Experiment Station Circular 71

The College of Earth and Mineral Sciences

Twenty-fifth Technical Conference on Petroleum Production

OCTOBER 19 - 21, 1966

The Pennsylvania State University

University Park, Pennsylvania

$5.00

Proceedings of the

25th Technical Conference on Petroleum Production

The Pennsylvania State University

October 19-21, 1966

Sponsored by

The Department of Petroleum and Natural Gas

in cooperation with

The Penn Grade Crude Oil Association

These proceedings are respectively dedicated to those individuals from industry and the University who were responsible for the very early research endeavors at Penn State.

From Industry:

Paul Torrey
Don Andrus
Ralph Zook
George Hanks
Harry Ryder
Art Simmons
Joe Moorhead
Wes Dunlap
George Holbrook
Jerry Bauer
Cliff Martin
Cornell Pfohl
Coy Hogg
Tony Saxe
Ed Booth
J. P. ("Dick") Jones
Bob Bossler
W. H. ("Tex") Young
John DePetro

From the University:

Dean Steidle
C. A. Bonine
Clark Barb
Arthur Honess
A. W. ("Doc") Gauger
Kenneth Barnes
George Fancher
James Lewis
Sam Yuster
Paul Krynine

PREFACE

The reaching of a milestone in what has been a most fruitful and continuing cooperative program between industry and the University should call for both reflection and celebration. Reflection on both the history of the Conference and the results of research programs carried out at Penn State is presented in these proceedings (Petroleum Production Research at Penn State in Retrospect, p. 405). In celebration of the Silver Anniversary of the Conference two symposia have been added to this year's meeting -- Mathematics and Mathematical Modelling and Geology of the Appalachian Basin. We feel that this is a most fitting way to honor the spirit of those that took part in the previous Conferences. It is hoped that the informality that has been a part of previous Conferences will prevail at the symposia. It has often been brought to our attention that the atmosphere for informal discussion is what makes the Conference so valuable.

The Department would like again to acknowledge the continuing friendship of the Penn Grade Crude Oil Association as well as the various oil companies and governmental agencies. We are proud to have had the opportunity to assemble these proceedings.

Richard N. Harding
David A. T. Donohue
Department of Petroleum and
Natural Gas

TABLE OF CONTENTS

ERRATA

p. 161

Below equation (1.12)

$$\eta_\alpha = 1,\ \alpha \in C_h^{**} + C_h^V + C_h^H\ ;\ \eta_\alpha = 0, \text{ otherwise.}$$

Below equation (1.14)

From (1.9), it is easily seen that $M_1 \underline{e} \leq \underline{8}\, \underline{\xi}$.

Equation (1.15)

$$M_1^{-1}\, \underline{\xi} \geq \frac{1}{8}\, \underline{e}.$$

Equation (1.16)

$$\underline{0} \leq M^{-1} R\, \underline{e} \leq \underline{e} - \frac{1}{8} M_2^{-1}\, \underline{e} < \underline{e},$$

p. 168

Equation (1.32)

$$h \leq \text{MIN}\left(\left(\frac{1}{q}\right)^{1/2}, \frac{\ln 2}{8r+4}, \frac{\ln 2}{8s+4}\right),$$

p. 185

Equation (2.9)

$$B^+ = D^{-1} H_1 D \geq 0.$$

SOME APPROXIMATE SOLUTIONS FOR CALCULATING THE TEMPERATURE DISTRIBUTION DURING HOT FLUID INJECTION

G. W. Thomas
Sinclair Oil & Gas Company
Tulsa Research Center

INTRODUCTION

Theoretical treatments of the problem of hot fluid injection into a petroleum reservoir have been given by a number of people.[1-12] Lauwerier[4] developed an analytical solution for calculating temperature distributions under certain restrictive assumptions. Later works of Avdonin[3] and Rubinshtein[10] either sought to examine the influence of these restrictions or remove them entirely. The additional analytical solutions they obtained are in the form of integrals, series, or combinations of both.

In this work we present two simpler closed form approximations for a radial system where the convection parameter is large and horizontal heat conduction in the bed can be neglected. Comparisons are made with the results of Lauwerier, Avdonin, Rubinshtein and an exact numerical solution of Spillette which indicate adequate agreement for most field calculations.

Finally, a third solution is presented employing a technique of approximate Laplace transform inversion developed by Schapery.[14] The steady state solution is also given.

FIRST METHOD OF APPROXIMATION

In the paper of Lauwerier[4] and later works of Avdonin[1,3] horizontal thermal conductivity in the bed was assumed to be zero. Avdonin[3] subsequently examined the influence of this supposition. He concluded that for large values of the convection parameter, ν, the convective heat flux dominates and the absolute error introduced by the assumption is generally

small.* Spillette's work[12] also supports this conclusion. Rubinshtein[11] developed an asymptotic series for the case of large convection parameter and presented the first two terms. These are satisfactory under some conditions, except in regions where the solution approaches zero. Subsequent terms are very complex and obtained only with much labor. The first method of approximation in this work is presented as an alternative to Rubinshtein's.

If we neglect horizontal conduction and assume infinite vertical thermal conductivity within the bed, we are led to the problem:**

$$\left.\begin{aligned} &u_{rr} + \frac{1}{r} u_r + u_{zz} = \frac{1}{\theta} u_t \,;\; 0<r<\infty,\; 0<z<\infty,\; t>0 \\ &-\frac{\nu}{r} u_r + u_z = u_t \,;\; z = 0,\; 0<r<\infty,\; t>0 \\ &u(r,z,0) = 0;\; u(0,0,t) = 1;\; u(r,z,t) \to 0, \text{ when } (r^2+z^2) \to \infty \end{aligned}\right\} \quad (1)$$

where

$$r = 2\bar{r}/h,\; z = 2\bar{z}/h,\; t = 4k_2\bar{t}/\rho_1 c_1 h^2,\; \theta = \rho_1 c_1/\rho_2 c_2,\; \nu = Q\rho_f c_f/2\pi h k_2 .$$

We now map (1) into a new coordinate system, ω, defined by

$$\omega \equiv z/\nu + r^2/\nu^2 \quad (2)$$

thus,

$$\left.\begin{aligned} &(1 + r^2/\nu^2)\, u_{\omega\omega} + u_\omega = \nu^2/\theta^2\, u_t \,;\; 0<\omega<\infty,\; t>0 \\ &u_t = 0 \text{ when } \omega = r^2/2\nu^2,\; t>0 \\ &u(\omega,0) = 0;\; u(0,t) = 1;\; u(\omega,t) \to 0 \text{ when } \omega \to \infty . \end{aligned}\right\} \quad (3)$$

If we assume that ν is sufficiently large such that for practical values of the dimensionless coordinate r, $(r/\nu)^2 \approx 0$ then (3) reduces to

$$\left.\begin{aligned} &u_{\omega\omega} + u_\omega = \nu^2/\theta\, u_t \\ &u(\omega,0) = 0;\; u(0,t) = 1 \\ &u(\omega,t) \to 0 \text{ when } \omega \to \infty . \end{aligned}\right\} \quad (4)$$

*Avdonin presents the following inequalities: $\sqrt{t}\,Q > 9450$; $\sqrt{t}/Q < 0.1588$, which, if satisfied, (for t in days and Q in bbls/day) results in an absolute error of less than 3% when horizontal conduction is neglected.

**Subscripts (except 1,2, & f) are used to indicate partial derivatives throughout this work.

Taking the Laplace transform of (4) yields

$$\frac{d^2\bar{u}}{d\omega^2} + \frac{d\bar{u}}{d\omega} - (p\nu^2/\theta)\bar{u} = 0$$

$$\bar{u}(0,p) = 1/p;\; \bar{u}(\omega,p) \to 0 \text{ when } \omega \to \infty . \quad (5)$$

Therefore, $\bar{u} = \frac{1}{p} \exp\{-\tfrac{1}{2}[1 + \sqrt{1 + (4p\nu^2/\theta)}]\,\omega\}$. (6)

The transform in (6) is readily inverted using the shifting rule and tables given in Carslaw and Jaeger.[13] Thus, we obtain the expression

$$u = \tfrac{1}{2}\left\{ e^{-\omega}\, \operatorname{erfc}\left(\frac{1}{2}\frac{\omega\nu}{\sqrt{\theta t}} - \frac{\sqrt{\theta t}}{2\nu}\right) + \operatorname{erfc}\left(\frac{1}{2}\frac{\omega\nu}{\sqrt{\theta t}} + \frac{\sqrt{\theta t}}{2\nu}\right)\right\} . \quad (7)$$

In Fig. 1, we compare the temperature distribution calculated by (7) with that obtained using the first two terms of Rubinshtein's asymptotic approximation.[11] In this case, $\nu = 166$. For small values of time, the use of the first two terms of Rubinshtein's asymptotic series leads to an underprediction of the temperature distribution. On the other hand, (7) tends to overpredict. Consequently the deviation between the two is appreciable at 135 days. However, as time increases the differences between the two curves becomes less, as reflected by the curves for 540 days.

Fig. 2 compares our results with those of Spillette[12] when $\nu = 15.8$. Spillette's curve represents an "exact" solution obtained by finite difference solution of the energy equations having no restrictive assumptions on the thermal constants. We notice again an improvement in correspondence for the larger time. Fig. 3 reproduces the curves of Fig. 2 and also shows the results of Lauwerier[4] and Avdonin.[2]

Since we are using Eq. (7) to represent the solution to (3), the approximation becomes poor as $(r/\nu)^2$ increases since we assumed this factor can be neglected. In Fig. 3 at a radius of 60 feet $(r/\nu)^2 = 0.577$. At t = 135 days the value of u obtained from (7) is about twice Spillette's --

a deviation of 100%. (Lauwerier's and Avdonin's results also present considerable deviations from the exact solution at this point.) However, at t = 540 days the deviation is less than 1% at 60 feet. Thus for larger times, the approximation becomes better and larger values of $(r/\nu)^2$ can be tolerated. For most field applications of hot fluid injection the maximum values of $(r/\nu)^2$ will generally be much less than those encountered in our comparison with Spillette's results.

It is apparent that isotherms at a given time will be prescribed by the relationship

$$|z| / \nu + r^2/2\nu^2 = k \tag{8}$$

where k is a unique constant for each isotherm. Thus, they all have the same parabolic shape in the r-z plane. To construct an isotherm, (7) is solved with ω replaced by z/ν (i.e. r = 0) for the specified time such that a range of values of u spanning the desired isotherm is generated. Simple interpolation within this range will yield a value of z and hence k ($=z/\nu$) for the isotherm. All other r-z coordinates of the isotherm are then determined from (8).

SECOND METHOD OF APPROXIMATION

A second approximation similar to (7) can be obtained readily, although it represents no significant improvement in the results. We present it merely as a means of demonstrating an alternate approach. First, we apply the Laplace transform to (1) and get

$$\left.\begin{aligned} &\bar{u}_{rr} + \frac{1}{r}\bar{u}_r + \bar{u}_{zz} = \frac{p}{\theta}\bar{u};\ 0<r<\infty,\ 0<z<\infty,\ p>0 \\ &-\frac{\nu}{r}\bar{u}_r + \bar{u}_z = p\bar{u};\ z = 0,\ 0<r<\infty,\ p>0 \\ &\bar{u}(0,0,p) = 1/p;\ \bar{u}(r,z,p) \to 0 \text{ when } (r^2+z^2) \to \infty . \end{aligned}\right\} \tag{9}$$

We now construct a function that satisfies the second equation in (9) and the boundary conditions exactly, i.e.,

$$\bar{u} = \frac{1}{p}\exp\left[\xi\, r^2/2\nu^2 + (\xi+p)\, z\right] \tag{10}$$

where ξ is < 0 and independent of the space coordinates. Substitution of (10) in the first equation of (9) and again assuming $(r/\nu)^2 \approx 0$ gives

$$\xi = -(p+1/\nu) - \sqrt{1/\nu^2 + 2p/\nu + p/\theta}\,. \tag{11}$$

Consequently,

$$\bar{u} = \frac{1}{p}\exp\left\{-\left[1+\sqrt{(2\nu+\nu^2/\theta)p+1}\right]\omega - pr^2/2\nu\right\} \tag{12}$$

where ω is defined in (2).

Inverting (12) yields

$$u = \frac{1}{2}\left\{ e^{-2\omega}\,\mathrm{erfc}\left[\frac{\omega}{2}\sqrt{\frac{\nu^2+2\theta\nu}{\theta\tau}} - \sqrt{\frac{\theta\tau}{\nu^2+2\theta\nu}}\right] + \mathrm{erfc}\left[\frac{\omega}{2}\sqrt{\frac{\nu^2+2\theta\nu}{\theta\tau}} + \sqrt{\frac{\theta\tau}{\nu^2+2\theta\nu}}\right]\right\} H(\tau) \tag{13}$$

where $\tau = t - r^2/2\nu$ and $H(\tau)$ is Heaviside's unit function. Fig. 4 presents the results of (13) again compared to Spillette's exact solution. Isotherms using this model are also given by (8).

THIRD METHOD OF APPROXIMATION

In many problems of applied mathematics one is frequently faced with the task of inverting Laplace transforms. Schapery[14] has devised some novel methods of approximate transform inversion where an exact analytical inversion is difficult. The problem in (1) results in an excellent example of a difficult transform which can be adequately approximated using Schapery's "direct method." In this, we claim no simplification of existing analytical solutions for hot fluid injection problems. Rather, our purpose is to illustrate the utility of Schapery's method in this area.

The first equation in (9) is satisfied by

$$\bar{u} = \int_0^\infty \lambda f(\lambda,p)\,\exp\left(-z\sqrt{\lambda^2+p/\theta}\right) J_o(\lambda r)\,d\lambda \tag{14}$$

which is obtained by separation of variables and superposition. Substitution of (14) into the second equation in (9) gives

$$\int_0^\infty \lambda f(\lambda,p)(\sqrt{\lambda^2+p/\theta} + p)\, J_o(\lambda r)d\lambda - \frac{\nu}{r}\int_0^\infty \lambda^2 f(\lambda,p)J_1(\lambda r)d\lambda = 0 . \quad (15)$$

The boundary condition $\bar{u}(0,0,p) = 1/p$ also yields

$$\int_0^\infty \lambda f(\lambda,p)d\lambda = 1/p . \quad (16)$$

From (15) and (16) we solve for $f(\lambda,p)$. To do this we employ the following lemma: Given two continuous functions $F(\lambda,p)$ and $G(\lambda,p)$ defined on the interval $[0,\infty]$ such that

$$\int_0^\infty \lambda F(\lambda,p)\, J_o(\lambda r)d\lambda = \frac{1}{r}\int_0^\infty G(\lambda,p)\, J_1(\lambda r)d\lambda$$

then

$$F_\lambda = - G/\lambda . \quad (17)$$

(A formal proof of (17) is given in the appendix.) In (15), $F(\lambda,p) = f(\lambda,p)(\sqrt{\lambda^2+p/\theta} + p)$ and $G(\lambda,p) = \lambda f(\lambda,p)$. Therefore from (17) we obtain

$$F_\lambda + \lambda\nu F/\sqrt{\lambda^2+p(1+1/\theta)} = 0 \quad (18)$$

which has the solution

$$F(\lambda,p) = k(p)\,(\sqrt{\lambda^2+p/\theta} + p)^{\nu p} \exp\,(-\nu\sqrt{\lambda^2+p/\theta}). \quad (19)$$

Therefore,

$$f(\lambda,p) = k(p)\,(\sqrt{\lambda^2+p/\theta} + p)^{\nu p-1} \exp\,(-\nu\sqrt{\lambda^2+p/\theta}) . \quad (20)$$

Substitution of (20) into (16) gives

$$\int_0^\infty k(p)(\sqrt{\lambda^2+p/\theta} + p)^{\nu p-1} \exp\,(-\nu\sqrt{\lambda^2+p/\theta})\lambda d\lambda = 1/p . \quad (21)$$

To determine $k(p)$ in (21) we make the following change of variable:

$$\left(\frac{\sqrt{\lambda^2+p/\theta} + p}{\sqrt{p/\theta} + p}\right)^p \exp\,(-\sqrt{\lambda^2+p/\theta} + \sqrt{p/\theta}) = \exp\,(-\zeta) . \quad (22)$$

Thus (21) becomes

$$k(p)\,[(\sqrt{p/\theta} + p)^p \exp\,(-\sqrt{p/\theta})]^\nu \int_0^\infty \exp\,(-\nu\zeta)\, d\zeta = 1/p \quad (23)$$

or

$$k(p) = \frac{\nu \exp\,(\nu\sqrt{p/\theta})}{p\,(\sqrt{p/\theta} + p)^{\nu p}} \quad (24)$$

and

$$f(\lambda,p) = \frac{\nu\,(\sqrt{\lambda^2+p/\theta} + p)^{\nu p-1} \exp\,[-\nu(\sqrt{\lambda^2+p/\theta} - \sqrt{p/\theta})]}{p(\sqrt{p/\theta} + p)^{\nu p}} . \quad (25)$$

Now we substitute (25) into (14) and obtain

$$\bar{u} = \int_0^\infty \lambda J_o(\lambda r)\left\{\frac{\nu(\sqrt{\lambda^2+p\theta} + p)^{\nu p-1} \exp\,[-(\nu+z)\sqrt{\lambda^2+p/\theta} + \nu\sqrt{p/\theta}]}{p(\sqrt{p/\theta} + p)^{\nu p}}\right\} d\lambda . \quad (26)$$

Attempts to analytically invert (26) have not met with success because of the complex nature of the argument. However, an approximate inversion can be obtained using Schapery's "direct method."[14] It simply involves evaluating $p\bar{u}$ with $p = c/t$ where c is a constant.* Consequently:

$$u \approx \int_0^\infty \lambda J_o(\lambda r)\left\{\frac{\nu(\sqrt{\lambda^2+c/\theta t} + c/t)^{\nu c/t-1} \exp\,[-(\nu+z)\sqrt{\lambda^2+c/\theta t} + \nu\sqrt{c/\theta t}]}{(\sqrt{c/\theta t} + c/t)^{\nu c/t}}\right\} d\lambda$$

... (27)

In Fig. 5, we compare the results obtained using (27) with Spillette's for $c = 0.5$. Again this approximation yields results that are sufficient for most engineering calculations.

The steady state solution to (1) can readily be found from (26) using Tauber's theorem.[16] Thus we find

$$\lim_{p\to 0} p\,\bar{u} = \nu\int_0^\infty J_o(\lambda r)\, \exp\,[\,-(\nu+z)\,\lambda]\, d\lambda \quad (28)$$

which is the well-known integral of Lipschitz.[17]

*From Schapery's theory, the constant c is the logarithm of Euler's number. However, it can be adjusted to allow for skewness. The method is generally applicable when $d[p\bar{u}(p)]/d(\log p)$ is a slowly varying function of $\log p$ ($\log \equiv \log_{10}$). See Ref. 14.

Therefore,

$$u = \frac{\nu}{\sqrt{r^2+(\nu+z)^2}} \quad \text{when } t \to \infty \ . \tag{29}$$

ACKNOWLEDGMENTS

Eugene Usdin of Southwestern Computing Service and Dr. Gordon Latta of the Stanford University Mathematics Department entered into several helpful discussions of this work. Their assistance is gratefully acknowledged.

NOMENCLATURE

c	- constant in Schapery's approximation, dimensionless
c_i	- heat capacity, BTU/lb^{o}F (i = 1,2, or f)
h	- bed thickness, feet
k	- constant for prescribing isotherms
k_i	- thermal conductivity, BTU/hr-ft^{o}F (i = 1, or 2)
p	- Laplace transform of dimensionless time, t
Q	- injection rate, bbls/day
$\bar{r}$	- radial coordinate, feet
r	- dimensionless radial coordinate
$\bar{t}$	- time, days
t	- dimensionless time
u	- dimensionless temperature
$\bar{z}$	- vertical coordinate, feet
z	- dimensionless vertical coordinate
θ	- dimensionless ratio, $\rho_1 c_1 / \rho_2 c_2$
ν	- convection parameter, dimensionless

ρ_i	- density, lbs/ft^3 (i = 1,2 or f)
τ	- dimensionless time

Subscripts

1	- refers to bed
2	- refers to bounding rock
f	- refers to injected fluid

REFERENCES

Theoretical Papers on Hot Fluid Injection

1. Avdonin, N. A.: "On a Certain Two-Layer Thermal Convection Problem," Dokl. Acad. Sci. USSR, Vol. 151, No. 4, 1963, p. 815.

2. Avdonin, N. A.: "Some Formulas for Calculating the Temperature Field of a Stratum Subject to Thermal Injection," Neft'i Gaz, Vol. 7, No. 3, 1964, p. 37.

3. Avdonin, N. A.: "On the Different Methods of Calculating the Temperature Fields of a Stratum during Thermal Injection," Neft'i Gas, Vol. 7, No. 8, 1964, p. 39.

4. Lauwerier, H. A.: "The Transport of Heat in an Oil Layer Caused by the Injection of Hot Fluid," Appl. Sci. Res., Sec. A, Vol. 5, 1955, p. 145.

5. Marx, J. W. and Langenheim, R. H.: "Reservoir Heating by Hot Fluid Injection," Trans.AIME, Vol. 216, 1959, p. 312.

6. Malofeev, G. E.: "Calculation of the Temperature Distribution in a Formation when Pumping Hot Fluid into a Well," Neft'i Gaz, Vol. 3, No. 7, 1960, p. 59.

7. Malofeev, G. E. and Sheinman, A. B.: "The Calculation of Oil Output of a Bed into which Hot Water is Injected," Neft. Khoz., No. 3, 1963, p. 31.

8. Ramey, H. J.: "How to Calculate Heat Transmission in Hot Fluid Injection," Petroleum Engineer, Nov. 1964, p. 110.

9. Rubinshtein, L. I.: "The Total Heat Losses in Injection of a Hot Liquid into a Stratum," Neft'i Gaz, Vol. 2, No. 9, 1959, p. 41.

10. Rubinshtein, L. I.: "A Contact Thermal Conduction Problem," Dan SSSR, Vol. 135, No. 4, 1960, p. 805.

11. Rubinshtein, L. I.: "An Asymptotic Solution of an Axially Symmetric Contact Problem in Thermal Convection for High Values of the Convection Parameter," Dan SSSR, Vol. 146, No. 5, 1962, p. 1043.

12. Spillette, A. G.: "Heat Transfer During Hot Fluid Injection into an Oil Reservoir," J. of Can. Petrol. Tech. Vol. 4, No. 4, October-December 1965, 213.

Other References

13. Carslaw, H. S. and Jaeger, J. C.: Conduction of Heat in Solids, Oxford U. Press, 2nd ed., p. 495, No. 19.

14. Schapery, R. A.: "Approximate Methods of Transform Inversion for Viscoelastic Stress Analysis," Proc. 4th Cong. Appl. Mechs., Vol. 2, 1962, 1075.

15. Sneddon, I. N.: Fourier Transforms, McGraw-Hill, 1951, 45.

16. Van der Pol, B. and Bremmer, H.: Operational Calculus Based on the Two-Sided Laplace Transform, Cambridge Press, 2nd ed., 1955, 123.

17. Watson, G. N.: Theory of Bessel Functions, Cambridge Press, 2nd ed., 384.

18. Watson, G. N.: ibid, 406.

APPENDIX

Lemma: Let $F(\lambda,p)$ and $G(\lambda,p)$ be continuous functions for $\lambda \geq 0$ and $p \geq 0$ defined on the interval $[o,\infty]$ such that

$$\int_o^\infty \lambda F(\lambda,p)\ J_o(\lambda r)\ d\lambda = \frac{1}{r}\int_o^\infty G(\lambda,p) J_1(\lambda r)\ d\lambda \qquad (A\text{-}1)$$

then $$\frac{\partial F}{\partial \lambda} = -\ G/\lambda . \qquad (A\text{-}2)$$

Proof: We define a function $M(r,p)$ as follows:

$$M(r,p) \equiv \int_o^\infty G(\lambda,p)\ J_1(\lambda r)\, d\lambda \qquad (A\text{-}3)$$

$$\therefore\ \frac{M(r,p)}{r} = \int_o^\infty \lambda F(\lambda,p)\ J_o(\lambda r)\ d\lambda\ . \qquad (A\text{-}4)$$

From the Hankel inversion theorem[15] we can write

$$F(\lambda,p) = \int_o^\infty M(r,p)\ J_o(\lambda r)\ dr \qquad (A\text{-}5)$$

$$= \int_o^\infty J_o(\lambda r) \int_o^\infty G(x,p)\ J_1(xr)\ dx\ dr \qquad (A\text{-}6)$$

$$= \int_o^\infty G(x,p) \int_o^\infty J_o(xr)\ J_1(xr)\ dr\ dx\ , \qquad (A\text{-}7)$$

The right-hand integral in (A-7) is a special case of Weber's discontinuous integral[18]

$$\therefore F(\lambda,p) = \int_o^\infty G(x,p)\ dx \left\{ \begin{matrix} \frac{1}{x}, & x>\lambda \\ 0, & x<\lambda \end{matrix} \right\} \qquad (A\text{-}8)$$

i.e.,

$$F(\lambda,p) = \int_\lambda^\infty \frac{G(x,p)}{x}\ dx\ . \qquad (A\text{-}9)$$

Differentiating (A-9) with respect to λ yields

$$\frac{\partial F(\lambda,p)}{\partial \lambda} = -\ \frac{G(\lambda,p)}{\lambda}\ . \qquad (A\text{-}10)$$

FIG. 1 COMPARISON OF APPROXIMATE TEMPERATURE DISTRIBUTIONS

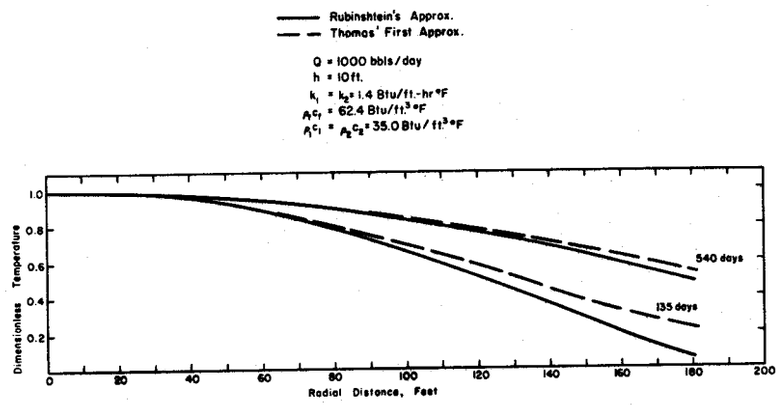

FIG. 2 COMPARISON OF FIRST APPROXIMATION WITH EXACT SOLUTION

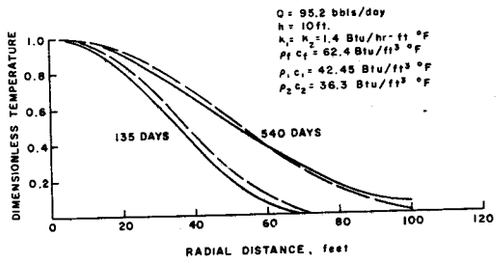

FIG. 3 COMPARISON OF FIRST APPROXIMATION WITH SOLUTIONS OF SPILLETTE, AVDONIN AND LAUWERIER

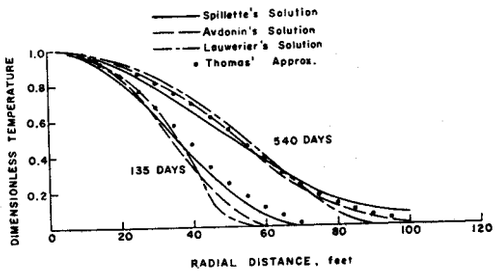

FIG.4 COMPARISON OF SECOND APPROXIMATION WITH EXACT SOLUTION

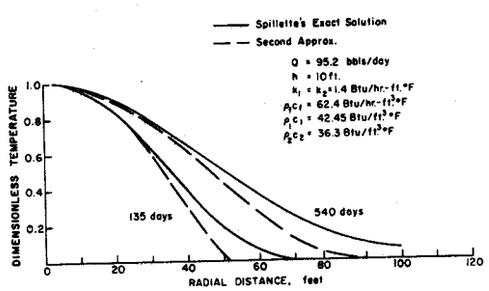

FIG. 5 COMPARISON OF THIRD APPROXIMATION WITH EXACT SOLUTION

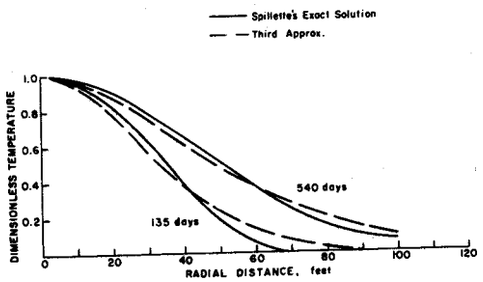

A Self-Similar Solution of Unsteady Flow of Gas Through Porous Media

Rafael J. Sandrea

Introduction

In the past many theoretical studies of ideal gas flow in porous media have been published.[1-4] Since the partial differential equation describing the unsteady-state motion of the gas is non-linear, many of these published solutions have been based on linear approximations. Moreover, in those cases where the original non-linear equation has been solved, numerical procedures similar to those applicable to the parabolic-type differential equation were employed. These procedures give origin to independent errors which are difficult to estimate. These errors mainly arise from round-off because of the repetitive nature of the iterative schemes that are compulsory, and also from the truncation of the series expansions used to obtain the finite difference approximations.

It is the object of this paper to present a particular solution of the transient motion of an ideal gas in an isotropic porous medium with constant properties. Both the isothermal and adiabatic cases are considered.

The method of solution differs from those previously published in that use is made of the self-similarity of the motion in order to obtain a transformation of the one-dimensional partial equation into an ordinary differential equation. The latter is then solved numerically. The effects of linearizing the original differential

equation are discussed.

Formulation of the Problem

In accordance with the development given by Muskat[5], the motion of ideal gases in porous media is governed by the expression

$$\nabla^2 p^{1+m} = \frac{1}{\alpha P} \frac{\partial p^{1+m}}{\partial t} \qquad (1)$$

where, for convenience, the following relationships are defined

$$P = \frac{p}{p_o} \quad ; \quad \alpha = \frac{k p_o}{m \mu \phi} \quad ; \quad m = \frac{c_v}{c_p} \qquad (2)$$

Specifically, it is proposed to solve the one-dimensional form of Eq. 1, for both radial and linear systems, subject to the following boundary conditions

$$\left.\begin{array}{lll} t = 0, & P = 1, & \text{for all } r,x \\ t > 0, & P = a, & r,x \rightarrow 0 \\ & P = 1, & r,x \rightarrow \infty \\ & a = p_w/p_o & \end{array}\right\} \qquad (3)$$

Equation 1, together with the boundary conditions 3 show that the system of characteristic parameters for the radial problem is α, r, t. Hence the dependent variable P can be a function only of these parameters, that is, $P(\alpha, r, t)$.

From the general considerations of dimensional analysis it follows that all the nondimensional quantities are a function of the

single independent combination, $y = r^2/4\alpha t$. It is therefore evident that the partial differential Eq. 1 for P reduces to an ordinary differential equation in the one unknown y. The motion of a compressible fluid which depends on such a combination is called self-similar[6]. By analogy, the similarity transformation for the linear case is $y = x^2/4\alpha t$.

Substituting the previously derived expressions for the independent variable y into Eq.1 gives for the radial case

$$\frac{d}{dy}\left(y \frac{dP^{1+m}}{dy}\right) + \frac{y}{P} \frac{dP^{1+m}}{dy} = 0 \qquad (4)$$

and for the linear case

$$\frac{d^2 P^{1+m}}{dy^2} + \frac{dP^{1+m}}{dy}\left(\frac{1}{2y} + \frac{1}{P}\right) = 0 \qquad (5)$$

The boundary conditions corresponding to the new variables are

$$\begin{array}{lll} P = a, & y \rightarrow 0 & 0 < a < 1 \\ P = 1, & y \rightarrow \infty & \end{array} \qquad (6)$$

Since analytical integration of the non-linear differential Eqs.4 and 5 is not possible, numerical methods are to be used. These equations, moreover, contain two singularities, y = 0 and P = 0, within the region of interest. The latter singularity P = 0, can be obviated easily by adequately defining the boundary conditions at $y \rightarrow 0$, such that $a \neq 0$. It is important, however, that the behavior of the

function P(y), in the vicinity of y→0, be determined prior to initiating the numerical integration. Likewise, the behavior of the function for large values of the argument must be derived.

For convenience we will discuss in detail the required analysis for the particular case of radial geometry and isothermal conditions. The pertinent equation, as obtained from Eq. 4, is then

$$\frac{d}{dy}\left(y\frac{dP^2}{dy}\right) + \frac{y}{P}\frac{dP^2}{dy} = 0 \qquad (7)$$

from which the asymtotic behavior of the function P(y) is readily obtained by equating P approximately to the limiting value P_∞=1 and integrating analytically. Hence the slope of the function is found to be

$$\frac{dP^2}{dy} = \frac{C_1}{y}\exp(-y) \qquad (8)$$

where C_1 is a constant of integration.

From Eq. 8 it is possible to estimate the error of an approximation in truncating the numerical solution at a finite value of the argument. The corresponding value of the derivative at y=10 is of the order $C_1 x 10^{-6}$.

Let us now analyse the function P(y) in the neighborhood of y→0. Following appropriate manipulation[7] Eq. 7 can be expressed in integral form as

$$P^2(y) = P^2(0) - 2\int_0^y \ln(y/\eta e)P(\eta)\,d\eta \qquad (9)$$

The limit of this integral is zero as y→0, thereby yielding the result that P^2 approaches a constant which we call a^2 in order to be consistent with the boundary conditions 6.

We now postulate that in the vicinity of y→0 a complete solution of Eq. 7 will be of the form

$$P^2 = a^2 + \delta(y) \qquad (10)$$

The function $\delta(y)$ is subsequently evaluated from Eq. 7. Equation 10 then becomes

$$P^2 = a^2 + C_2 y \qquad (11)$$

where, from the nature of the problem, C_2 must be positive.

The analysis of the behavior of the function P(y) is now complete, and thus Eq. 7 can be solved numerically in conjunction with Eq. 11. The method of Runge-Kutta was used to initiate the solution, which was subsequently continued with the Adams' formula. The results are shown in Fig. 1 for several values of a^2.

Following the approach previously described, the behavior of the function P(y) in the vicinity of y→0 can be determined for the generalized forms of Eqs. 4 and 5. Figure 2 illustrates typical results of the numerical integration of these equations for radial and linear systems producing under adiabatic and isothermal conditions. Specifically, the case of a^2 = .10 is given. In addition the adiabatic computation refers to air (m = .71).

Discussion

Although the problem treated in this paper is idealized in so far as the boundary conditions are concerned, advantage can now be taken of the fact that an exact solution of the original non-linear equation of motion is available. In this respect, it is possible to check the validity of various approximate methods of solving the original equation; and in particular, it is important to investigate the non-linear character of the equation itself.

One could intuitively argue that the non-linear term 1/P in Eqs. 4 and 5 could be replaced by a constant if the variations in P are small compared to the value of P. Indeed, if this constant is unity then the original differential equation (Eq. 1) becomes the classical diffusivity equation for which numerous analytic solutions are available.

The possibility of linearizing the differential eqs. 4 and 5 was studied for both isothermal and adiabatic conditions. The variable P in the non-linear term was replaced by constants varying in value from the initial condition a to the asymtotic value of the function.

It was found in all cases that the linearized solutions approached more closely the corresponding non-linear solutions when P was replaced by unity. Moreover, as it is to be expected, the discrepancy between the two types of solutions is substantially reduced as the pressure drop across the system is decreased. Figures 3 and 4 illustrate the comparative results of the linearized (P=1) and non-linearized solutions, for systems of both linear and radial geometry. These results are for the case of $a^2=.10$, which corresponds to approximately 70 percent pressure drop.

Two important conclusions are evident from these figures. Firstly, the results point out that while there exists some degree of difference between the linearized and non-linearized solutions, essentially the non-linear effects are insignificant for systems of radial geometry. This behavior is manifested for both the isothermal and adiabatic cases.

In addition, an interesting result of the calculations is that the linearized solutions of the isothermal problem corresponds almost identically with the non-linear solutions of the adiabatic problem. This is fortunate, since it is well known that disturbances propagate more nearly under adiabatic, rather than isothermal, conditions.

As will be recalled from the previous discussions the singularity at P=0 in Eqs. 4 and 5 was conveniently obviated by redefining the boundary conditions. For this reason it was only possible to study the behavior of the systems under a maximum pressure drop of approximately 80 percent ($a^2=.04$). The relative effects of linearization, previously discussed, were found to be equally valid in this range also.

From the aforesaid the results further establish that the non-linear character of the differential equations is not manifested except, perhaps in systems subjected to high pressure draw-downs (over 80 percent). An approximate explanation of this phenomenon is suggested by Eq. 1. Here the coefficient of the time derivative, $1/\alpha$, is of small order of magnitude ($\sim 10^{-5}$). This, therefore, minimizes the effects of the non-linear term except when P is very small. Therefore, we may venture to conclude that the non-linearity of the original equation of motion appears to be more of a mathematical nature than physical.

Conclusions

An exact solution of the non-linear equation describing the dynamics of an ideal gas in a porous medium of radial and linear geometry is presented. Results indicate that the non-linear character of this equation may be important only in systems subjected to large pressure draw-downs (more than 80%). The non-linearity appears to be more of a mathematical nature than physical, especially for systems of radial geometry. Moreover, it is found that linearized solutions of the isothermal problem correspond almost identically to non-linear solutions of the adiabatic problem.

Bibliography

1. Katz, D. L., Cornell, D., Kobayashi, R., Poettman, F. H., Vary, J. A., Elenbaas, J. R. and Weinaug, C. F.: Handbook of Natural Gas Engineering, McGraw-Hill Book Co., Inc., New York (1959).

2. Aronofsky, J. S. and Jenkins, R.: Unsteady Flow of Gas Through Porous Media: One-dimensional Case, Proc. 1 st. U. S. Natl. Congr. Appl. Mech., 763, (1952).

3. **Warren, J. E.: The Unsteady State Behavior of Linear Gas Storage Reservoirs, Pet. Engr., 38 (12): B60 (1956).**

4. Bruce, G., Peaceman, D., Rachford, H. H. and Rice, J.: Calculations of Unsteady State Gas Flow through Porous Media, Trans. AIME, 198: 79 (1953).

5. Muskat, M.: The Flow of Homogeneous Fluids through Porous Media, McGraw-Hill Book Co., Inc., New York (1937).

6. Sedov, L. I., On Certain Unsteady Compressible Fluid Motions, Appl. Math. Mech. Leningr. 9, 4, 294 (1945).

7. Moyer, R. D., Private Communication.

Acknowledgement

The author is indebted to Dr. David P. Hoult for his guidance throughout the course of this study.

Nomenclature

c_v	specific heat at constant volume
c_p	specific heat at constant pressure
e	constant, 2.718
k	permeability
P	dimensionless pressure, p/p_o
p	pressure
p_o	original pressure of the system
p_w	well pressure
ϕ	porosity
μ	viscosity

May 11, 1966

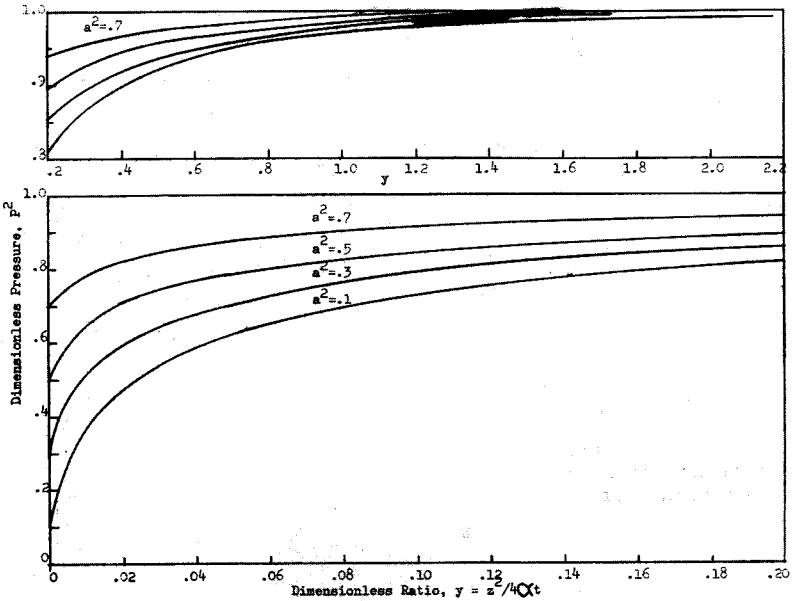

Figure 1.- Pressure Distribution in an Isothermal and Radial System

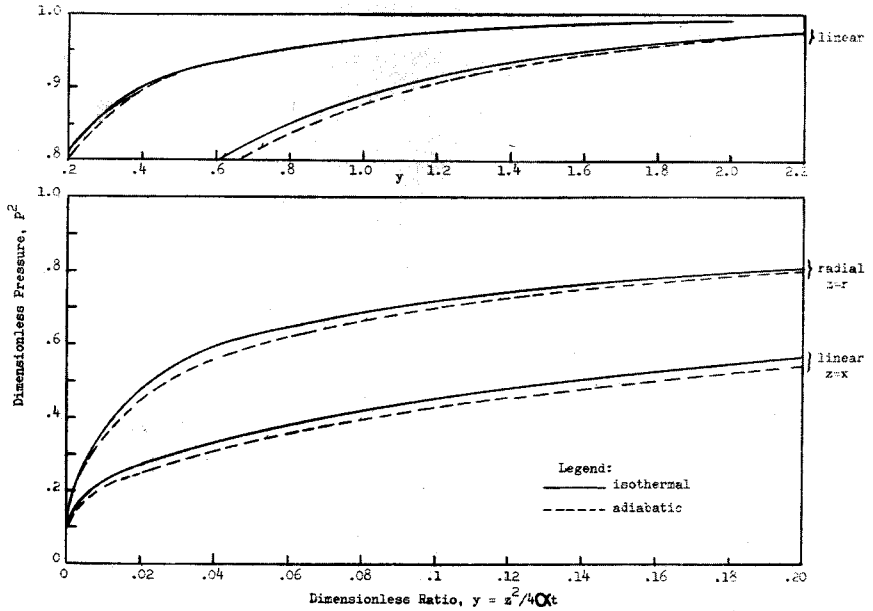

Figure 2.- Comparative Pressure Distributions for Adiabatic and Isothermal Systems (a^2 = .10)

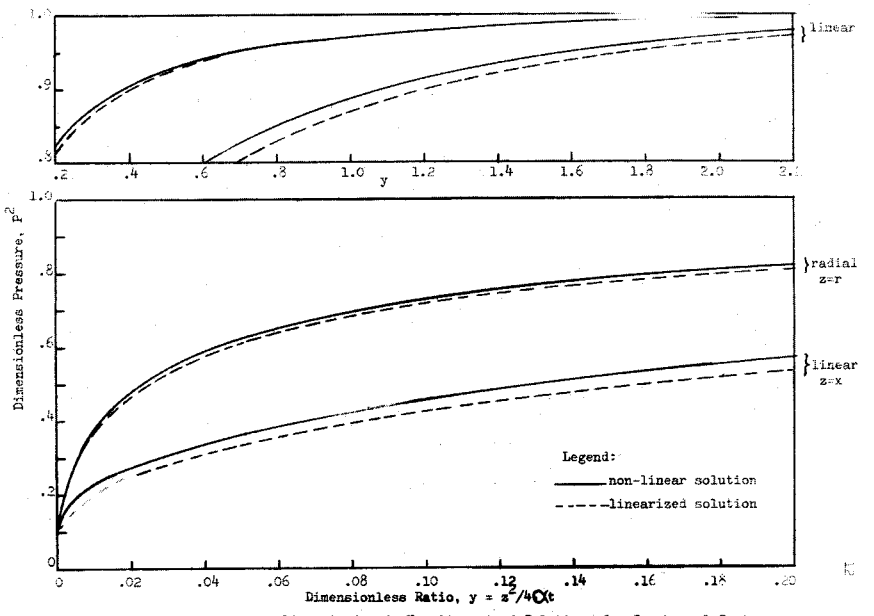

Figure 3.- Comparison of the Linearized and Non-linearized Solutions for Isothermal Systems ($a^2 = .10$)

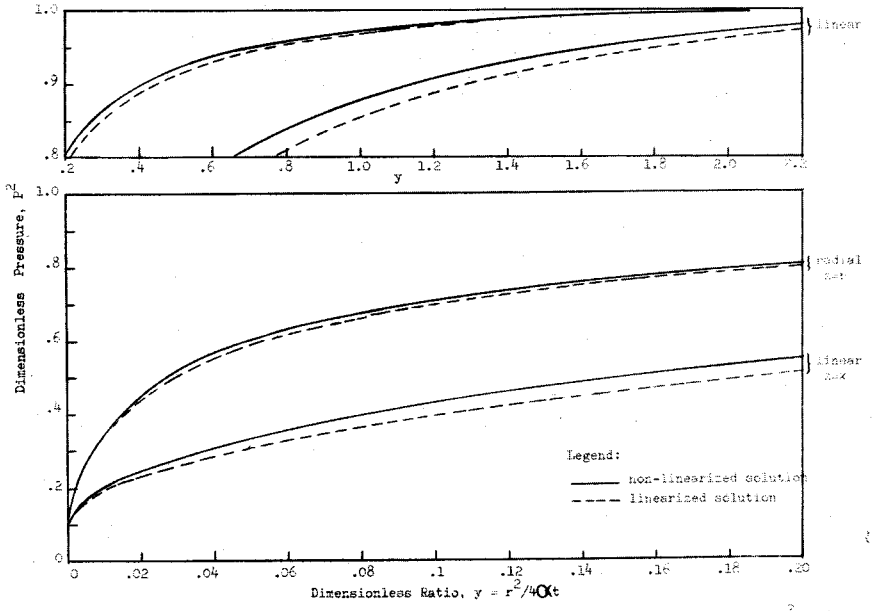

Figure 4.- Comparison of the Linearized and Non-linearized Solutions for Adiabatic Systems ($a^2 = .10$)

RESERVOIR ENGINEERING, REFORMULATED

By

Walter Rose

University of Illinois

ABSTRACT

Reservoir performance, as observed for example during exploitation of petroleum reservoirs, may be described aptly and adequately by reference to the modern principles of continuum mechanics to which the constitutive assumptions of nonequilibrium thermodynamics have been appended. Such a description makes explicit reference to the well-known coupled transport processes of mass and energy transfer. Accordingly it becomes clear that engineering applications of the theory are hampered unless extensive laboratory work is done in particular cases to provide experimental values for the needed transport coefficients.

INTRODUCTION

Condensed in this paper are ideas about the reformulation of reservoir engineering transport problems that avoid using Darcy's famous empirical law (1856) as the starting place of the analysis. Detailed explanations can be found in the papers of Bear and Bachmat,[1] and of Rose,[2] while the underlying theory is fully developed in the monumental work of Truesdell and Toupin.[3]

Like other important fields of technology, reservoir engineering is one that has been exposed to the impact of the scientific revolution now ushered in by the appearance of the high speed computer. Data processing and numerical methods for solving the intricate boundary valued problems of continuum physics make it possible for the reservoir engineer

to attempt refinements in analysis that just a few years ago could not be envisioned (much less attempted).

At the same time, but in a somewhat less spectacular and less advertised way, great progress has been and continues to be achieved in the development of the laboratory methods that provide necessary experimental data as input information and confirmation for the theoretical studies.

One might suppose, therefore, that the current practice of reservoir engineering here and abroad would reflect the manifold possibilities for realization and for achievement in this new era. And, indeed, one does see evidence of a new spirit, a new interest, and a new ambition in the reservoir engineering papers appearing in the current literature.

Concepts and ideas are generated more quickly, however, than they ever are utilized and applied. For one thing, there is an inertia to continue doing things in time-tested ways. Also, there is a natural distrust of innovations, compounded by the further problem of making the innovations widely known. But perhaps the greatest impediment to progress comes from the fact that here we are dealing with <u>systems</u>, and it is not always possible or straightforward for the reservoir engineer to use his improved understanding of one part of the reservoir system unless and until an improved understanding of other interlocked parts also is realized.

In this paper, we shall attempt to reformulate a statement of what is intended to be an integrated and self-contained approach to the solution of the classical reservoir engineering problems. And as might be expected, some of the ideas involved will be recognized as old and non-controversial, while others are new and essentially untested in the applications under discussion.

The successful practice of reservoir engineering in every case is facilitated whenever the underlying scientific aspects are understood. It is true, of course, that the reservoir engineer simply is involved in a problem-solving game where occasionally (and, for example, with luck) a satisfactory answer sometimes may be obtained without reference to all of the technological details. Consideration of the details, however, can only serve to improve the answer otherwise obtained. Accordingly, the goal in reservoir engineering is to optimize methods for generating wanted information so that the needs for the information are adequately met while the costs, labor and time spent are held at a minimum.

Here a general theory underlying the practice of reservoir engineering will be developed from physical science considerations alone. Involved are many familiar topics of Newtonian (continuum) mechanics, physical chemistry and implicitly geology. And, as will be evident, frequent appeal must be made to the results of laboratory and field experiments, before the theory can be applied in specific cases with any measure of completeness.

A subtle point to be noted in these connections is the duality in the practice of engineering analysis, where links must be sought continuously between the theoretical models of reality and the observational representations of the natural phenomena of interest. It is clear that experiments prompt the appearance of theoretical statements, and vice versa, in the ordinary evolution of scientific understanding. But a chain can be no stronger than its weakest link, and in this paper the point will be illustrated how the reservoir engineer often lacks enough empirical information to take full advantage of his skill in theoretical analysis. The difficulty being confronted here mirrors the scientist's inherent limitations and imperfections in developing a complete description of physical phenomena from theory (i.e. "first principles") alone.

With the motivation provided by the access to high speed computer and the remarkable progress in numerical methods for solving differential equations, it is now possible in rapidly expanding ways to examine in detail the consequences of highly involved theories of reservoir performance. But as new plateaus in the facility for analysis are reached, complicated processes of interest become easy to simulate. Accordingly, it then is all the more urgent now that pertinent models are chosen in the first place.

Obviously, it would be foolish to ridicule the mushrooming abilities of the theoretical analyst, but it is self-defeating not to

strengthen analysis first by supplying the missing input information that theory fails to provide. And so, in this paper, as new theories of reservoir performance are developed, and as old ones are restated, the crucial role played by laboratory experiment will be exposed. And the reader will be shown examples of where the theory is usable only if certain data are available as input information, and only if certain experiments are performed to serve as a check on the theoretical predictions.

From one point of view we can say that reservoir engineering is an art, and from another we can say it is a kind of a problem-solving game. Dealt with are the reservoir systems that are comprised of the reservoir proper together with the wells and their mechanical paraphernalia that serve to provide access needed for the fluids to be withdrawn or injected from surface to subsurface locations.

The reservoirs themselves can be any of those more-or-less bounded underground rock units that are sufficiently porous to be containers and conductors of fluids, and that are sufficiently large so that commercial uses can be envisioned and realized.

Reservoirs commonly are used as sources of fluids (for example, petroleum, fresh and saline waters, certain inorganic gases such as helium and carbon dioxide, etc.). They also are used as places for the storage or the disposal of fluids (as in the case of the underground storage of natural gas, or as in the case of the underground disposal

of industrial waste materials). Occasionally reservoirs are used as conduits for the transport of fluids (as illustrated by the practice of injecting water into aquifers at one place to enable production at another). And finally, we may mention the use of reservoirs as underground chemical reactors, which use has developed, among other things, as an outgrowth of in situ combustion (oil recovery) methods where the catalytic role played by the interstitial clays is of importance.

All the uses mentioned above can be realized as long as access to the porous formations is provided, for example, by one or more wells or systems of wells, and as long as there is a commercial justification for the use. Obviously there are many occurences of subsurface rock units in nature that potentially might be classified as reservoirs.

In the final analysis, the reservoir engineer is concerned mainly with forecasting and controlling reservoir behavior so that an optimum result is obtained, namely, so that an effective reservoir use is made that maximizes the realization of the aims and objectives while minimizing the attending costs and labor. And since reservoir uses in one way or another involve the transport of large quantities of fluids into and/or out of the porous rocks (usually through the well system), we find that the central topic to be understood and mastered by the reservoir engineer has to do with the description of transport phenomena in porous media systems.

This then is what is to be discussed here, namely, the fundamental principles of reservoir mechanics that describe the fluid flow feature

of many of the reservoir processes that are of practical interest. While fluid flow must be emphasized since all reservoir uses involve the movement of large quantities of fluids into and out of subsurface locations, subsidiary transport effects such as diffusion of mass and heat sometimes also have to be taken into account.

We have pointed out already that reservoirs are bounded regions of the crustal earth environment. The boundaries have various forms such as the cap (impervious) rock overlying anticlinal structures, or such as gouge-filled joints and fault planes, or such as the shale strata and laminae surrounding or streaking through otherwise porous rocks. A water-oil contact or a liquid-gas free surface also may be taken as a convenient boundary even when they are non-stationary, and of course many other types of structural and stratigraphic boundaries are recognized and may be described (e.g., the surface of a salt-plug intrution, unconformities, gradational contacts between clean and shaley sands, and so forth). The point is that without them the reservoir could not be a satisfactory container or conductor of fluids even though the other prerequisites of high porosity and permeability were met.

The business of the reservoir engineer then is to be skillful in treating the questions attending various commercial uses of the fluid-filled reservoirs that are (as it turns out) widely but unevenly scattered in the sedimentary strata and other rocks of the continental land areas and the continental shelves and slopes. To be skillful means that good results consistently are obtained, and therefore there is

always a strong incentive to replace uncertain "trail and error" method of analysis by "logical" methods that depend upon making systematic use of valid mathematical models of the reservoir processes of interest. In what follows, therefore we intend to outline how the required models conceptually can be constructed. The practicing reservoir engineer then will be left only with the requirement to develop the auxiliary but practical techniques where concepts are reduced to particular programs of computation.

GENERAL THEORY

We start with the general conservation theorem (cf. Truesdell and Toupin,[3] page 468) of the form:

$$\partial(\rho\gamma)/\partial t + \text{div}\ (\rho\gamma\underline{v}') = \sigma \qquad (1)$$

where $\rho=\rho(x_i,t)$ is the mass density of a material particle that varies in space and in time; $\gamma=\gamma(x_i,t)$ is the local value per unit mass of some intensive property of the material particle; $\underline{v}'=\underline{v}'(x_i,t)$ is a velocity vector chosen such that $\rho\gamma\underline{v}'$ represents the flux of the property, $\rho\gamma$; and σ is the associated source-sink function (if any) by which the local values of the property, $\rho\gamma$, change via internal mechanisms (e.g. chemical reactions, energy conversions, entropy production, etc.)

Specifically, the intensive property, γ, may be associated with a corresponding extensive property, G, by the volume integral definition:

$$G = \int \rho(x_i,t)\ \gamma(x_i,t)\ dx_i \qquad (2)$$

where G for example can represent such things as the total system mass, energy, entropy, etc., property to which the conservation theorem (1) implicitly refers and applies. For example, let G be the total mass of the k^{th}-component in the partitioned system space of a porous solid occupied by some multi-component (interstitial) fluid phase, then by (1) we have:

$$\partial\rho_k/\partial t + \text{div}\ (\rho_k \underline{\overset{\prime}{v}}_k) = \sigma_k \qquad (3)$$

where ρ_k refers to the local values of the density of the k^{th}-component, and where σ_k will take into account local changes in ρ_k due to chemical reactions and to phase changes (if any). Obviously, by summing the k-set of equations (3), we can recover the ordinary mass conservation theorem, or:

$$\partial\rho/\partial t + \text{div}\ \rho\underline{v} = 0 \qquad (4)$$

where $\underline{v}$ has the special meaning of the center of mass velocity of a material particle, that is, $\underline{v}$ is the mass average value of the local $\underline{\overset{\prime}{v}}_k$ values, or $\rho\underline{v} = \sum \rho_k \underline{\overset{\prime}{v}}_k$.

In describing dissipative transport phenomena, however, we need to use (1) additionally as an energy and entropy conservation theorem, and furthermore we need to introduce certain constitutive assumptions in order to arrive at determinate formulations of particular processes of interest. In connection with the latter we make particular use of the Onsager formalism (cf. for example, de Groot and Mazur,[4] also Luikov and Mikhailov,[5] also Fitts,[6] etc., etc.) which reflects the

expected linearity for low intensity transport phenomena between generalized fluxes, J_i, and generalized forces, X_j, of the form:

$$J_i = D_{ij}X_j \text{ with } D_{ij} = D_{ji} \tag{5}$$

where D_{ij} is a transport coefficient of tensorial rank equal either to the sum of the tensorial ranks of J_i and X_j (anisotropic cases), or to the difference of these ranks (isotropic cases). Note further that the summations called for by (5) must be in accord with Curie's Theorem as regards the equivalence of tensorial rank of all summed terms.

For our purposes in treating uncoupled processes, and keeping in mind relevant dimensional considerations, we give (5) the explicit form:

$$\varphi^{1/2}(\underline{v}' - \underline{v}) = -D\cdot(\text{grad } \varphi^{1/2}) \tag{6}$$

where φ represents the total local energy per unit mass of material particles; hence $\underline{\text{grad } \varphi}$ is proportional to the driving force giving rise to the transport process of interest. Obviously, we may set $\gamma=\varphi$ in equation (1), which when combined with (4) and (6) yields:

$$\rho[(\partial\varphi/\partial t) + \underline{v}\cdot(\text{grad } \varphi)] = \sigma + \text{div}[(\rho D/2)(\text{grad } \varphi)] \tag{7}$$

where σ now can be set equal to zero since we assume energy is neither being created nor destroyed (i.e., $\sum \varphi = \text{const.}$).

Furthermore, an auxiliary useful relationship, expressing the rate of entropy production per unit mass, $\dot{S}$, for uncoupled and coupled processes, respectively, is given by:

$$S\theta = -(D/4\varphi)(\text{grad } \varphi)^2(\cos \beta) = D_{ij}(X_i)(X_j) \qquad (8)$$

where β is the angle between the directions of the vectors J_i and X_i (as will be non-zero for anisotropic cases), and where θ is the local thermodynamic temperature.

Now, in the important case of "Le Chatelier" coupling, as is to be expected for the case of interpenetrating continuums (where each serves as the system space for separate but interacting transport processes), in addition to the total energy equation (7), we would also make use of the analogous sets of equations derived from (1) and (5) of the form:

$$\rho_k[(\partial\varphi_i/\partial t) + \underline{v}_k \cdot (\text{grad } \varphi_i)] =$$

$$\text{div } [(\rho_k/2)\ \{D_{ii}(\text{grad } \varphi_i) + D_{ij}(\varphi_i/\varphi_j)^{1/2}(\text{grad } \varphi_j)\}] \qquad (9)$$

where the D_{ij} are the coupling coefficients which are to be determined by suitable experimentation. Similarly, the D_{ii} diagonal coefficients are to obtained by special experiments with coupling avoided, and the D-coefficient of equation (7) is to be obtained by the experiment indicated upon taking note of the equality: $\sum\varphi_i = \varphi$. The auxiliary condition provided by (8) will be of use in these connections.

Furthermore, in applying the procedures outlined above to the consideration of transport phenomena in the fluid-filled interstitial paths of porous solids, an additional relationship would be required between the internally unobservable microscopic fluid particle velocity vector, $\underline{v}$, and the externally observed macroscopic (approach) velocity

vector, $\underline{q}$. Evidently (cf. Saffman[8]) the latter is given by:

$$\underline{q} = f \frac{\int \underline{v}\, dx_i}{\int dx_i} \tag{10}$$

where f is the fraction of the total volume of a macroscopic representative volume element occupied by fluid-filled pore space, and where further as a simplification it is implied that f(=porosity) is locally a time-independent constant.

Now, ordinarily it is assumed that Darcy's Law describes the flow of homogeneous fluids through inert porous media when the Renyolds Number is low. At least many experimental results have been cited in the literature (Muskat[7]) which can be taken as particular integral solutions of:

$$\underline{q} = -(k\rho/\eta)\ \text{grad}\ \varphi_f \tag{11}$$

where $\underline{q}$ is the approach velocity vector, φ_f is the force potential (the gradient of which involves the sum of the pressure and gravity forces per unit mass), k is the so-called coefficient of permeability, and ρ and η respectively are the fluid density and viscosity.

To make (11) determinate additional statements are needed to interrelate the various dependent variables. For simplicity we limit attention first to isothermal flow of fluids in isotropic and homogeneous media (therefore k is a simple scalar constant), where η is taken independent of pressure, and where density and pressure, p, ideally are interrelated by state equations such as:

$$\left.\begin{aligned} p/\rho &= \text{constant} \qquad \text{(Ideal gas law)} \\ (\partial\rho/\partial p)/\rho &= -\beta_F = \text{const.} \end{aligned}\right\} \tag{12}$$

Otherwise empirical correlations have to be established by special laboratory phase behavior studies.

Furthermore, in the case of gas flow we assume that the mean free path is small compared to the characteristic pore dimensions so that microscopically a zero velocity boundary condition can be assigned at the solid surfaces defining the pore walls. In any case we treat the solid matrix as rigid, and also as chemically inert with reference to the contained flowing fluid (e.g. electrokinetic effects are to be ignored).

Various workers [cf. especially Hubbert[8]] have taken note of the fact that (11) may be thought of as derived from the Navier-Stokes transport equations, where the interconnection simply involves accepting the three identities:

$$\int (\text{grad } \varphi)^{dx_i} = \text{constant}$$

$$\int \underline{v}(\text{grad } \underline{v})\ dx_i = 0$$

$$\int (\text{lap } \underline{v})\ dx_i = -(\underline{g}/k) \int dx_i \tag{13}$$

that are supposed to hold when attention is limited to steady flow (i.e. $\partial\underline{v}/\partial t = 0$).

To relate Darcy's Law (11) to the fundamental conservation postulates of Newtonian mechanics, of course would provide confidence that good results are to be expected. Indeed experiments (based on a dimensional analysis of the Navier-Stokes equations) lead to the conclusion that (11) fits observations for a somewhat broader range of cases than would be anticipated by the restrictions imposed above where (11) was linked to the steady-state form of the Navier-Stokes equations through the equalities of (13). Specifically, it has been claimed (Muskat[9]) that Darcy's Law can be applied to cases of unsteady flow of compressible fluids in elastic, inhomogeneous and/or anisotropic media, even when the pore space is filled with more than one immiscible fluid (i.e. the multiphase flow problem). Furthermore, it has been supposed that Darcy's Law also leads to good results when heat transfer and mass transfer (diffusion) superimpose on the flow phenomena. Accordingly, it is commonly concluded that (11) is an important limiting transport equation which is (sometimes, if not invariably) meaningful in the treatment of porous media hydrodynamics, as in relating the macroscopic fluxes to the driving forces. Combining (11) and (12) with a mass continuity statement derived from (4) and (10), that is, with:

$$f\,\partial\rho/\partial t + \mathrm{div}\,(\rho\underline{q}) = 0 \qquad (14)$$

then is assumed to give the wanted equation of motion in terms of a single dependent variable. A potential flow form often is thereby indicated (Muskat,[9] Polubarinova-Kochina,[10] etc.).

In the above paragraphs we have indicated the frequently cited basis for accepting Darcy's Law, (11), tacitly as the starting point in ensuing analyses of reservoir performance. Without fully examining the consequences, we have asserted that this procedure has been justified because of the alleged links between (11) and the underlying microscopic descriptions as derived from Newtonian (continuum) mechanics. It is clear however that in the final analysis, direct appeal must be made to experiment to be reassured that Darcy's Law leads to good results in particular cases. Furthermore, it is necessary to show the degree of consistancy between Darcy's Law (11), and the basic transport equations, (7) and (9).

Thus, we are now ready to consider from a new point of view an important application, namely the isothermal, single phase flow of a homogeneous fluid through locally homogeneous elements of porous solids that themselves can be regarded as rigid and chemically inert. For this case we retain the Darcian assumption that the driving force giving rise to the bulk flow can be expressed in terms of the gradient in the mechanical energy, φ_f, as defined by:

$$\varphi_f = \int \frac{dp}{\rho} + \underline{g} \int dz + \text{constant} \qquad (15)$$

where $\underline{g}$ is the acceleration due to gravity vector, and z is some relative elevation above an arbitrarily selected datum plane. This is because, in the case chosen, no other energy changes in time or space occur. It is thus clear that φ_f represents the mechanical

energy per unit mass associated with the coordinates x_i and t, made up of the sum of the pressure energy and the potential (gravitational) energy per unit mass. If explicit reference also were to be made to the kinetic energy (inertial force) part, then we might write an acceleration potential in the form:

$$\varphi'_f = \int \frac{dp}{\rho} + \underline{g} \int dz + (\underline{q}\cdot\underline{q})/2f + \text{constant} \qquad (16)$$

where by the reasoning of taking the averages of (13) we are justified in saying that the kinetic energy per unit mass is proportional to the square of the absolute value of the vector, $\underline{q}$, divided by the porosity.

In these connections, however, when we recall that we shall be dealing with the gradient of the potential as the driving force, we shall soon find a basis for showing that in many practical cases:

$$\text{grad } \varphi'_f \cong \text{grad } \varphi_f = (1/\rho)\text{grad } p + \underline{g} \qquad (17)$$

since by calculation we find that the acceleration force will assume values a thousand or more times smaller than the pressure and gravity forces.

Now, taking $\gamma=\rho\varphi$=the local value of the mechanical energy per unit pore volume of the element, dx_i, we may combine (7) and (10) to yield (for porosity constant):

$$f\rho(\partial\varphi_f/\partial t) + \rho\underline{q}\cdot(\text{grad } \varphi_f) = \sigma + \text{div}[(\rho fD/2)\ (\text{grad } \varphi_f)]. \qquad (18)$$

To make (18) determinate we must put the source function, σ, in explicit form, and this is done by making use of the idea that the

mechanical energy driving force acts only against fluid (viscous) friction in causing flow.

Specifically, we say that σ in this case is identically equal to zero. This follows from the observation that in our system it is only the mechanical energy as defined by (15) that is changing in time and in space during the flow transport process. All other components of the local total energy remain fixed and unchanging, and beyond the small amount of heat generated by the friction of the motion, there are no energy conversions from one form to another. And from (8), it is clear that the entropy production associated with the transport will be given by:

$$\dot{S}\theta = -(fD/4\varphi)(\text{grad } \varphi_f)^2. \tag{19}$$

In any case, with $\sigma=0$, (18) expands to:

$$\partial\varphi/\partial t + (\underline{g}/f)\cdot(\text{grad } \varphi_f) =$$
$$(D/2\rho)(\text{grad } \varphi_f)\cdot(\text{grad } \rho) + (D/2)(\text{lap } \varphi_f) + (1/2)(\text{grad } \varphi_f)\cdot(\text{grad } D). \tag{20}$$

Now (20) is a partial differential equation that involves three dependent variables of the x_i,t-coordinates, namely φ_f, ρ and $\underline{g}$. Taking porosity as a constant, we have from (14) the mass conservation statement interrelating density and the vector $\underline{g}$. We also have from the definition of (15) a relationship between φ_f, ρ and pressure, meaning that appeal still must be made to an equation of state, say an empirical one of the form of (12), so that ρ and p become interrelated.

That is, we reduce the implied degrees of freedom in order to arrive at a determinate transport equation by making use of the principle of mass and energy conservation, and of an equation of state. Additionally however, we must say something about the functional form of the transport coefficient, D.

Evidently the function $D=D(x_i,t....)$ can be put in explicit form only by the interpretation of results of a set of relevant experiments, or by making use of the postulate of a phenomenological model. To illustrate this idea we now considerably simplify the problem under consideration by limiting attention to the low intensity, isothermal and steady flow of an incompressible fluid in an isotropic porous medium that is rigid, inert and geometrically homogeneous. As already noted, for this special case there is ample experimental evidence to leave the fact unquestioned that Darcy's Law (11) holds. For this special case form (14) we would have:

$$\text{div } \underline{q} = 0 \quad \underline{\text{hence}} \quad \text{lap } \varphi_f = \text{lap } p = 0 \tag{21}$$

Accordingly, we can take advantage of the fact that both $\underline{q}$ and grad φ_f are constants having the same vector direction in the isotropic case, hence it is a simple matter to find the integrals of (11) and (21) so that the permeability coefficient, k, can be directly evaluated by observing the components of $\underline{q}$ and the associated components of grad p [that is, we can do this as long as the fluid properties, η and ρ, are independently known].

Defining a Renyolds Number arbitrarily as $(k^{1/2}\rho)/\eta$, many observations have been reported to show that there is little to question about the applicability of (11) for the special case under discussion when this Renyolds Number is sufficiently low (say less than 10). Furthermore, we can gain further confidence in Darcy's Law, upon taking note of Hubbert's derivation[8] of (11) from the Navier-Stokes equation for the steady-state case where ρ is taken as a constant. Lastly, we may note that (11) has the linear form analogous to other transport equations of Ohm, Fick, and Fourier, as might have been expected on intuitive grounds alone.

Accepting, then, (11) as valid for the special limiting case under discussion, we now reduce the general flow equation (20) to apply to the same special case. That is: (a) we drop the time-dependent term; (b) take density as constant; (c) recall from (21) that lap φ_f = zero; and (d) observe that the scalar product of two vectors having the same orientation is equal to the produce of the absolute magnitudes of these vectors. This gives finally:

$$\underline{q} = (f/2)(\text{grad } D) \tag{22}$$

Combining (22) with Darcy's Law (11) then yields:

$$D = -(2k\rho\varphi_f/\eta f) \tag{23}$$

Equation (23) only expresses the result of a particular set of experiments, and indeed we have already noted the necessity of always making an appeal to observational information in order to

finally render the generalized transport equations determinate for each special case. What this means is that if subsequently we want to describe a more general class of flow processes, for example, where unsteady-states of compressible fluid flow are considered, we cannot presume that D as given by (23) constitutes a proper universal functional relationship for the more general flow cases. A proof of this idea will be given shortly, at least by the way of citing some examples, but first we examine an important implication of (23) as this relates to the case of steady flow of an incompressible fluid.

Combining (22) and (23) we see immediately that for the special case under discussion, Darcy's Law may be rewritten in the form of a velocity potential, or:

$$\underline{q} = -\text{grad}\,[(k\rho/\eta)(\varphi_f)] = \text{grad}\,[(f/2)(D)] \qquad (24)$$

Now it is well known that the existence of a velocity potential connotes the idea of a reversible transport process occurring in a conservative system. This follows from the vector identity which states that the curl of a scalar gradient is zero, hence the macroscopic equation (24) appears to describe an irrotational motion even though we realize that microscopically a finite vorticity exists (i.e. curl $\underline{v} \neq 0$). In interpretation of the implications of this observation, we note by combining (19) and (23) that the rate of energy dissipation per unit volume is given by $\rho\underline{q}\cdot\text{grad}\ \varphi_f = 1/2(k\rho^2/\eta)(\text{grad}\ \varphi_f)^2$. Given the case of where grad φ_f does not exceed one atmosphere per centimeter, and where k

does not exceed 10^{-7} cms^2 ($\cong$10 Darcy units), then for the case of flow of water (ρ=1, η=10^{-2}), the energy dissipation is measured by the exceedingly small quantity of 0.5 Joules per second per cubic centimeter ($\approx$0.5 watts of power). In other words, in close approximation we may say that flow transport from the macroscopic point of view occurs as an isothermal process in the absence of any externally superimposed temperature gradients. (Note the specific heat of water is about 85 Joules per gram at 20°C. Furthermore, in the above case, g=10 cm/sec).

With the above remarks now made, we are ready to examine the doubtful and so-far unverified postulate that Darcy's Law also describes the more general regimes of porous medium flow. Three limiting cases will be discussed first, namely: (a) the steady flow of a slightly compressible liquid where the density-pressure variation is that given by (12); (b) the steady flow of an ideal gas in isothermal expansion, where the density is taken as linearly proportional to pressure; and (c) the unsteady flow of an incompressible fluid. In all of these cases we choose for simplicity to ignore the effect of gravity forces; hence we are permitted to take the local pressure as a measure of the local value of the potential function. Thus, by (11) and (14) for these three cases we would have: (a) lap ρ=0; (b) lap ρ^2=0; and (c) lap φ=0, respectively.

By simple algebra then, we may obtain from (20) with the aid of the other relations already prescribed, the following compatibility condition:

$$\Delta + \underline{q} + (Df\lambda/2)(\text{grad } \omega) - (f/2)(\text{grad } D) = 0 \qquad (25)$$

where for the three cases under discussion, the parameters, Δ and λ have the following values:

	Δ	λ
case (a)	0	$\beta_F \rho$
case (b)	0	ρ_o/p_o
case (c)	$f(\partial p/\partial t)/(\text{grad } p)$	0

In any case we see that (25) reduces to (22) only whenever both Δ and λ are zero; hence we would conclude that Darcy's Law is not precisely compatible with the general theory embodied in (20) for the three cases under discussion.

On the other hand, a numerical check will show that the <u>degree</u> of incompatibility is not necessarily large, for example, if the mean pressure is not high. Thus, for the steady flow cases, when Darcy's Law is substituted back into (25), we find that the closeness of the term, $(1-\varphi\lambda)$, to unity measures the degree of incompatibility. And for water at ten atmospheres, $\varphi\lambda$ is of the order of 5×10^{-4}, while for air at ten atmospheres, $\varphi\lambda$ is of the order of 1.3×10^{-2}. On the other hand, for the unsteady flow case (c), it is easy to demonstrate that a rather violent change in pressure with time is required before the ratio of Δ to $|\underline{q}|$ is large enough to indicate an observable discrepancy between the presumption of the validity of Darcy's Law and the acceptance of the general theory outlined above.

In these connections, however, it will be realized that we have only attempted to demonstrate the degree of compatibility; hence the point may be made that any compatibility condition, while necessary, is not sufficient to preclude the possibility that experiment will show significant departures from Darcy's Law for the general flow situations. That is, we acknowledge that by experiment we may find that the transport coefficient, D, as reflecting the material properties may have a form in the more general cases quite different from that given by (23).

Furthermore, in practical cases the relationships between density and pressure for various gases and liquids may depart significantly from the ideal relationships mentioned above, in which case the compatibility relationship (25) itself no longer applies.

Additionally, we are prompted to consider the possibility that the solid matrix itself is deformable as reflecting a balance between the internal pore fluid pressure and the externally imposed mechanical stressing of the solid matrix. For example, β_S, the compressibility of, the solid rock elements, may be finite, and additionally we may imagine that the bulk volume of the solid matrix changes (via subsidence) with the internal pore pressure as measured by the compaction factor: $\beta_C = + (1/V_b)(\partial V_b/\partial p)$, where V_b is the bulk volume. Accordingly, (14) would take on the more general form:

$$[\{(\beta_S+\beta_C)(1-f)/\beta_F\} + f]\ (\partial\rho/\partial t) + \text{div}\ \rho\underline{q} = 0 \qquad (26)$$

Furthermore, with porosity now changing with time and position, equations (21) and (10) yield in addition to the terms appearing in (20) the following: $\rho\varphi(\partial f/\partial t) + [(D\rho/2)(\text{grad } \varphi)(\text{grad } f)]$. Since the derivative of porosity ($\partial f/\partial t$, grad f) appearing in these terms are all each proportional to the "compressibility" coefficient of (26), namely: $(\beta_S+\beta_C)(1-f)/\beta_F$, the compatibility of Darcy's Law with the general theory becomes accordingly progressively weakened.

With the question raised above in simple cases, an even greater uncertainty remains about the meaningfulness of employing Darcy's Law for the even more general cases of common interest, (say) such as refer to the unsteady flow of compressible fluids in anisotropic media, or to unsaturated flow of heterogeneous fluids, with gravity forces taken into account, etc.

Indeed, the last remark brings us to the main point of this paper, namely, the proposition that (20) constitutes the only logical description of flow of homogeneous fluids for the general cases, while Darcy's Law (11) constitutes a particular solution of (20) for a very special limiting case of steady flow of incompressible fluids. Furthermore (20) can not be reduced to determinate form until the functional form of $D=D(x_i,t,\ldots)$ has been established by relevant experiments.

If a rough but instructive analogy will be permitted, we may say that (20) bears the same parent relationship to (11) as the Navier-Stokes equations do to Poiseuille's Law. For example, Darcy's Law and

Poiseuille's Law are both only verified experimentally for the very special case of steady flow of an incompressible fluid; hence substituting (11) back into (20) lacks the same logic and involves the same hazards as supposing that the unsteady flow of a compressible fluid in a tube can be expressed properly by making use of the Poiseuille hypothesis of linearity between a certain flux and driving force.

The fact is clear and herewith brought into focus, that no real progress can be made in understanding flow transport in porous solids until the transport coefficient, D, appearing in (20) has been ascertained experimentally under carefully controlled experimental conditions.

DISCUSSION

In some valid respects the porous medium system space can be thought of as a "black box." We note that the system space serves as the environment in which transport occurs, and has the physical boundaries that either isolate the system space from the surroundings, or provide the surfaces across which mass and energy exchanges with the surroundings occur (if any). If the initial state of the system is an equilibrium one, then at least we can say that all forms of energy are evenly and uniformly distributed within the confines of that black box, and that no fluxes of mass or energy are occurring across the system boundaries. Otherwise, we can say little without further consideration.

Suppose now the system is disturbed in some prescribed way, as by introducing mass and/or energy across some portion of the system boundary. An input function will describe this disturbance, and the possibility always exists to observe an output response as the system accommodates itself to the constraints imposed by the input function. And whenever the input disturbance is finally removed, thereafter the system response is one of spontaneous (if gradual) approach to a future equilibrium state.

Now here we have been treating transport processes deterministically rather than stochasitically. That is, we presume a given input function will always produce the same certain output function, rather than just the probability of an outcome as given in the form of a distribution function. Hence, it has been our aim to develop a general theory where, upon the experimental verification of the associated constitutive assumptions, the black box becomes adequately if not fully characterized. Then, given the input function, we can predict the output function through the thereby attained knowledge of the system response.

To schematize things further, we know that mass and energy are conserved in the transport processes of interest. Also we know that for low intensity transport processes, a linearity between fluxes and forces of the Onsager form can be presumed. This latter is the generalized constitutive assumption, which states further that the

force has the form of an energy gradient function. We next take note of the fact that several dependent variables may enter into the specification of a particular problem, hence we must ascertain their interrelationships from other auxiliary conditions (e.g. from appropriate equations of state, etc.). Finally we are satisfied when we have as many conditions prescribed as there are dependent variables, for then we are in a position (at least implicitly) simultaneously to solve the interlocked equations in order to produce a single equation in terms of one dependent variable. In this equation, however, the transport coefficients, D also will appear always.

Let us suppose we have chosen (arbitrarily it must be noted) to have the resultant transport coefficient expressed in terms of E, the total energy per unit mass associated with the local fluid particles in motion, where:

$$E = e_1 + e_2 + \ldots\ldots e_j + \ldots e_N \,. \tag{27}$$

That is, the e_j are the local values of the various energy forms (e.g. mechanical, thermal, chemical, etc.). As a simplification which loses no generality, we limit attention only to those e_j where $(\partial e_j/\partial t)_{x_i}$ and $(\partial e_j/\partial x_i)_t$ are non-zero. Furthermore, for any particular system space we choose the e_j so that they are all independent of each other, in the sense assuring that we avoid the need to consider the reversible changes from one energy form to another. For example, instead of talking about kinetic, pressure and gravity energy separately, we

lump these forms together and talk only about the total mechanical energy. Thereby the source function, σ, usually can be taken as equal to zero.

Accordingly, we are permitted to suggest that each (grad e_j) serves as the driving force for a particular type of dissipative transport process.[+] Coupling then occurs between these processes (or at least the possibility of this must be allowed until independently proven false) whenever N in (27) is two or larger. And the total entropy production associated with the transport will be proportional to the associated force-flux summed products.

For simplicity, let us consider two coupled processes (N=2), that is situations where we have superimposed transport arising due to the driving force, grad e_1, with transport of a different sort arising due to some other driving force, grad e_2. If porosity is constant, and if the pore space is occupied by a single fluid phase, we may write immediately:

$$f\rho(\partial E/\partial t) + \rho \underline{q}\cdot(\text{grad } E) = \text{div } [(\rho f D/2)(\text{grad } E)] \qquad (28)$$

Now, since density will be given by an equation of state of the form: $\rho=\rho(E)$, and since $\underline{q}$ and ρ are interrelated by the mass conservation statement, it is clear that the form of the transport coefficient, $D=D(x_i,t)$, in (28) can be obtained by suitable experimental work.

[+] In the case of interpenetrating continua, we may wish to consider the same e_j types in the adjacent spaces separated by a phase interface [cf. eq. (35)].

Furthermore, we also have the relationships:

$$f\rho(\partial e_1/\partial t) + \rho\underline{g}\cdot(\text{grad } e_1) = \text{div}\,[(\rho f/2)\{D_{11}(\text{grad } e_1)+D_{12}(e_1/e_2)^{1/2}(\text{grad } e_2)\}]$$

and

$$f\rho(\partial e_2/\partial t) + \rho\underline{g}\cdot(\text{grad } e_2) = \text{div}\,[(\rho f/2)\{D_{12}(e_2/e_1)^{1/2}(\text{grad } e_1) + D_{22}(\text{grad } e_2)\}] \qquad (29)$$

where the D_{11} and D_{22} transport coefficients characterize the nature of the two transport processes, respectively, as they would occur each in the absence of the other; and where the D_{12} are the coupling coefficients. In any case, by making use of (27), the two equations (29) may be added and then combined with (28) to yield:

$$\text{div}\,[\rho\{D(\text{grad } E) - (D_{11}+D_{12}[\frac{e_1}{e_2}]^{1/2})(\text{grad } e_1)-(D_{22}+D_{12}[\frac{e_1}{e_2}]^{1/2})(\text{grad } e_2)\}]=0 \qquad (30)$$

Also, by making use of the entropy production theorem, and the energy flux equation, the D, D_{11}, D_{12} and D_{22} transport coefficients further are interrelated by the auxiliary relationships:

$$(D_{11}/e_1)(\text{grad } e_1)^2+2D_{12}(\text{grad } e_1)(\text{grad } e_2)/(e_1e_2)^{1/2}+(D_{22}/e_2)(\text{grad } e_2)^2=$$

$$D(\text{grad } E)^2/E = (D/E)(\text{grad } e_1)^2+(\text{grad } e_2)^2+2(\text{grad } e_1)(\text{grad } e_2) =$$

$$(D_{11}+D_{12})(\text{grad } e_1)(\text{grad } E)/(Ee_1)^{1/2}+(D_{22}+D_{12})(\text{grad } e_2)(\text{grad } E)/Ee_2)^{1/2}. \qquad (31)$$

We have already shown in connection with (28), however, that D can be evaluated experimentally; hence we see quickly from (29) with

(30) or (31) that we have the determinate set of implicit parametric equations:

$$F_1(D_{11}, D_{12}) = 0$$
$$F_2(D_{22}, D_{12}) = 0$$
$$F_3(D_{11}, D_{22}, D_{12}) = 0 \qquad (32)$$

which is to say that the other transport coefficients D_{11}, D_{12} and D_{22}, also can be evaluated experimentally. Thus, with all of the transport coefficients thereby determined, equations (29) then can be used with confidence to predict future events in particular transport systems for a variety of other cases that may have not been studied systematically in the laboratory.

In these connections we must remark that, in general, the transport coefficients obtained by one set of experiments cannot be used necessarily when fed back into the transport equations to predict events, except in certain particular cases. Thus we may imagine a hierarchy of transport situations extending as a spectrum from the most general cases to the most simple ones. For example, the unsteady flow of a compressible fluid refers to a considerably more general case than does the steady flow of an incompressible fluid. We simply say that the experiment whereby D is evaluated must be performed under somewhat more general conditions than those that apply when the predetermined D-function is subsequently used in arriving at calculated predictions.[+]

[+] Here we should cite Truesdell's opinion[3] that viscosity as evaluated by a Poiseuille experiment really gives no information about the nature of the transport coefficient as needed at the Navier-Stokes level of reference.

Before discussing some examples of coupled processes, we can further point out that the evaluation of the set (32) can be further simplified by undertaking subsidery experiments where, successively, (grad e_1) and (grad e_2) are set equal to zero. Thereby, the coefficients, D_{11} and D_{22}, respectively are given since the coupling between process artificially but effectively has been avoided.

Additionally, we have a basis for knowing a priori something about the coupling coefficient, D_{12}. In the limiting case, of course, D_{12} will be zero, which would reflect the situation that the concurrent processes for some reason have no influence one upon the other. As an example, solid state diffusion in the matrix of a porous solid generally would in no way modify fluid flow through the pore space.

On the other hand, we recognize that the entropy production for dissipative processes must be positive definite, and this by itself puts an identifiable constraint on the magnitude of the transport coefficients. Thus we would say that the left-hand side of (31) is a positive number, or:

$$D_{11}\lambda^2 + 2D_{12}\lambda + D_{22} > 0 \qquad (33)$$

where $\lambda = (e_2/e_1)^{1/2}(\text{grad } e_1)/(\text{grad } e_2)$.

It immediately follows, therefore, that:

$$(D_{12})^2 > (D_{11})(D_{22}) \qquad (34)$$

in order to insure real roots for the quadratic (33). Thus we see that the coupling coefficients, D_{ij}, will be of the same order of the

diagonal coefficients, D_{ii}, in the event that the D_{ii} themselves are of the same order -- otherwise D_{ij} will be zero (implying no coupling). On the other hand, if the D_{ii} differ from each other (by whatever amount the D_{ij} (if not zero) will display intermediate values which will be closer to the smaller rather than the larger of the D_{ii} values. Furthermore, given the constraint of Curie's Theorem, the inequality (34) provides no information whenever the various $(J_i \cdot X_i)$ terms have differing tensorial rank.

We are now ready to make a detailed analysis of some important coupled processes. We choose first to examine the rather simple case of steady two-phase flow (W=wetting fluid, N=nonwetting fluid), where the two fluids are both incompressible and have the same density, ρ, and viscosity, η. As a further simplicity, we say (grad ϕ_W) = (grad ϕ_N) = (grad ϕ), implying for example that we limit attention to situations where the saturation and the capillary pressure gradients are zero.

From one point of view we imagine we are dealing with a uniformly partitioned pore space, that is with two locally homogeneous and interpenetrating continua each filled with its own immiscible fluid; still there will be a fluid-fluid interface of contact which amounts to a distinctly different sort of boundary conditions as that provided by the various fluid-solid surfaces.

Accordingly, from (29) we have:

$$2q_W/f = (\text{grad } D_{11})(s_W) + \alpha(\text{grad } D_{12}) + D_{12}(\text{grad } \alpha)$$

and $2\underline{q}_N/f = \beta(\text{grad } D_{12}) + D_{12}(\text{grad } \beta) + (\text{grad } D_{22})(1-s_W)$ (35)

where $\alpha=(s_W s_N \varphi_W/\varphi_N)^{1/2}$ and where $\beta=(s_W s_N \varphi_N/\varphi_W)^{1/2}$. Note, in (35) we may substitute:

$$(\text{grad } \alpha) = -(\varphi_W/\varphi_N)(\text{grad } \beta) = (s_W s_N/\varphi_W\varphi_N)^{1/2}(p_c/2\rho\varphi_N)(\text{grad } \varphi) \quad (36)$$

where p_c is the capillary pressure defined by the local pressure difference between nonwetting and wetting fluids at their interfacial contacts, or: $p_c = \rho(\varphi_N-\varphi_W)$ for systems where gravity forces can be ignored. In any case, published experimental data verify that coupling does occur for the multiphase flow process under discussion, since it is observed that the sum, $\underline{q}_W+\underline{q}_N$, invariably is less than the Darcian flow, $\underline{q}$, as would be calculated by (11) in the event that the saturation of either of the immiscible pore saturants was increased to 100-percent.

Indeed, on the presumption that the coupling coefficient, D_{12}, is a negative function, we see from (35) that the consequence of this coupling is that the nonwetting fluid and the wetting fluid alike seem to have a reduced conductivity, than would be the case in the absence of coupling.

Specifically, in (35) we are tempted to use the definitions:

$$(\text{grad } D_{11}) = (2\, k'_w\rho/f\, s_w\eta)(\text{grad } \varphi_W)$$

and $$(\text{grad } D_{22}) = (2\, k'_N\rho/f\, s_N\eta)(\text{grad } \varphi_N) \quad (37)$$

where the analogy with the empirically established form of (23) will be evident. This is to say that in the absence of coupling we would

expect the Darcian permeability, k, to be equal to the sum of the effective permeabilities to the wetting and nonwetting fluids, namely: $k=k_W'+k_N'$ in such a case. This idea is consistent with the model of electrical resistors in parallel where the total conductance is given by the sum of the conductances of the separate elements. But evidently in two-phase flow in porous solids, the proper and more realistic model is one of a complicated network form of branched resistors in both series and parallel array, from which we derive the expectation that the presence of elements of one of the immiscible fluids blocks and provides impedence to the transport of the other. The resultant effect, then, is to be measured by the coupling coefficient, D_{12}.

The evaluation of this coupling coefficient empirically is a straight-forward process, however. Combining (35) and (37) with Darcy's Law (11), for example, yields:

$$s_W(\text{grad } D_{11}) + s_N(\text{grad } D_{22}) = (2\, k\rho/f\eta)(\text{grad } \varphi)$$

and

$$-(2/f)(k_W+k_N-k)(\rho/\eta)(\text{grad } \varphi) = (\alpha+\beta)(\text{grad } D_{12})+D_{12}(\text{grad } \alpha)(\varphi_W+\varphi_N)/\varphi_W \qquad (38)$$

where k is the specific permeability. In the second of (38) we have an ordinary linear differential equation in D_{12} that can be solved easily in terms of the saturation parameter. Indeed, as a close approximation valid for the high permeability cases where we may take $\varphi_W \tilde{=} \varphi_N$ (i.e. $p_c \tilde{=} 0$, hence $\alpha \tilde{=} \beta$ and grad α=grad β=0), the right-hand

member of the second of equations (38) reduces to a particularly simple form. On the other hand, if we relax the constraint imposed above where we set $\eta_W=\eta_N=$ constant and $\rho_W=\rho_N=$ constant, then the first of equations (38) takes on the more complicated form of involving (grad D_{11}) and (grad D_{22}) terms explicitly, in which case special experiments are required to observe $\underline{q_W}$ with (grad φ_N)=0, and $\underline{q_N}$ with (grad φ_W)=0, respectively.

Many other cases of coupled processes could be discussed such as those involving superimposed thermal gradients perturbing fields of bulk fluid flow, and such as those that give rise to the well-known electrokinetic effects. Such processes rigorously are to be treated by the methods outlined here, but for our final illustrations of the principles involved we consider the coupling aspect involved both in the case of the miscible and immiscible displacement processes.

Thus according to the theory of coupled process now under discussion, we would be inclined to describe miscible displacement by the set of equations:

$$\rho f(\partial\mu/\partial t)+\rho\underline{q}\cdot(\text{grad }\mu) = (f/2)\,\text{div}\{[D_{11}(\text{grad }\mu)+D_{12}(\mu/\varphi)^{1/2}(\text{grad }\varphi)]\rho\}$$
$$\rho f(\partial\varphi/\partial t)+\rho\underline{q}\cdot(\text{grad }\varphi) = (f/2)\,\text{div}\{[D_{12}(\varphi/\mu)^{1/2}(\text{grad }\mu)+D_{22}(\text{grad }\varphi)]\rho\} \qquad (39)$$

where μ is the chemical potential, φ is the mechanical energy potential, D_{11} is the molecular diffusity, D_{22} is the Darcian flow conductivity coefficient, and D_{12} again represents the coupling coefficient. In

these connections, of course, the special equation of state must be employed in evaluating the mechanical energy function, φ (cf. Guggenheim, page 406).

As for the treatment of the transients of two-phase immiscible displacement processes, we adopt first the idea that the total energy balance statement is given in the form of equation (28). Furthermore, for (29) expressing mechanical energy conservation in each of the incompressible fluid phases (filling the two halves of the partitioned pore space) we write:

$$fs_W(\partial\varphi_W/\partial t)+\underline{q}_W\cdot(\text{grad }\varphi_W)=(f/2)\,\text{div}[D_{11}(\text{grad }\varphi_W s_W)+\alpha D_{12}(\text{grad }\varphi_N s_N)]$$
$$fs_N(\partial\varphi_N/\partial t)+\underline{q}_N\cdot(\text{grad }\varphi_N)=(f/2)\,\text{div}[(D_{12}/\alpha)(\text{grad }\varphi_W s_W)+D_{22}(\text{grad }\varphi_N s_N)] \qquad (40)$$

where it will be immediately seen that (35) represents the steady flow special case consequence of (40). Here $\alpha=[(s_W\varphi_W)/(s_N\varphi_N)]^{1/2}$.

Accordingly, we conclude that (40) is needed along with the total energy equation in order to have the coupling aspect of the immiscible displacement process taken explicitly into account. Again, however, the analysis as here given is sterile and impotent unless and until the transport coefficients have been evaluated by experimental methods.

Above we have set out to formulate the general description of low intensity transport processes as observed in the interstices or porous solids, in a way that introduces a minimum of constitutive assumptions, and in a way that reveals just what experiments must be

undertaken so that these constitutive assumptions may be verified for particular cases. We find that even for the case of uncoupled processes the general theory suggests that the ordinary (classical) methods of treating the attending transport problems in some cases have been over-simplified. The extent of the discrepancies, if any, between the nature of these transport processes as usually described versus as their nature actually is, cannot be quantitatively forecast at this stage. This is because much experimental work remains to be undertaken before answers even to the simple questions can be given with assurance. The most we can say now is that the anticipated discrepanices between methods of analysis as outlined here, versus as ordinarily practiced, should prove especially significant in the important case of coupled transport processes.

CONCLUSIONS

In the previous sections we have derived in implicit (and sometimes explicit) form the transport equations governing certain limiting cases of oil recovery processes. For example, we could have had in mind oil recovery by volumetric expansion, by miscible displacement processes, by depletion drive, by replacing the produced fluid with another immiscible one, by gravity drainage, or by gas cycling to entrain the vapor of a residual liquid fraction.

The transport equations all were derived from the conservation (of mass, energy, momentum, etc.) concepts that are in fact consistant

with statistical mechanics interpretations, and that also form the fundamental theorems of Newtonian (continuum) mechanics as well. In presenting them, however, only a few limiting cases were treated, and two reasons may be mentioned to explain why no effort was made to be systematic in treating all possible cases in detail. First, generalizing a set of equations to cover the more complicated cases usually will be no more difficult than deriving them in the first place as applying to the simplified special cases. For example, treating a recovery process involving three phase rather than two phase flow does not increase the conceptual difficulty of stating the problem, although in most instances it will greatly increase analysis difficulties.

Indeed here we have made no reference at all to how the transport equations are to be solved in practice. This is because such an exercise in applied mathematics would have taken us well beyond the intendedscope of this paper. And so this than becomes the second reason why illustrative cases have been cited at random rather than systematically, for we have taken the position that it is premature to present a "cook book of recipes" as a guide to the practicing reservoir engineer. While it represents a somewhat exaggerated claim even yet, still for the sake of argument one can take the position that as access to high speed computers increases, and as skill in achieving stability and convergence in numerical methods of solving differential equations becomes commonplace, the mathematical part of the reservoir engineer's work can be left to the technicians and the program writers.

In a nutshell, it becomes the true responsibility of the reservoir engineer to be sure that the mathematical models that are postulated and that are to be adopted, are physically meaningful. In effect the reservoir engineer's role is to state the problem to be solved in a germane way, and then to tell the technician where he can obtain the required input information appertaining to initial and boundary condition, and appertaining to the empirical data corrleations that render the theoretical statement complete. In this frame of reference, the reservoir engineer is then left free to sit back (or to work on other problems), until the mathematical solution of the problem has been obtained by the technician, at which time the reservoir engineer can then become involved in the interpretation of the results so obtained.

Perhaps it can be fairly said that the foregoing Utopian life is not one which many reservoir engineers are free to enjoy today. For one thing, a progress is implied above, which admittedly has not yet been broadly achieved. Still this paper has been written in anticipation of what the general possibilities will be in the foreseeable (if not the immediate) future. And most will agree that progress and the possibility of progress are emerging at such an accelerating pace that a visionary approach to these questions is abundantly justified.

In conclusion, it has been shown that stating the governing transport equations that describe oil recovery processes can be done

without great difficulty. The same then must also be true with concocting valid descriptions of the reservoir behavior aspects of all questions related to the various reservoir uses, including uses of reservoirs for storage, disposal, and transport of fluids, and uses of reservoirs as natural (catalytic) environments for chemical reactions.

The more difficult part of reservoir engineering is supplying the input information needed to complement the theoretical concepts, so that finally a determinate problem is formulated. Admittedly there still remains the need to know how to generate solutions without undue labor, cost or involvement of the engineer's time. Having made the point, however, this latter aspect need not be discussed here further. Also beyond the scope of this paper is any treatment of the interpretation problems, and of the checks for reliability that must follow and complete any reservoir engineering analysis.

Perhaps the most interesting conclusion to be drawn from this paper is in the way close analogies can be drawn between the form of the analytical description of the different transport processes.

Indeed these analogies extend beyond the similarities in form of the governing transport equations. Thus, it has been shown, for example, that precisely the same types of experiments and measurement problems must be undertaken and faced before the required empirical data are obtained as needed to complete and make determinate the various cited applications of the basic theoretical statements.

Furthermore, it appears in general that the major impediment to progress now has to do with how development of experimental techniques has not always kept pace with developments in theory and analysis.

NOTATION

curl	the curl (vorticity) operator
D_{ij}	a transport coefficient
div	the divergence operator
e,E	local energy of fluid particles (per unit mass)
f	fractional porosity of medium
F	designation of a functional relationship
$\underline{g}$	acceleration due to gravity vector
grad	gradient operator
G	some extensive property corresponding to ν
J_i	some generalized flux
k	permeability coefficient
lap	Laplacian operator
p, p_c	fluid pressure, capillary pressure
$\underline{q}$	Darcian flow velocity vector
$\hat{S}$	entropy production rate (per unit mass)
S_w, S_N	fluid saturation parameters (fractional)
t	time
$\underline{v}$, $\underline{\hat{v}}$	microscopic fluid particle velocity vectors
V_b	bulk volume of a reference porous medium ($= \int dx_i$)
x_i	Cartesian space coordinate
X_i	generalized force
α, β	parameters, see eq. (35)

$\beta_F, \beta_S, \beta_C$	compressibility facotrs
γ	intensive property corresponding to G
Δ, λ	parameters, see eq. (25)
η, μ, ρ	fluid viscosity, chemical potential, density
θ	temperature
σ	source function
φ	energy functions

REFERENCES

1. J. Bear and Y. Bachmat (July 1965), "A unified approach to transport phenomena in porous media," Technion Research and Development Foundation Research Project CV-54, Progress Report 3. (Haifa, Israel).

2. W. Rose, "Transport through Interstitial Paths," Chapter 5 in Flow through Porous Media, R. J. De Wiest, Editor, Academic Press Inc. (In press, 1967).

3. C. Truesdell and R. A. Toupin (1960), "The classical field theories Handbuch der Physik, v. III/1, p. 226.

4. S. R. De Groot and P. Mazur (1962), Nonequilibrium Thermodynamics, North-Holland Publishing Co.

5. A. V. Luikov and Yu. A. Mikhailov (1965), Theory of Energy and Mass Transfer, Pergamon Press.

6. D. D. Fitts (1962), Nonequilibrium Thermodynamics, McGraw Hill.

7. M. Muskat (1937), The Flow of Homogeneous Fluids through Porous Media, McGraw Hill.

8. M. King Hubbert (1956), "Darcy's law and the field equations of the flow of underground fluids," Trans A.I.M.E., v. 207, p. 222.

9. M. Muskat (1949), Physical Principles of Oil Production, McGraw Hill.

10. P. Ja. Polubarinova-Kochina (1952), Theory of Ground Water Movement Moscow. (Translated 1963 Princeton University Press.

11. E. A. Guggenheim (1959), Thermodynamics, North-Holland Publishing Company.

ACKNOWLEDGEMENT

This paper, presented at the 25th Anniversary Penn State Conference on Petroleum Production, collects ideas first developed by the author in lectures to engineers of Petroleos Mexicanos (in 1964 in Mexico City, Coatzacoalces, Pozo Rica and Tampico), and before the Hydrology Institute at Princeton (in 1965, sponsored by the National Science Foundation).

Recalling the remarkable inquisitiveness of the early Penn State workers, I have done my best here to reflect the adventureous mood of yesteryear before so many workers became computerized and programmed to conform to the stereotyped viewpoints common today.

A rebirth (if not my reformulation) of reservoir engineering is surely needed. But where will the seeds of new ideas be found, and who will know how -- and be free, and be disposed -- to fertilize them, and when again will the universities and the industrial laboratories serve as hotbeds for the growth? And how can the unconvinced Director of Research be answered, who (for example, upon seeing the material discussed herein) commented as follows:

> ".....I believe that you are flogging a dead horse; certainly you seem to have ignored much relevant work while including much I thought was decently buried ....Quot homines, et cetera....."

My response: Judgments will yield lots learned if examined, such as insight disclosing thoughts held in secret!

One seldom hears of engineers
Suspecting flaws in Darcian laws,
Or sees absurd to have it heard
That Newton knew what fluids do
When sheared and stressed and decompressed,
And caused to flow however slow.

How sweet a hoax! How nice for Stokes
Who, grabbing claim to Navier's fame,
Saw scattered dots in data plots,
Thus was deceived in what he believed,
And missed the law that Poiseuille saw.

Forgetting what we see is not,
We think it wise to improvise,
And good to quote what great men wrote,
Glad (with them dead) Truth stays unsaid.

...attributed to S. T. Yuster...

COUPLING PHENOMENON DURING MISCIBLE DISPLACEMENT

Hans-Olaf Pfannkuch

Introduction

The physical phenomenon of hydrodynamic dispersion is defined as the process of mixing that occurs when heterogeneous but fully miscible fluid particles move through a defined interstitial pore space in single phase hydrodynamic flow.

In technical systems these conditions are found in miscible displacement processes, as secondary recovery methods or in the intrusion of sea water into coastal aquifers. The following discussion will limit itself to ideal conditions. That is, the porous matrix will be considered rigid and chemically inert. It is assumed to be locally isotropic and homogeneous. The fluids have the same physical properties, especially identical viscosity and density. The different species of fluid particles may have different chemical potentials or they may be only marked differently as radioactive tracer elements, say. The microscopic flow laws are defined by Darcy's relation for single phase fluids. Under these conditions the factors contributing to the mixing are the fluctuation of the local flow velocities around the mean displacement velocity and the molecular diffusion. The local flow velocity in a pore varies with its shape, size and orientation with respect to the principal flow direction. Thus in linear flow a number of marked fluid particles released at the same instant and same cross-section into the stream will arrive at different times at a subsequent sampling point due to the different lengths of their tortuous flow paths and due to the different velocities encountered in pore channels of different diameter.

This phenomenon can best be visualized by a simple experiment where an abrupt concentration change is effectuated at the inlet of a linear flow system and the subsequent concentration distribution is obtained at a sampling point downstream. It is characterized by a delay or dead time and a dispersion. The delay is linked to the macroscopic propagation phenomenon and measured by the ratio of the travel distance by the over-all translation velocity of the center of mass of the quantity under consideration. The dispersion is a physical process that can finally be attributed to the law of increasing entropy (Fig. 1).

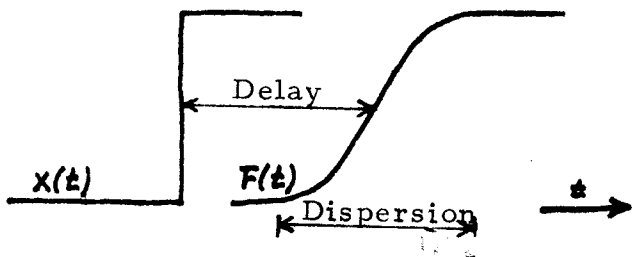

If $\Phi(t)$ is the response of the linear process to an unit step input, $F(t)$, the general response to an arbitrary disturbance $x(t)$, then their relations can be expressed in general form by using the convolution or superposition theorem

$$F(t) = \int_{-\infty}^{t} x(t-t')\, d\Phi(t') \qquad (1)$$

where t' is the delay time. From these response characteristics deterministic or probabilistic interpretations as to the mechanism underlying the microscopical processes can be made.

The S-shaped response function in Fig. 1 immediately leads to a comparison with error function curves, that are special solutions of the diffusion equation. As a matter of fact, some of the earlier attempts to describe dispersion phenomena, especially for the case of linear miscible displacements, consisted of fitting experimental data points of breakthrough curves to error function curves (cf. von Rosenberg (19), Aronofsky and Heller (2) Blackwell (4)). The fit for these preliminary investigations was considered to be sufficient, and hence the underlying mechanism was described to be of the diffusion type without further quantitative specifications. The transport coefficients had to be found by experiment.

However, a close fit of experimental points with the error function curve is only obtained for the central part in the most cases, whereas deviation occurs on the leading and tailing end of the breakthrough curve (cf. Pfannkuch (14)). The deviation is always in the direction of a greater dispersion than that expected if standard mean deviations are obtained from the center part of the curve. The magnitude of the deviation is greater than can be accounted for by experimental inaccuracy. Several attempts to explain the phenomenon have been made. Warren and Skiba (28) investigate heterogeneity and anisotropy effects of the porous medium itself. The possible influence of retention of original saturating fluid in dead-end pores expressed by a capacitance model and subsequent diffusion out of these pores into the flowing stream has been discussed by Coats and Smith (5)* who introduce an additional "Quasi-source function" term responsible for the distortion in the concentration profile.

This paper proposes to investigate other possible explanations for the experimentally observed deviations. It will consider the situation when coupling effects between bulk flow and molecular

*see also discussion of their paper by Rose (16).

diffusion can be expected. In order to determine under what circumstances this coupling may occur the main theories dealing with hydrodynamic dispersion and miscible displacement will be reviewed.

Model Concepts of Dispersion in Porous Media

The older theories explaining the mechanisms of hydrodynamic dispersion can be divided into two groups. The first uses simple physical phenomena for which particular solutions on a microscopic scale are known. These solved cases are then adapted and extended to greatly simplified physical models of the complex situation in the porous solid. Examples are diffusion in a capillary tube and mixing in cells. The second approach, in circumvening the ignorance of microscopic conditions and the impossibility of a deterministic solution, takes statistical averages to obtain the macroscopic parameters. Essentially it describes the probability function of a given particle to be at a certain place at a certain time $\Psi(x, y, z, t)$. A number of combinations of both try to join the advantages and to eliminate the shortcomings inherent in each one of these theories. A third approach develops a theory of transport processes in porous media from a continuum mechanics and irreversible thermodynamics point of view.

Physical Models

Dispersion in a Capillary Tube. All theories making use of the capillary analogy go back to the work of G. I. Taylor (26) who defines an effective diffusion coefficient describing the dispersion of a soluble matter (dye) in axial direction while flowing through a capillary tube. His treatment is an example of a straight-forward solution of the physical problem. Some limiting assumptions are made as to the time scale for which the molecular diffusion will smooth out concentration variations over the cross-section of the tube with radius a. This time scale has to be small enough so that no appreciable effects of molecular diffusion in axial direction will be noted. Furthermore the coefficient of molecular diffusion is assumed to be independent of the concentration. Defining boundary conditions and dropping terms according to the limiting assumptions the diffusion equation given in cylindrical coordinates can be stated as follows:

$$D\left(\frac{\partial^2 c}{\partial r^2} + \frac{1}{r}\frac{\partial c}{\partial r} + \frac{\partial^2 c}{\partial x^2}\right) = \frac{\partial c}{\partial t} + u_0\left(1 - \frac{r^2}{a^2}\right)\frac{\partial c}{\partial x} \qquad (2)$$

where D = coefficient of molecular diffusion

C = concentration

r = radial distance

a = radius

x = axial distance

t = time

u_o = maximum velocity at r = o

The mean concentration C_m over a cross section will then disperse relative to a plane moving with the mean velocity $u_m = 1/2\ u_o$ as though it were diffused by a process obeying the laws of molecular diffusion:

$$K_L \frac{\partial^2 C_m}{\partial x^2} = \frac{\partial C_m}{\partial t} \qquad (3)$$

where the effective diffusion coefficient in the longitudinal direction K_L is related to the molecular diffusion coefficient D by

$$K_L = \frac{a^2 u_o^2}{192\ D} = \frac{a^2 u_m^2}{48\ D}$$

An error function solution is obtained for a step input in concentration.

The fact that the same form of solution is obtained as displayed by experimental results for porous media does not mean that the underlying mechanisms of dispersion are the same. Hence attempts to extend Taylor's treatment to porous media represented by bundles of straight capillaries with different radii have not rendered any significant insight into the phenomenon. The solution of the equation for dispersion in a capillary tube will be important for the description of the microscopic behavior in a pore when statistical approaches are used.

Mixing Cells. Another physical model concept for dispersion in porous media comes from the study of reactors. The porous medium is considered to consist of a series or chain of connected cells. A fluid entering will displace its own volume and then mix with the remaining contents. In the next step part of the mixture will enter the following cell and the process is repeated. The mixing of entering and stagnant fluid is supposed to be perfect and to occur instantaneously. Aris and Amundson (1) show that the final concentration distribution is a Poisson distribution which will tend to a normal one when the number of steps is sufficiently great. This treatment does not indicate how

perfect mixing is achieved in each unit cell nor does it identify the contribution from different mechanisms such as jet mixing, eddy diffusion or molecular diffusion. Furthermore, the simpler theories do not provide for any possibilities to explain transversal dispersion normal to the direction of general flow observed in actual experiments.

Statistical Models.

Random Walk. The ideas of statistical mechanics in porous media have been developed and used extensively by Scheidegger. (For summaries of older works and more recent developments see references (23) and (24) where the original literature is referred to.)

Actually the flow of fluids in a porous medium is a deterministic process a mathematical solution of which could be obtained, like in the case of the capillary tube, if all the boundary conditions were known. The latter of course is not the case. Furthermore, even if these conditions were known the mathematical formulation of the geometry of the pore surface would be far too complicated to yield any useful analytical expressions of the flow equations. Hence dispersion processes may be treated statistically as if they were random (21). Basically one asks the probability of a particle to be at a given point at a given time

$$\Psi\ (x, y, z, t)$$

If the particle has been in motion for a very long time compared to the time for passing one pore it can be assumed that it will encounter all conditions present in the flow domain. According to the ergodic hypothesis, time averages of any quantity in any system can be interchanged with ensemble averages of the same quantity taken over the space. This means for instance that the time average of the probability distribution for one particle at a fixed time t can be interchanged with the spatial distribution at that time of a great number of particles released into the flow stream at the same initial instant t_o. The probability density for one particle can then be interchanged for the tracer concentration provided the number of steps is very great.

$$\Psi\ (x, y, z, t) \rightarrow C\ (x, y, z, t)$$

For the treatment of a practical problem Scheidegger proposes that one first has to choose and fix (1) the ensemble with which to do statistics, (2) the type of statistics to be used, and (3) the microscopic flow laws to which each small fluid volume is subject. In his random walk model, the total time t is split into a number N of equal time intervals τ so that

$$t = \sum \tau \qquad \text{and } N = \frac{t}{\tau}$$

It is supposed that the porous medium be isotropic, laminar flow prevail and there be no correlation between two steps. The latter means that at the end of one step a particle has equal probability to move in any direction. The progress of a particle during an interval τ is some random function. If the mean progress during τ is $\bar{\xi}$ the deviation from $\bar{\xi}$ is random. In this case the function (x, y, z, t) by virtue of the Central Limit theorem becomes asymptotically normal and statistically independent. No explicit indication, however, is given by what mechanism randomness of velocity fluctuations around $\bar{\xi}$ is obtained. With these assumptions, the basic flow equation becomes

$$\frac{\partial \Psi}{\partial t} = \frac{\partial}{\partial x'} K \frac{\partial \Psi}{\partial x'} \qquad (4)$$

if the system moves with the center of mass, or in fixed coordinates with $x' = x - u t$ and $t' = t$

$$\frac{\partial \Psi}{\partial t} = \frac{\partial}{\partial x} K \frac{\partial \Psi}{\partial x} - u \frac{\partial \Psi}{\partial x} \qquad (5)$$

where u is the velocity of the center of mass and depends on the macroscopic parameters as pressure difference, permeability and viscosity. If Ψ is only to be a function of position then it is independent of the flow velocity, hence

$$K \propto u$$

This statement means that no particles change streamlines or better that there is no mass transport across the boundaries of adjacent streamtubes. Molecular diffusion is thus neglected.

In order to account for the fact of experimentally observed transversal dispersion in unidirectional flow equation (5) has to be written

$$\frac{\partial \Psi}{\partial t} = \frac{\partial}{\partial x_i} K_{ik} \frac{\partial \Psi}{\partial x_k} - u \frac{\partial \Psi}{\partial x_i} \qquad (6)$$

where K_{ik} becomes a dispersivity tensor. Again the form of K_{ik} does not follow explicitly from the basic development of the theory.

Random Networks. De Josselin de Jong (11) improves the above model by considering the porous medium as a network of randomly oriented straight capillary tubes of equal length. The local velocities vary with the orientation of the capillary with respect to the direction of general flow. He also defines a directional probability of a particle after leaving a capillary at the junction points. He relates the discharge into a particular direction to the total discharge. Introduced at this microscopic level these assumptions lead to a transversal dispersion term with K_T coefficient of transversal dispersion. Again the probability of a particle to be at a certain point at time t becomes a Gaussian distribution in space for a great number of steps.

The magnitude of dispersion in the direction of general flow and normal to it are function of two different dispersion coefficients K_L and K_T respectively where

$$K_L / K_T \approx 3$$

Since molecular diffusion was only introduced to justify the assumption of a uniform concentration distribution over the cross section of the elementary tube the coefficients of dispersion are proportional to the mean flow velocity

$$K_L, K_T \propto u$$

Saffman's (20) statistical treatment is similar to the previous one. But here the effects of molecular diffusion are explicitly taken into account on the microscopic level. His porous medium is represented by a homogeneous and isotropic network of capillaries of equal length (l) and diameter (a) where $l \gg a$. As a consequence of Taylor's treatment, time scales are defined so that the parabolic velocity distribution in an elementary capillary can be neglected. The local velocity is a function of the direction of the capillary with a term added to take care of the contribution of molecular diffusion. The directional choice of a particle at a junction point is incorporated in the treatment of correlating the different velocities by Lagrange functions. The final form of the longitudinal dispersion coefficient appearing in the diffusion equation is

$$K_L = \frac{1}{3} D + \frac{3}{80} \frac{a^2 u^2}{D} + \frac{l^2 u^2}{4} \int_0^1 (3\vartheta^2 - 1)^2 \frac{M \coth M - 1}{K_s - M^2} \, d\vartheta \qquad (7)$$

$$M = \frac{3}{2} \frac{u l \vartheta}{K_s} \qquad K_s = D + \frac{3}{16} \vartheta^2 \frac{a^2 u^2}{D}$$

with

- u = mean velocity in the pore
- ϑ = $\cos \theta$
- θ = angle of direction of capillary with respect to general flow direction.

The first term on the right side corresponds to the contribution of the molecular diffusion in the longitudinal direction. The second term is comparable to the dispersion in a capillary tube for the conditions given by Taylor. The third expresses the complex interaction between molecular diffusion and hydrodynamic dispersion. The resulting dispersion coefficient is some power function of u

$$K_l \propto u^n$$

Saffman's theory explicitly accounts for transversal dispersion and defines a transversal coefficient K_T.

Bear and Bachmat (3) use a statistical approach but define the microscopic conditions in very great detail and for a more generalized situation. Their approach is mainly concerned with the tensorial character of the dispersion coefficient and the inherent dispersivity of the porous medium.

Gibbsian Statistics. Scheidegger (22) has applied a more general statistical treatment to the flow in porous media and shows that through a thermodynamic analogy Gibbsian statistics can be applied for the equilibrium case and theorems of non-equilibrium thermodynamics for small deviations from the equilibrium state as specified by the Onsager relations. General diffusivity equations can be derived. They are independent of special assumptions concerning the particular quantity (heat, concentration, etc.) involved in a transport process. Applied to the special conditions for dispersion in a porous medium the same equations as for the random walk model are immediately obtained.

The statistical methods only give the probability of a particle to be at a certain point at a given time. Different treatments of the microscopic conditions allow more or less explicitly for transversal dispersion. The particle in question differs from other fluid particles only by some imaginary marking or tagging. Only for this case or for a perfect solution can the thermodynamic probability for one particle be interchanged for the concentration distribution. The application of the ergodic principle is not possible, however, when the concentration change is accompanied by some change in internal energy, such as the chemical energy expressed by μ (Tuwiner (27)). Hence the interchange of Ψ for C is rigorous only for the mathematical model, permissible in certain cases of highly diluted tracer flow, but certainly not applicable to the exact theoretical treatment of miscible displacements that are characterized by steep concentration gradients at the liquid interfaces (sea water intrusions, waste disposal and miscible recovery procesees).

Thermodynamic Model.

All the above described theories of dispersion in porous media do not provide for any interaction or coupling between bulk flow, mechanical dispersion and molecular diffusion. A general theory of transport processes in porous media has been formulated by Rose (17) (18) in the reference frame of continuum mechanics and irreversible thermodynamics. The usual conservation theorems are extended to the conservation of energy and entropy for dissipative transport phenomena. The constitutive assumptions needed to formulate particular

processes are derived from the linear phenomenological relations between generalized flows and forces. Furthermore, the auxiliary relationships of positive definite entropy production from irreversible thermodynamics are used. Expressing the driving force in terms of the total local energy Ψ the transport equation can be written

$$\rho\left[\left(\frac{\partial \Psi}{\partial t}\right)+v\cdot(\mathrm{grad}\,\Psi)\right]=\sigma+\mathrm{div}\left[\left(\frac{\rho D}{\epsilon}\right)(\mathrm{grad}\,\Psi)\right] \qquad (8)$$

with ρ = mass density of material particle

v = center of mass velocity of a material particle

D = transport coefficient

σ = source or sink function.

For derivation see eq. (9) Rose (17). Choosing one particular form of energy and relating it to its conjugated flux, the classical laws of transport phenomena in porous media (Darcy's law) as well as a number of less conventional relationships can be derived. The advantage of this approach lies in the fact that the energy term of transport equation expresses the total energy per unit mass associated with the local particle in motion. This means that it can be decomposed into the local values of the different possible energy forms such as mechanical, thermal, electrical, chemical, etc. Separate equations for each transport process can be written and combined into a general set of linear relations between currents and driving forces of the form

$$J_i=\sum_j L_{ij}X_j \qquad (9)$$

with J_i = flux

L_{ij} = general linear coefficient

X_j = conjugate force

This means that each flow is not only related linearily to its conjugate force but also to all other forces contributing to the entropy production of the system. This relation does not prove any coupling of processes (for which $L_{ij} \neq 0$ when $i \neq j$); it does, however, imply a possibility. Rose applies these relationships to coupled processes chiefly in the study of a two phase displacement, where the general driving force can be decomposed in a pressure gradient and a surface energy gradient expressed by a saturation gradient. He tentatively writes the general equation for coupled transport processes in porous media when the gradient of chemical potential and the pressure gradient are the driving forces, as it would be represented by the case of a miscible displacement. The set of equations is:

$$Pf\left(\frac{\partial \mu}{\partial t}\right) + Pq \cdot (\text{grad}\,\mu) = \frac{f}{2}\,\text{div}\left\{P\left[L_{11}(\text{grad}\,\mu) + L_{12}\left(\frac{\mu}{\varphi}\right)^{\frac{1}{2}}(\text{grad}\,\varphi)\right]\right\} \tag{10a}$$

$$Pf\left(\frac{\partial \varphi}{\partial t}\right) + Pq \cdot (\text{grad}\,\varphi) = \frac{f}{2}\,\text{div}\left\{P\left[L_{21}\left(\frac{\varphi}{\mu}\right)^{\frac{1}{2}}(\text{grad}\,\mu) + L_{22}(\text{grad}\,\varphi)\right]\right\} \tag{10b}$$

where μ = chemical potential

φ = mechanical energy potential

f = porosity

L_{11} = phenomenological coefficient of molecular diffusion

L_{22} = phenomenological coefficient for darcian flow conductivity

L_{12} = L_{21} coupling coefficients

These relationships as well as the other general considerations applicable to the special conditions in porous media will be the basis of the following discussion.

Thermodynamic Treatment of Transport Processes in Porous Media

Discussion of Coupling Phenomena.

General Theory. The methods of irreversible thermodynamics make available a tool to treat complicated natural processes. On the basis of a generalized Gibbs equation energy and entropy balances are carried out. The entropy production and energy dissipation near the equilibrium state are analyzed and the relations between generalized fluxes and their conjugate forces are established.

The first step is to define the generalized flows by the quantities transported and to relate them to the driving forces that give rise to the flux.

J_i = $\dot{v}$

X = grad γ

where J = generalized flux

X = generalized force

γ = entity in question per unit mass

grad γ = gradient giving rise to flow of γ

$\dot{v}$ = local diffusional velocity

From Gibbs equation

$$dS = \frac{dE}{T} + \frac{P}{T}\,dV - \sum_j \frac{\mu_j}{T}\,dn_j \tag{11}$$

with E = internal energy

S = entropy

T = ambient temperature

μ_j = chemical energy of component j

n_j = mole number of component j

P = pressure

V = volume

the source function for entropy production due to the irreversible part of the process can be generated (Fitts (7), Haase (9), (10)).

$$\frac{dS}{dt} = \frac{1}{T}\sum_i J_i X_i > 0 \tag{12}$$

where i denotes the number of different, independent processes under consideration. The inequality states that the process has to be positive definite.

The energy dissipation function Θ is given by

$$\Theta = \frac{dS}{dt}\,T \tag{13}$$

The fluxes J_i and their conjugated forces X_j vanish when the system is at thermodynamic equilibrium if their dimensions are properly chosen. In a first approximation the deviation of the system from equilibrium is taken to be small. In this case the irreversible process may be described by a linear relationship between the fluxes and forces. The general expression has been given by Onsager (13) as the phenomenological relation already stated in eq. (9) where the L_{ij} are the phenomenological coefficients, independent of J and X. They are not thermodynamic functions but rather kinetic quantities that have to be defined for each particular transport process. Written in matrix representation when $i = j \geqslant 2$ the diagonal coefficients describe simple processes for i = j,as simple heat conduction or electrical conduction. The cross coefficients ($i \neq j$) would express coupling effects between two concurrent processes.

When all J'_is and X'_js are taken from expression (12) for the entropy production, and if they are independent then the phenomenological conditions satisfy the Onsager symmetry relations

$$L_{ij} = L_{ji} \tag{14}$$

When the two expressions (9) and (12) are combined, the dissipation function takes the form

$$\frac{dS}{dt} T = L_{ij} X_i X_j > 0 \tag{15}$$

applying the summation convention. From eq. (15) useful relations can be derived to determine the upper limits of the cross coefficients when the pure coefficient L_{ii} is known. In the case of two processes $i = 1, 2$ $j = 1, 2$ it leads to

$$(L_{11} L_{22}) > (L_{12})^2 \tag{16}$$

These relations themselves only imply the possible relations of the coefficients, they do not prove the existence of cross coefficients nor their symmetry. Detailed derivation and physical justifications are to be found in the standard monographs on the subject (7) (8) (10).

Experimental Evidence. Experimental observation of coupling effects is abundant. They are easily observed in thermoelectric phenomena (Peltier-Thomson effects) and in thermodiffusion (Sorel-Dufour effects). Electrokinetic effects are identified by the schema of relations for the phenomenological coefficients. Saxen's equations (1894) have been known for a long time, but only recently have they been recognized as a consequence of Onsager relations. On the other hand, phenomena such as the mechanocaloric effect for liquid Helium II have been predicted on the basis of thermodynamic considerations (Tisza cf. Haase (9) p. 111) and were observed later.

Onsager's symmetry relations have been verified by laboratory methods to be accurate within the experimental error for a great number of processes (Miller (12), Schlögl(25), Rastogy (15)).

Diffusion-Pressure Interrelations. The quantities of interest in an isothermal dispersion-diffusion process are, of course, pressure and concentration and their interrelations.

Numerous experimental observations of pressure-diffusion interrelations exist for discontinuous systems as represented by two different homogeneous sub-systems separated by a porous membrane, capillary tube or a very small opening. The ensuing osmotic effects show that a bulk flow can be associated with a concentration gradient (osmotic transport, osmotic pressure build up) and that separation of matter (concentration) can be associated with pressure gradients (ultrafiltration). These examples of well known facts only serve as illustrations of a qualitative nature since they occur in different systems than the one under consideration.

The porous medium is here only considered as a phase separation so small that phenomena occurring within can be neglected.

Pressure and diffusional interdependence for continuous systems has been discussed by Haase (10) for the isothermal case.

The simultaneous occurrence of diffusion and dfifusion due to a pressure gradient in a fluid medium with two species of neutral particles is given by the expression

$$J_i = - \frac{1 - w_i}{1 - x_i} c \left(D \operatorname{grad} x_i \mp D_p \frac{\operatorname{grad} P}{P} \right) \tag{17}$$

The sign in the brackets is negative for $i = 1$, positive for $i = 2$. The quantities are

w_i = weight factors to obtain weighted average of the reference velocity w, $w_1 + w_2 = 1$

x_i = partial mole fraction of particle i with $x_1 + x_2 = 1$

c = total molar volume concentration with $c = c_1 + c_2$

J_i = mass flux

D = coefficient of molecular diffusion

D_p = coefficient of diffusion due to a prsssure gradient

P = pressure.

The theoretical foundations for eq. (17) are to be found on p. 354, reference (10). Apparently no experimental observations of this phenomenon have been reported yet. All eq. (17) does is to relate the different parameters in a way consistent with the theory of irreversible thermodynamics, where the existence of D and D_p and their magnitude have to be determined by experiment. For $D_p = 0$ or grad $P = 0$ eq. (17) reduces to Fick's law of diffusion.

Transport Processes in Porous Media.

Diffusion. The generalized force-flux relationships are given in a square root form for dimensional consistency in eq. (6) of reference (17). The usual but looser notation is:

$$\Psi(\dot{v}) = - \frac{D}{2} (\operatorname{grad} \Psi) \tag{18}$$

with Ψ = total local energy per unit mass.

If Ψ consists of only two forms of energy, a mechanical potential φ and a chemical potential μ, then using eq. (18) Rose's relations (10) on a unit volume basis become

$$\rho f\left(\frac{\partial \mu}{\partial t}\right)+\rho q\cdot(\operatorname{grad}\mu) = \frac{f}{2}\operatorname{div}\left\{\rho\left[L_{11}(\operatorname{grad}\mu)+L_{12}(\operatorname{grad}\varphi)\right]\right\} \qquad (19a)$$

$$\rho f\left(\frac{\partial \mu}{\partial t}\right)+\rho q\cdot(\operatorname{grad}\mu) = \frac{f}{2}\operatorname{div}\left\{\rho\left[L_{21}(\operatorname{grad}\mu)+L_{22}(\operatorname{grad}\varphi)\right]\right\} \qquad (19b)$$

in which the L_{ij} are the phenomenological coefficients and q the seepage velocity. It can be shown (Fitts (7) p. 80, Haase (10) p. 306) that the gradients of chemical potential are easily transformed into concentration gradients in a system with constant temperature T and pressure P:

$$(\operatorname{grad}\mu_j)_{TP} = \sum\left(\frac{\partial \mu_j}{\partial \rho_j}\right)_{TP}\operatorname{grad}\rho_j \qquad (2)$$

where

μ_j = chemical potential of j^{th} component

ρ_j = partial mass density

From the definition equation for the generalized flux:

$$J_i = \sum L_{ij}(\operatorname{grad}\mu_j)_{TP} = \sum_i\sum_j L_{ij}\left(\frac{\partial \mu_i}{\partial \rho_j}\right)_{TP}\operatorname{grad}\rho_j \qquad (21)$$

and for

$$D_{ij} = \sum L_{ij}\left(\frac{\partial \mu_i}{\partial \rho_j}\right) \qquad (22)$$

If no coupling occurs eq. (19a) reduces to Fick's 2nd law with a convection term containing q. It must be stated, however, that the simple diffusion coefficients measuring the transport of mass due to concentration gradients do not obey the Onsager symmetry relations. In order to verify the latter the D_{ij}, more readily obtained in experiments, have to be transformed back into the phenomenological coefficients with relations analogous to eq. (21) and (22).

Eq. (19b) can be reduced to Darcy's equation when there is no coupling with a darcian transport coefficient of the form $L_{22} = (2k\rho\varphi)/f\eta$ involving permeability k, viscosity η, porosity f, density ρ and mechanical energy φ.

The magnitude of the coefficients $L_{12} = L_{21}$ will give an indication of the coupling of mass diffusion due to interaction of chemical potential gradients and a mechanical energy gradient.

From equations (19) it can be seen that Rose's treatment describes one phase of the miscible drive process, namely mass transport due to a concentration gradient, and possibly coupled with this a mass transport due to a mechanical energy gradient. It does not, explicitly, take into account the dispersion due to the geometrical dispersivity of the porous medium itself.

Dispersion. In order to interrelate molecular diffusion and hydrodynamic dispersion in porous media they have to be described from a thermodynamic point of view.

From the foregoing the position in space at time t of a given fluid particle in a miscible displacement process is determined by two basically different processes. One of the contributing mechanisms is the mass diffusion due to a gradient in chemical potential with the possibility of a coupling term arising due to a gradient in mechanical energy. Here thermodynamic driving forces and fluxes have been identified by Rose (18). The second mechanism is that of hydrodynamic dispersion for tracer flow, where in the case of no flow (q = 0) the tagged particles will be subject to an autodiffusional movement due to their own kinetic energy. In the flow case ($u \neq 0$) particles will be mixed due to the dispersivity of the porous medium. However, no generalized thermodynamic force for this mass transport can be defined in the context of irreversible thermodynamics. The reason is that the concentration, expressed as C or ρ, used in the gradient, does not reflect the existence of a chemical potential differential but a probability state. The analogy with the kinetic theory is obvious.

If the entropy production is to be examined from an energetic point of view, it has to be borne in mind that in the development of the theory for pure dispersion one of the basic assumptions is the identity of physical properties of all particles. The only means of differentiation is by some imaginary marking or tagging of species 1 and species 2. Since these particles are energetically all in the same state, their dispersion with respect to coordinates moving with the center of mass during flow through a porous medium would be unobservable if the marking were removed. Then dispersion will not give rise to an energy dissipation function of the form described in eq. (13).

On the other hand, it is observed that tagged particles separated initially in an orderly arrangement (as in an unit impulse or unit step input functinn) will tend to complete disorder in an irreversible way. The entropy production connected with this phenomenon is only a statistical analogy of the thermodynamic entropy. It indicates the case where increasing entropy describes a state of increasing

disorder in the geometrical arrangement (Fast (6) p. 49 ff). Here the term entropy production has the same sense as in kinetic theory for monatomic gases where complete reversibility from an energetic point of view is postulated.

Conclusion

An answer to the question of how and to what extent the different mechanisms of mass transport during flow through a porous medium interact may be given by the insight obtained from the statistical and thermodynamical model of dispersion processes.

In the thermodynamic treatment it has been indicated that coupling effects between mass transport due to concentration gradients and due to mechanical energy gradients are possible. The final proof of this matter, however, lies with experiment. It should be pointed out again that mass transport due to a combination of chemical potential and mechanical energy gradients can be a factor in distorting concentration profiles as described in (5) and (28). The spread or distortion is in the direction of a greater entropy production.

On the other hand, the same thermodynamic treatment seems to indicate that no coupling may exist between the mechanical dispersion of mass due to the geometrical configuration of the pore space and diffusion due to a concentration gradient. From an energy point of view both processes are different so that their entropy productions cannot be compared or interrelated for use in the fundamental relations describing coupling phenomena. In a typical miscible displacement experiment the results of the geometrical dispersivity are felt to be superposable on molecular diffusion effects. To determine the exact form of these additive effects which would be different from coupling, experiments should be conducted for a flow situation with very low velocities. Then the influence of diffusion and dispersion are of the same order of magnitude and experimental constraints on one or the other will produce the most visible effects (cf. 14).

Until experimental answers to the above questions have been obtained nothing more can be said in conclusion than that it seems not permissible to apply the results obtained from the statistical model for single phase non-homogeneous flow directly to the treatment of a miscible displacement process just because the form of the solutions look alike. This extrapolation may be useful for a rough description, especially of practical cases, where ideal conditions do not prevail as postulated in the theory. The distinction has to be made, even in the case of tracer flow, when a deeper insight into transport phenomena in porous media is wanted.

REFERENCES

(1) Aris, R. and N. R. Amundson, "Some remarks on longitudinal mixing or diffusion in fixed beds," AIChE Journ., vol. 3, p. 280, 1957.

(2) Aronofsky, J. S. and J. P. Heller, "A diffusion model to explain mixing of flowing miscible fluids in a porous media," Trans. AIME, vol. 210, p. 345, 1957.

(3) Bear, J. and Y. Bachmat, "A unified approach to transport phenomena in porous media," Technion Research and Development Foundation Research Project CV-54 Progress Report 3, Haifa, Israel, 1965.

(4) Blackwell, R. J., "Experiments on mixing by fluid flow in porous media," Preprint no. 29, SPE-AIChE, 52 Ann. Meeting, 1959.

(5) Coats, K. H. and B. D. Smith, "Dead-end pore volume and dispersion in porous media," Soc. Pet. Eng. Journ., v. 4, p. 73, 1964.

(6) Fast, J. D., Entropy, McGraw-Hill, New York, 1962.

(7) Fitts, D. D., Non-equilibrium Thermodynamics, McGraw-Hill, New York, 1962.

(8) de Groot, S. R. and P. Mazur, Non-equilibrium Thermodynamics, North-Holland Publ. Co., Amsterdam, 1962.

(9) Haase, R., "Thermodynamisch-phänomenologische Theorie der irreversiblen Prozesse," Ergebnisse d. exakt. Naturwiss, vol. 26, pp. 56-164, 1952 (Springer-Berlin-Göttingen-Heidelberg).

(10) Haase, R., Thermodynamik der irreversiblen Prozesse, Dr. D. Steinkopff Verl., Darmstadt, 1963.

(11) de Josselin de Jong, G., "Longitudinal and transverse diffusion in granular deposits," Trans. Am. Geophys. Un., vol. 39, no. 1, p. 67, 1958.

(12) Miller, D., "Thermodynamics of irreversible processes," Chem. Reviews, vol. 60, no. 1, pp. 15-37, February 1960.

(13) Onsager, L., "Reciprocal relations in irreversible processes," Part I: Phys. Review, vol. 37, p. 405, 1931; Part II: Phys. Review, vol. 38, p. 2265, 1931.

(14) Pfannkuch, H. O., "Contribution a l'etude des deplacements de fluides miscibles dans un milieu poreux," Rev. Institut Francais du Petrole et Ann. des Combustibles Liquides, vol. 18, no. 2, pp. 215-270, 1963.

(15) Rastogi, R. P. and K. M. Jha, "Cross-phenomenological coefficients," Trans. Farad. Soc., vol. 62, no. 519, part 3, pp. 585-594, March 1966.

(16) Rose, W. D., Discussion of "Dead-end pore volume and dispersion in porous media" by Coats and Smith, Soc. Petr. E. Journ., vol. 4, p. 282, 1964.

(17) Rose, W., "Reservoir engineering reformulated," Paper presented at 25th Technical Conference on Petroleum Production, October 19-21, 1966, University Park, Penna.

(18) Rose, W., "Transport through interstitial paths," Chapter 5 in Flow Through Porous Media, Academic Press, New York (in press, 1967).

(19) von Rosenberg, D. U., "Mechanics of steady state single phase fluid displacement from porous media," AIChE Journ., vol. 2, no. 1, p. 55, 1956.

(20) Saffmann, P. G., "Dispersion due to molecular diffusion and macroscopic mixing in flow through a network of capillaries," J. Fluid Mech. G. B., vol. 7, no. 2, p. 194, 1960.

(21) Scheidegger, A. E., "Statistical hydrodynamics in porous media," Journ. Appl. Phys., vol. 25, no. 8, pp. 994-1001, August 1954.

(22) Scheidegger, A. E., "On the statistical properties of some transport equations," Can. J. Phys., vol. 39, pp. 1573-1580, 1961.

(23) Scheidegger, A. E., "Statistical hydrodynamics in porous media," Advances in Hydroscience, vol. 1, pp. 161-181, Academic Press, New York and London, 1964.

(24) Scheidegger, A. E., "Statistical theory of flow through porous media," Trans. of the Soc. of Rheology, vol. 9, no. 1, pp. 313-319, 1965.

(25) Schlögl, R., Stofftransport durch Membranen, Fortschritte der Physikalischen Chemie, vol. 9, Dr. Dietrich Steinkopff Verlag, Darmstadt, 1964.

(26) Taylor, Sir G. I., "Dispersion of soluble matter in solvent flowing slowly through a tube," Proc. Royal Soc. of London, Series A, vol. 219, no. 1137, pp. 186-203, August 1953.

(27) Tuwiner, S. B., Diffusion and Membrane Technology, AChS Monograph, Reinhold Publishing Co., New York, 1962.

(28) Warren, J. E. and F. F. Skiba, "Macroscopic dispersion," Soc. Pet. Eng. Journ., vol. 4, September 1964.

Calculation of Transient Behavior of Gravity Counterflow Segregation

By

Paul F. Fulton, University of Pittsburgh

R. F. Nielsen, The Pennsylvania State University

INTRODUCTION

Displacement Theory

Since the publication of the classic paper of Buckley and Leverett[1] in 1942, the petroleum literature has contained a great number of papers dealing with the displacement of one fluid by another in porous systems and the distribution of those fluids within the system. The reason for this interest, of course, is that petroleum production is basically a displacement process and an understanding of the displacement process is essential to the optimum recovery of our petroleum resources. Indeed, a whole new profession - that of the petroleum reservoir engineer - has developed to apply this knowledge of displacement of fluids in porous systems to increasing recovery of oil and natural gas, and, incidentally, to the development of underground storage facilities for off-season storage of natural gas.

The very important contribution of the Buckley-Leverett paper was the development of the frontal advance equation, which makes possible the calculation of the saturation distribution at various times in the injection history as a function of injection rate and fractional flow, where fractional flow is the ratio of the rate of displacing fluid flow to the total flow at any saturation. It is a function of the relative permeability characteristics of the porous system and the viscosities of the fluids. The usual method, based on the equation, applied only to linear systems where the two fluids were immiscible, or nearly so, and gravity and capillary effects were excluded. The

combined effect of gravity and capillary pressure was studied by Terwilliger et al.[2] They introduced the "stabilized zone concept" of frontal advance which established that the leading edge of the advancing displacing fluid assumed some saturation profile early in the injection history, which thereafter remained constant and moved through with a constant velocity at uniform injection rates.

Rapoport and Leas[3] also studied the effects of capillary pressure in the Buckley-Leverett equation. Their resulting equation was a non-linear, parabolic type partial differential equation which is not subject to formal solution. In the same paper they presented experimental evidence to show that, in a linear system, the displacement behavior is dependent upon the length of the system, the rate of injection, and the ratio of viscosities of the two fluids. Of particular importance was the conclusion that, at the rates of injection normally used in field operations, the effects of capillarity are negligible and the behavior follows closely that predicted by the simple Buckley-Leverett equation. Jones-Parra and Calhoun[4] have presented a method applying the above-mentioned parameters to the Terwilliger et al. theory to solve for the length of this stabilized zone.

Even though the Buckley-Leverett method may produce the physically impossible triple values of saturation at some positions along the length of the system, simple material balance concepts provide a satisfactory engineering solution to this dilemma.[1,5] Welge's[6] form of the theory eliminates the triple value by modifying some of the data that go into the displacement calculations. Cardwell[7] offered a

theoretical explanation for the triple value using the method of characteristics to show that "shocks" or discontinuities exist within the system and hence the frontal advance equation is not valid in this region. Sheldon, Zondek, and Cardwell[8] have presented a graphical method for this type of computation, making use of "characteristic lines." Nielsen[9] has pointed out that some doubt arises as to preserving material balance in determining the position of shock since the intersection of characteristic lines corresponds to the first appearance of triple (or double, depending on whether or not an initial displacing fluid saturation exists) values rather than to a material balance.

In 1958, Douglas, Blair and Wagner[10] presented a method for calculating saturation distributions in a displacement system which included the effects of capillary pressure but did not include gravity effects. They arrived at the same form of the equation that Rapoport and Leas had derived earlier; i.e., a second order partial differential equation which was non-linear in the derivative. By a change of variable they transformed the equation to a semi-linear partial differential equation which was solved by numerical methods on a high speed digital computer. McEwen[11] repeated their work but changed the outflow end conditions and assumed no flow of water ahead of the flood front. A short time later Fayers and Sheldon[12] solved the Rapoport and Leas form of the equation by using a finite difference form. They included both the capillary pressure and gravity terms in their solution but the time necessary to attain a particular saturation distribution could not be obtained. More recently (1961), Hovanessian and Fayers[13] extended the

work of Douglas et al. to include gravity effects. They computed not only saturation distribution but the pressure distribution as well.

Gravity Drainage and Counterflow

Gravitational and capillary forces are responsible for the original segregation of fluids within a reservoir. One of the earliest observations of petroleum reservoir engineers was that these same gravitational forces played an important part in the recovery of oil from those reservoirs where considerable structure exists.[14-18] During the later stages of depletion of an oil reservoir produced by dissolved gas alone, when the gas will have been virtually exhausted and the reservoir pressure very low, gravity becomes the dominant force in causing continued oil movement to the well bore.[19] Current but relatively minor production from many of our older oil fields is due almost entirely to this form of gravity drainage. Of much greater importance in terms of recoverable oil were the conclusions reached early by most reservoir engineers that:

"(1) Where gravity drainage is important, the reservoir pressure should be maintained by gas injection at the crest of the structure to prevent shrinkage of the oil in place and to keep a low viscosity so the oil can drain at the fastest possible rate.

"(2) Recovery by gravity drainage is rate sensitive."[2]

However, it was not until the publication of the work of Terwilliger et al., that a method was presented for accurately predicting performance of a gravity drainage system. Since then, in addition to the references cited above dealing with gravity effects, other theoretical and computational work has appeared in the literature.[20-24]

The gravity term as incorporated into the displacement theory by these earlier authors applied to downward displacement by gas with all fluids moving downward. With counterflow, the less dense fluid moves upward and the more dense fluid moves downward, hence for this situation the theory again had to be modified. For the situation in which all fluids moved downward, fractional flow rates are used in the calculations. In the case of counterflow, this could result in negative values, values greater than unity, and when rates are equal and opposite, in infinite values. Sheldon et al.[8] and Fayers and Sheldon[12] pointed out that actual flow rates, even though they may be opposite in sign, may be used just as well as fractional flows, thereby eliminating this difficulty.

Recently, Templeton et al.[9] ran some experiments on gravity counterflow to test this theory and concluded that the Darcy equations, as modified for the separate phases, are adequate for counterflow due to density differences. They also concluded that the method of predicting saturation changes, which involves a continuity equation and the elimination of the unknown pressure gradient from the flow equations should therefore apply. More recently, Briggs[25] also investigated gravity counterflow in gas-liquid systems, starting with a high gas saturation in the bottom of the system. The purpose was to simulate the gas bubble created in the lower portion of an aquifer during underground gas storage. Briggs used the

method of Douglas, Peaceman, and Rachford[26] to calculate the transient behavior in the system and compared the computed results with experimental values. One important conclusion from his work was that the use of ordinary drainage and imbibition capillary curves in calculating transient behavior in such systems leads to erroneous results.

STATEMENT OF THE PROBLEM

This study was initially undertaken for the purpose of investigating the conclusion of Templeton et al.[9] that the method of predicting saturation changes which involves a continuity equation and elimination of the unknown pressure gradient should apply to counterflow conditions. This was done by using a computer solution to check their experimental results. Then, providing the above could be established, the problem was to determine by these same computational methods, the effect on the transient behavior during counterflow, of varying certain of the parameters of the system, with particular interest in the final equilibrium districation and the time necessary to attain various degrees of that equilibrium.

The models studied were limited to immiscible liquid-liquid systems with fairly uniform initial saturation distribution.

EQUATIONS USED AND METHOD OF SOLUTION

Equations describing the two-phase flow of incompressible fluids in a linear system can be derived by solving

simultaneously the equation for the conservation of mass and Darcy's Law for two-phase flow. The resulting equation is a non-linear, second order, partial differential equation with one dependent variable, the saturation of one phase. The independent variables are position and time. The derivation of this equation has appeared in the literature in several forms.[3,8,10,12]

Briefly, the equation of continuity is

$$\phi\frac{\partial S}{\partial t} + f'(S)\ \frac{\partial S}{\partial x} = 0 \qquad (1)$$

and this combined with the flow equation

$$\frac{u_w}{\phi} = f(S) = \frac{K}{\phi}\left(\frac{1}{M_o} + \frac{1}{M_w}\right)^{-1}\left(\frac{dP_c}{dS}\cdot\frac{\partial S}{\partial X}\cdot N_c + \frac{u_t}{KM_o} - (\rho_w - \rho_o)\right) \qquad (2)$$

produces this equation,

$$\frac{\partial S}{\partial T} + N_c \cdot \frac{\partial}{\partial X}\left[C(S)\ \frac{\partial S}{\partial X}\right] + \frac{d}{\partial S}\left[G(S)\right]\ \frac{\partial S}{\partial X} = 0 \qquad (3)$$

where

$N_c = \frac{\overline{P}c}{L}$ with $\overline{P}_c$ being that value on the capillary pressure where its slope becomes quite large, and L is the length of the system,

$$X = \frac{x}{L}$$

$$T = \frac{tK}{\phi L}$$

C(S), the capillary pressure term, $= \left(\frac{1}{M_o} + \frac{1}{M_w}\right)^{-1}\ \frac{dP_c}{dS}$

with

$$\underline{P}_c = \frac{P_c}{\overline{P}_c}$$

and

G(S), the total flow and gravity term, =

$$+\left(\frac{1}{M_o} + \frac{1}{M_w}\right)^{-1}\left[\left(\frac{u_t}{KM_o} - \rho_w - \rho_o\right)g\right]$$

In all of these calculations there was no flow across the boundaries, hence $u_o = -u_w$ and

$$G(S) = -\left(\frac{1}{M_o} + \frac{1}{M_w}\right)^{-1}\left(\rho_w - \rho_o\right)g$$

All other symbols are those recommended by the Society of Petroleum Engineers. The details of the derivation of Equation 3 are given in reference 32.

Equation 3 is the equation which Fayers and Sheldon referred to as "the Eulerian form for the fluid flow system since S in this equation is the saturation which an observer located at X would observe as a function of T." From this equation they also derived what they call the Lagrangian form.

$$\frac{\partial X}{\partial T} = \frac{d[G(S)]}{dS} + N_c \frac{\partial}{\partial S}\left[C(S)\Big/\partial X/\partial S\right] \qquad (4)$$

which is essentially the more familiar Buckley-Leverett[1] and Terwilliger, et al.[2] relationship and represents in "X" the position an observer moving along with a fluid element carrying saturation S would observe as a function of "T".

Both the second and third terms of Equation 3 are non-linear and thus the equation cannot be solved by classical techniques. The second term is particularly difficult since it is in values of the derivatives of a non-linear term. It is possible to resolve this problem of the non-linearity in the derivative term by making the following change of variables:

Let

$$r(S) = \frac{1}{Z}\int_{S_{wi}}^{S} C(\xi)\, d\xi \qquad (5)$$

Where Z normalizes r(S), i.e.,

$$Z = \int_{S_{wi}}^{S_{1-S_{or}}} C(\xi)\, d\xi \qquad (6)$$

Making this substitution into Equation 3 produces the "r" form of the equation

$$\frac{1}{C(r)}\frac{\partial r}{\partial T} + \frac{1}{Z}\frac{d\,G(r)}{dr}\cdot\frac{\partial r}{\partial X} + N_c\frac{\partial^2 r}{\partial X^2} = 0 \qquad (7)$$

This is the equation to be solved in this problem. It is still non-linear but not in the derivative. This makes a solution by numerical methods possible.

In the solution of Equation 7 initial and boundary conditions must be stipulated. Initial conditions are represented by the arbitrarily chosen saturation distribution in the system. In these problems there is no flow of fluids

across the boundaries (at X = 0 and X = 1). This is satisfied by setting f(S) in Equation 2 equal to zero. Thus at the boundaries, either

$$\left(\frac{1}{M_w} + \frac{1}{M_o}\right)^{-1} = 0 \qquad (8)$$

or

$$\frac{\partial S}{\partial X}\cdot\frac{dP_c}{dS}\cdot N_c - (\rho_w - \rho_o)\, g = 0 \qquad (9)$$

Rewriting Equation 9 in the "r" form yields

$$\frac{\partial r}{\partial X} = \frac{(\rho_w - \rho_o)g}{N_c}\cdot\frac{1}{dP_c/dr} \qquad (10)$$

During the early part of the fluid movement the boundary conditions must satisfy Equation 10 which sets the slope at the boundary as a function of $P_c(r)$. Once the saturation at either end reaches either residual, the other condition (Equation 8) takes over and the slope boundary must be relaxed. Thereafter the saturation at the end is fixed at the residual.

PROCEDURE OF THE INVESTIGATION

General

The systems assumed in all of the calculations were porous media of varying heights, initially fairly uniformly saturated along the height with brine and an oil. The systems are completely closed and the fluids allowed to redistribute themselves under gravitational and capillary forces.

The method of solution used in all of the computations is similar to that introduced by Douglas et al.[10] and later modified by Hovanessian and Fayers[13] for the calculation of satura-

tion distribution in a horizontal linear water flood. However the solution is somewhat more complicated than that presented in these papers for two reasons: (1) the no-flow boundary conditions, and (2) the fact that at any time part of the flow will be governed by wetting liquid drainage conditions and the remainder by wetting liquid imbibition conditions. This latter condition results from the fact that the wetting liquid saturation will be increasing in the lower portion of the model while simultaneously decreasing in the upper part. Depending on the initial saturation distribution, a third condition is also possible, i.e., a section of the model could exhibit successively imbibition and then drainage. This will be discussed in a later section. One approach to the solution of the drainage-imbibition problem is to synthesize curves either from experimental relative permeability and capillary pressure data or empirical equations such that the portion of the curves covering wetting liquid saturations greater than the initial represents imbibition, and that portion covering the lower saturations is representative of drainage. A second possibility is to attempt to write the computer program in such a way that if the wetting liquid saturation at any point is decreasing, drainage data will be used and if it is increasing, imbibition data will be used in the calculations. In the calculations presented here the first approach was used.

The computer time necessary to get the complete transient behavior of each of the several systems calculated varied from 4 to about 10 hours.

A material balance check was made on all calculated distributions by planimetering the plotted results. In many of the calculations, in order to preserve material balance, the upper slope boundary condition had to be relaxed and the fluids in the upper portion of the system "speeded up." This was done by fixing the saturation at the upper boundary such that the curve did preserve material balance. In retrospect it would have been more realistic to "slow down" the movement of the fluids in the lower portion of the system.

Details of Individual Runs

A total of eleven separate sets of calculations were made in the following sequence: the first two to check the computed saturations with the experimental results of Templeton, et al.;[9] an unconsolidated sand pack; a consolidated sandstone; three glass bead systems where only the length of the system was varied; and four additional calculations on the glass bead system, each with a different value of initial average saturation.

The values of permeability, porosity, length of the system, initial water saturation, $\bar{P}_c$, and the fluids used in each run are shown in Table 1. The properties of the fluids are shown in Table 2.

Runs 1 and 2 - Templeton's Glass Beads

In order to check the experimental results of Templeton, some improvising was necessary, since relative permeability and capillary pressure data for the glass bead pack he used are not known. Wygal and Naar[27] have determined these curves for a great number of glass bead packs and the ones used here are shown in Figures 1 and 2. Figure 1 shows both drainage and imbibition relative permeability relationships. The dashed line represents the compromise imbibition-drainage oil relative permeability (K_{ro}) used in the calculations. Since the drainage and imbitition wetting liquid curves differ very little, the drainage data were used for the water relative permeability (K_{rw}). It is interesting to note that the relative positions of the drainage and imbibition K_{ro} curves are reversed from those normally shown. Wygal's data show this to be consistently so for packs of glass beads. A discussion of this apparent anomalous behavior has been presented by Naar and Wygal.[28]

The synthesized capillary pressure curve is shown by the dashed line in Figure 2. It will be shown later that it is the slope of the capillary pressure curve that is important in the solution of the equations, hence the curve as drawn attemps to retain the slope of the drainage curve throughout most of the lower saturation region and the slope of the imbibition curve in most of the region of higher saturations. The value of $\bar{P}_c$ (that point on the capillary pressure curve where the slope becomes very steep, i.e., the value of P_c at approximately the irreducible water saturation) for Templeton's glass bead pack

was determined from the final distribution curve of his air-brine experiment and corrected for the difference in interfacial tension.

Run 3 - Unconsolidated Sand

The relative permeability curves for the unconsolidated sand, Figure 3, were calculated from the equations of Corey, Henderson, and Naar.[31]

For drainage:

$$K_{rw} = (1 - S)^3 \qquad \text{Where } S = \frac{S_o}{1 - S_{wi}} \tag{11}$$

$$K_{ro} = S^3 \tag{12}$$

For Imbibition:

$$K_{rw} = S^3 \qquad \text{Where } S = \frac{S_w - S_{wi}}{1 - S_{wi}} \tag{13}$$

$$K_{ro} = (1 - S)^3 \tag{14}$$

The curves as shown were calculated by Equations 11 and 12 for the lower half of the saturation range and by Equations 13 and 14 for the upper half.

The capillary pressure relationship was calculated from the empirical equation,

$$\underline{P}_c = .58753 - .17506\ S^* \pm 422.37\ (S^* - .5)^{10}$$

where $\underline{P}_c$ is the dimensionless capillary pressure, P_c/F_c and $S^* = \frac{S_w - S_{wi}}{1 - S_{wi}}$. The plus sign applies to the drainage portion of the curve and the minus sign to the imbibition portion. In order to plot Figure 4 the calculated $\underline{P}_c$ was converted to the

equivalent height of a brine-naphtha system by applying the proper density correction.

In this computer solution, of course, the calculation of relative permeabilities and capillary pressure was incorporated into the program.

Run 4 - Consolidated Sand

The consolidated sand model chosen was a Berea sandstone for which capillary pressure data were available. (Figure 5). The combined drainage-imbibition curve was obtained by altering the higher saturation portion of the curve as shown by the dashed line. Figure 6 is a replot of the curve with capillary pressure expressed as equivalent height.

Relative permeabilities were calculated using the equations of Corey, Naar and Henderson[31] for consolidation systems:

For drainage:

$$K_{rw} = (1 - S)^4$$

$$\text{Where } S = \frac{S_o}{1 - S_{wi}} \qquad (15)$$

$$K_{ro} = S^3 (2 - S) \qquad (16)$$

For imbibition:

$$K_{rw} = S^4$$

$$\text{Where } S = \frac{S_w - S_{wi}}{1 - S_{wi}} \qquad (17)$$

$$K_{ro} = (1 - 2S)^{3/2} (2 - (1 - 2S)^{.5}) \qquad (18)$$

The two sets of equations were used as in the unconsolidated system to produce the desired combination of drainage and imbibition. A plot of the calculated curves is shown in Figure 7.

Runs 5, 6, and 7 - Length Varied

In this series of calculations the system was assumed to be packed with a mixture of glass beads, 73.8% of which were 10-12 mesh and 26.2% of which were 120 to 140 mesh size, and packed according to the method of Naar and Wygal.[27] The relative permeability and capillary pressure data for this pack as shown by Naar and Wygal were used for the calculations checking Templeton's data and are shown in Figures 1 and 2. The only difference in these three calculations was the length of the system, varying from four feet in Run 5 to approximately eight feet in Run 6, to sixteen feet in Run 7. The capillary pressure curve of Figure 2 is shown replotted as equivalent height of the brine-naphtha system in Figure 8.

Runs 8 - 11 - Initial Saturation Varied

A pack identical to that of the fifth run was used in each of these calculations, and hence the relative permeability and capillary pressure curves of Figures 1 and 2 again apply. Initial saturation (including Run 5) varied in the following sequence: 0.25, 0.375, 0.50, 0.625 and 0.75.

RESULTS OF THE INVESTIGATION

Results of the calculations are the transient history of the saturation distribution for each of the systems as shown in Figures 9 through 19. In all curves the water saturation is plotted as the abscissa and distance from the bottom as the ordinate.

Figure 9 is a comparison of the calculated saturations with the experimental results of the brine-naphtha test of Templeton, et al.[9] This is designated as Run 1 in this paper.

Figure 10 is a similar comparison of the Templeton brine-Bradford crude test (Run 2).

An unconsolidated sand model was used for Run 3. Results of the calculations are shown in Figure 11 on which are shown points taken from the capillary pressure curve of Figure 4. The consolidated sand data (Run 4) are similarly plotted in Figure 12 along with points from the capillary pressure curve of Figure 6.

Figures 13, 14, and 15, are the results of Runs 5, 6, and 7 where the only variable in the system was its length.

The results of the final set of calculations, Runs 8, 9, 10, and 11, are shown in Figures 16, 17, 18, and 19. The only variable in these systems was the initial water saturation.

On all of these curves presented, the equilibrium data which were taken from the capillary pressure curve for the system are also plotted. How these points were located and their significance are discussed in the section, DISCUSSION

AND THEORETICAL CONSIDERATIONS.

The time required for the movement of various fractions of the total fluid moved at equilibrium are shown in Figures 22, 23, and 24.

Finally, the effect of (1) initial brine saturation and (2) the grouping [K/ϕL] on the time necessary to reach various fractions of the fluid moved to equilibrium are plotted in Figures 25 and 26.

THEORETICAL CONSIDERATIONS AND DISCUSSION OF RESULTS

Check on Experimental Work

Before entering into a detailed and lengthy program of calculations designed to investigate the transient counter-flow behavior of fluids in porous systems, it had to be ascertained that the synthesized relative permeability and capillary pressure relationships as used in the calculation procedure produced results representative of actual behavior. Fortunately, the experimental work of Templeton et al.[9] provided the necessary data for such a check. Comparisons of the computed results with those of Templeton are shown in Figures 9 and 10. The results in Figure 9 are those for a brine-haphtha system and those in Figure 10 for a brine-Bradford crude system. Considering the fact that the exact relative permeability and capillary pressure relationships were not known for this system, the agreement is good. The reason for the slight bulge that appears near the bottom of the experimentally determined curves is not readily apparent.

The work of Briggs[25] shows experimental results where a similar bulge appears near the top of the system and is much more severe than that shown by Templeton. He attributes this to a "hysteresis zone" in the system where it is alternately going through drainage and imbibition. Such behavior would be expected where the initial wetting liquid saturation is higher at the top of the system than at the bottom. Such a system was used in his experiments. If the initial saturation distribution was continuously decreasing from top to bottom, or even if a uniform initial saturation (re Templeton) were used, one would expect only a drainage zone in the top portion and an imbibition zone in the lower portion, the fraction of the total length exhibiting each condition being dependent upon the original saturation and material balance considerations. The bulge shown in the Templeton data which appears in approximately the same position in both runs could be attributed to a lower permeability section in the glass bead pack.

Additional Calculations and Discussions

One of the problems arising in calculations of this type is that of determining when equilibrium has been established or how close to equilibrium the calculations have progressed. Obviously if the computer were run long enough to establish that the saturation distribution was not changing and material balance was preserved, the equilibrium distribution would have been reached. However, in many of the runs this would have involved additional hours of computing time and

cost would have been prohibitive. Also, obviously, the final distribution should fall along that portion of the capillary pressure curve which maintains material balance about the initial saturation, i.e., equal amounts of wetting liquid must move into the imbibition zone and out of the drainage zone. Thus the equilibrium saturation distribution can be obtained by "skidding" the original capillary pressure curve vertically until material balance is preserved. Material balance was checked by planimetering the areas between the initial saturation line and the "skidded" capillary pressure curve. When the areas in the imbibition zone and drainage zone are equal, material balance is established. The equilibrium curve thus located is shown on each of the Figures 9 through 19. It appears from these figures that the calculations had essentially proceeded to equilibrium in Runs 1, 2, 3, 5, and 11, however the saturations were actually still changing at a very slow rate. It is obvious that equilibrium had not been reached in Runs 4, 6, 7, 8, 9, and 10.

Run 3

The calculations on the unconsolidated sand model as shown in Figure 11 required less computer time than most of the other runs because the calculations were carried through to completion without any need to make material balance adjustments as they progressed. This was expected, since the relative permeability and capillary pressure curves as calculated were symmetric about the original brine saturation value.

Run 4

The futility of attempting any laboratory gravity segregation experiments using consolidated systems is illustrated in Figure 12. Since the length of the system (121.9 cm) is only a small fraction of the length (over 2000 cm) of the capillary pressure curve of Figure 6, the equilibrium curve will be quite steep about the original brine saturation of 33% and hence only a small volume of fluid must be moved before equilibrium is attained. Even so, after 192 hours of elapsed time, the system which had a permeability of 1 Darcy (relatively high for consolidated sands) had not attained equilibrium.

Runs 5, 6, and 7

Analysis of Figures 13, 14, and 15 reveals that if the system is long enough a "stabilized zone" similar to that first observed by Terwilliger et al.[2] appears to form and move through the imbibition zone. There is very slight, if any, indication of the formation of such a zone in Figure 13 representing a system length of 4 feet, but in the 8 foot model* of Figure 14 the indication is somewhat more positive, and finally the shape of the zone definitely shows up in the 16 foot model of Figure 15. However, while the shape of the zone remains quite constant, in contrast with the conventional stabilized zone concept, the rate of advance is definitely

*It should be pointed out that the 8 foot length is very close to the total length of the capillary pressure curve where the capillary pressure is expressed as the equivalent height of the two liquid system.

not constant beyond a certain time. In order to better understand the significance of this, the following review is presented.

The continuity equation for vertical flow,

$$\frac{\partial S_w}{\partial t} = -\frac{1}{\phi}\frac{\partial u_w}{\partial x} \tag{19}$$

leads to the frontal advance or characteristic equation[1,7,8]

$$\left(\frac{\partial x}{\partial t}\right)_{S^*} = \frac{1}{\phi}\left(\frac{\partial u_w}{\partial S_w}\right)_{S^*} \tag{20}$$

where $\partial x/\partial t$ is the velocity of some saturation S^*. If a stabilized zone is formed Welge[6] has shown that the derivative is that of the highest saturation in the zone and can be determined graphically. Equation 12 derived earlier,

$$f(S) = \frac{u_w}{\phi} = \frac{K}{\phi}\left(\frac{1}{M_o} + \frac{1}{M_w}\right)^{-1}\cdot\left(\frac{dP_c}{dS_w}\cdot\frac{\partial S}{\partial X}\cdot\frac{\overline{P}_c}{L} + \frac{u_t}{KM_o} - (\rho_w - \rho_o)g\right) \tag{12}$$

leads to

$$u_w = K\left(\frac{1}{M_o} + \frac{1}{M_w}\right)^{-1}(\rho_o - \rho_w)\,g \tag{21}$$

if capillary pressure effects are ignored and $u_t = o$. Thus

$$\frac{\partial u_w}{\partial S} = K(\rho_o - \rho_w)\,g\,\frac{\partial}{\partial S}\left[\frac{1}{M_o}\quad\frac{1}{M_w}\right]^{-1} \tag{22}$$

and the Welge tangent rule can be applied to the plot of $\left(\frac{1}{M_o} + \frac{1}{M_w}\right)^{-1}$ vs. S_w and the slope determined. Figure 20 is such a plot for the systems under discussion with the tangent line drawn in. Even though the decrease in slope of the right end of the bell shaped curve is not apparent, the calculation is conventionally made as if the slope at this point suddenly decreased

to zero. The velocity, u_w is thus proportional to the secant AB and for this system was calculated to be 88 cm/day. It is apparent that a tangent cannot be drawn from the original brine saturation of 50% to the left side of the curve and hence no stabilized oil zone should be formed in the drainage portion of the system. Figures 13, 14, and 1[illegible] show this to be so.

The positions of the stabilized or "shock" zone at 8, 16, 32 and 64 hours are plotted in Figure 21 (which is an enlarged plot of the lower portion of the system) along with the computed positions at the same times. Interestingly, in spite of the fact that capillary forces were ignored in this simplified approach, the agreement is good up through 32 hours of elapsed time. The fact that the simplified calculations break down for a closed system such as this as equilibrium is approached is indicated by the relative positions of the two "fronts" after 64 hours. Since material balance has been preserved in the computer solutions and since no stabilized oil zone forms in the lower brine saturation region, the saturation distributions as calculated for that region would be the same as those determined by the Welge method except for the 64 hour curve which would have to be shifted to the left to preserve material balance. These results indicate that if a system is of sufficient length, the movement of the fluids is governed by gravitational effects throughout a fairly large percentage of its transient history.

Runs 8 - 11

The final set of calculations was performed for the purpose of evaluating the effect of initial brine saturation on the transient behavior of the system and especially to observe its effect on the time necessary to reach equilibrium. The transient behavior is illustrated in Figures 16, 17, 13, 18, and 19.

Because of the uncertainties involved in determining the exact time at which equilibrium is established, it was thought better to analyse the data from the standpoint of the time necessary to reach various "fractions of equilibrium." By this is meant the ratio of the volume of brine moved into the imbibition zone at any time to the volume moved into the zone at equilibrium. Because material balance must be preserved at all times this is also the ratio of the oil moved into the drainage zone to the total oil moved into that zone at equilibrium. These ratios were determined by planimetering and are tabulated in Table 3 for all runs and plotted in Figures 22, 23, and 24. Note that Runs 1, 2, 3, 5 and 11 all reached apparent equilibrium, but the exact path the curves take as equilibrium is approached is uncertain. Theoretically, the curves should approach unity on the vertical scale asymptotically.

From the curves of Figure 24, the time necessary to reach the 0.25, 0.50 and 0.75 fractions of equilibrium were determined and tabulated in Table 4. Figure 25 is a plot of $1/S_{wi}$ versus the time necessary to reach various stages of equilibrium as shown in Table 4. A

linear relationship is firmly established for each curve, however, the slope decreases as the fraction of equilibrium assumed is increased. The linear relationship is in contrast to the results of Briggs[25] who found that a double logarithmic plot was necessary to produce a straight line relationship between $1/S_{wi}$ and the time of equilibrium. This further emphasizes the advantage of working with the time necessary to reach various stages of equilibrium rather than the equilibrium time itself.

Additional Correlation

In addition to the initial water saturation variation, the other obvious parameter available from this study for correlation purposes is the $K/\phi L$ group. It will be recalled that the time parameter used in the calculations was $T = Kt/\phi L$ where K is the permeability of the system in darcys, t is the time in seconds, ϕ is the porosity, and L is the length of the system in centimeters. As shown by Table 5, a sufficient spread of the $K/\phi L$ values (with all other parameters essentially constant) was available from Runs 1, 3, 5, 6 and 7 for satisfactory correlation. Intuitively, one would expect a linear relationship between $\phi L/K$ and the time necessary to reach various fractions of equilibrium even though concommitant with variations in K are variations in capillary pressure-saturation relationships. Figure 26 shows this relationship between $(K/\phi L)^{-1}$ and the time necessary to reach various fractions of equilibrium to be indeed linear. As with the

$1/S_{wi}$ relationship, the slope of the lines became less as the assumed degree of equilibrium is increased.

SUMMARY AND CONCLUSIONS

In summary, the work has demonstrated that the calculation method of Douglas, Blair, and Wagner, as used in this study does satisfactorily predict the transient behavior of gravity counterflow in closed systems of fairly uniform initial saturation distribution. With modification, the method should be applicable to the practical problems of predicting behavior of natural reservoir systems operated under counterflow conditions. Examples of such problems are the recovery of inaccessible "attic oil" by injection of gas downstructure with subsequent counterflow, upward migration of natural gas being stored in aquifers, and water injection in upstructure wells in petroleum reservoirs.

The following conclusions can be drawn from the results of this investigation:

1. For systems whose length is greater than the length of the capillary pressure scale (where capillary pressure is expressed in equivalent height of fluids), a stabilized zone is formed and its movement is governed largely by gravitational forces throughout a large portion of its travel.
2. A linear relationship exists between $1/S_{wi}$ and the time necessary to reach various fractional degrees of equilibrium.
3. A linear relationship exists between $L\phi/K$ and the time necessary to reach various stages of equilibrium.

ACKNOWLEDGMENTS

The authors are appreciative of the help of Dr. Terry L. Loucks who aided immeasurably in the development of the computer programs. Acknowledgment is also due The Computer Center at the University of Pittsburgh whose facilities and equipment were used for all calculations. These facilities are partially supported by the National Science Foundation Grant No. G-11309.

BIBLIOGRAPHY

1. Buckley, S.E., and Leverett, M.C. "Mechanism of Fluid Displacement in Sands," Trans. A.I.M.E., 1942, 146, 117.

2. Terwilliger, P.L., Wilsey, L.E., Hall, H.N., Bridges, P.M., and Morse, R.A. "An Experimental and Theoretical Investigation of Gravity Drainage Performance," Trans. A.I.M.E. 1951, 192, 285.

3. Rapoport, L.A., and Leas, W.J. "Properties of Linear Waterfloods," Trans. A.I.M.E. 1953, 198, 139.

4. Jones-Parra, J., and Calhoun, J.C., Jr. "Computation of a Linear Flood by the Stabilized Zone Method," Trans. A.I.M.E. 1953, 198, 335.

5. Calhoun, J.C. "Fundamentals of Reservoir Engineering," University of Oklahoma Press 1953, 340.

6. Welge, H.J. "Simplified Method for Computing Oil Recovery by Gas or Water Drive," Trans. A.I.M.E. 1952, 195, 91.

7. Cardwell, W.T., Jr. "The Meaning of the Triple Value in Non-capillary Buckley-Leverett Theory," Trans. A.I.M.E. 1959, 179, 199.

8. Sheldon, J.W., Zondek, B., and Cardwell, W.T. "One-Dimensional, Incompressible, Noncapillary, Two-Phase Fluid Flow in a Porous Medium," Trans. A.I.M.E. 1959, 216, 290.

9. Templeton, E.E., Nielsen, R.F., and Stahl, C.D. "A Study of Counterflow Segregation," Society of Petroleum Engineers Journal, Vol. 2, No. 2, June 1962, 185.

10. Douglas, Jim, Blair, P.M., and Wagner, R.J. "Calculation of Linear Waterflood Behavior Including the Effects of Capillary Pressure," Trans. A.I.M.E. 1958, 213, 96.

11. McEwen, C.R. "A Numerical Solution of the Linear Displacement Equation with Capillary Pressure," Trans. A.I.M.E. 1959, 216, 412.

12. Fayers, F.J., and Sheldon, J.W. "The Effect of Capillary Pressure & Gravity on Two-Phase Fluid Flow in a Porous Medium," Trans. A.I.M.E. 1959, 216, 147.

13. Hovanessian, S.A., and Fayers, F.J. "Linear Water Flood with Gravity and Capillary Effects," Society of Petroleum Engineers Journal, Vol. 1, No. 1, March 1961, 32.

14. Katz, D.L. "Possibilities of Secondary Recovery for the Oklahoma City Wilcox Sand," Trans. A.I.M.E. 1942, 146, 28.

15. Stahl, R.F., Martin, W.A., Huntington, R.L. "Gravity Drainage of Liquid from Unconsolidated Wilcox Sand," Trans. A.I.M.E. 1943, 153, 138.

16. Lewis, J.O. "Gravity Drainage in Oil Fields," Trans. A.I.M.E. 1944, 155, 133.

17. Burtchaell, E.P. "Reservoir Performance of a High Relief Pool," Trans. A.I.M.E. 1949, 186, 171.

18. Elkins, L.F., French, R.W., and Glenn, W.E. "Lance Creek Sundance Reservoir Performance - A Unitized Pressure-Maintenance Project," Trans. A.I.M.E. 1949, 179, 222.

19. Buckley, et al. "Petroleum Conservation," A.I.M.E. publication, 1951.

20. Shreve, D.R., and Welch, L.W. "Gas Drive and Gravity Drainage for Pressure Maintenance Operations," Trans. A.I.M.E. 1956, 207, 136.

21. Martin, John C. "Some Mathematical Aspects of Two-Phase Flow with Applications to Flooding and Gravity Segregation Problems," Producers Monthly April 1958, 22.

22. Martin, John C. "Reservoir Analysis for Pressure Maintenance Operations Based on Complete Segregation of Mobile Fluids," Trans. A.I.M.E. 1958, 213, 220.

23. Cook, R.E. "Analysis of Gravity Segregation Performance During Natural Depletion," Society of Petroleum Engineers Journal, Sept. 1962, Vol. 2, No. 3, 261.

24. Gilmore, H. "Gas and Oil Segregation in Oilfield Reservoirs," Journal Institute of Petroleum, Dec. 1960, Vol. 46, No. 444, 1.

25. Briggs, J.R. "Countercurrent Gravity Segregation in Porous Media," Ph.D. Thesis, Dept. of Chemical Engineering, University of Michigan, 1963.

26. Douglas, Jim, Jr., Peaceman, D.W., Rachford, H.H., Jr. "A Method for Calculating Multi-Dimensional Immiscible Displacement," Trans. A.I.M.E. 1959, 216, 297.

27. Naar, J., and Wygal, R.J. "Physical and Flow Properties of Unconsolidated Aggregates. Application to Scaled Model Studies," Unpublished report of the Reservoir Mechanics Division of Gulf Research and Development Co.

28. Naar, J., and Wygal, R.J. "Structure and Properties of Unconsolidated Aggregates," Canadian Journal of Physics, 1962, 40, 218.

29. Peaceman, D.W., and Rachford, H.H., Jr. "The Numerical Solution of Parabolic and Elliptical Differential Equations," Journal Society of Ind. Appl. Math., 1955, 3, 28.

30. McCarty, D.G., and Barfield, E.C. "The Use of High Speed Computers for Predicting Flood-out Patterns," Trans. A.I.M.E. 1958, 213, 139.

31. Warren, J.E., and Cosgrove, J.J. "The Effective Mobility Ratio for Immiscible Fluids," Presented at Twenty-fourth Technical Conference on Petroleum Production, The Pennsylvania State University, 1963.

32. Fulton, P.F., "Calculation of Transient Behavior of Gravity Counterflow Segregation," Ph.D. Thesis, Department of Petroleum and Natural Gas Engr., The Pennsylvania State University, 1964.

APPENDIX A

Details of Calculation of Rate of Advance of Stabilized Zone

$$u_w = K\left(\rho_o - \rho_w\right)g \cdot \frac{\partial}{\partial S_w}\left(\frac{1}{M_o} + \frac{1}{M_w}\right)^{-1}$$

From Figure 32

$$\frac{\partial}{\partial S_w}\left(\frac{1}{M_o} + \frac{1}{M_w}\right)^{-1} = -\frac{0.051}{.875 - .5} = -0.136$$

$$\frac{\partial u_w}{\partial S_w} = -0.136\, K\left(\rho_o - \rho_w\right)g$$

$$= -0.136 \cdot 4.5 \cdot 6.3\ (.72-1.01) \cdot 62.4/144$$

$$= .485$$

$$\frac{\partial x}{\partial t} = \frac{1}{\phi}\frac{\partial u_s}{\partial S_w}$$

$$= \frac{.485}{.168} = 2.88 \text{ feet per day}$$

$$= 88 \text{ cm./day}$$

Where 6.3 is the correction factor for converting permeability in darcies to "perms."

TABLE 1

PROPERTIES OF POROUS SYSTEMS

Run	K Darcys	Φ	L cm.	Initial S_w	P_c Atmos.	Fluids	Description
1	28.2	.369	121.9	.62	.041	Brine-Naphtha	Templeton-Glass beads
2	28.2	.369	121.9	.43	.060	Brine-Bradford Crude	Templeton-Glass beads
3	15.0	.36	121.9	.525	.574	Brine-Naphtha	Unconsolidated sand
4	1.0	.22	121.9	.335	.070	Brine-Naphtha	Consolidated sand
5	4.5	.168	121.9	.50	.070	Brine-Naphtha	Ballotini glass beads
6	4.5	.168	248	.50	.070	Brine-Naphtha	Ballotini glass beads
7	4.5	.168	488	.50	.070	Brine-Naphtha	Ballotini glass beads
8	4.5	.168	121.9	.25	.070	Brine-Naphtha	Ballotini glass beads
9	4.5	.168	121.9	.375	.070	Brine-Naphtha	Ballotini glass beads
10	4.5	.168	121.9	.625	.070	Brine-Naphtha	Ballotini glass beads
11	4.5	.168	121.9	.75	.070	Brine-Naphtha	Ballotini glass beads

TABLE 2

PROPERTIES OF FLUIDS

Fluid	Density gm/cc.	Viscosity cp.	Interfacial Tension With Brine Dynes/cm.
Brine	1.01	1.02	-
Naphtha	.72	.52	41
Bradford crude	.80	4.33	35

TABLE 3

RATIO OF LIQUID MOVED AT VARIOUS TIMES TO TOTAL LIQUID MOVED AT EQUILIBRIUM

Time Hrs.	Ratio: Run 1	3	5	6	7	8	9	10	11
.5	.184	.20	.057	.025	.012	.015	.036	.09	.199
2	.626	-	.139	.079	.038	.059	.122	.302	.43
4	.854	.74	.358	.169	.068	.120	.212	.605	.686
6	.648	.748	-	-	-	-	-	-	-
9	-	.807	.628	.293	.144	.246	.362	.822	.845
14	1.0	-	-	-	-	-	-	-	-
16	-	.904	.883	.554	.270	.508	.606	.945	1.0
32	-	1.0	1.0	.819	.513	-	-	-	-
64	-	-	-	-	.794	-	-	-	-

TABLE 4

TIME REQUIRED TO REACH VARIOUS STAGES OF EQUILIBRIUM AS FUNCTION OF INITIAL S_w

S_{wi}	Ratio:	Time (Hrs.) .25	.50	.75
.25		9.25	16	37.5
.375		5.0	12	22.5
.50		3.0	5.25	11
.625		1.5	3.5	6.75
.75		.5	2	4.5

TABLE 5

TIME REQUIRED TO REACH VARIOUS STAGES OF EQUILIBRIUM AS FUNCTION OF K/Øl

K/Øl	Ratio:	Time (Hrs.) .25	.50	.75
.055		32.5	32	65
.11		5.25	14.5	26.5
.22		2	6	11
.34		1	2	6
.63		.5	-	4.5

FIGURE 1

RELATIVE PERMEABILITY CURVES
BINARY MIXTURE OF GLASS BEADS

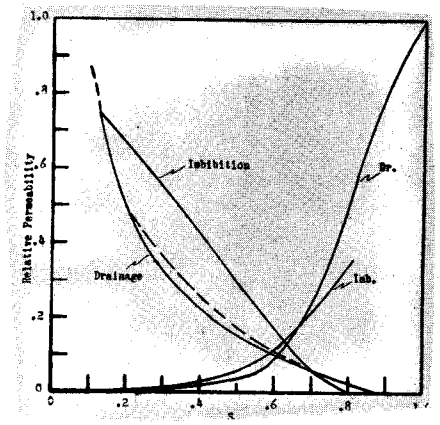

FIGURE 2

CAPILLARY PRESSURE CURVES
BINARY MIXTURE

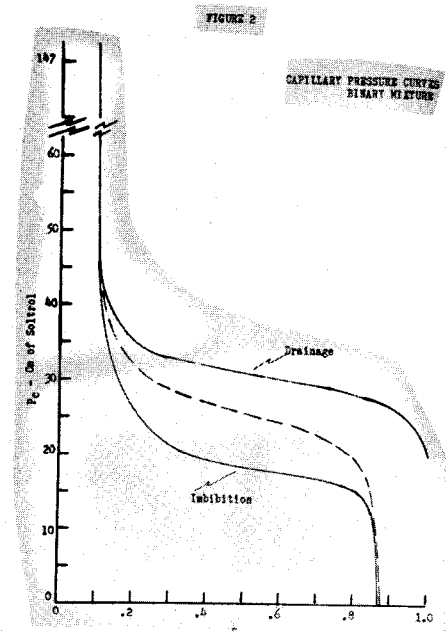

FIGURE 3

RELATIVE PERMEABILITY RE COREY, ET AL
UNCONSOLIDATED SAND

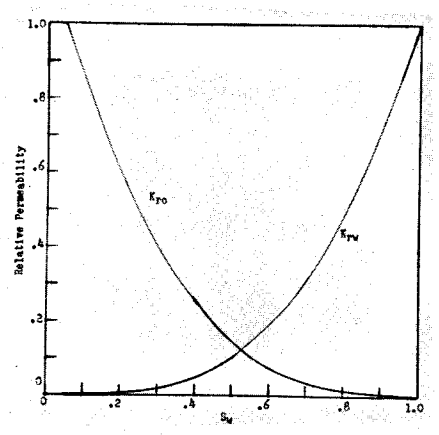

FIGURE 4

P_c (HEIGHT) VS. S_w
UNCONSOLIDATED SAND

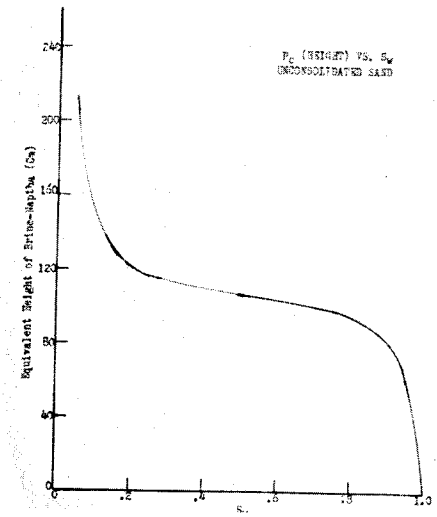

FIGURE 5

CAPILLARY PRESSURE CURVE FOR
CONSOLIDATED SAND

Air-Soltrol System
σ =23.5 dynes/cm

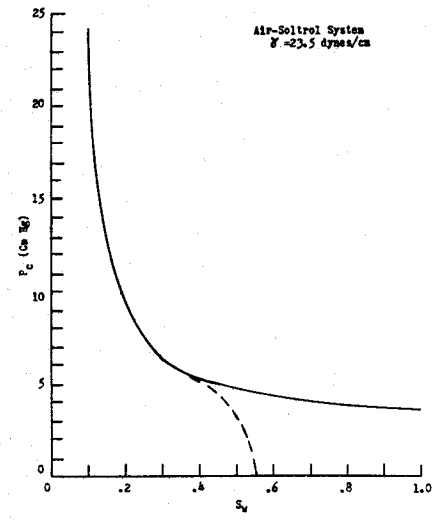

FIGURE 6

P_c (HEIGHT) VS S_w
CONSOLIDATED SAND

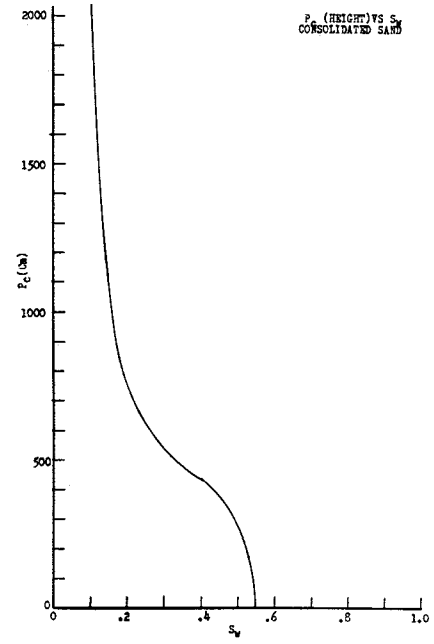

FIGURE 7

RELATIVE PERMEABILITY RE COREY, ET AL
CONSOLIDATED SAND

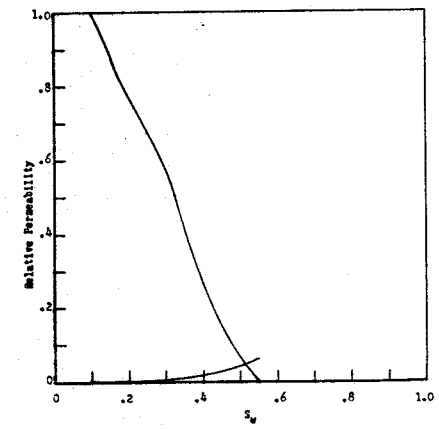

FIGURE 8

CAPILLARY PRESSURE CURVE FOR
NAAR-WYGAL GLASS BEADS CONVERTED
TO EQUIVALENT HEIGHT OF BRINE-NAPHTHA

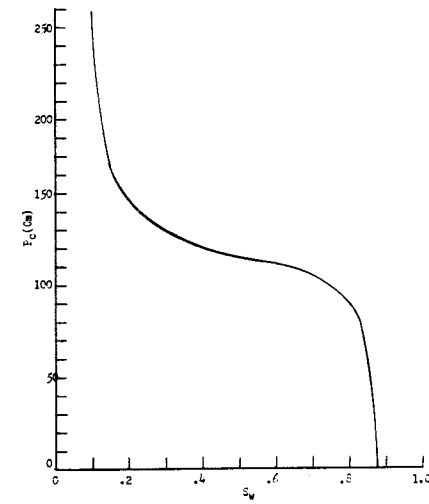

FIGURE 9

RUN 1 - CHECK ON TEMPLETON'S BRINE-NAPHTHA EXPERIMENT

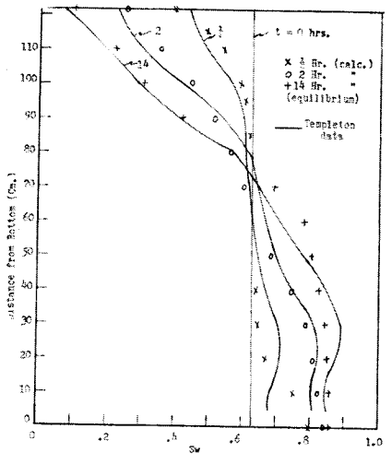

FIGURE 10

RUN 2 - CHECK ON TEMPLETON'S BRINE-CRUDE EXPERIMENTS

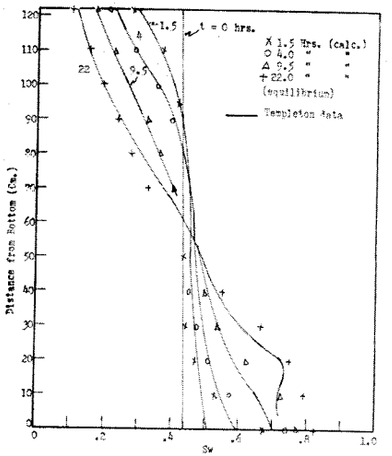

FIGURE 11

RUN 3 - UNCONSOLIDATED SAND

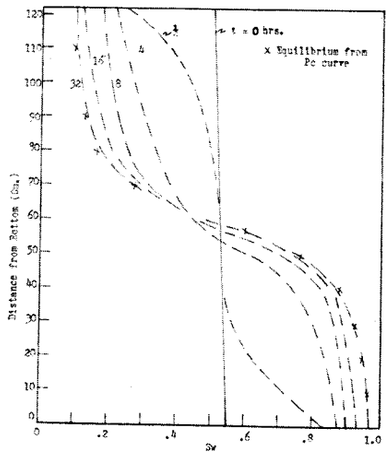

FIGURE 12

RUN 4 CONSOLIDATED SAND

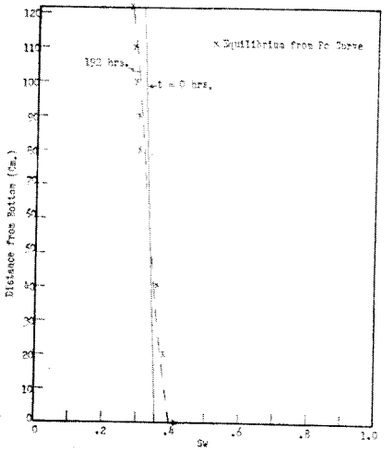

FIGURE 13

RUN 5 : LENGTH = 4 Ft.
S_{wi} = .50

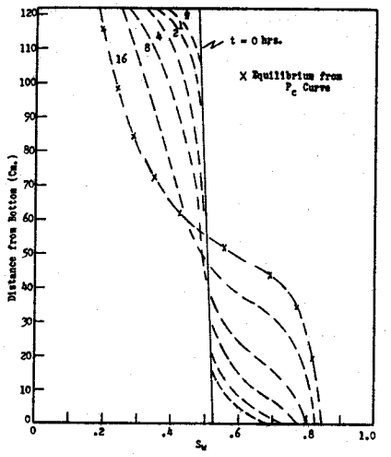

FIGURE 14

RUN 6 : LENGTH = 8'
S_{wi} = .50

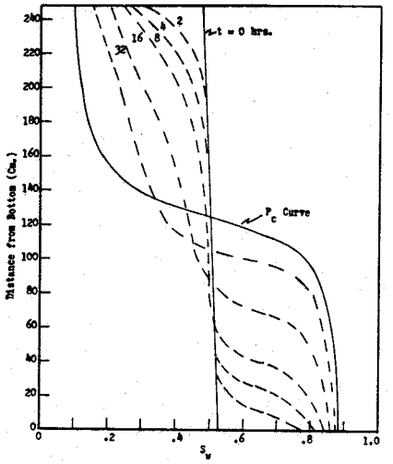

FIGURE 15

RUN 7 : LENGTH = 16'
S_{wi} = .5

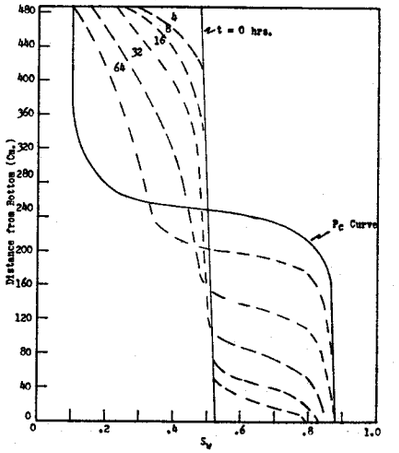

FIGURE 16

RUN 8 : S_{wi} = .25
Length = 4'

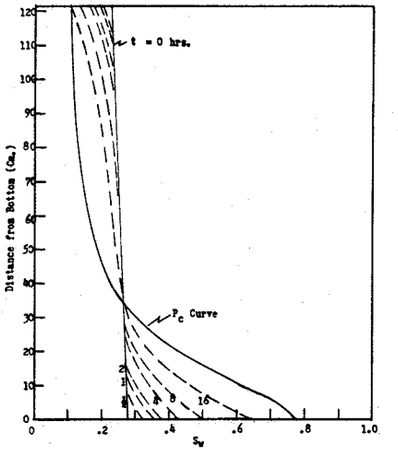

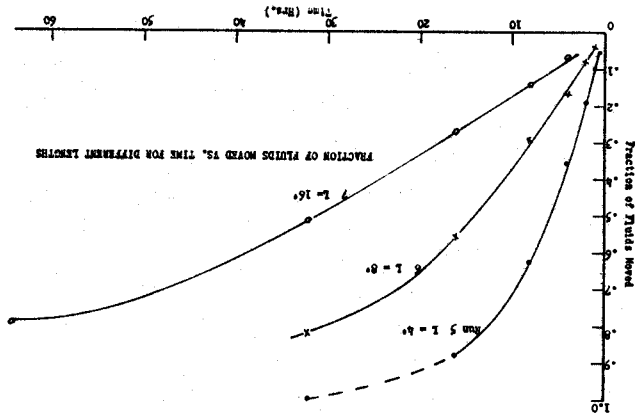

FRACTION OF FLUIDS MOVED VS. TIME FOR DIFFERENT LENGTHS

FIGURE 23

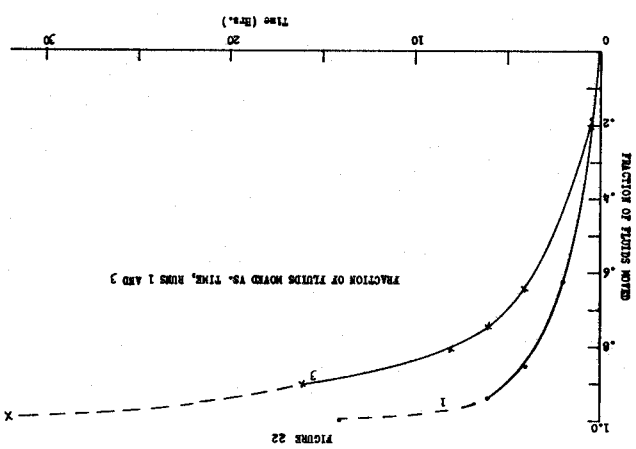

FRACTION OF FLUIDS MOVED VS. TIME, RUNS 1 AND 3

FIGURE 22

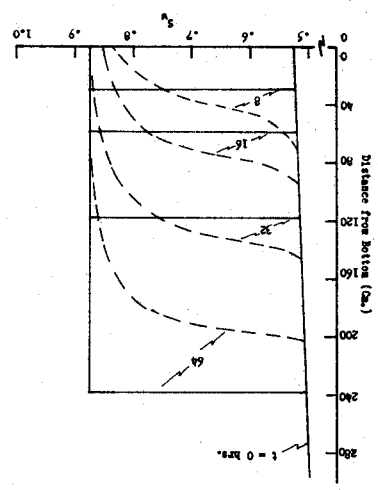

COMPARISON OF SATURATION DISTRIBUTION AS CALCULATED WITH THAT DETERMINED BY RADIO TRACKER NOLE

FIGURE 21

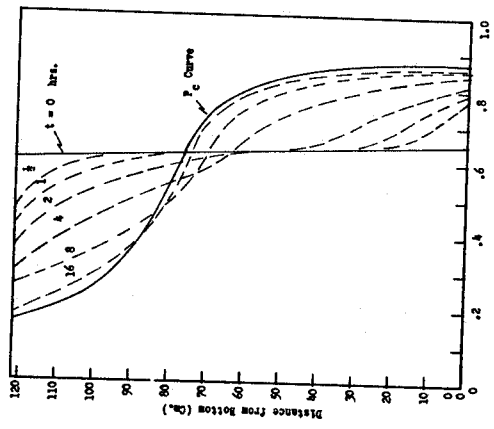

RUN 10 : S_{wi} = .625
Length = 4'

FIGURE 18

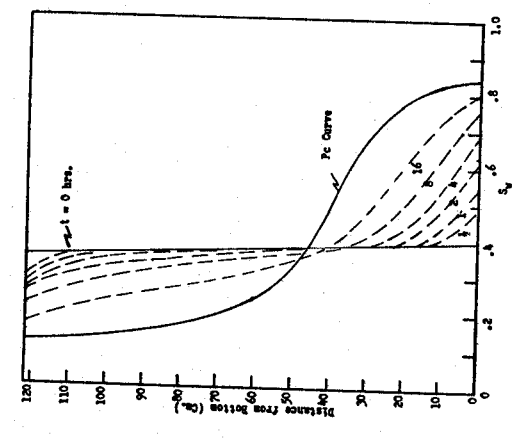

RUN 9 : S_{wi} = .395
Length = 4'

FIGURE 17

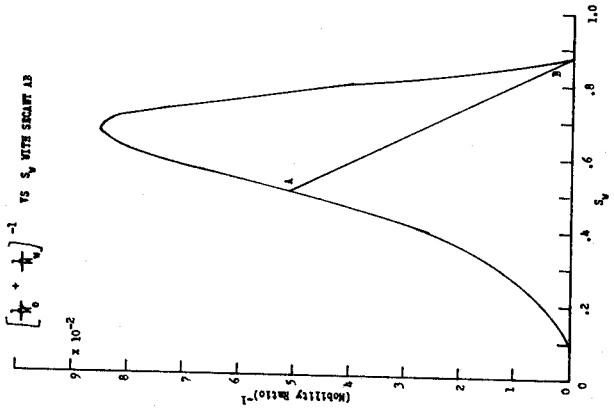

$\left[\frac{1}{k_o} + \frac{1}{k_w}\right]^{-1}$ VS S_w WITH SECANT AB

FIGURE 20

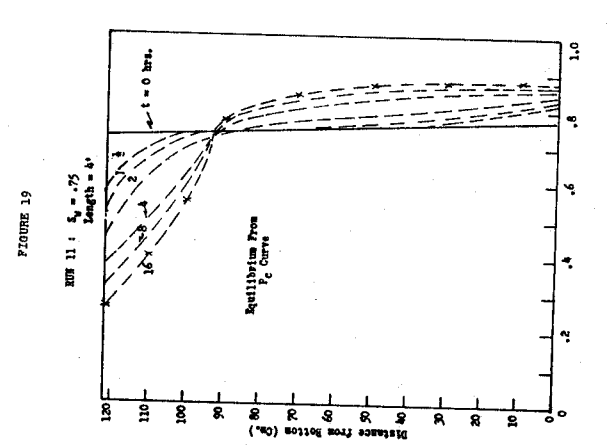

RUN 11 : S_{wi} = .75
Length = 4'

FIGURE 19

FIGURE 24

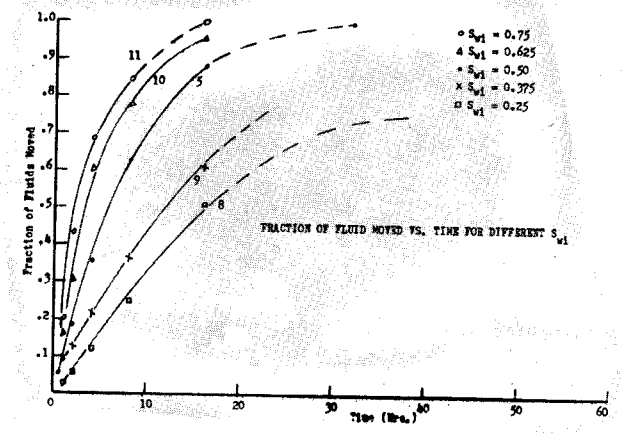

FIGURE 25

EFFECT OF INITIAL S_w ON TIME TO REACH VARIOUS FRACTIONS OF EQUILIBRIUM

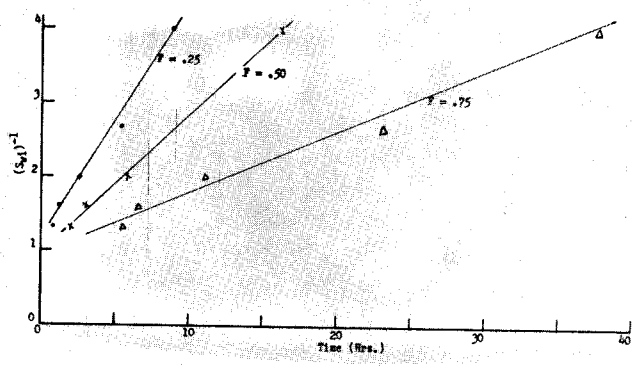

FIGURE 26

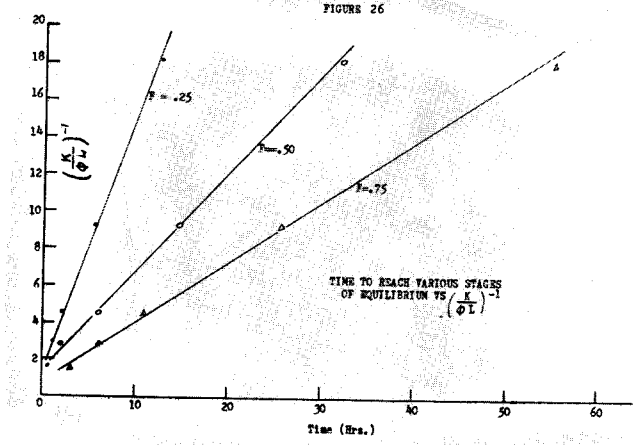

THE ANALYTICAL SOLUTION OF A SEMI-DISCRETE FORM OF THE DARCY-CONTINUITY EQUATION *

by

Quon, D., Dranchuk, P.M. and Darsi, C.R.

ABSTRACT

The Darcy-Continuity equation may be transformed into a matrix differential equation by discretizing the space variables. For the particular case where the variation of viscosity and compressibility with pressure is small the resulting equation is linear. Therefore an analytical solution may be obtained through the use of some operational methods of linear algebra. The solution gives the pressures as functions of time at chosen discrete points in the reservoir. The resulting pressure vector may be calculated explicitly in terms of a matrix, which describes the spatial distribution of reservoir properties, and vectors describing the initial and boundary conditions.

This method has two important advantages, namely, that the resulting solutions appear in closed form and that the principle of superposition may be applied to them. However, it involves the manipulation of matrices and as a result becomes somewhat cumbersome when the pressure vector contains more than a few hundred elements. Despite this shortcoming the method is suitable for application to a large class of two-dimensional reservoir problems.

In order to demonstrate the principles involved, a problem dealing with a forty element pressure vector is presented.

---

* Contribution from the Department of Chemical and Petroleum Engineering, University of Alberta, Edmonton, Alberta.

INTRODUCTION

Whenever available, analytical solutions are generally preferred to numerical ones for a number of well-known reasons - the errors can be more easily estimated and controlled; better insight is provided into the structure of the problem; and in the case of initial value problems, the analytical solution does not require intermediate calculations.

Unfortunately, rigorous analytical solutions to the Darcy Continuity equation have been limited to homogeneous, one-dimensional reservoirs(1),(2).

In the present paper, the space variables in the Darcy-Continuity equation are discretized, giving rise to a matrix differential equation. The latter is then integrated analytically. This semi-analytical approach allows any spatial variation in reservoir properties to be taken into account. Furthermore, many two-dimensional problems can be handled in this manner.

MATHEMATICAL DEVELOPMENT

The Darcy-Continuity equation for a volumetric two-dimensional reservoir R, bounded by a closed curve C, may be written as:

$$\frac{\partial}{\partial t}(\phi\, hS_f\rho) = \frac{\partial}{\partial x}\left(\frac{kh\rho}{\mu}\frac{\partial p}{\partial x}\right) + \frac{\partial}{\partial y}\left(\frac{kh\rho}{\mu}\frac{\partial p}{\partial y}\right) - \omega(x,y,t) \qquad (1)$$

with typical boundary conditions

$$\text{I.C.} \qquad p = p_o \quad \text{at} \quad t = 0 \qquad x,y \in R$$

$$\text{B.C.} \qquad \frac{\partial p}{\partial r} = 0 \quad \text{on } C \qquad t \geq 0$$

where r is the direction normal to C.

The following conditions are also commonly encountered:

1) ϕ, h, S_f and k are functions of position only.

2) The behavior of the fluid is described by:

$$c = \frac{1}{\rho}\frac{\partial \rho}{\partial p}$$

3) Both c and μ can be considered constant.

Under these conditions, Dranchuk and Quon(3) have shown that equation (1) can be linearized according to either of two schemes;

1) If cp<<<1.0, then linearization by deletion is warranted, resulting in:

$$\phi h S_f c \frac{\partial p}{\partial t} = \frac{\partial}{\partial x}\left(\frac{kh}{\mu}\frac{\partial p}{\partial x}\right) + \frac{\partial}{\partial y}\left(\frac{kh}{\mu}\frac{\partial p}{\partial y}\right) - \frac{\omega}{\rho} \qquad (2)$$

2) Otherwise, linearization by transformation of variables is suggested. Let

$$\pi = \frac{1}{c}(e^{cp} - 1) \qquad (3)$$

This substitution, after suitable arithmetic operations on equation (1), will give:

$$\phi h S_f c \frac{\partial \pi}{\partial t} = \frac{\partial}{\partial x}\left(\frac{kh}{\mu}\frac{\partial \pi}{\partial x}\right) + \frac{\partial}{\partial y}\left(\frac{kh}{\mu}\frac{\partial \pi}{\partial y}\right) - \frac{\omega}{\rho_o} \qquad (4)$$

where ρ_o is the density at p = 0.

This procedure is, of course, useful only when the transformation of variables does not introduce non-linearities into the boundary conditions.

Whatever scheme is chosen, equations (2) and (4) have the same form; and subsequent derivations will deal only with the latter.

Equation (4) may be converted into semi-discrete form by discretization of the space variables only, using a procedure described by Varga(4). The method is illustrated for a hypothetical reservoir, which is of the shape shown in Figure 1. Enough points in the reservoir - in this case, forty - are selected in order to provide a sufficiently detailed spatial definition of the geometry and to adequately describe the positional variation in property values. Although in the example, the points form a square grid pattern, other patterns might well be used. Elemental areas corresponding to each point are constructed by making the boundary between two adjacent points a straight side which is normal to and bisects the line segment joining the points. Elemental areas on the boundary of the reservoir may be irregular shaped but all interior elemental areas are polygons.

Mathematically, the first step is to multiply both sides of equation (4) by dx·dy to give:

$$(\phi\ h\ S_f\ c\ dx{\cdot}dy)\ \frac{\partial \pi}{\partial t} = \left\{\frac{\partial}{\partial x}\left(\frac{kh}{\mu}\ \frac{\partial \pi}{\partial x}\right) + \frac{\partial}{\partial y}\left(\frac{kh}{\mu}\ \frac{\partial \pi}{\partial y}\right)\right\} dx{\cdot}dy$$

$$- \ q{\cdot}dx{\cdot}dy \qquad (5)$$

where

$$q = \omega/\rho_o \qquad (6)$$

For the i^{th} elemental area, which may be designated as r_i, a double integration, term by term, on equation (5), gives the following ordinary differential equation.

$$\left(\iint_{r_i} \phi \, h \, S_f \, c \, dx \cdot dy \right) \frac{d\pi_i}{dt} = \iint_{r_i} \left\{ \frac{\partial}{\partial x} \left(\frac{kh}{\mu} \frac{\partial \pi}{\partial x} \right) + \frac{\partial}{\partial y} \left(\frac{kh}{\mu} \frac{\partial \pi}{\partial y} \right) \right\} dx \cdot dy - \iint_{r_i} q \cdot dx \cdot dy \qquad (7)$$

There is no problem in evaluating the integral on the L.H.S. and the last term on the R.H.S. to the desired degree of accuracy. The remaining integral is handled, using Green's Theorem, i.e.

$$\iint_{r_i} \left(\frac{\partial S}{\partial x} - \frac{\partial T}{\partial y} \right) dx \cdot dy = \int_{c_i} (T dx + S dy) \qquad (8)$$

where the integral on the R.H.S. is simply the line integral along c_i, the boundary of the area r_i. This procedure is illustrated in Appendix A.

The set of N first order ordinary differential equations, one corresponding to each elemental area, may be written compactly in matrix form as:

$$\underline{G} \frac{d\underline{\pi}}{dt} = \underline{K} \, \underline{\pi} + \underline{s(t)} \qquad (9)$$

where $\underline{G}$ is a diagonal, positive definite matrix, whose entries represent the values of the integral for each area given on the L.H.S. of equation (7); $\underline{\pi}$ is the potential vector, in this case a modified pressure vector; $\underline{K}$ is a diagonally dominant, symmetric, negative definite matrix, derived by evaluating the line integral for each area, given by the first term on the R.H.S. of equation (7);

$\underline{s(t)}$ is a vector incorporating all the boundary conditions, including the specified withdrawal of fluid from certain designated elemental areas.

Under these conditions, equation (9) may be integrated analytically (See Appendix B) to give:

$$\underline{\pi} = \underline{G}^{-\frac{1}{2}}\ \underline{Q}\ \underline{E(t)}\ \underline{Q}^{T}\ \underline{G}^{\frac{1}{2}} \left[\underline{\pi}^{(0)} + \int_{0}^{t} \underline{G}^{-\frac{1}{2}}\ \underline{Q}\ \underline{E^{-1}(\sigma)}\ \underline{Q}^{T}\ \underline{G}^{-\frac{1}{2}}\ \underline{s(\sigma)}\ d\sigma \right] \tag{10}$$

where

$\underline{Q}$ is a matrix consisting of the normalized eigen vectors of the matrix $(\underline{G}^{-\frac{1}{2}}\ \underline{K}\ \underline{G}^{-\frac{1}{2}})$ arranged columnwise.

$E(t)$ is a diagonal matrix whose entries are $e^{\lambda_i t}$ where λ_i is the i^{th} eigen value of the matrix $(\underline{G}^{-\frac{1}{2}}\ \underline{K}\ \underline{G}^{-\frac{1}{2}})$

$\underline{\pi}^{(0)}$ is the value of the modified pressure vector at $t = 0$

σ is merely a dummy variable.

Since $\underline{K}$ is symmetric, and $\underline{G}^{-\frac{1}{2}}$ is diagonal and non-singular, then the matrix $(\underline{G}^{-\frac{1}{2}}\underline{K}\ \underline{G}^{-\frac{1}{2}})$ must also be symmetric and will have real distinct eigen values and real, orthogonal eigen vectors.

It should be noted that while equation (10) is an exact solution to equation (9), the latter is only a first order correct approximation to the original equation (4).

The main computational problem, of course, is in evaluating the eigen values and eigen vectors of the matrix $(\underline{G}^{-\frac{1}{2}}\ \underline{K}\ \underline{G}^{-\frac{1}{2}})$. In the example problem, involving a 40 x 40 matrix, determination of all the eigen values and eigen vectors, using Householder's method(5), required about 2 minutes of IBM 7040 computing time. It has been

estimated by the Computing Center, University of Alberta, that a 100 x 100 matrix would require about 5 minutes of IBM 7090 time. From these considerations, the analytical approach is probably feasible for reservoirs which can be adequately defined by several hundred grid points.

The utility of the semi-analytical solution rests in the fact that once the geometry of the reservoir and its properties have been defined, then the solution vector $\underline{\pi}$, which gives the modified pressure distribution in the reservoir, can be expressed explicitly in matrix form for any initial or boundary conditions. Thus, any production policy can be evaluated simply, using the principle of superposition which follows directly from the matrix solution. A closed form solution, of course, has other advantages. Problems of stability and truncation errors in discretizing the time variable do not arise.

EXAMPLE PROBLEM

The geometry of a hypothetical reservoir is given in Figure 1, the distance between grid points being 0.25 mile.

Production is from 3 wells as follows:

Elemental Area No.	Production Std.bbl./day
8	100
19	100
25	200

The ϕh or porosity-formation thickness distribution in the reservoir is given in Table 1; the kh or permeability-formation thickness distribution in Table 2.

The fluid saturation S_f is assumed to be unity throughout. The compressibility factor c is 1.25×10^{-6} psi^{-1} and the viscosity μ is 2.4 centipoises; both are assumed to be independent of pressure.

The initial pressure is assumed to be uniform at 1500 psia. The pressure distribution, at the end of 280 days, is shown in Table 3. The total production as calculated from the withdrawal rates is 1,120,000 std. bbls. while that calculated from a material balance on the reservoir is 1,119,000 std. bbls. The close agreement is a check on the consistency of the internal arithmetic.

CONCLUSION

A semi-analytical solution has been developed for a volumetric two-dimensional petroleum reservoir in which the compressibility and the viscosity are essentially independent of pressure. This approach is capable of handling a much wider range of cases than the classical analytical approach.

NOMENCLATURE

Scalars

c	oil compressibility factor
h	formation thickness
k	formation permeability
p	pressure
q	volumetric rate of withdrawal of oil (under standard conditions) per unit area of reservoir
S_f	fluid saturation
t	time
ω	mass rate of withdrawal of oil per unit area of reservoir
λ	eigen value of matrix $\underline{B}$
μ	fluid viscosity
π	modified pressure, defined by equation (3)
ρ	density of oil
σ	dummy variable
ϕ	formation volume factor

Vectors, Matrices

$\underline{a}$	defined by equation (A16)
$\underline{r}$	eigen vector of matrix $\underline{B}$
$\underline{s(t)}$	boundary condition vector
$\underline{s^*(t)}$	modified boundary condition vector, defined by equation (A7)
$\underline{u}$	defined by equation (A4)
$\underline{v}$	defined by equation (A9)
$\underline{\pi}$	modified pressure vector

$\underline{B}$	defined by equation (A6)
$\underline{E(t)}$	diagonal matrix, whose entries are $e^{\lambda_i t}$
$\underline{G}$	diagonal matrix used to describe the volumetric capacity of the reservoir.
$\underline{K}$	rate coefficient matrix
$\underline{P}$	diagonal matrix of eigen values of $\underline{B}$
$\underline{Q}$	matrix of eigen vectors of $\underline{B}$, arranged columnwise

REFERENCES

1. Muskat, M., "The Flow of Homogeneous Fluids Through Porous Media", p. 630, McGraw-Hill Book Company Inc., New York, 1937.

2. Van Everdingen, A.F. and Hurst, W., "The Application of the Laplace Transformation to Flow Problems in Reservoirs", AIME Trans., 186, 305 (1949).

3. Dranchuk, P.M. and Quon, D., "Analysis of the Darcy-Continuity Equation", presented to the 17th Annual Meeting of the Petroleum Society of CIM, May 6th, 1966.

4. Varga, R.S., "Matrix Iterative Analysis", p. 181, Prentice-Hall Inc., Englewood Cliffs, N.J., 1962.

5. Wilkinson, J.H., Computer J., 3, 23, (1961).

APPENDIX A

Elemental area has odd-shaped boundaries, with two of its sides forming part of the boundary of the reservoir as shown below

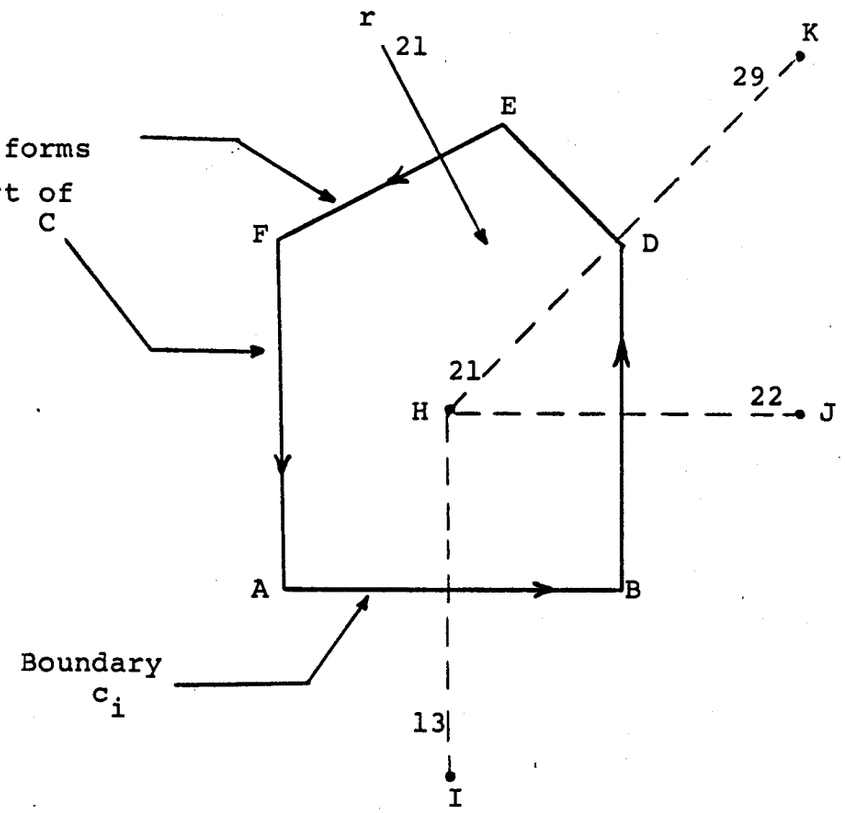

The line integral is evaluated in a counter clockwise direction, starting at point A.

$$v_{21}c\frac{d\pi_{21}}{dt} = \left(\frac{\left(\frac{kh}{\mu}\right)_{13} + \left(\frac{kh}{\mu}\right)_{21}}{2}\right)\left(\frac{\pi_{13} - \pi_{21}}{\overline{IH}}\right)\overline{AB} \qquad \text{Path A to B}$$

$$+ \left(\frac{\left(\frac{kh}{\mu}\right)_{22} + \left(\frac{kh}{\mu}\right)_{21}}{2}\right)\left(\frac{\pi_{22} - \pi_{21}}{\overline{JH}}\right)\overline{BD} \qquad \text{B to D}$$

$$+ \left(\frac{\left(\frac{kh}{\mu}\right)_{29} + \left(\frac{kh}{\mu}\right)_{21}}{2}\right)\left(\frac{\pi_{29} - \pi_{21}}{\overline{HK}}\right)\overline{DE} \qquad \text{D to E}$$

$$+ 0 \qquad \text{E to F}$$

$$+ 0 \qquad \text{F to A}$$

$$+ Q_{21} \qquad \text{(A1)}$$

where

$$V_{21} = \iint_{r_{21}} \phi\, h\, S_f\, dx\, dy \qquad \text{(A2)}$$

Q_{21} = instantaneous withdrawal of oil in std. bbls./day

APPENDIX B

We are required to solve the matrix differential equation

$$\underline{G}\,\frac{d\underline{\pi}}{dt} = \underline{K}\,\underline{\pi} + \underline{s(t)} \tag{A3}$$

where $\underline{G}$ is a diagonal, positive definite matrix of order N

$\underline{K}$ is a real, symmetric matrix of order N

Let

$$\underline{\pi} = \underline{G}^{-\frac{1}{2}}\,\underline{u} \tag{A4}$$

Replacing in (A3) and premultiplying both sides by $\underline{G}^{-\frac{1}{2}}$, we get

$$\frac{d\underline{u}}{dt} = \underline{G}^{-\frac{1}{2}}\,\underline{K}\,\underline{G}^{-\frac{1}{2}}\,\underline{u} + \underline{G}^{-\frac{1}{2}}\,\underline{s(t)} \tag{A5}$$

Let

$$\underline{B} = \underline{G}^{-\frac{1}{2}}\,\underline{K}\,\underline{G}^{-\frac{1}{2}} \tag{A6}$$

and

$$\underline{s^*(t)} = \underline{G}^{-\frac{1}{2}}\,\underline{s(t)} \tag{A7}$$

Therefore,

$$\frac{d\underline{u}}{dt} = \underline{B}\,\underline{u} + \underline{s^*(t)} \tag{A8}$$

Since both $\underline{K}$ and $\underline{G}^{-\frac{1}{2}}$ are symmetric, it can be readily shown, using the reversal rule for transpose matrices, that $\underline{B}$ is also symmetric.

Let

$$\underline{u} = \underline{Q}\,\underline{v} \tag{A9}$$

where

$$\underline{Q} = (\underline{r}_1 \cdots \underline{r}_N) \tag{A10}$$

and $\underline{r}_1 \cdots \underline{r}_N$ are the normalized eigen vectors of $\underline{B}$.

Replacing (A9) in (A8) and premultiplying both sides by $\underline{Q}^{-1}$ gives:

$$\frac{d\underline{v}}{dt} = \underline{Q}^{-1}\,\underline{B}\,\underline{Q}\,\underline{v} + \underline{Q}^{-1}\,\underline{s^*(t)} \qquad \text{(A11)}$$

However, the operation $\underline{Q}^{-1}\,\underline{B}\,\underline{Q}$ can be shown* to be a similarity transformation which produces a diagonal matrix, which may be called $\underline{P}$ whose entries λ_i are the eigen values of $\underline{B}$. Furthermore, since $\underline{B}$ is symmetric, all its eigen vectors are orthogonal. Hence,

$$\underline{Q}^{-1} = \underline{Q}^{T} \qquad \text{(A12)}$$

Equation (A11) now becomes

$$\frac{d\underline{v}}{dt} = \underline{P}\,\underline{v} + \underline{Q}^{T}\,\underline{s^*(t)} \qquad \text{(A13)}$$

and the individual equations may be written as:

$$\frac{dv_i}{dt} = \lambda_i v_i + \underline{r}_i^{T}\,\underline{s^*(t)} \qquad \text{(A14)}$$

Thus, we have a set of first order linear differential equations which have been effectively decoupled from each other and may be solved separately as follows:

$$v_i = e^{\lambda_i t}\left(v_i^{(0)} + \int_0^t e^{-\lambda_i \sigma}\,\underline{r}_i^{T}\,s^*(\sigma)\,d\sigma\right) \qquad \text{(A15)}$$

where $v_i^{(0)}$ is the value of v_i at $t = 0$.

---

* Lapidus, L., "Digital Computation for Chemical Engineers", p. 215, McGraw-Hill, New York, (1953).

Let

$$\underline{a} = \begin{bmatrix} \int_0^t e^{-\lambda_i \sigma} \, \underline{r}_i^T \, \underline{s^*(\sigma)} \, d\sigma \\ \vdots \\ \int_0^t e^{-\lambda_N \sigma} \, \underline{r}_N^T \, \underline{s^*(\sigma)} \, d\sigma \end{bmatrix} = \int_0^t \underline{E^{-1}(\sigma)} \, \underline{Q}^T \, \underline{s^*(\sigma)} d\sigma \tag{A16}$$

Then

$$\underline{v} = \underline{E(t)} \, (\underline{v}^{(0)} + \underline{a}) \tag{A17}$$

where $\underline{E(t)}$ is a diagonal matrix whose entries are $e^{\lambda_i t}$

However,

$$\underline{\pi} = \underline{G}^{-\frac{1}{2}} \, \underline{u} = \underline{G}^{-\frac{1}{2}} \, \underline{Q} \, \underline{v} \tag{A18}$$

and

$$\underline{v}^{(0)} = \underline{Q}^T \, \underline{G}^{\frac{1}{2}} \, \underline{\pi}^{(0)} \tag{A19}$$

Substituting we get

$$\underline{\pi} = \underline{G}^{-\frac{1}{2}} \, \underline{Q} \, \underline{E(t)} \, \underline{Q}^T \, \underline{G}^{\frac{1}{2}} \left[\underline{\pi}^{(0)} + \int_0^t \underline{G}^{-\frac{1}{2}} \, \underline{Q} \, \underline{E^{-1}(\sigma)} \, \underline{Q}^T \, \underline{G}^{-\frac{1}{2}} \, \underline{s(\sigma)} \, d\sigma \right] \tag{A20}$$

Q.E.D.

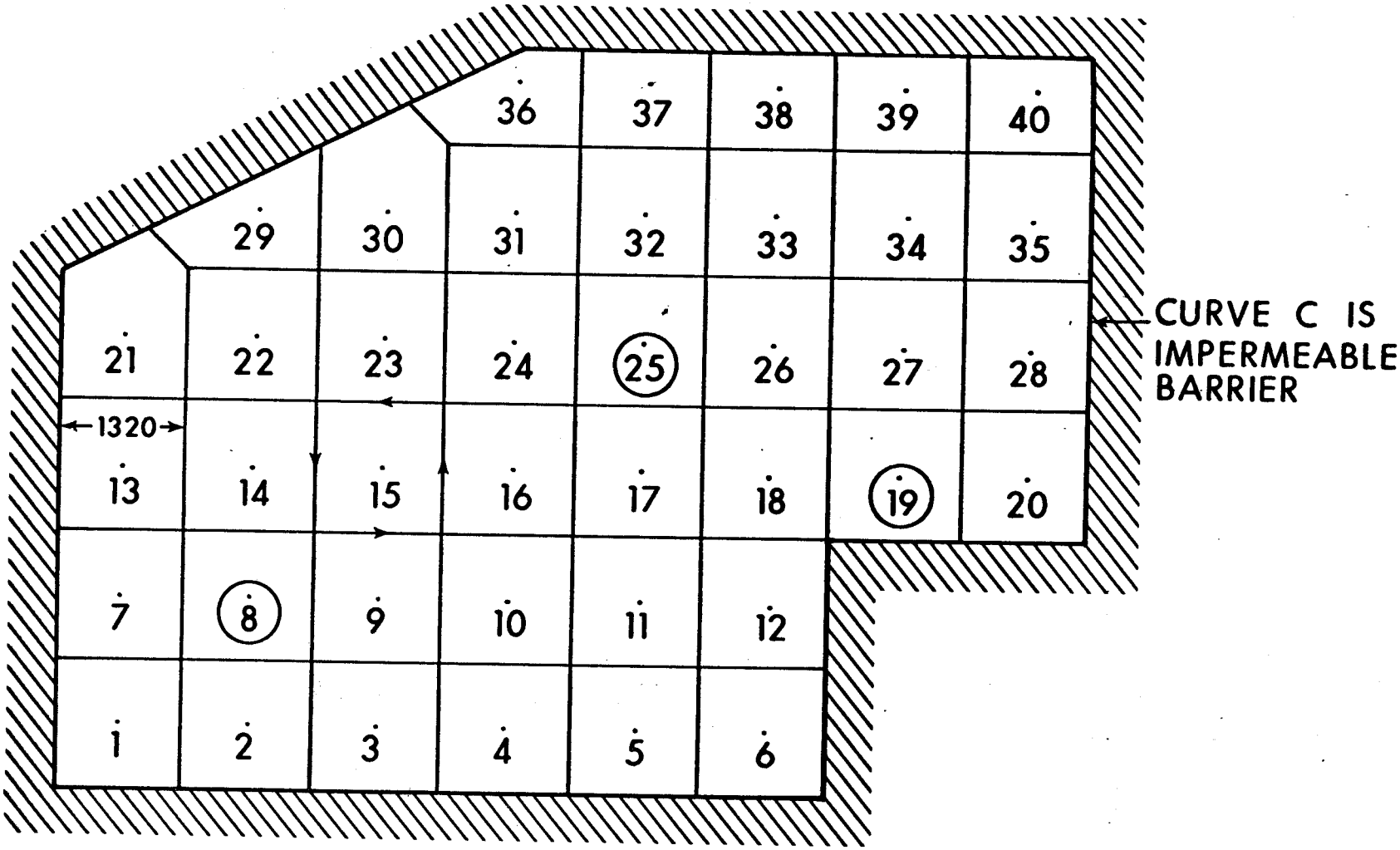

FIGURE 1 A TWO - DIMENSIONAL PETROLEUM RESERVOIR

Table 1

ϕ h Matrix, feet

			47.00	57.00	62.00	68.00	61.00
	80.00	69.00	47.00	51.00	62.00	64.00	58.00
69.00	62.00	62.00	77.00	74.00	69.00	87.00	91.00
81.00	84.00	68.00	69.00	54.00	47.00	50.00	48.00
69.00	52.00	53.00	53.00	83.00	80.00		
101.00	88.00	80.00	69.00	65.00	64.00		

Table 2

kh Matrix, Darcy feet

			3.00	2.70	2.60	4.10	5.20
	6.00	6.30	4.20	4.60	5.30	5.00	3.70
7.40	6.80	6.70	8.30	7.70	6.80	6.00	5.80
8.80	9.70	14.20	8.00	10.30	11.00	12.50	12.20
15.10	12.80	13.20	13.20	9.60	9.00		
10.90	9.50	9.30	11.00	14.20	14.10		

Table 3

Pressure Distribution after 280 Days (psia)

			522.76	522.27	522.19	522.21	522.26
	524.53	524.28	522.57	521.87	522.02	522.05	522.11
524.78	524.52	524.01	522.77	520.64	521.74	521.69	521.90
524.74	524.44	524.29	523.64	522.85	522.53	520.70	521.70
524.69	523.73	524.47	524.36	524.03	523.87		
524.81	524.58	524.72	524.73	524.61	524.52		

ON DIFFERENCE APPROXIMATIONS FOR SOLVING MATHEMATICAL MODELS OF FLUID FLOW IN POROUS MEDIA

by

H. S. Price

Gulf Research & Development Company

INTRODUCTION

The development and solution of mathematical models simulating fluid flow in porous media have become an important part of Reservoir Engineering. Because reservoir simulation is such a useful tool, the "art" of solving complex partial differential equation using finite difference methods has developed much faster than the necessary mathematical rigor. This could be a serious problem if the engineer using these models were not aware of the necessary mathematics and were not to encourage the mathematicians to catch up. It is the purpose of this paper to present some mathematical tools, which are very useful for analyzing finite difference methods, and their applications to some very accurate approximate methods.

In solving boundary value problems by finite difference methods, there are two problems which are fundamental. One is to solve the matrix equations arising from the discrete approximation to a differential equation. The second is to estimate, in terms of the mesh spacing h, the difference between the approximate solution and the exact solution (discretization error). Until recently, most of the research papers considered these problems only for finite difference approximations whose associated square matrices are M-matrices*. This paper treats both of the problems described above for a class of difference equations whose associated matrices are not M-matrices, but belong to the more general class of monotone matrices, i.e., matrices with non-negative inverses.

---

* See text for definition.

After some necessary proofs and definitions from matrix theory, we study the problem of estimating discretization errors. The fundamental paper on obtaining pointwise error bounds dates back to Gershgorin (1930). He established a technique, in the framework of M-matrices, with wide applicability. Many others, Batschelet (1952), Collatz (1933) and (1960), and Forsythe and Wasow (1960) to name a few, have generalized Gershgorin's basic work, but their methods still used only M-matrices. Recently, Bramble and Hubbard (1964a) and (1964b) considered a class of finite difference approximations without the M-matrix sign property, except for points adjacent to the boundary. They established a technique for recognizing monotone matrices and extended Gershgorin's work to a whole class of high order difference approximations whose associated matrices were monotone rather than M-matrices. We continue their work by presenting an easily applied criterion for recognizing monotone matrices. The procedure we use has the additional advantage of simplifying the work necessary to obtain pointwise error bounds. Using these new tools, we study the discretization error of a very accurate finite difference approximation to a second order elliptic differential equation.

Our interests then shift from estimating discretization errors of certain finite difference approximations to obtaining information about the eigenvalues and eigenvectors of their associated matrices. Using the concepts of oscillation matrices, introduced by Gantmacher and Krein (1950), we show that the associated matrix of the previously introduced high order difference approximation has real, positive and distinct eigenvalues. This property is quite

important for solving certain parabolic problems of the conduction-convection type, Price, Warren and Varga (1966).

Finally, we apply the results concerning oscillation matrices to the problem of solving the matrix equations associated with the above-mentioned high order finite difference approximation. We indicate what conditions are necessary, Widlund (1966), for rigorously applying the Peaceman-Rachford (1955) variant of the Implicit Alternating Direction Method to solving these difference equations. This paper is concluded with some numerical results indicating the practical advantage of using high order difference approximations where possible.

Section 1. Monotone Type Approximations for Elliptic Problems

This section is concerned with estimating the discretization error of a very accurate finite difference approximation whose associated matrix is not an M-matrix but is monotone. We begin this section by briefly introducing definitions and concepts needed throughout the paper, and establishing necessary and sufficient conditions that a given square matrix be monotone.

We then apply these conditions to obtain pointwise error bounds for a high order difference approximation to a second order elliptic partial differential equation on a rectangle. These results are then extended to a general two-dimensional region.

Matrix Preliminaries and Definitions

Let us begin our study of discretization errors with some basic definitions:

Definition 1.1. A real n x n matrix $A = (a_{i,j})$ with $a_{i,j} \leq 0$ for all $i \neq j$ is an M-matrix if A is non-singular, and $A^{-1} \geq 0$*.

Definition 1.2. A real n x n matrix A is monotone (cf. Collatz, 1960, p. 43) if for any vector $\underline{r}$, $A\underline{r} \geq \underline{0}$ implies $\underline{r} \geq \underline{0}$.

Another characterization of monotone matrices is given by the following well-known theorem of Collatz (1960, p. 43):

Theorem 1.1. A real n x n matrix $A = (a_{i,j})$ is monotone if and only if $A^{-1} \geq 0$.

Theorem 1.1 and Definition 1.1 then imply that M-matrices are a subclass of monotone matrices. The structure of M-matrices

---

* The rectangular matrix inequality $A \geq 0$ is taken to mean all elements of A are non-negative.

is very complete, (cf. Ostrowski (1955), and Varga (1962, p. 81)), and consequently they are very easy to recognize when encountered in practice. However, the general class of monotone matrices is not easily recognized and almost no useful structure theorem for them exists. Therefore, Theorem 1.3 below, which gives necessary and sufficient conditions that an arbitrary matrix be monotone, is quite useful.

We include the following basic definitions for completeness (cf. Varga, (1962, p. 13)).

Definition 1.3. The n x n complex matrix A is said to be convergent if the sequence of matrices A, A^2, A^3,...converges to the null matrix 0, and divergent otherwise.

Definition 1.4. Let λ_i, $1 \leq i \leq n$ be the eigenvalues of the n x n matrix A. Then

$$\rho(A) \equiv \underset{1 \leq i \leq n}{\text{MAX}} \; |\lambda_i|$$

is the spectral radius of A. The following theorem is an equivalent statement of Definition 1.3.

Theorem 1.2. The n x n matrix A is convergent if and only if $\rho(A) < 1$.

For a proof of this theorem, see Varga (1962, p. 13).

We are now ready to state:

Theorem 1.3. Let $A = (a_{i,j})$ be a real n x n matrix. Then, A is monotone if and only if there exists a real n x n matrix R with the following properties:

1) $M = A + R$ is monotone

2) $M^{-1}R \geq 0$

3) $\rho(M^{-1}R) < 1$.

Proof: If A is monotone, R can be chosen to be the null matrix 0, and the above properties are trivially satisfied.

Now suppose A is a real n x n matrix and R is a real n x n matrix satisfying properties 1, 2 and 3 above. Then,

$$A = M - R = M(I - M^{-1}R)$$

and

$$A^{-1} = (I - M^{-1}R)^{-1}M^{-1}$$

Since, by Theorem 1.2, $M^{-1}R$ is convergent, we can express A^{-1} as in Varga (1962, p. 82),

$$A^{-1} = \left[I + M^{-1}R + (M^{-1}R)^2 + (M^{-1}R)^3 + \ldots\right]M^{-1} \qquad (1.1)$$

As $M^{-1}R$ and M^{-1} are both non-negative, we see from (1.1) that A^{-1} is non-negative, and thus by Theorem 1.1, A is monotone. Q.E.D.

It is interesting to note that if R can be chosen to be non-negative then Theorem 1.3 is equivalent to a (if and only if) statement of Theorem 3.13 of Varga (1962, p. 89). When R is of mixed sign, this theorem is a slightly stronger statement of Theorem 2.7 of Bramble and Hubbard (1964b). As will be seen later, it is much easier to find a monotone matrix M which dominates A, giving a non-negative R, than to choose R such that property (2) of Theorem 1.3 is satisfied. This is one of the major deviations between this development and Bramble and Hubbard's in (1964a, 1964b). Also

for this reason, we shall, from now on, be concerned with constructing the matrix M rather than the matrix R.

We shall now conclude this section by defining some vector and matrix norms which we shall use in the subsequent development.

Let $V_n(C)$ be the n-dimensional vector space of column vectors $\underline{x}$, $\underline{y}$, $\underline{z}$, etc., with components x_i, y_i, z_i, $1 \le i \le n$, in the complex number field C.

Definition 1.5. Let $\underline{x}$ be a column vector of $V_n(C)$. Then,

$$\| \underline{x} \|_2^2 \equiv \underline{x}^* \underline{x} = \sum_{i=1}^{n} |x_i|^2$$

is the Euclidean (or L_2) norm of $\underline{x}$.

Definition 1.6. Let $\underline{x}$ be a column vector of $V_n(C)$. Then

$$\| \underline{x} \|_\infty \equiv \max_{1 \le i \le n} |x_i|$$

is the maximum (or L_∞) norm of $\underline{x}$.

The matrix norms associated with the above vector norms are given by:

Definition 1.7. If $A = (a_{i,j})$ is an n x n complex matrix, then

$$\| A \|_2 \equiv \sup_{\underline{x} \neq \underline{0}} \frac{\| A \underline{x} \|_2}{\| \underline{x} \|_2} = \left[\rho(A^* A) \right]^{1/2}$$

is the spectral (or L_2) norm of A.

Definition 1.8. If $A = (a_{i,j})$ is an n x n complex matrix, then

$$\| A \|_\infty \equiv \sup_{\underline{x} \neq \underline{0}} \frac{\| A \underline{x} \|_\infty}{\| \underline{x} \|_\infty} = \max_{1 \le i \le n} \sum_{j=1}^{n} |a_{i,j}|$$

is the maximum (or L_∞) norm of A.

A Very Accurate Difference Approximation in a Rectangle

For simplicity, we shall consider a rectangle, R, in two dimensions, with a square mesh (size h) which fits R exactly. Later, we shall consider the modifications necessary to obtain pointwise $O(h^4)$ discretization error estimates for general bounded domains. This will of course include rectangular regions which are not fit exactly by a square mesh.

Let us consider the numerical solution of the following second order elliptic boundary value problem in the rectangle R with boundary C:

$$- \frac{\partial^2 u}{\partial x^2} - \frac{\partial^2 u}{\partial y^2} + r(x,y) \frac{\partial u}{\partial x} - s(x,y) \frac{\partial u}{\partial y}$$

$$+ q(x,y) u = f(x,y); \quad (x,y) \in R, \tag{1.2}$$

$$u = g(x,y) \quad ; \quad (x,y) \in C.$$

We also assume that $q(x,y) \ge 0$ in $\bar{R}$, the closure of R.

With the aid of Figure 1, we shall define the following sets of mesh points, assuming the "English or typewriter ordering" (i.e., numbering the mesh points from left to right, top to bottom),

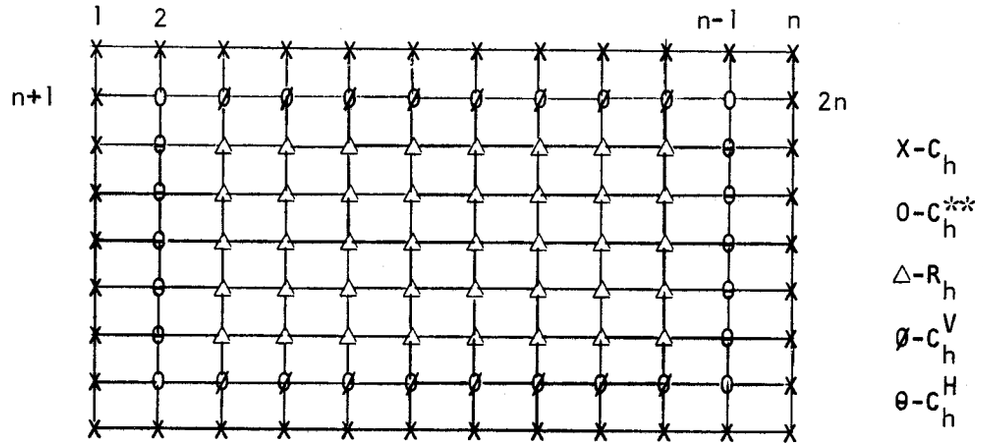

FIGURE 1

with α the running index. This is illustrated in Figure 1.

Definition 1.10. C_h is the set of indices, α, of grid points which lie on C, the boundary of R.

Definition 1.11. C_h^{**} is the set of indices, α, of interior grid points which have two of their four nearest neighbors in C_h.

Definition 1.12 C_h^V and C_h^H are, respectively, the set of indices, α, of the interior grid points with exactly one of the two, vertical or horizontal, respectively, nearest neighbors in C_h.

Definition 1.13. R_h is the set of indices, α, of interior grid points not in $C_h^{**} + C_h^H + C_h^V$.

The various indices are illustrated in Figure 1 above.

Now, by means of Taylor's series, assuming $u(x,y)$ has six continuous derivatives in $\bar{R}$, (i.e., $u \in C^6(\bar{R})$), we can derive the following finite difference approximation to (1.2):

$$D A \underline{u} = \underline{f} + \underline{I} . \tag{1.3}$$

The vectors $\underline{u}$ and $\underline{f}$ are defined to have components u_α and f_α which are just the functions $u(x,y)$ and $f(x,y)$ of (1.2) evaluated at the mesh points. The N x N diagonal matrix D has entries $d_{\alpha,\alpha}$ given by

$$d_{\alpha,\alpha} = 1, \ \alpha \in C_h, \ d_{\alpha,\alpha} = \frac{1}{12\ h^2} \text{ otherwise}, \tag{1.4}$$

and the N x N matrix $A = (a_{i,j})$ is defined as

$$\begin{aligned}
(Aw)_\alpha &= w_\alpha \quad , \quad \alpha \in C_h; \\
(Aw)_\alpha &= -(12 + 6\, s_\alpha h)w_{\alpha-n} - (12 + 6\, r_\alpha h)w_{\alpha-1} \\
&\quad + (48 + 12\, q_\alpha h^2)w_\alpha - (12 - 6\, r_\alpha h)w_{\alpha+1} \\
&\quad - (12 - 6\, s_\alpha h)w_{\alpha+n} \quad , \quad \alpha \in C_h^{**}; \\
(Aw)_\alpha &= -(12 + 6\, s_\alpha h)w_{\alpha-n} + (1 + r_\alpha h)w_{\alpha-2} - (16 + 8\, r_\alpha h)w_{\alpha-1} \\
&\quad + (54 + 12\, q_\alpha h^2)w_\alpha - (16 - 8\, r_\alpha h)w_{\alpha+1} + (1 - r_\alpha h)w_{\alpha+2} \\
&\quad - (12 - 6\, s_\alpha h)w_{\alpha+n} \quad , \quad \alpha \in C_h^V ;
\end{aligned} \tag{1.5}$$

$$(Aw)_\alpha = (1 + s_\alpha h)w_{\alpha-2n} - (16 + 8\, s_\alpha h)w_{\alpha-n} - (12 + 6\, r_\alpha h)w_{\alpha-1}$$

$$+ (54 + 12\, q_\alpha h^2)w_\alpha - (12 - 6\, r_\alpha h)w_{\alpha+1} - (16 - 8\, s_\alpha h)w_{\alpha+n}$$

$$+ (1 - s_\alpha h)w_{\alpha+2n} \quad , \quad \alpha \in C_h^H \ ;$$

$$(Aw)_\alpha = (1 + s_\alpha h)w_{\alpha-2n} - (16 + 8\, s_\alpha h)w_{\alpha-n} + (1 + r_\alpha h)w_{\alpha-2}$$

$$- (16 + 8\, r_\alpha h)w_{\alpha-1} + (60 + 12\, q_\alpha h^2)w_\alpha - (16 - 8\, r_\alpha h)w_{\alpha+1}$$

$$+ (1 - r_\alpha h)w_{\alpha+2} - (16 - 8\, s_\alpha h)w_{\alpha+n} + (1 - s_\alpha h)w_{\alpha+2n}, \ \alpha \in R_h;$$

where n is the number of mesh points in one row and m is the number of rows. Thus, $N = m\,n$. Finally, the vector $\underline{\tau}$ of (1.3) has components τ_α, given by

$$\tau_\alpha = O(h^2), \ \alpha \in C_h^{**} + C_h^V + C_h^H \ ; \ \tau_\alpha = O(h^4), \ \alpha \in R_h; \tag{1.6}$$

$$\tau_\alpha = 0, \ \alpha \in C_h.$$

We shall now define

$$r \equiv \underset{(x,y)\in\bar{R}}{MAX} \left| r(x,y) \right|$$

$$s \equiv \underset{(x,y)\in\bar{R}}{MAX} \left| s(x,y) \right| \tag{1.7}$$

$$q \equiv \underset{(x,y)\in\bar{R}}{MAX} \left| q(x,y) \right| .$$

We are now ready to state the following:

Lemma 1.1. There exists a monotone matrix M, such that for A as defined by (1.5), $M \geq A$ for all

$$h \leq MIN\left\{ \frac{1}{3r} , \frac{1}{3s} , \frac{1}{(q)^{1/2}} \right\} . \tag{1.8}$$

Proof: We will construct M as the product of two M-matrices, i.e., $M = M_1 M_2$. With M_1 and M_2 defined by

$$(M_1 w)_\alpha = 4w_\alpha \quad , \quad \alpha \in C_h;$$

$$(M_1 w)_\alpha = -(1 + r_\alpha h)w_{\alpha-1} + 8\, w_\alpha - (1 - r_\alpha h)w_{\alpha+1}, \ \alpha \in C_h^V \ ;$$

$$(M_1 w)_\alpha = -(1 + s_\alpha h)w_{\alpha-n} + 8\, w_\alpha - (1 - s_\alpha h)w_{\alpha+n}, \ \alpha \in C_h^H \ ;$$

$$(M_1 w)_\alpha = 8\, w_\alpha \quad , \quad \alpha \in C_h^{**} \ ; \tag{1.9}$$

$$(M_1 w)_\alpha = -(1 + s_\alpha h)w_{\alpha-n} - (1 + r_\alpha h)w_{\alpha-1} + 8\, w_\alpha - (1 - r_\alpha h)w_{\alpha+1}$$

$$- (1 - s_\alpha h)w_{\alpha+n} \quad , \quad \alpha \in R_h;$$

and

$$(M_2 w)_\alpha = 4w_\alpha \quad , \quad \alpha \in C_h;$$

$$(M_2 w)_\alpha = -w_{\alpha-n} - w_{\alpha-1} + 8\, w_\alpha - w_{\alpha+1} - w_{\alpha+n}, \text{ otherwise;} \tag{1.10}$$

it is easily verified by direct multiplication that $M \equiv M_1 M_2$ is given by,

$$(Mw)_\alpha = 16\, w_\alpha \quad , \quad \alpha \in C_h;$$

$$(Mw)_\alpha = -8\, w_{\alpha-n} - 8\, w_{\alpha-1} + 64\, w_\alpha - 8\, w_{\alpha+1} - 8\, w_{\alpha+n}, \ \alpha \in C_h^{**};$$

$$\begin{aligned}(Mw)_\alpha = {} & (1 + r_\alpha h)w_{\alpha-n-1} - 8\, w_{\alpha-n} + (1 - r_\alpha h)w_{\alpha-n+1} + (1 + r_\alpha h)w_{\alpha-2} \\ & - (16 + 8\, r_\alpha h)w_{\alpha-1} + 66\, w_\alpha - (16 - 8\, r_\alpha h)w_{\alpha+1} + (1 - r_\alpha h)w_{\alpha+2} \\ & + (1 + r_\alpha h)w_{\alpha+n-1} - 8\, w_{\alpha+n} + (1 - r_\alpha h)w_{\alpha+n+1}, \ \alpha \in C_h^V;\end{aligned}$$

$$\begin{aligned}(Mw)_\alpha = {} & (1 + s_\alpha h)w_{\alpha-2n} + (1 + s_\alpha h)w_{\alpha-n-1} - (16 + 8\, s_\alpha h)w_{\alpha-n} \\ & + (1 + s_\alpha h)w_{\alpha-n+1} - 8\, w_{\alpha-1} + 66\, w_\alpha - 8\, w_{\alpha+1} \\ & + (1 - s_\alpha h)w_{\alpha+n-1} - (16 - 8\, s_\alpha h)w_{\alpha+n} + (1 - s_\alpha h)w_{\alpha+n+1} \\ & + (1 - s_\alpha h)w_{\alpha+2n} \quad , \quad \alpha \in C_h^H; \end{aligned} \tag{1.11}$$

$$\begin{aligned}(Mw)_\alpha = {} & (1 + s_\alpha h)w_{\alpha-2n} + (2 + s_\alpha h + r_\alpha h)w_{\alpha-n-1} - (16 + 8\, s_\alpha h)w_{\alpha-n} \\ & + (2 + s_\alpha h - r_\alpha h)w_{\alpha-n+1} + (1 + r_\alpha h)w_{\alpha-2} - (16 + 8\, r_\alpha h)w_{\alpha-1} \\ & + 68\, w_\alpha - (16 - 8\, r_\alpha h)w_{\alpha+1} + (1 - r_\alpha h)w_{\alpha+2} \\ & + (2 + r_\alpha h - s_\alpha h)w_{\alpha+n-1} - (16 - 8\, s_\alpha h)w_{\alpha+n} \\ & + (2 - s_\alpha h - r_\alpha h)w_{\alpha+n+1} + (1 - s_\alpha h)w_{\alpha+2n}, \ \alpha \in R_h.\end{aligned}$$

Now, for all h satisfying (1.8), it is easily seen that $M \geq A$, and since (1.8) implies that $|r_\alpha h| < 1$ and $|s_\alpha h| < 1$,

M_1 and M_2 are both M-matrices by Theorem 3.10 of Varga (1962, p. 84). Since $M^{-1} = M_2^{-1} M_1^{-1} \geq 0$, M is monotone. Q.E.D.

Theorem 1.4. The matrix A defined by (1.5) is monotone for all h satisfying (1.8).

Proof: We shall now show that $\rho(M^{-1}R) < 1$, where $R \equiv M - A$. Define the vectors $\underline{e}$, $\underline{\xi}$, and $\underline{\eta}$ to have components

$$e_\alpha = 1 \quad , \quad \text{for all } \alpha;$$

$$\xi_\alpha = 1 \quad , \quad \alpha \in C_h; \ \xi_\alpha = 0, \text{ otherwise;} \tag{1.12}$$

$$\eta_\alpha = 1, \ \alpha \in C_h^{**} + C_h^V + C_h^H; \ \xi_\alpha = 0, \text{ otherwise.}$$

Since $q_\alpha \geq 0$ for all α, we have from (1.5) that

$$A\, \underline{e} \geq \underline{\xi}. \tag{1.13}$$

Since $M \geq A$ and M is monotone, we have from (1.13) that

$$\underline{0} \leq M^{-1} R\, \underline{e} \leq \underline{e} - M^{-1} A\, \underline{e} \leq \underline{e} - M^{-1} \underline{\xi} = \underline{e} - M_2^{-1} M_1^{-1} \underline{\xi}. \tag{1.14}$$

From (1.9), it is easily seen that $M_1 \underline{e} \geq 4\, \underline{\xi}$ and since M_1 is an M-matrix

$$M_1^{-1} \underline{\xi} \leq \frac{1}{4}\, \underline{e}. \tag{1.15}$$

Using this in (1.14), we have

$$\underline{0} \leq M^{-1} R\, \underline{e} \leq \underline{e} - \frac{1}{4}\, M_2^{-1} \underline{e} < \underline{e}, \tag{1.16}$$

where the last inequality follows since $M_2^{-1} \underline{e} > 0$, which

is obvious from Definitions 1.1 and (1.12). Thus, we deduce from (1.16), that $\| M^{-1} R \|_\infty < 1$. Hence, from the simply proved inequality (see Varga (1962, p. 32))

$$\rho(A) \leq \| A \|_\infty$$

we obtain the desired result

$$\rho(M^{-1} R) < 1. \tag{1.17}$$

Thus, (1.17) and Lemma (1.1) imply that A satisfies the hypothesis of Theorem 1.3. This proves that A as defined by (1.5) is monotone. Q.E.

We will now examine the truncation error from approximating (1.3) by

$$D A \underline{v} = \underline{f}. \tag{1.18}$$

Subtracting (1.18) from (1.3) we have from the definitions (1.4), (1.6) and (1.12),

$$\| \underline{v} - \underline{u} \|_\infty = \| A^{-1} D^{-1} \underline{T} \|_\infty \leq K_1 h^4 \| A^{-1} \underline{\tau} \|_\infty$$

$$+ K_2 h^6 \| A^{-1} (\underline{e} - \underline{\tau} - \underline{\xi}) \|_\infty . \tag{1.19}$$

With A_o derived from A by setting q = 0 in (1.5), we have by a well-known result (cf. Henrici (1962, p. 362)) that A_o is monotone and

$$A_o^{-1} \geq A^{-1} \geq 0. \tag{1.20}$$

The next Lemma is due to Roudebus (1963, p. 34).

Lemma 1.2. Let $\underline{e}$, $\underline{\xi}$, and $\underline{\eta}$ be defined by (1.12). Then, for A defined by (1.5)

$$\| A^{-1} (\underline{e} - \underline{\xi} - \underline{\eta}) \|_\infty \leq K_3 h^{-2} \tag{1.21}$$

for all

$$h \leq \text{MIN} \left\{ \frac{\ln 2}{4(2s+1)} , \frac{\ln 2}{4(2r+1)} \right\} , \tag{1.22}$$

where r and s are defined by (1.7).

Proof: Following Roudebush (1963), we define the function $\gamma(x,y)$ to be

$$\gamma(x,y) \equiv \mu - e^{(2r+1)x} - e^{(2s+1)y} , \quad (x,y) \in \bar{R} ,$$

where $\mu \geq e^{(r+s+1)2d}$ and d is the diameter of $\bar{R}$. Let $\underline{\chi}$ be the vector whose αth component, (where α corresponds to the (i,j)th mesh point), is given by

$$\chi_\alpha = \gamma(x_i y_j), \quad \alpha \in R_h + C_h + C_h^{**} + C_h^V + C_h^H .$$

By Taylor's theorem, with A_o defined as above, we have

$$\frac{1}{2h^2} (A_o \underline{\chi})_\alpha = - \left. \frac{\partial^2 \gamma}{\partial x^2} \right|_{x_i^{(1)}} + r_\alpha \left. \frac{\partial \gamma}{\partial x} \right|_{x_i^{(2)}}$$

$$- \left. \frac{\partial^2 \gamma}{\partial y^2} \right|_{y_j^{(1)}} - s_\alpha \left. \frac{\partial \gamma}{\partial y} \right|_{y_j^{(2)}}, \alpha \in R_h + C_h^{**} + C_h^V + C_h^H$$

where

$$(i - 2)h \le x_i^{(1)},\ x_i^{(2)} \le (i+2)h, \quad 2 \le i \le n-2,$$

$$(j - 2)h \le y_j^{(1)},\ y_j^{(2)} \le (j+2)h, \quad 2 \le j \le m-2,$$

and

$$(i - 1)h \le x_i^{(1)},\ x_i^{(2)} \le (i+1)h, \quad i=1,\ n-1,$$

$$(j - 1)h \le y_j^{(1)},\ y_j^{(2)} \le (j+1)h, \quad j=1,\ m-1.$$

Therefore,

$$\frac{1}{12\ h^2}\ (A_o\chi)_\alpha = (2r+1)^2\ e^{(2r+1)x_i^{(1)}} - r_\alpha(2r+1)e^{(2r+1)x_i^{(2)}}$$

$$+ (2s+1)^2\ e^{(2s+1)y_j^{(1)}} + s_\alpha(2s+1)e^{(2s+1)y_j^{(2)}} \ge 1, \alpha \in R_h$$

for all h satisfying (1.22). Since

$$\frac{1}{12\ h^2}\ (A_o\chi)_\alpha \ge 0 \text{ for } \alpha \in C_h^{**} + C_h^V + C_h^H + C_h,$$

we have finally,

$$\frac{1}{12\ h^2}\ (A_o\chi) \ge (\underline{e} - \underline{\xi} - \underline{\eta}),$$

from which (1.21) follows using also (1.20). Q.E.D.

Lemma 1.3. With the definitions of this section,

$$\left\| A^{-1}\underline{\eta} \right\|_\infty \le \frac{1}{4}\ . \tag{1.23}$$

Proof: With A_o derived from A by setting $q_\alpha \equiv 0$ in (1.5), we have from (1.20)

$$0 \le A^{-1}\underline{\eta} \le A_o^{-1}\underline{\eta}\ . \tag{1.24}$$

We now compute $R_o \equiv M - A_o$, using (1.11), to be

$$(R_o w)_\alpha = 15\ w_\alpha \quad , \quad \alpha \in C_h;$$

$$(R_o w)_\alpha = (4 + 6\ s_\alpha h)w_{\alpha-n} + (4 + 6\ r_\alpha h)w_{\alpha-1} + 16\ w_\alpha$$

$$+ (4 - 6\ r_\alpha h)w_{\alpha+1} + (4 - 6\ s_\alpha h)w_{\alpha+n} \quad , \quad \alpha \in C_h^{**};$$

$$(R_o w)_\alpha = (1 + r_\alpha h)w_{\alpha-n-1} + (4 + 6\ s_\alpha h)w_{\alpha-n} + (1 - r_\alpha h)w_{\alpha-n+1}$$

$$+ 12\ w_\alpha + (1 + r_\alpha h)w_{\alpha+n-1} + (4 - 6\ s_\alpha h)w_{\alpha+n}$$

$$+ (1 - r_\alpha h)w_{\alpha+n+1}, \quad \alpha \in C_h^V\ ; \tag{1.25}$$

$$(R_o w)_\alpha = (1 + s_\alpha h)w_{\alpha-n-1} + (1 + s_\alpha h)w_{\alpha-n+1} + (4 + 6\ r_\alpha h)w_{\alpha-1}$$

$$+ 12\ w_\alpha + (4 - 6\ r_\alpha h)w_{\alpha+1} + (1 - s_\alpha h)w_{\alpha+n-1}$$

$$+ (1 - s_\alpha h)_{\alpha+n+1} \quad , \quad \alpha \in C_h^H\ ;$$

$$(R_o w)_\alpha = (2 + s_\alpha h + r_\alpha h)w_{\alpha-n-1} + (2 + s_\alpha h - r_\alpha h)w_{\alpha-n+1} + 8\, w_\alpha$$

$$+ (2 + r_\alpha h - s_\alpha h)w_{\alpha+n-1} + (2 - r_\alpha h - s_\alpha h)w_{\alpha+n+1} ,$$

$$\alpha \in R_h .$$

Let us define the diagonal matrix $\hat{D}$ to have diagonal entries $\hat{d}_{\alpha,\alpha}$ given by

$$\hat{d}_{\alpha,\alpha} = 2,\ \alpha \in C_h + C_h^{**} ;\ \hat{d}_{\alpha,\alpha} = 3/2,\ \alpha \in C_h^V + C_h^H ;$$

$$\hat{d}_\alpha = 1, \quad \alpha \in R_h . \tag{1.26}$$

With $\underline{e}$, $\underline{\xi}$ and $\underline{\eta}$ as defined by (1.12) we readily verify using (1.8), that

$$R_o(\underline{e} - \underline{\xi}) \le 16\, \hat{D}(\underline{e} - \underline{\xi}) - 4\underline{\eta} . \tag{1.27}$$

From (1.9) and (1.10), we compute directly

$$M_1(\underline{e} - \underline{\xi}) = 4\hat{D}(\underline{e} - \underline{\xi}) \ge 4(\underline{e} - \underline{\xi}), \tag{1.28}$$

$$M_2(\underline{e} - \underline{\xi}) \ge 4(\underline{e} - \underline{\xi}), \tag{1.28'}$$

and, since M_1 and M_2 are M-matrices,

$$\frac{1}{4}(\underline{e} - \underline{\xi}) = M_1^{-1}\hat{D}(\underline{e} - \underline{\xi}) \ge M_1^{-1}(\underline{e} - \underline{\xi}), \tag{1.29}$$

$$\frac{1}{4}(\underline{e} - \underline{\xi}) \ge M_2^{-1}(\underline{e} - \underline{\xi}). \tag{1.29'}$$

Using (1.27), (1.29) and (1.29'), it is easily seen that

$$R_o M_2^{-1} M_1^{-1}\hat{D}(\underline{e} - \underline{\xi}) \le \hat{D}(\underline{e} - \underline{\xi}) - \frac{1}{4}\underline{\eta} ,$$

from which it follows that

$$(I - R_o M_2^{-1} M_1^{-1})\hat{D}(\underline{e} - \underline{\xi}) \ge \frac{1}{4}\underline{\eta} . \tag{1.30}$$

Collecting these results, we have

$$A_o(\underline{e} - \underline{\xi}) = (I - R_o M_2^{-1} M_1^{-1}) M_1 M_2 (\underline{e} - \underline{\xi})$$

$$\ge 16\ (I - R_o M_2^{-1} M_1^{-1})\hat{D}(\underline{e} - \underline{\xi}) \ge 4\underline{\eta}, \tag{1.31}$$

and since A_o is monotone, (1.23) follows easily from (1.24) and (1.31).

Now, using (1.21) and (1.23) in (1.19), we have

Theorem* 1.5. If $u(x,y)$, the solution of (1.2) in the region R, has bounded sixth derivatives in $\bar{R}$, and $\underline{u}$ is a vector whose

---

*Remark: It should be noted here that all the results of this section are equally valid for a region R which is the sum of squares, and therefore, Theorem (1.5) is valid for this type of region.

αth component, where α corresponds to the (i,j)th mesh point, is given by $u_\alpha = u(x_i, y_j)$, and if $\underline{v}$ is the solution of (1.18), then for

$$h \leq \text{MIN}\left\{\left(\frac{1}{q}\right)^{1/2}, \frac{\ln 2}{8r+r}, \frac{\ln 2}{8s+s}\right\}, \tag{1.32}$$

we have

$$\|\underline{u} - \underline{v}\|_\infty \leq K_4 h^4,$$

where K_4 is independent of h. The constants r, s and q are defined by (1.7).

The result of this theorem generalizes a known result of Bramble and Hubbard (1964b) to the case where $r(x) \not\equiv 0$. Moreover, the proof given here is substantially different from theirs, and gives a computable sufficient upper bound for h, (1.32), while their paper establishes only the existence of such a bound.

An $O(h^4)$ Difference Approximation in a General Bounded Region

We again consider the partial differential equation of (1.2), but we assume now that R is a general bounded domain with boundary C. If we construct a square grid (size h) covering $\bar{R}$, it can be seen from Figure 2, that, in addition to the sets of grid points defined above, we need

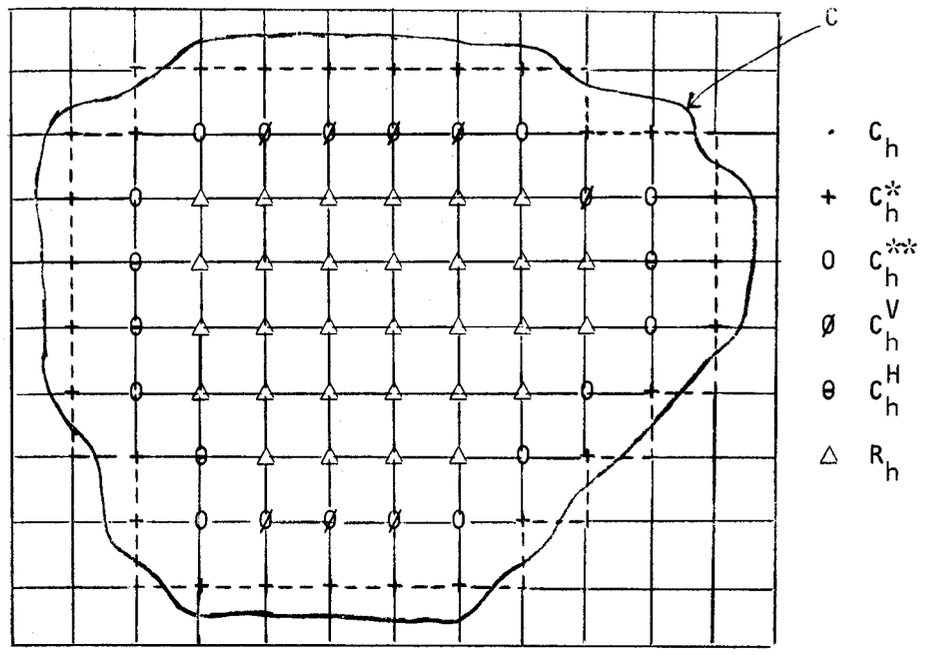

FIGURE 2

Definition 1.13. C_h^* is the set of indices, α, of interior grid points which have at least one and at most two of its four nearest neighbors in R^C, the complement of R.

Note that the assumption that points in C_h^* can have at most two nearest neighbors in R^C, may eliminate certain regions with corners having acute angles†. However, if C has a continuously turning tangent and h is sufficiently small, this assumption can always be satisfied.

†We point out here that if the smallest boundary angle is $\alpha > 0$, then using a $\Delta X \neq \Delta y$ would allow us to cover such angles. The assumption, $\Delta X \neq \Delta y$, does not change the results of the previous section, so we actually can consider most cases of interest by a suitable choice of

$$\frac{\Delta X}{\Delta y} \equiv K,$$

and h sufficiently small, where $h \equiv \text{MAX}\left\{\Delta X, \Delta y\right\}$.

We shall now define a finite difference approximation to (1.2), assuming $u \in C^6(\bar{R})$, in matrix notation as

$$\frac{1}{12\,h^2}\,\tilde{A}\,\underline{u} = \underline{f} + \underline{I}\,. \tag{1.33}$$

For the sets of grid points C_h^{**}, C_h^V, C_h^H, and R_h the equations of (1.33) are defined exactly as before, (cf. (1.4), (1.5), (1.6). We therefore need only define the equations of (1.33) for grid points $\alpha \in C_h^*$. If a point is in C_h^*, there are many different cases to consider (i.e., its nearest neighbor on the left, right, bottom, or top, in R^C, as well as its two nearest neighbors on the left and top, top and right, right and bottom, or bottom and left, are in R^C). For simplicity, we shall list only two of these eight possibilities since, from these, the others will be obvious. First assume for $\alpha \in C_h^*$ that the points below and to the left of the αth point are in R^C, as shown in Figure 3. Then,

$$\begin{aligned}
&\frac{1}{12\,h^2}\left\{\frac{12(1-\lambda)}{\lambda+2}\,u_{\alpha+2} - \left(24\,\frac{(2-\lambda)}{\lambda+1} - \frac{12\,r_\alpha\,\lambda h}{\lambda+1}\right)u_{\alpha+1}\right.\\
&\quad - \left(\frac{72}{\lambda(\lambda+1)(\lambda+2)} + \frac{12\,r_\alpha h}{\lambda(\lambda+1)}\right)g(x-\lambda h, y)\\
&\quad + \left(12\,q_\alpha h^2 + \frac{12(3-\lambda)+12\,r_\alpha h(\lambda-1)}{\lambda} + \frac{12(3-\mu)+12\,s_\alpha h(\mu-1)}{\mu}\right)u_\alpha\\
&\quad + \frac{12(1-\mu)}{\mu+2}\,u_{\alpha+2n} - \left(\frac{24(2-\mu)}{\mu+1} - \frac{12\,s_\alpha \mu h}{\mu+1}\right)u_{\alpha+n}\\
&\quad \left. - \left(\frac{72}{\mu(\mu+1)(\mu+2)} + \frac{12\,s_\alpha h}{\mu(\mu+1)}\right)g(x, y-\mu h)\right\}\\
&\quad = 12\,h^2 f_\alpha + 0(h^4)
\end{aligned} \tag{1.34}$$

where λh is the distance, in the x-direction, and μh is the distance, in the y-direction, to the nearest boundary, $0 < \lambda, \mu < 1$ (see Figure 3).

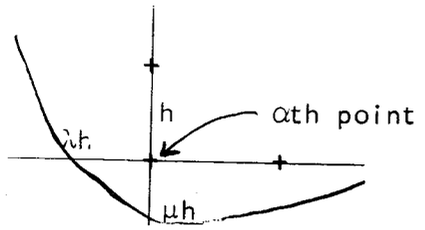

FIGURE 3

If for $\alpha \in C_h^*$ only the point to the left is in R^C we have

$$\begin{aligned}
&\frac{1}{12\,h^2}\left\{\frac{12(1-\lambda)}{\lambda+2}\,u_{\alpha+2} - \left(\frac{24(2-\lambda)}{\lambda+1} - \frac{12\,r_\alpha h\lambda}{\lambda+1}\right)u_{\alpha+1}\right.\\
&\quad - \left(\frac{72}{\lambda(\lambda+1)(\lambda+2)} + \frac{12\,r_\alpha h}{\lambda(\lambda+1)}\right)g(x-\lambda h, y) +\\
&\quad + \left(12\,q_\alpha h^2 + 24 + \frac{12(3-\lambda)}{\lambda}\right)u_\alpha - (12 + 6\,s_\alpha h)u_{\alpha-n}\\
&\quad \left. - (12 - 6\,s_\alpha h)u_{\alpha+n}\right\} = 12\,h^2 f_\alpha + 0(h^4).
\end{aligned} \tag{1.35}$$

Notice that now we are not carrying along dummy equations for the points $\alpha \in C_h$.

If the boundary of our region R were just the collection of horizontal and vertical line segments connecting points of C_h^*, the dashed line of Figure 2, then the finite difference approximation to (1.2) on this region would be given by (1.3). Also, we have that

$$\tilde{A}\,\underline{x} = D_1 A\,\underline{x} + \underline{k}(x) \tag{1.36}$$

where D_1 is a diagonal matrix whose diagonal entries $d^{(1)}_{\alpha,\alpha}$ are given by

$$d^{(1)}_{\alpha,\alpha} = \tilde{a}_{\alpha,\alpha} \quad , \quad \alpha \in C^*_h \ , \ d^{(1)}_{\alpha,\alpha} = 1, \text{ otherwise,}$$

and $\underline{k}(x)$ is a vector whose components $k_\alpha(x)$ are

$$k_\alpha(x) = \sum_{j \neq \alpha} \tilde{a}_{\alpha,j}\, x_j \ , \ \alpha \in C^*_h \ , \ k_\alpha(x)=0, \text{ otherwise.}$$

Using (1.37) we may now rewrite (1.33) as

$$A\,\underline{u} = 12\,h^2 D_1^{-1}\underline{f} - D_1^{-1}\underline{k}(u) + 12\,h^2\,D_1^{-1}\underline{T}, \tag{1.37}$$

and if $\underline{v}$ is the solution of

$$A\,\underline{v} = 12\,h^2 D_1^{-1}\underline{f} - D_1^{-1}\underline{k}(v), \tag{1.38}$$

we have that the truncation error $\underline{\epsilon} \equiv (\underline{u} - \underline{v})$ satisfies

$$A\,\underline{\epsilon} = 12\,h^2\,D_1^{-1}\underline{T} - D_1^{-1}\underline{k}(\epsilon).$$

An easy calculation using (1.34), (1.35) and the definitions of D_1 and $\underline{k}$, gives

$$\max_\alpha \left|(D_1^{-1}\underline{k}(\epsilon))_\alpha\right| = \max_{\alpha \in C^*_h} \left|(D_1^{-1}\underline{k}(\epsilon))_\alpha\right| \leq \sum_{j\neq\alpha} \frac{|\tilde{a}_{\alpha,j}|\,|\epsilon_j|}{\tilde{a}_{\alpha,\alpha}}$$

$$\leq \frac{10}{11}\left\|\underline{\epsilon}\right\|_\infty . \tag{1.39}$$

Since $\left\|D_1^{-1}\right\|_\infty = 1$ and A, by Theorem 1.4, is monotone if h satisfies (1.32), we have

$$\left|\underline{\epsilon}\right| \leq (K_1 h^4 + \frac{10}{11}\left\|\underline{\epsilon}\right\|_\infty)\underline{\xi} + K_2 h^4 A^{-1}\underline{\eta} + K_3 h^6 A^{-1}(\underline{e} - \underline{\xi} - \underline{\eta}),$$

where $\underline{e}$, $\underline{\xi}$, and $\underline{\eta}$ are defined by (1.12). Using Lemma 1.2 and Lemma 1.3, we have

$$\left\|\underline{\epsilon}\right\|_\infty \leq K\,h^4 + \frac{10}{11}\left\|\underline{\epsilon}\right\|_\infty$$

from which follows

Theorem 1.6. If u (x,y), the solution of (1.2) in a general bounded region $R^\dagger$ with boundary C, has bounded sixth derivatives in $\bar{R}$, and $\underline{u}$ is a vector whose αth component, $(\alpha \equiv (i,j))$, is $u_\alpha = u(x_i,y_j), (x_i,y_j) \in R_h + C^{**}_h + C^*_h + C^V_h + C^H_h$, and if $\underline{v}$ is the solution of (1.38), then

$$\left\|\underline{\epsilon}\right\|_\infty = \left\|\underline{u} - \underline{v}\right\|_\infty \leq K\,h^4, \tag{1.40}$$

for all h satisfying (1.32)

The results of this section extend the results above, which held for regions which were sums of squares, to fairly general bounded domains. This extension follows closely a similar extension of Bramble and Hubbard (1964b), and differs only in that we consider a more general class of problems.

In the preceeding, we have presented a detailed proof of convergence of the solution of a finite difference approximation to the solution of the continuous partial differential equation.

---

† Excluding regions where points of C^*_h would have more than two nearest neighbors in R^C.

The tools presented are widely applicable and proofs of this sort should be available before attempting to solve a partial differential equation on a computer. Many petroleum problems do not admit convergence proofs of this sort because of the non-linearities present; however, before going to a computer, one should at least be able to obtain a proof of this sort for the linearized problem. Hopefully, in the near future, mathematicians will develop tools which will enable us to prove convergence even for the badly non-linear equations which simulate fluid flow in porous media.

Section 2. Oscillation Matrices and Applications to Non-Symmetric Difference Equations

In Section 1, we considered the truncation error of a high order difference approximation without concern about how one would solve the resulting system of linear equations. For one-dimensional problems, this is not a serious consideration since Gaussian Elimination can be used efficiently. This is basically due to the fact that the associated matrices are band matrices of fixed widths. However, for two-dimensional problems like the one considered in the previous section, Gaussian Elimination is quite inefficient, because the associated band matrices have widths which increase with decreasing mesh size. Therefore, we need to consider other approaches.

For cases where the matrices, arising from finite difference approximations, are symmetric and positive definite many block successive over-relaxation methods may be used (Varga (1962, p. 77)). Also, for this case, a variant of ADI, like the Peaceman-Rachford method (1955), may be used. In this instance, convergence for a single fixed parameter can be proved (cf Birkhoff and Varga (1959)) and, in some instances, rapid convergence can be shown using many parameters cyclically (cf Birkhoff and Varga (1959)), Pearcy (1962), and Widlund (1966). For the case of Alternating Direction Implicit methods, the assumption of symmetry may be weakened to some statement about the eigenvalues and the eigenvectors of the matrices. Knowing properties about the eigenvalues of finite difference matrices is also very important when considering conduction-convection-type

problems (Price, et al (1966)). Therefore, in this section. we shall obtain results about the eigenvalues and the eigenvectors of matrices arising from difference approximations.

We begin by introducing the concept of oscillation matrices, originally due to Gantmacher and Krein (1950), along with their properties. These properties are then applied to show that the H and V matrices, chosen when using a variant of ADI, have real positive distinct eigenvalues. This result will be shown to be the foundation for proving rapid convergence for the Peaceman-Rachford variant of ADI.

Finally, some numerical results will be presented which confirm both the $0(h^4)$ truncation error estimates of Section 1 and the rapid convergence of ADI for solving these finite difference equations.

Oscillation Matrices and Their Properties

We will begin our study of oscillation matrices with some basic definitions:

Definition 2.1. An n x n matrix $A = (a_{i,j})$ will be called totally non-negative (totally positive) if all its minors of any order are non-negative (positive):

$$A\begin{pmatrix} i_1, i_2, \ldots, i_p \\ k_1, k_2, \ldots, k_p \end{pmatrix} \geq 0 \qquad \left(1 \leq \begin{matrix} i_1 < i_2 < \ldots < i_p \\ \\ k_1 < k_2 < \ldots < k_p \end{matrix} \leq n \right)$$

$$(p = 1,2\ldots,n).$$

The square bracket notation

$$A\begin{bmatrix} i_1, i_2, \ldots, i_p \\ k_1, k_2, \ldots, k_p \end{bmatrix} \equiv \begin{bmatrix} a_{i_1,k_1} & a_{i_1,k_2} \cdots a_{i_1,k_p} \\ a_{i_2,k_1} & a_{i_2,k_2} \cdots a_{i_2,k_p} \\ \cdots\cdots\cdots\cdots \\ a_{i_p,k_1} & a_{i_p,k_2} \cdots a_{i_p,k_p} \end{bmatrix}$$

denotes square submatrices, while parentheses denote determinants of such square submatrices:

$$A\begin{pmatrix} i_1, i_2, \ldots, i_p \\ k_1, k_2, \ldots, k_p \end{pmatrix} \equiv \det A\begin{bmatrix} i_1, i_2, \ldots, i_p \\ k_1, k_2, \ldots, k_p \end{bmatrix}.$$

Some simple properties of totally non-negative matrices are given by

Theorem 2.1

(1) The product of two totally non-negative matrices is totally non-negative.

(2) The product of a totally positive matrix and a non-singular totally non-negative matrix is totally positive.

The proofs of the theorems given in this section are omitted because they involve concepts which are too lengthy to develop here. They may be found in either Gantmacher and Krein (1950, Chapter II), or Price (1965, Chapter II).

Continuing now with our development, we are ready to define an oscillation matrix.

Definition 2.2. An $n \times n$ matrix $A = (a_{i,j})$ is an oscillation matrix if A is totally non-negative and some power of A, A^p, $p \geq 1$, is totally positive.

The following theorem gives some of the simplest properties of oscillation matrices.

Theorem 2.2.

(1) An oscillation matrix is non-singular.

(2) Any power of an oscillation matrix is an oscillation matrix.

(3) The product of two oscillation matrices is an oscillation matrix.

The following is the basic theorem about oscillation matrices. Its proof may be found in Gantmacher (1953, p. 105), and Gantmacher and Krein (1950, p. 123).

Theorem 2.3. If an $n \times n$ matrix $A = (a_{i,j})$ is an oscillation matrix, then

(1) The eigenvalues of A are positive distinct real numbers

$$\lambda_1 > \lambda_2 > \ldots > \lambda_n > 0.$$

(2) If $\underline{u}^{(k)}$ is an eigenvector of A corresponding to the kth largest eigenvalue, then there are exactly $k-1$ sign changes among the coordinates of the vector, $\underline{u}^{(k)}$.

We shall see later in this section that many matrices which arise from finite difference approximations of second order differential equations are in fact diagonally similar to oscillation matrices. It is now necessary to develop some easy tests to determine if a given matrix A is an oscillation matrix. We will state, without proof, such a criterion.

Theorem 2.4. An $n \times n$ matrix $A = (a_{i,j})$ is an oscillation matrix if and only if

(1) A is non-singular and totally non-negative, and

(2) $a_{i,i+1} > 0$ and $a_{i+1,i} > 0$ $(i = 1,2,\ldots,n-1)$.

The proof of this theorem can be found in Gantmacher and Krein (1950, p. 139).

Since it is quite simple to determine when the superdiagonal and subdiagonal of a matrix are positive, it is necessary only to determine if a given matrix is totally non-negative. We will therefore need the following

Theorem 2.5. If the $n \times n$ non-singular matrix $A = (a_{i,j})$ has $r > 1$ superdiagonals and $s > 1$ subdiagonals, i.e.,

$$a_{i,j} = 0 \text{ unless } -r \leq i - j \leq s,$$

and if for any $p < n$

$$A\begin{pmatrix} i, i+1, \ldots, i+p-1 \\ k, k+1, \ldots, k+p-1 \end{pmatrix} > 0,$$

$$(i,k = 1,2,\ldots,n-p+1;\ 1-r \leq i-k \leq s-1),$$

then A is an oscillation matrix.

The proof of this theorem is developed completely in Price (1965).

The Peaceman-Rachford Method for the Rectangle

Let us consider the problem

$$-\frac{\partial^2 u}{\partial x^2} + \lambda(x)\frac{\partial u}{\partial x} - \frac{\partial^2 u}{\partial y^2} - s(y)\frac{\partial u}{\partial y} + (q^{(1)}(x)+q^{(2)}(y))u = f(x,y)$$

$$(x,y)\epsilon R, \qquad (2.1)$$

$$u(x,y) = g(x,y) \quad , \quad (x,y)\epsilon C,$$

where R is the rectangle defined by

$$R \equiv \left\{(x,y) \;\middle|\; 0 < x < L,\ 0 < y < W\right\}$$

and C is the boundary of R. We shall now place a uniform mesh on R, (i.e., $\Delta x = \frac{L}{N+1}$, where N is the number of interior mesh points in the x-direction and $\Delta y = \frac{W}{M+1}$, where M is the number of interior mesh points in the y-direction), and define the totality of difference approximations to (2.1) by

$$(H + V)\underline{v} = \underline{k} \; . \qquad (2.2)$$

The matrices H and V are defined by

$$(H\underline{v})_{1,j} \equiv \frac{1}{\Delta x^2}\left\{(24 + 12\, q_1^{(1)}\Delta x^2)v_{1,j} - (12 - 6\,\lambda_1\Delta x)v_{2,j}\right\},$$

$$1 \le j \le M \; ;$$

$$(H\underline{v})_{2,j} \equiv \frac{1}{\Delta x^2}\left\{-(16 + 8\,\lambda_2\Delta x)v_{1,j} + (30 + 12\, q_2^{(1)}\Delta x^2)v_{2,j}\right.$$

$$\left. - (16 - 8\,\lambda_2\Delta x)v_{3,j} + (1 - \lambda_2\Delta x)v_{4,j}\right\}, \; 1 \le j \le M;$$

$$(H\underline{v})_{i,j} \equiv \frac{1}{\Delta x^2}\left\{(1 + \lambda_i\Delta x)v_{i-2,j} - (16 + 8\,\lambda_i\Delta x)v_{i-1,j}\right.$$

$$+ (30 + 12\, q_i^{(1)}\Delta x^2)v_{i,j} - (16 - 8\,\lambda_i\Delta x)v_{i+1,j} \qquad (2.3)$$

$$\left. + (1 - \lambda_i\Delta x)v_{i+2,j}\right\}, \; 2 \le i \le N-2, \; 1 \le j \le M;$$

$$(H\underline{v})_{N-1,j} \equiv \frac{1}{\Delta x^2}\left\{(1 + \lambda_{N-1}\Delta x)v_{N-3,j} - (16 + 8\,\lambda_{N-1}\Delta x)v_{N-2,j}\right.$$

$$\left. + (30 + 12\, q_{N-1}^{(1)}\Delta x^2)v_{N-1,j} - (16 - 8\,\lambda_{N-1}\Delta x)v_{N,j}\right\},$$

$$1 \le j \le M \; ;$$

$$(H\underline{v})_{N,j} \equiv \frac{1}{\Delta x^2}\left\{-(12 + 6\,\lambda_N\Delta x)v_{N-1,j} + (24 + 12\, q_N^{(1)}\Delta x^2)v_{N,j}\right\},$$

$$1 \le j \le M \; ;$$

and

$$(V\underline{v})_{i,1} \equiv \frac{1}{\Delta y^2}\left\{(24 + 12\, q_1^{(2)}\Delta y^2)v_{i,1} - (12 - 6\, s_1\Delta x)v_{i,2}\right\},$$

$$1 \le i \le N;$$

$$(V\underline{v})_{i,2} \equiv \frac{1}{\Delta y^2}\Big\{-(16 + 8\, s_2\Delta y)v_{i,1} + (30 + 12\, q_2^{(2)}\Delta y^2)v_{2,j}$$

$$-(16 - 8\, s_2\Delta y)v_{i,3} + (1 - s_2\Delta y)v_{i,4}\Big\},\ 1 \le i \le N;$$

$$(V\underline{v})_{i,j} \equiv \frac{1}{\Delta y^2}\Big\{(1 + s_j\Delta y)v_{i,j-2} - (16 + 8\, s_j\Delta y)v_{i,j-1}$$

$$+ (30 + 12\, q_j^{(2)}\Delta y^2)v_{i,j} - (16 - 8\, s_j\Delta y)v_{i,j+1}$$

$$+ (1 - s_j\Delta y)v_{i,j+2}\Big\},\quad 1 \le i \le N,\ 2 \le j \le M-2; \tag{2.4}$$

$$(V\underline{v})_{i,M-1} \equiv \frac{1}{\Delta y^2}\Big\{(1 + s_{M-1}\Delta y)v_{i,M-3} - (16 + 8\, s_{M-1}\Delta y)v_{i,M-2}$$

$$+ (30 + 12\, q_{M-1}^{(2)}\Delta y^2)v_{i,M-1} - (16 - 8\, s_{M-1}\Delta y)v_{i,M}\Big\},$$

$$1 \le i \le N;$$

$$(V\underline{v})_{i,M} \equiv \frac{1}{\Delta y^2}\Big\{-(12 + 6\, s_M\Delta y)v_{i,M-1} + (24 + 12\, q_M^{(2)}\Delta y^2)v_{i,M}\Big\},$$

$$1 \le i \le N;$$

and $\underline{k}$ is a vector with $n \equiv NM$ components $k_{i,j}$ given by

$k_{i,j} \equiv 12\, f_{i,j}$ + (contributions from couplings to the boundary).

For simplicity, we have not written out in full the exact contributions of couplings to the boundary, but these are analogous to our treatment in the past.

Following Varga (1962, p. 212), we define the Peaceman-Rachford variant of ADI by

$$(H + r_{m+1}I)\underline{v}^{(m+\frac{1}{2})} \equiv (r_{m+1}I - V)\underline{v}^{(m)} + \underline{k},$$

$$(V + r_{m+1}I)\underline{v}^{(m+1)} \equiv (r_{m+1}I - H)\underline{v}^{(m+\frac{1}{2})} + \underline{k},\ m \ge 0, \tag{2.5}$$

where $\underline{v}^{(0)}$ is some initial guess and the r_m's are positive <u>acceleration parameters</u>. Combining the two equations (2.5), we have

$$\underline{v}^{(m+1)} \equiv T_{r_{m+1}}\underline{v}^{(m)} + \underline{g}_{r_{m+1}}(\underline{k}),\ m \ge 0$$

where

$$T_r \equiv (V + rI)^{-1}(rI - H)(H + rI)^{-1}(rI - V),$$

$$\underline{g}_r \equiv (V + rI)^{-1}\left\{(rI - H)(H + rI)^{-1} + I\right\}\underline{k}. \tag{2.6}$$

Since $(H + V)$ is monotone, (2.2) admits a unique solution $\underline{v}$. Therefore, if $\underline{\epsilon}^{(m)} \equiv \underline{v}^{(m)} - \underline{v}$ is the error after m iterations, then $\epsilon^{(m+1)} \equiv T_{r_{m+1}}\underline{\epsilon}^{(m)}$, and in general

$$\underline{\varepsilon}^{(m)} = \left(\prod_{k=1}^{m} T_{r_k} \right) \underline{\varepsilon}^{(0)}, \quad m \geq 1. \tag{2.7}$$

Since H and V, as defined by (2.3) and (2.4), are the sum of five diagonal matrices, $(H_j,\ 1 \leq j \leq M;\ V_i,\ 1 \leq i \leq N)$, such that $H_1 = H_2 = \ldots H_M$, and $V_1 = V_2 = \ldots = V_N$, it is easily seen that H and V have the same eigenvectors $\underline{\alpha}^{(k,\ell)}$. Now defining

$$\lambda = \sup_{0 \leq x \leq L} \left| \lambda(x) \right|,$$

$$s = \sup_{0 \leq y \leq W} \left| s(y) \right|, \tag{2.8}$$

$$q^{(1)} = \sup_{0 \leq x \leq L} \left| q^{(1)}(x) \right|,$$

$$q^{(2)} = \sup_{0 \leq x \leq W} \left| q^{(2)}(y) \right|,$$

we are ready to prove

$$0 < \Delta x \leq \text{MIN} \left\{ \frac{1}{3\lambda}, \left(\frac{2}{q^{(1)}} \right)^{1/2} \right\},$$

$$0 < \Delta y \leq \text{MIN} \left\{ \frac{1}{3s}, \left(\frac{2}{q^{(2)}} \right)^{1/2} \right\},$$

the submatrices H_i and V_j defined in (2.3) and (2.4) are diagonally similar to oscillation matrices, and therefore have the following properties:

(1) If $(\tau_k,\ 1 \leq k \leq N)$ and $(\mu_\ell,\ 1 \leq \ell \leq M)$ are the eigenvalues of the submatrices H_i and V_j respectively, then $0 < \tau_1 < \tau_2 < \ldots < \tau_N$, and $0 < \mu_1 < \mu_2 < \ldots < \mu_M$.

(2) If $(\underline{x}^{(k)}, 1 \leq k \leq N)$ and $(\underline{y}^{(\ell)},\ 1 \leq \ell \leq M)$ are the eigenvectors of the submatrices H_i and V_j respectively, then each forms a linearly independent set. Moreover, the eigenvectors, $\alpha^{(k,\ell)}$ form a basis for the n-dimensional vector space $V_n(C)$ where $n = MN$.

Proof: Since properties (1) and (2) follow directly from Theorem 2.3 and $H_1 = H_2 = \ldots H_M$, and $V_1 = V_2 = \ldots V_N$, all that need be shown is that H_1 and V_1 are diagonally similar to oscillation matrices. Let D be the diagonal matrix whose diagonal entries $d_{i,i}$ are given by

$$d_{i,i} = (-1)^{i+1}, \quad 1 \leq i \leq N,$$

then it is easily verified that the matrix B^+ defined by

$$B^+ \equiv D^{-1} H D \geq 0. \tag{2.9}$$

Since B^+ is a non-negative matrix with two super-diagonals and two subdiagonals, we shall establish the hypotheses

of Theorem 2.5 in order to obtain this result. Let us consider the following cases:

Case I

$$B^{+}\begin{bmatrix} i,i+1,\ldots,i+p-1 \\ i+1,i+2,\ldots,i+p \end{bmatrix}, \quad 1 \le i \le N-p-1;\ 1 \le p \le N-2,$$

$$B^{+}\begin{bmatrix} i+1,i+2,\ldots,i+p \\ i,i+1,\ldots,i+p-1 \end{bmatrix}, \quad 1 \le i \le N-p-1;\ 1 \le p \le N-2.$$

Let us choose $S^{(p)}$ to be a p x p diagonal matrix whose diagonal entries $s_{i,i}$ are given by

$$s_{i,i} = (6)^{i-1}, \quad 1 \le i \le p.$$

Then, it is easy to verify that,

$$\left(S^{(p)}\right)^{-1} B^{+}\begin{bmatrix} i,i+1,\ldots,i+p-1 \\ i+1,i+2,\ldots,i+p \end{bmatrix} S^{(p)}$$

and

$$\left(S^{(p)}\right) B^{+}\begin{bmatrix} i+1,i+2,\ldots,i+p \\ i,i+2,\ldots,i+p-1 \end{bmatrix} \left(S^{(p)}\right)^{-1},$$

for all

$$1 \le p \le N-2,$$

are strictly diagonally dominant matrices and therefore,

$$B^{+}\begin{pmatrix} i,i+1,\ldots,i+p-1 \\ k,k+1,\ldots,k+p-1 \end{pmatrix} > 0,$$

for all

$$i,k = 1,2,\ldots,N-p-1\ ;\ i-k=1,-1\ ;\ 1 \le p \le N-2.$$

Case II.

$$B^{+}\begin{bmatrix} i,i+1,\ldots,i+p-1 \\ i,i+1,\ldots,i+p-1 \end{bmatrix}, \quad 1 \le i \le N-p\ ;\ 1 \le p \le N-1.$$

From arguments similar to those given in Section 1, we have that the matrix

$$H_1 = H_1\begin{bmatrix} 1,\ldots,N-1 \\ 1,\ldots,N-1 \end{bmatrix}$$

is monotone. If $H_1^{-1} = (\alpha_{i,j})$, then it is easily seen that

$$\alpha_{1,N-1} = B^{+}\begin{pmatrix} 1,2,\ldots,N-2 \\ 2,3,\ldots,N-1 \end{pmatrix} \Big/ H_1\begin{pmatrix} 1,2,\ldots,N-1 \\ 1,2,\ldots,N-1 \end{pmatrix}.$$

Since H_1 is non-singular and

$$B^{+}\begin{pmatrix} 1,2,\ldots,N-2 \\ 2,3,\ldots,N-1 \end{pmatrix} > 0,$$

from Case I, we have, since $\alpha_{1,N-1} \ge 0$, that

$$H_1\begin{pmatrix} 1,2,\ldots,N-1 \\ 1,2,\ldots,N-1 \end{pmatrix} > 0.$$

By similar arguments, if $H_1(i,p)$, where

$$H_1(i,p) \equiv H_1 \begin{bmatrix} i, i+1, \ldots, i+p-1 \\ \\ i, i+1, \ldots, i+p-1 \end{bmatrix} = \left(h_{k,j}^{(i,p)} \right),$$

is monotone for all $(i=1,2,\ldots,N-p \; ; \; 1 \le p \le N-1)$, then defining

$$\left(H_1(i,p) \right)^{-1} \equiv \left(\alpha_{k,j}^{(i,p)} \right),$$

we have

$$0 \le \alpha_{1,p}^{(i,p)} = B^{+} \begin{pmatrix} i, i+1, \ldots, i+p-1 \\ \\ i+1, i+2, \ldots, i+p \end{pmatrix} \Big/ H_1 \begin{pmatrix} i, i+1, \ldots, i+p-1 \\ \\ i, i+1, \ldots, i+p-1 \end{pmatrix}.$$

Therefore from Case I and the monotonicity of $H_1(i,p)$, we have

$$\det(H_1(i,p)) \equiv H_1 \begin{pmatrix} i, i+1, \ldots, i+p-1 \\ \\ i, i+1, \ldots, i+p-1 \end{pmatrix} > 0$$

for all

$$(1 \le i \le N-p \; ; \; 1 \le p \le N-1).$$

The matrix $H_1(i,p)$ can be easily shown to be monotone for all $(1 \le p \le N-1)$ by applying the methods of Section 1. Therefore, collecting the results of Cases I and II, we see that B^{+} is an oscillation matrix by Theorem 2.5. Since H_1 is similar to

B^{+}, the theorem is established for H_1 and by identical arguments V_1 can be shown to be similar to an oxcillation matrix. Q.E.D.

We shall now state, without proof, a particular theorem from Householder (1964, p. 47).

Theorem 2.7. Associated with an n x n complex matrix A is a convex body K, depending only on the eigenvectors of A, and a norm, $\| A \|_K$, such that

$$\| A \|_K = \rho(A),$$

if and only if, for every eigenvalue β_i of A such that $|\beta_i| = \rho(A)$, the number of linearly independent eigenvectors belonging to β_i equals its multiplicity.

Clearly from Theorem (2.6) there exists such a norm for the matrices H and V which is the same for both, since they have the same eigenvectors.

Now, following Varga (1962, Ch 7) and using this norm, it is clear that all the results obtainable from the commutative theory for the Peaceman-Rachford variant of ADI are applicable to the finite difference equations defined by (2.3) and (2.4). The most important of these is

Theorem 2.8. If α and β are the bounds for the eigenvalues τ_i and μ_i of the matrices H and V defined in (2.3) and (2.4), i.e.,

$$0 < \alpha \le \tau_i, \; \mu_i \le \beta, \; 1 \le i \le n,$$

and if the acceleration parameters $\left\{ r_k \right\}_{k=1}^{m}$ are chosen in some optimum fashion (cf. Varga (1962, p. 226) or Wachspress (1963))

then, the average rate of convergence of the iterative method defined by (2.5) is

$$R \equiv -\ln \rho\left(\prod_{j=1}^{m} T_{r_j}\right) > \frac{K}{\ln(\beta/\alpha)} \quad . \tag{2.10}$$

The result of (2.10) states that if we can obtain bounds on the eigenvalue spectrums of H and V, given by (2.3) and (2.4), then at least for the separable problem we can use variants of ADI to solve, very efficiently, the matrix equations of (2.2). We also have experimental evidence which indicates that the Peaceman-Rachford variant is very effective for non-separable problems. This has been reported by Young and Ehrlich (1960) and Price and Varga (1962) for the standard $0(h^2)$ finite difference equations. A very recent paper by Widlund (1966) allows us to extend the result of (2.10) to the non-separable problem given by (1.2) but still for rectangular regions.

The iterative solution of matrix equations for which the associated matrix is non-symmetric and is not of the M-matrix type has also been considered by Rockoff (1964), who in contrast used the successive overrelaxation iterative method and tools different from those resulting from the theory of oscillation matrices. The results of this section are apparently the first such applications of the theory of oscillation matrices to alternating direction implicit iterative methods.

ADI for Non-Rectangular Regions

The Peaceman-Rachford matrix T_r for a single fixed parameter is given, from (2.6), by

$$T_r = (V + rI)^{-1}(rI - H)(H + rI)^{-1}(rI - V) \quad . \tag{2.11}$$

Using (2.7), we have

$$\underline{\varepsilon}^{(m)} = (T_r)^m \, \underline{\varepsilon}^{(0)}, \quad m \geq 1,$$

so from Theorem 1.2, the iteration procedure, defined by (2.5), for a single fixed parameter converges if and only if $\rho(T_r) < 1$. Defining

$$\tilde{T}_r \equiv (V + rI)\, T_r\, (V + rI)^{-1}$$

$$= (rI - H)(rI + H)^{-1}(rI - V)(rI + V)^{-1}$$

we have

$$\rho(T_r) = \rho(\tilde{T}_r) \leq \left\|\tilde{T}_r\right\|_2$$

$$\leq \left\|(rI - H)(rI + H)^{-1}\right\|_2 \left\|(rI - V)(rI + V)^{-1}\right\|_2 ,$$

where $\|\quad\|_2$ is defined in Section 1. Therefore, to prove T_r is convergent we need only show

$$\left\|(rI - H)(rI + H)^{-1}\right\|_2 < 1$$

and (2.12)

$$\left\| (rI - V)(r + V)^{-1} \right\|_2 < 1.$$

In order to establish sufficient conditions on H and V so that (2.12) holds, we shall use a theorem due to Feingold and Spohn (1963). Results of this sort have been reported as well by Wachspress and Habather (1960) and Birkhoff, Varga and Young (1962).

Definition 2.3. If S is a Hermitian and positive definite n x n matrix, then

$$\left\| \underline{x} \right\|_S \equiv (x^* S x)^{1/2}$$

denotes a vector norm, and the induced matrix norm is defined by

$$\left\| A \right\|_S = \sup_{x \neq 0} \left(\left\| A\underline{x} \right\|_S / \left\| x \right\|_S \right).$$

We shall now prove

Theorem 2.9. (Feingold and Spohn) Let A and B be n x n matrices with A non-singular and A-B Hermitian and positive definite. Then $\left\| A^{-1}B \right\|_{(A-B)} < 1$ and $\left\| BA^{-1} \right\|_{(A-B)^{-1}} < 1$ if and only if $A^* + B$ is positive definite.

Proof: Since

$$A^{-1}B = I - A^{-1}(A - B),$$

then from Definition 2.3 $\left\| A^{-1}B \right\|_{(A-B)} < 1$ is equivalent to

$$\left\| (I - A^{-1}(A - B))\underline{x} \right\|_{(A-B)} \leq \left\| \underline{x} \right\|_{(A-B)}, \text{ for all } \underline{x} \neq \underline{0}. \quad (2.13)$$

Letting

$$A^{-1}(A - B)\underline{x} = \underline{y},$$

then (2.13) becomes

$$\left\| (A - B)^{-1}Ay - y \right\|_{(A-B)} < \left\| (A - B)^{-1}Ay \right\|_{(A-B)} \text{ for all } \underline{y} \neq \underline{0}.$$

Again using Definition 2.3, and remembering that A - B is Hermitian, we have

$$y^*(A - B)\, y - y^* Ay + y^* A^* (A - B)^{-1}Ay - y^* A^* y < y^* A^* (A - B)^{-1}Ay,$$

which is equivalent to

$$y^* A^* y + y^* Ay - y^*(A - B)y > 0,$$

which is equivalent to

$$y^*(A^* + B)y > 0,$$

which completes the first part of this result. The proof of the second part is similar. Q.E.D.

If we let A = rI + P and B = P - rI, for any r > 0 we have that A - B = 2 rI is Hermitian and positive definite, so we have immediately

Corollary 2.1. If P is an n x n matrix, with (rI + P) non-singular for all r > 0, then

$$\left\| (rI + P)^{-1}(P - rI) \right\|_1 < 1$$

if and only if P* + P is positive definite.

Since from Definition 2.3 and Definition 1.7

$$\| A \|_1 = \| A \|_2 ,$$

we have that (2.12) holds if and only if $H^T + H$ and $V^T + V$ are positive definite. Therefore, if we wish to solve the finite difference equations (1.33)

$$(H + V)\underline{x} = A\,\underline{x} = \underline{k}$$

using (2.5), it is sufficient to show that $H + H^T$ and $V + V^T$ are positive definite.

We shall proceed by showing that the matrix P, representing the $O(h^4)$ finite difference approximation to (1.2) for an arbitrary row or column of our mesh region R of Figure 2 (see Section 1), is such that $P + P^T$ is positive definite. For simplicity, we shall neglect the first derivative terms in (1.2) since they greatly complicate the algebra and add only mesh spacing restrictions to the final result. The n x n matrix P, representing an arbitrary row or colum of our region is given by:

$$(Pu)_1 \equiv \left(12\,\frac{(3-\lambda)}{\lambda} + 12\,h^2 q_1\right)u_1 - 24\,\frac{(2-\lambda)}{\lambda+1}\,u_2 + 12\,\frac{(1-\lambda)}{\lambda+2}\,u_3 \quad , \quad 0 < \lambda < 1,$$

$$(Pu)_i \equiv -12\,u_{i-1} + (24 + 12\,h^2 q_i)u_i - 12\,u_{i+1} \quad , \quad i=2,\ n-1,$$

$$(Pu)_i \equiv u_{i-2} - 16\,u_{i-1} + (30 + 12\,h^2 q_i)u_i - 16\,u_{i+1} + w_{i+2} \quad , \quad 3 \le i \le n-2,$$

$$(Pu)_n \equiv \left(12\,\frac{(3-\mu)}{\mu} + 12\,h^2 q_n\right)u_n - 24\,\frac{(2-\mu)}{\mu+1}\,u_{n-1} + 12\,\frac{(1-\mu)}{\mu+2}\,u_n, \quad 0 < \mu < 1. \qquad (2.14)$$

If Q is the matrix derived from P in (2.14) by setting the q_i's to zero, we have,

$$x^T(P + P^T)x \ge x^T(Q + Q^T)x \qquad (2.15)$$

since by assumption $q_i \ge 0$, $1 \le i \le n$. It is easily verified, using straightforward inequalities, such as

$$(x_i - x_{i+2})^2 \le 2(x_i - x_{i+1})^2 + 2(x_{i+1} - x_{i+2})^2,$$

that,

$$x^T(Q + Q^T)x \geq \left(12\,\frac{(3-\lambda)}{\lambda} \right) x_1^2 - \left(12\,\frac{(5\lambda-1)}{\lambda+1} \right) x_1 x_2$$

$$+ \left(\frac{14-11\lambda}{(\lambda+2)} \right) x_1 x_3 + 9\,\frac{1}{2}\,x_2^2 + x_3^2$$

$$+ 11 \sum_{i=2}^{n-2} (x_i - x_{i+1})^2 + x_{n-2}^2 + 9\,\frac{1}{2}\,x_{n-1}^2$$

$$+ \left(\frac{14-11\mu}{\mu+2} \right) x_n x_{n-2} - \left(\frac{12(5\mu-1)}{\mu+1} \right) x_n x_{n-1}$$

$$+ \left(\frac{12(3-\mu)}{\mu} \right) x_n^2 = \left(12\,\frac{(3-\lambda)}{\lambda} - a_\lambda - b_\lambda \right) x_1^2$$

$$+ \left(a_\lambda x_1 - \sqrt{\frac{19}{2}}\, x_2 \right)^2 + \left(b_\lambda x_1 + x_3 \right)^2$$

$$+ 11 \sum_{i=2}^{n-2} (x_i - x_{i+1})^2 + (b_\mu x_n + x_{n-2})^2$$

$$+ (b_\mu x_n - \sqrt{\frac{19}{2}}\, x_{n-1})^2$$

$$+ \left(12\,\frac{(3-\mu)}{\mu} - a_\mu - b_\mu \right) x_n^2 \qquad (2.16)$$

where

$$a_\gamma^2 = \frac{72}{19} \left(\frac{5\gamma - 1}{\gamma+1} \right)^2 , \quad \gamma = \lambda, \mu,$$

$$b_\gamma^2 = \left(\frac{14-11\gamma}{2(\gamma+2)} \right)^2 , \quad \gamma = \lambda, \mu.$$

Also by a simple calculation, we have

$$\left(\frac{12(3-\gamma)}{\gamma} - a_\gamma - b_\gamma \right) > 0 \text{ for all } 0 < \gamma < 1,$$

giving finally

$$\underline{x}^T(P + P^T)\underline{x} \geq \underline{x}^T(Q + Q^T)\underline{x} > \underline{0} \text{ for all } \underline{x} \neq \underline{0}.$$

Collecting these results, we have

Theorem 2.10. The Peaceman-Rachford variant of ADI defined by (2.5) converges for any single, positive, fixed, parameter, r, when used to solve the matrix equations (1.33), for all h sufficiently small.

Theorem 2.10 along with Theorem 2.8 gives us as complete a theory for the Peaceman-Rachford variant of ADI for the high order finite difference equations of Section 1 as exists for the $O(h^2)$, standard, central, difference approximations. In the absence of a more complete theory for the non-separable case, we recommend using 2^m Wachspress parameters, once reasonable bounds for the eigenvalue spectrum have been found. An excellent upper bound β is obtained by using the Gershgorin Circle Theorem [see Gershgorin (1931)], which is equivalent to

$$\beta \equiv \text{MAX} \left\{ \|H\|_\infty , \|V\|_\infty \right\}.$$

Also, since H and V are both monotone, the inverse power method of Wielandt, [see Varga (1962, p. 288)], may be used to obtain the lower bound α. Excellent results are obtained by using these bounds and the Wachspress parameters, as seen from the numerical results of Tables 1 and 2.

Numerical Results

We consider here numerical solution of the following problem:

$$\frac{\partial^2 u}{\partial x^2} + \frac{\partial^2 u}{\partial y^2} = 32\, e^{4x}\, e^{4y}, \quad (x,y)\epsilon R_i$$

$$u(x,y) = e^{4x}\, e^{4y}, \quad (x,y)\epsilon C_i, \tag{2.17}$$

where the R_i are the regions of interest with boundaries C_i. The solution of (2.17) is easily verified to be

$$u(x,y) = e^{4x}\, e^{4y}, \quad (x,y)\epsilon \bar{R}_i.$$

For each example, we again solve both the high accuracy, $0(h^4)$, finite difference equations, presented in Section 1, and the standard, $0(h^2)$, finite difference equations for a sequence of mesh spacings (h) tending to zero.

In all cases the Peaceman-Rachford variant of ADI, described above, is used to solve the matrix equations. The upper bound, b, of the eigenvalue spectrums of H and V, is chosen to be

$$b = \text{MAX}\left\{ \|H\|_\infty, \ \|V\|_\infty \right\}.$$

The lower bound, a, is found by doing ten iterations of Wielandt's inverse power method [see Varga (1962, p. 288)]. We use, cyclically, 2^m acceleration parameters generated using formulas presented by Wachspress (1962). The number m is chosen, in all cases, to be the smallest integer such that

$$\frac{b_m - a_m}{b_m + a_m} \leq \delta = 1 \times 10^{-5}$$

where

$$a_o = a \quad ; \quad b_o = b;$$

$$a_{i+1} = \sqrt{a_i b_i} \quad ; \quad b_{i+1} = \frac{a_i + b_i}{2} \quad ; \quad i \geq 0 .$$

This is just a suggestion made by Wachspress (1962), where δ is the desired accuracy. The iterations are stopped when

$$\text{MAX}_i \left| \frac{u_i^{(k)} - u_i^{(k-1)}}{u_i^{(k)}} \right| < 1 \times 10^{-5}; \ k \geq 1, \tag{2.18}$$

where $\underline{u}^{(k)}$ is the solution of the iterative procedure after k cycles of m parameters and $u^{(0)} \equiv 0$.

We then compare the approximate solution of the matrix equations to the exact solution of (2.17) and compute $\|\underline{\varepsilon}\|_\infty$, and α, the order of accuracy. Tabulated also are the number of parameters 2^m which were used, and the number of cycles (k) needed to satisfy (2.18).

Example 1 Unit Square

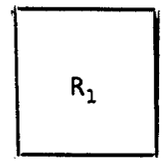

	Standard				High Accuracy			
h	$\|\|\underline{\epsilon}\|\|_\infty$	α	2^m	k	$\|\|\underline{\epsilon}\|\|_\infty$	α	2^m	k
.125	.175	-	8	3	$.355 \times 10^{-1}$	-	8	3
.0625	$.454 \times 10^{-1}$	1.95	16	2	$.266 \times 10^{-2}$	3.74	16	2
.03125	$.114 \times 10^{-1}$	1.99	16	3	$.184 \times 10^{-3}$	3.86	16	3
.015625	$.288 \times 10^{-2}$	2.0	16	3	$.115 \times 10^{-4}$	3.99	16	3

TABLE 1

Clearly the theoretical estimates of Section 1 are confirmed, as well as the earlier results of Section 2. We see from Table 1, that for a mesh size h = .03125, which is 1024 mesh points, a 100 to 1 improvement in the relative error is obtained with the high accuracy method. Also we see for this example, that the high accuracy difference equations require only 1/15th as much computer time as the standard difference equations to obtain a given accuracy.

Example 2 An L Shaped Region

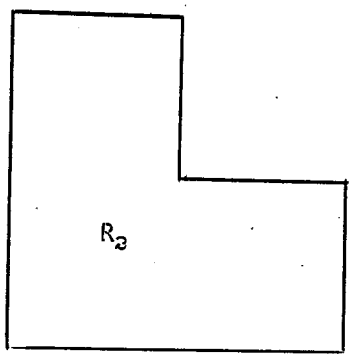

	Standard				High Accuracy			
h	$\|\|\underline{\epsilon}\|\|_\infty$	α	2^m	k	$\|\|\underline{\epsilon}\|\|_\infty$	α	2^m	k
.125	$.477 \times 10^{-1}$	-	8	3	$.148 \times 10^{-1}$	-	8	3
.0625	$.126 \times 10^{-1}$	1.92	8	3	$.105 \times 10^{-2}$	3.82	8	3
.03125	$.323 \times 10^{-2}$	1.96	16	3	$.690 \times 10^{-4}$	3.92	16	3
.015625	$.812 \times 10^{-3}$	1.99	16	3	$.436 \times 10^{-5}$	3.98	16	3

TABLE 2

Clearly the theoretical results of Section 1 are borne out by the numerical experiments. Moreover, the Peaceman-Rachford variant of ADI appears as efficient for non-separable problems as it is for separable problems. This observation has been reported by Young and Ehrlich (1960) and Price and Varga (1962) for the standard, $O(h^2)$, finite difference equations.

We have seen then how effective high accuracy difference equations can be. Even though none of the examples considered here could be called practical problems, these results are certainly impressive. Because the high accuracy methods, in many cases, allow one to use fewer mesh points to obtain a given accuracy, computer time and storage can be saved.

Both the theoretical results in the body of this paper and the numerical results presented here indicate that, when solving practical problems, high accuracy finite difference equations should be considered.

BIBLIOGRAPHY

Batschelet, E. (1952), "Über die numerische Auflösung von Randwertproblem bei elliptischen partiellen Differentialgleichungen," Z. angew. Math. Physik, 3, 165-193.

Birkhoff, G. and Varga, R. S. (1959), "Implicit Alternating Direction Methods," Trans. Amer. Math. Soc., 92, 13-24.

Birkhoff, G., Varga, R. S., and Young, D. M., (1962), "Alternating direction implicit methods," Advances in Computers, Vol. 3, Academic Press, New York.

Bramble, J. H. and Hubbard, B. E. (1964a), "On a Finite Difference Analogue of an Elliptic Boundary Problem Which is Neither Diagonally Dominant nor of Non-Negative Type," J. of Math and Physics, No. 43, 117-132.

Bramble, J. H. and Hubbard, B. E. (1964b), "New Monotone Type Approximations for Elliptic Problems," Math. of Computation, Vol. 18, No. 87, 349-367.

Collatz, L. (1933), "Bermerkungen zur Fehlerabschätzung für das Differenzenverfahren bei partiellen Differentialgleichungen," Z. Angew. Math. Mech., Vol. 13, 56-57.

Collatz, L. (1960), Numerical Treatment of Differential Equations, 3rd ed., Springer, Berlin.

Feingold, D. and Spohn, D. (1963), "Un théoréme simple sur normes de matrices et ses conséquences," C. R. Acad. Sci. Paris, 256, pp 2758-2760.

Forsythe, G. E. and Wasow, W. R. (1960), Finite-Difference Methods for Partial Differential Equations, Wiley, New York.

Gantmacher, F. P. and Krein, M. G. (1950), Oscillation Matrices and Small Vibrations of Mechanical Systems, Moscow, Leningrad. Trans. Available - Office of Technical Service, Dept. of Commerce, Washington 25, D.C.

Gantmacher, F. P. (1959), The Theory of Matrices, Vol. II, Translated and revised by K. A. Hirsch, Chelsea, New York.

Gerschgorin, S. (1930), "Fehlerabschätzung für das Differenzenverfahren zur Lösung partiellen Differential-gleichungen," Z. Angew. Math. Mech. 10, 373-382.

Gerschgorin, S. (1931), "Über die Abrenzung der Eigenwerte eiven Matrix," Izv. Akad. Nauk SSSR Ser. Mat. 7, 749-754.

Henrici, P. (1962), Discrete Variable Methods in Ordinary Differential Equations, John Wiley and Sons, Inc., New York.

Householder, A. S. (1964), The Theory of Matrices in Numerical Analysis, Blaisdell Publishing Company, New York,

Ostrowski, A. M. (1955), "Determination mit überwiegender Hauptdiagonals und die absolute Konvergenz von linearen Iterationsprozcssen, Comm. Math. Helv. 30, 175-210.

Peaceman, D. W. and Rachford, H. H. (1955), "The Numerical Solution of Parabolic and Elliptic Differential Equations," J. of Soc. Indust. Appl. Math. 3, 28-41.

Pearcy, C. (1962), "On Convergence of Alternating Direction Procedure," Numerische Math. 4, 172-176.

Price, H. S. (1965), "Monotone and Oscillation Matrices Applied to Finite Difference Approximations," Doctoral Thesis, Case Institute.

Price, H. S. and Varga, R. S. (1962), "Recent Numerical Experiments Comparing Successive Overrelaxation Iterative Methods with Implicit Alternating Direction Methods," Gulf Research & Development Company, Report No. 91, Reservoir Mechanics Division.

Price, H. S., Varga, R. S., and Warren, J. E. (1966), "Application of Oscillation Matrices to Conduction-Convection Equations," to appear in the Journal of Math and Physics.

Rockoff, M. L. (1964), "Comparison of Some Iterative Methods for Solving Large Systems of Linear Equations," Nat. Bureau of Standards Report 8577.

Roudebush, W. H. (1963), "Analysis of Discretization Error for Differential Equations with Discontinuous Coefficients," Doctoral Thesis, Case Institute.

Wachspress, E. L. (1962), "Optimum Alternating-Direction-Implicit Iteration Parameters for a Model Problem," J. Soc. Indust. Appl. Math. 8, 403-424.

Wachspress, E. L. (1963), "Extended Applications of Alternating Direction-Implicit Iteration Model Problem Theory," J. Soc. Indust. Appl. Math. 11, 994-1016.

Wachspress, E. L. and Habetler, G. J. (1960), "An Alternating Direction-Implicit Iteration Technique," J. Soc. Indust. Appl. Math. 8, 403-424.

Widlund, O. B. (1966), "On the Rate of Convergence of an Alternating Direction Implicit Method in A Non-Commutative Case," to appear.

Varga, R. S. (1962), Matrix Iterative Analysis, Prentice Hall, Englewood Cliffs, New Jersey.

Young, D. M. and Ehrlich, L. (1960), "Some Numerical Studies of Iterative Methods for Solving Elliptic Difference Equations," Boundary Problems in Differential Equations, University of Wisconsin Press, Madison, pp. 143-162.

CALCULATION OF WATER DISPLACEMENT BY GAS IN DEVELOPMENT OF AQUIFER STORAGE

By

K. H. Coats*
J. G. Richardson*

INTRODUCTION

In recent years natural gas has been stored near markets in aquifers where insufficient storage capacity is available in depleted fields. Operators of these aquifer storage reservoirs have encountered technical problems relating to the gas-water displacement accompanying initial growth of the gas bubble. The injected gas tends to override the water, with a resultant low displacement efficiency and high rate of gas travel downstructure toward spill points. Low displacement efficiency makes it difficult to sustain water-free gas production. Sometimes the fingering of gas downstructure may be so pronounced that the injection rate must be severly curtailed, which excessively lengthens the time required for bubble growth.

This paper is concerned with estimating - for given aquifer characteristics and fluid properties - the displacement efficiency, rate of gas movement down-structure, and rate of gravity drainage of water behind the gas front. Several published articles relate to the simulative capability necessary to handle this problem. The Dietz formula[1] and Buckley-Leverett method[2] have some applicability to the problem;

*Esso Production Research Company, Houston, Texas

Woods and Comer[3] reported one-dimensional, radial calculations which accounted for the two-phase flow of gas and water. Most of the recent research directed toward understanding of aquifer behavior in relation to gas storage has concentrated on single-phase flow in the aquifer.[4] Douglas, Peaceman, and Rachford[5] presented a method for calculating multidimensional two-phase flow in reservoirs; their method has been applied in work reported by Nielsen[6], Blair and Peaceman[7], and Goddin[8].

The purpose of this paper is to illustrate the use of two-dimensional, two-phase flow calculations in simulating the gas-water displacement. The calculations described account for capillary and gravity forces, relative permeability, and reservoir heterogeneity. An example reservoir is described and calculated results are presented for a variety of injection rates and values of permeability, reservoir thickness, and dip angle. The results are compared with those obtained from the Buckley-Leverett and Dietz formulas.

EQUATIONS EMPLOYED

The well-known, basic equations governing two-phase flow in porous media are:

(a) Darcy's Law for each fluid phase,

(b) the continuity equation expressing conservation of mass, and

(c) the definition of capillary pressure.

These three equations are combined as shown in Appendix A to give Equations (1).[5]

The gas and water are treated as incompressible.

$$\vec{\nabla}\cdot\left(k\frac{k_{rw}}{\mu_w}\vec{\nabla}\Phi_w\right) - B_w q_w = \phi S'\frac{\partial \Phi_g}{\partial t} + \phi S'\frac{\partial \Phi_g}{\partial t}; \qquad (1a)$$

$$\vec{\nabla}\cdot\left(k\frac{k_{rg}}{\mu_g}\vec{\nabla}\Phi_g\right) + B_g q_g = \phi S'\frac{\partial \Phi_g}{\partial t} - \phi S'\frac{\partial \Phi_g}{\partial t}. \qquad (1b)$$

Equation (2) gives the critical rate[9] as a function of formation and fluid properties,

$$q_{gc} = 1.124 \times 10^{-6}\frac{kA}{B_g}\frac{\rho_w - \rho_g}{\mu_w - \mu_g}\sin\alpha_d \ \text{MMCFD}, \qquad (2)$$

where A is cross-sectional area perpendicular to the direction of flow.

This formula is derived by balancing viscous and gravitational forces about a small finger of gas extending downstructure into the water parallel to the bedding plane.* Sustained gas injection above the critical rate is undesirable, since the displacement of water will be inefficient and the gas will finger unstably downstructure at a high rate. The critical rate thus serves as a useful guide or reference rate in establishing the gas injection rate during bubble growth. Where

*Equation (2) and the following Dietz Equation (3) may be written with k/k_{rw}, μ_g/k_{rg} replacing μ_w and μ_g. However, this replacement requires choice of thegas saturation (e.g., frontal saturation or average saturation behind front) at which k_{rg} is to be evaluated. That question deserves extensive consideration and has in fact been the subject of several previous papers. For the sake of simplicity, and to avoid lengthy discussion of a subject somewhat apart from the purpose of this paper, k_{rg} is excluded from Equations (2) and (3). The critical rate given by Equation (2) is therefore employed here only as a reference rate; it is not viewed as a rate at which unstable fingering of gas necessarily begins. Rates above the critical rate given by Equation (2) may, in fact, yield a favorable mobility ratio at the displacement front.

the critical rate is far lower than the desired injection rate, gravity segregation plays little role in preventing a rapid rate of gas travel downstructure.

For injection rates below the critical, the Dietz formula, Equation (3), gives the angle between the bedding plane and the gas-water interface as a function of rate and formation and fluid properties.[1]

$$\tan\theta = \tan\alpha_d - 0.89 \times 10^6 \frac{q_g B_g}{k A} \frac{\mu_w - \mu_g}{(\rho_w - \rho_g)\cos\alpha_d} . \qquad (3)$$

To evaluate the utility of this formula, the predicted angle is compared with results calculated from Equations (1).

One of the reservoir scaling groups derived by Rapoport and Leas[1] for incompressible, two-phase flow is the ratio of viscous to gravitational forces, $\frac{q\mu_w/Lk}{L\,\Delta\rho}$. Since injection rate q, and permeability k appear only as the ratio q/k, their effects on reservoir performance can be considered as the single effect of the ratio, q/k.

DISPLACEMENT STUDIES

Scope

Two-dimensional calculations employing Equation (1) were performed to simulate the growth of a gas bubble in a slightly dipping aquifer. The example aquifer or reservoir was represented by the homogeneous, vertical cross section described below. Calculations were performed for various values of injection rate, permeability, reservoir thickness, and dip angle. A severely stratified case was also treated to illustrate the effect of heterogeneity. The two-dimensional calculations

were performed on a vertical cross section in order to describe the gas overriding the water. This overriding tendency has a great effect on the efficiency with which water is displaced. On the other hand, areal coverage tends to be fairly good when the gas overrides so the displacement behavior in the vertical cross section is of greater interest than that in the areal grid.

Description of Example Reservoir

The example reservoir treated here is patterned roughly after the Mt. Simon aquifer storage field.[11] Fig. 1 illustrates the homogeneous vertical slice or cross section, 3000 ft. long and 100 ft. thick, with a 3° dip angle. Gas injection rate is based on a width of 7500 ft. The injection rate and fluid and rock properties for the reservoir, given in Table 1, constitute the base case (or Case 1) for the calculations. The relative permeability and capillary pressure curves listed in Table 1 were averaged from data on a number of permeable Eocene sandstone core samples.

Table 2 gives data and results for all seven cases calculated. Cases 2-7 involve variations in permeability, reservoir thickness, dip angle, and gas injection rate. For each case in Table 2, data not reported are identical with those given in Table 1. Table 2 also includes the ratio of injection rate to critical rate for each case.

Procedure

Equations (1) were solved simultaneously, employing ADIP as

described in the literature.[5] The cross section was represented by a 30 x 10 grid, yielding a block 100 ft long x 10 ft thick (30 x 5 grid in cases involving 50-ft thickness). Gas was injected into the top, corner block of the reservoir as shown in Fig. 1. Water was produced from all ten blocks through the thickness at the downdip end of the section.

Iterations at each time step were continued until the incremental material balance was less than 0.003—i.e., until the sum of the changes in block gas saturations multiplied by block pore volume differed by less than 0.3 percent from the amount of gas injected during the time step. About 8 iterations per time step were required. Cumulative material balance, defined as total gas in place divided by total gas actually injected, was generally less than 0.5 percent, always less than one percent in error. Time steps were limited so that the maximum block saturation change was less than 10 percent in one time step.

As an example of computer time requirements, using 57 time steps to simulate injection at one MMCF/D for 1050 days (Case 2) required 16.84 minutes of IBM 7044 time ($200 per hour).

Base Case Results

Data for the base case are given in Table 1. The injection rate is 5 MMCF/D into a 200-millidarcy formation 100 ft thick and 7500 ft wide. Fig. 1 shows the calculated position of the gas-water interface after 210 days, or cumulative injection of 1.05 Bcf. The 5 MMCF/D rate is 3.62 times the critical rate and results in a severe gas override

as shown in the scale representation of the cross section; the tongue of gas reaches over 2100 ft downstructure. The displacement efficiency, defined as the percentage of the water initially in place that we displaced from the region invaded by gas*, is 37.2 percent. Fig. 2 shows depth-averaged gas saturation vs distance along the cross section. Fig. 3 shows the rate of gas travel downstructure. The gas front travels 800 ft in 60 days and continues to move linearly with time.

Comparison With Buckley-Leverett Results

The Buckley-Leverett technique was applied to the base-case data of Table 1 to calculate saturation versus distance after 210 days of injection. Fig. 4 shows that the Buckley-Leverett and 2-D results are in poor agreement; the Buckley-Leverett technique gives a gas movement downstructure of only 700 ft compared with the 2100 ft predicted by the 2-D method.

Fig. 5 shows equally poor agreement between Buckley-Leverett and 2-D results for an injection rate less than the critical rate (Case 2, Table 2). The primary reason for this poor agreement is the inability of the Buckley-Leverett method to account for the two-dimensional nature of the displacement—i.e., for the pronounced override of the water by the gas.

The lack of applicability of the Buckley-Leverett results indicates the need for 2-D or 3-D calculations in simulating gravity override of water by injected gas.

*Since relative permeability to water is 0 at a water saturation of 22 percent (see Table 1), the maximum possible displacement efficiency is 78 percent.

Comparison of 2-D Results With Dietz Equation

Two-dimensional calculations were performed for an injection ra less than the critical rate in order to compare the inclination of th gas-water interface with the inclination yielded by the Dietz Equatio (3). Fig. 6 shows the position of the gas-water interface given by two-dimensional calculations simulating 1050 days of injection at one MMCF/D (Case 2, Table 2). Insertion of the Case 2 data into Equation (3) yields tan θ = 0.0142. In Fig. 6, the line drawn corresponding t that angle corresponds to a 100 percent displacement of mobile water, a displacement efficiency of 78 percent. The figure shows that the Dietz angle provides a good approximation to the inclination of the interface over the flat portion. However, the Dietz equation predict only the angle, not the position of the interface. Positioning of th interface requires that the average displacement efficiency behind th front be known, and determination of this efficiency requires 2-D cal culations.

Effects of Permeability, Dip Angle, and Thickness

The 2-D results for Case 2 show how permeability affects the ga water displacement. This case is identical with the base case except that injection rate is one MMCF/D, less than critical. Injection rat and permeability affect reservoir performance only through the ratio q/k, as discussed above. Therefore, Case 2 results are identical wit those for the case of five MMCF/D rate of injection into a 100-md for ation. Thus comparison of Case 1 and Case 2 results shows how a five-

fold larger permeability affects the displacement.

Fig. 6 shows the position of the gas-water interface after injection of 1.05 Bcf. Comparison with Fig. 1 shows that the higher permeability results in a more nearly horizontal interface, lesser extent of gas travel downstructure, and higher displacement efficiency. For the 1000-md permeability, the gas traveled only 1300 ft downstructure compared with 2100 ft in the 200-md case. The displacement efficiency for 1000 md was 46.3 percent, compared with 37.2 percent for 200 md.

Case 3, as noted in Table 2, differs from the base case only in that the sine of the dip angle is increased from 0.05 to 0.25. As noted in Table 2, the higher dip angle reduces the gas travel downstructure after injection of 1.05 Bcf from 2100 ft in the base case to 800 ft. The displacement efficiency rises from 37.2 percent to 46 percent. The injection rate of 5 MMCF/D for Case 3 is below critical, as noted in Table 2. These considerable effects of dip angle on rate of gas movement and displacement efficiency indicate the desirability of locating steeply dipping structures for storage purposes.

Case 4 illustrates the effect of a 50 percent reduction in injection rate to 2.5 MMCF/D. As noted in Table 2, displacement efficiency after injection of 1.05 Bcf rises from the base case 37.2 percent to 43.3 percent, and gas travel downstructure decreases from the 2100-ft base case to 1800 ft.

Case 5 shows how reservoir thickness affects displacement efficiency. Data for this case are identical with those for Case 4 except

that reservoir thickness is reduced 50 percent, to 50 ft. Displacement efficiency, after 0.525 Bcf injection, dropped from the 39.4 percent of Case 4 to 33.5 percent. Gas travel downstructure increased, reaching 1600 ft as compared with 1100 ft. These results indicate the desirability of thick sands in aquifer storage structures.

Heterogeneous Case

Cases 6 and 7 illustrate the effect of severe heterogeneity. Case 6 is a stratified formation with five layers varying from 20 to 500 md in permeability. The layer thicknesses and vertical permeabilities are given in Table 3. Case 7 is identical with Case 6 except that the reservoir is homogeneous with the same millidarcy-feet product. Fig. 7 compares calculated positions of the gas-water interface after injection of 0.525 Bcf for the stratified and homogeneous cases. In the stratified formation, a finger or wafer of gas in high-permeability layer 4 reaches over 2600 ft downstructure; in the homogeneous formation (equivalent Case 7), it reaches only 1700 ft. Gas entered the tight layers 1 and 3 in the stratified reservoir almost entirely by percolation upward from high-permeability layers 2 and 4. The displacement efficiency in the stratified formation (Case 6) is only 9.35 percent, compared with 32 percent for the equivalent homogeneous formation (Case 7).

Fig. 8 shows calculated gas saturation contours for the stratified aquifer. The 5 percent saturation contour exhibits the same character as the interface contour of Fig. 7, in that it is further advanced in

tight layer 3 than in loose layer 2. However, the 10 percent saturation contour exhibits the contrary behavior of further advancement in layer 2 than in layer 3. The reason for this situation is that the gas enters tight layer 3 by percolating upward from layer 4, and for small saturations (e.g., 5 percent or less) the low relative permeability to gas in layer 3 retards further percolation upward to layer 2. However, with higher gas saturations in layer 3 (e.g., 10 percent or more), sufficiently high relative permeabilities to gas exist to allow significant flow upward to layer 2, thus causing the character of the 10 percent saturation profile shown in Fig. 8.

The significant effect of heterogeneity in Case 6 shows the need for reservoir description. It is probably true that our ability to simulate reservoirs at the present time exceeds our ability to describe them. Considerable reliance on simulated performance is justified where sufficient core data, well tests, and some history for matching purposes are available. Simulation of performance can still be useful when little is known about the reservoir properties, however, since calculations assuming a homogeneous sand will generally give a conservative estimate of the rate of gas travel downstructure and an upper limit on the displacement efficiency.* If calculations assuming a homogeneous sand indicate intolerably low displacement efficiencies and high rates of

*This statement holds for random arrangements of layers of differing permeability. However, it is not strictly true since one could easily design a stratification that would retard the gas fingering along the caprock and thereby increase displacement efficiency relative to the homogeneous case.

gas travel, perhaps past spill points, then they justify dismissal of the structure as a potential storage site. However, where permeabilit distributions are known for a potential storage reservoir, these shoul be included in the calculations.

CONCLUSIONS

Based on the two-phase, two-dimensional calculations conducted i this study, and on comparisons of these with results of one-dimensiona calculations, the following conclusions are reached:

1. Two-phase, two-dimensional calculations appear to be necessa for reliable estimates of displacement efficiency and rates of gas mov ment downstructure in aquifer storage projects.

2. Where at all possible, calculations should include the perm- eability distribution of the aquifer in question. Generally, when the sand is assumed to be homogeneous, displacement efficiencies are too high and rates of gas movement are too low.

3. One-dimensional calculations such as the Buckley-Leverett technique predict displacement efficiencies that are too high and rate of gas movement that are too low.

References

1. Dietz, D. N.: "A Theoretical Approach to the Problem of Encroaching and By-Passing Edge Water," Prec. Kan. Neder. Adad., Wetenshaffen (1953) Series B-56, 83.

2. Buckley, S. E., and Leverett, M. C.: Trans. AIME, 146:107 (1942).

3. Woods, E. G., and Comer, A. G.: "Saturation Distribution and Injection Pressure for a Radial Gas Storage Reservoir," Trans. AIME, 1962.

4. Katz, D. L., et al.: "Movement of Underground Water in Contact with Natural Gas," AGA Monograph on Project No. 31, New York, New York, 1963.

5. Douglas, J., Jr., Peaceman, D. W., and Rachford, H. H., Jr.: "A Method for Calculating Multi-Dimensional Immiscible Displacements," Trans. AIME 216:297 (1959).

6. Nielsen, R. L., Doctoral Dissertation: "On the Flow of Two Immiscible Incompressible Fluids in Porous Media," Univ. of Michigan, 1962.

7. Blair, P. M., and Peaceman, D. W.: "An Experimental Verification of of a Two-Dimensional Technique for Computing Performance of Gas-Drive Reservoirs," Trans. AIME 228, 19-II, 1963.

8. Goddin, C. S., Jr., et al.: "A Numerical Study of Waterflood Performance in a Stratified System With Crossflow," Jour. of Pet. Tech., June 1966, p. 765.

9. Hill, S.: Genie Chemique, Chem. Eng. Sci. I (6): 246 (1952).

10. Rapoport, L. A., and Leas, W. J.: Trans. AIME, 198:159 (1953).

11. Rzepczynski, W. M., Katz, D. L., Tek, M. R., and Coats, K. H.: "How the Mt. Simon Gas Storage Project Was Developed," The Oil and Gas Journal, June 19, 1961.

TABLE I

DATA FOR EXAMPLE RESERVOIR, BASE CASE

Water density	.433 psi/ft
Gas density	.0208 psi/ft
Water viscosity	1 cp
Gas viscosity	.013 cp
Water formation volume factor	1 RB/STB
Gas formation volume factor	2.55 RB/MCF
Permeability	200 md
Porosity	.15
Reservoir length	3000 ft
Reservoir width	7500 ft
Reservoir thickness	100 ft
Dip angle, sine	.05
Initial saturation	100% water
Injection rate	MMCFD
2-D grid	30 x 10
Critical Rate, q_{gc}	1.38 MMCFD

CAPILLARY PRESSURE-RELATIVE PERMEABILITY DATA

Water Saturation (fraction)	Capillary Pressure (psi)	Water Relative Permeability (fraction)	Gas Relative Permeability (fraction)
.22	15.	.0	1.
.23	8.8	.00018	.977
.25	6.2	.00045	.925
.3	3.57	.0013	.802
.35	2.76	.00215	.683
.4	2.45	.003	.573
.45	2.16	.006	.466
.5	1.86	.012	.372
.55	1.57	.022	.287
.6	1.29	.04	.211
.65	1.	.065	.152
.7	.71	.099	.106
.75	.42	.146	.069
.8	.09	.202	.043
.85	- .22	.285	.023
.9	- .56	.418	.008
.95	- .91	.675	.002
.99	-1.3	.932	.0
1.	-1.5	1.	.0
1.	-200.	1.	.0

TABLE 2

DATA AND RESULTS FOR CASES 1 - 7

Case	Permeability	Sine of Dip Angle	Thickness	Injection Rate MMCFD	Cumulative Injection BCF	Injection Rate/ Critical Rate	Displacement Efficiency	Distance of Gas Travel Down-Structure
	200 md	.05	100 ft	5	1.05	3.62	37.2 %	2100 ft
1					1.05	.725	46.3	1300
2	200	.05	100	1	1.05	.725	46.	800
3	200	.25	100	5	1.05	1.81	43.3	1800
4	200	.05	100	2.5	.525	1.81	39.4	1100
4	200	.05	100	2.5	.525	3.62	33.5	1600
5	200	.05	50	2.5	.525	-	9.35	2500
6	See Table 3	.05	50	2.5	.525	4.6	32.	1700
7	158	.05	50	2.5				

TABLE 3

DESCRIPTION OF STRATIFIED AQUIFER, CASE 6

Layer #, i	Horizontal Permeability	Vertical Permeability Between Layers i & i+1	Thickness
1	50 md	1.6 md	10 ft
2	200	.727	10
3	20	.385	10
4	500	7.7	10
5	20	0.	10

Porosity = 0.15

See Table 1 for other data

APPENDIX

3-D Flow Equations

The basic equations governing incompressible, two-phase flow in porous media are:

(a) The continuity, or material balance, equations for each phase

$$-\vec{\nabla}\cdot(\vec{v}_w) + B_w q_w = \frac{\partial}{\partial t}\cdot(\phi S_w) \tag{A1a}$$

$$-\vec{\nabla}\cdot(\vec{v}_n) + B_n q_n = \frac{\partial}{\partial t}(\phi S_n) \tag{A1b}$$

(b) Darcy's Law relating superficial velocities to flow potential

$$\vec{v}_w = -k\frac{k_w}{\mu_w}\vec{\nabla}\Phi_w$$

$$\vec{v}_n = -k\frac{k_n}{\mu_n}\vec{\nabla}\Phi_n \tag{A2}$$

(c) The capillary pressure definition

$$P_c = P_n - P_w$$

Equation (A3), along with the definition of Φ,

$$\Phi_w = P_w - P_{wh}$$

$$\Phi_n = P_n - P_{nh} \tag{A4}$$

allows expression of the saturation derivative $\frac{\partial S_w}{\partial t}$ in terms of the potentials,

$$\frac{\partial S_w}{\partial t} = S'\left[\frac{\partial \Phi_n}{\partial t} - \frac{\partial \Phi_w}{\partial t}\right] \tag{A5}$$

Substitution of (A2) and (A5) into (A1) yields two equations in two dependent variables Φ_w and Φ_n:

$$\vec{\nabla} \cdot \left(k \frac{k_w}{\mu_w} \overrightarrow{\nabla \Phi_w}\right) + B_w q_w = - \phi S' \frac{\partial \Phi_w}{\partial t} + \phi S' \frac{\partial \Phi_n}{\partial t} \qquad \text{(A6a)}$$

$$\vec{\nabla} \cdot \left(k \frac{k_n}{\mu_n} \overrightarrow{\nabla \Phi_n}\right) + B_n q_n = \phi S' \frac{\partial \Phi_w}{\partial t} - \phi S' \frac{\partial \Phi_n}{\partial t} \qquad \text{(A6b)}$$

where $S' = dS_w/dPc$. Multiplying equations (A6) by the block volume $\Delta x\, \Delta y\, \Delta z$ and writing derivations in difference form yields

$$\Delta A_w \Delta \Phi_w + B_w Q_w = - G \Delta_t \Phi_w + G \Delta_t \Phi_n$$

$$\Delta A_n \Delta \Phi_n + B_n Q_n = G \Delta_t \Phi_w - G \Delta_t \Phi_n$$

where

$$\Delta A \Delta \Phi = \Delta_x AX \Delta_x \Phi + \Delta_y AY \Delta_y \Phi + \Delta_z AZ \Delta_z \Phi$$

$$\Delta_x AX \Delta_x \Phi = AX_{i+\frac{1}{2},j,k} (\Phi_{i+1,j,k} - \Phi_{ijk}) - AX_{i-\frac{1}{2},j,k} (\Phi_{ijk} - \Phi_{i,j,k})$$

$$AX_{i+\frac{1}{2},j,k} = \left(k \frac{k_r}{m} \frac{\Delta y \Delta z}{\Delta x}\right)_{i+\frac{1}{2},j,k}$$

$$G = \frac{PV\, S'}{\Delta t} = \frac{\phi \Delta x \Delta y \Delta z\, S'}{\Delta t}$$

$$\Delta_t \Phi = \Phi^{n+1}_{ijk} - \Phi^{n}_{ijk}$$

$$x = i\Delta x \quad y = j\Delta y \quad z = k\Delta z \quad t = n\Delta t$$

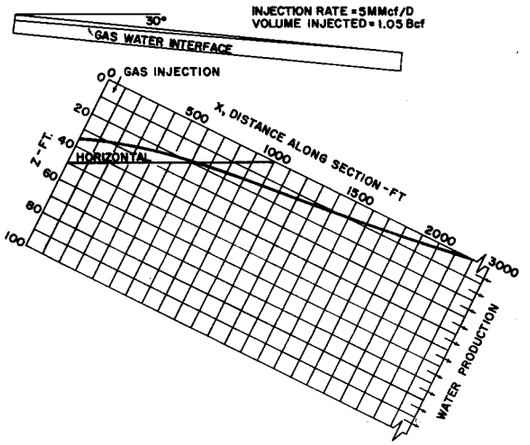

FIG. 1 CALCULATED POSITION OF GAS-WATER INTERFACE - BASE CASE

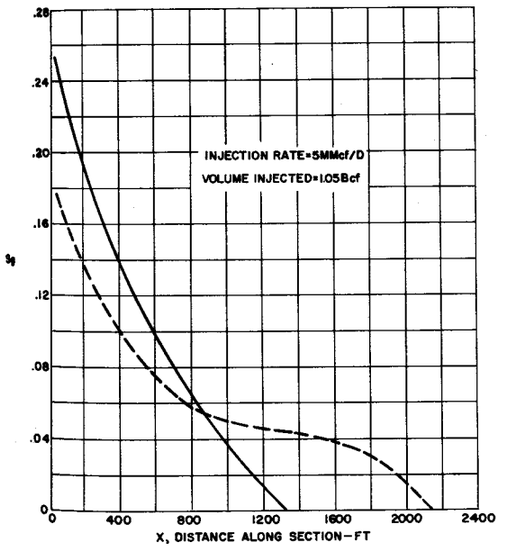

FIG. 2. DEPTH-AVERAGED GAS SATURATION PROFILE—BASE CASE

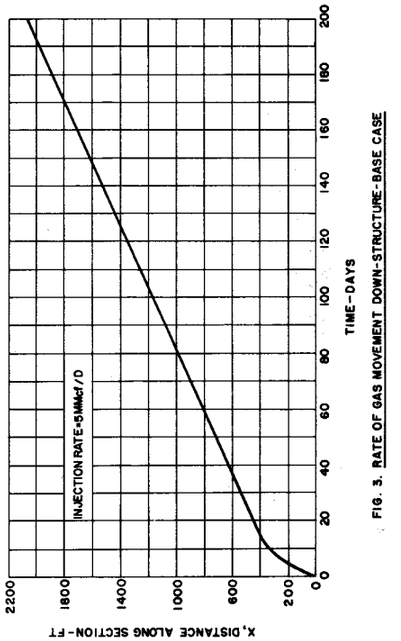

FIG. 3. RATE OF GAS MOVEMENT DOWN-STRUCTURE-BASE CASE

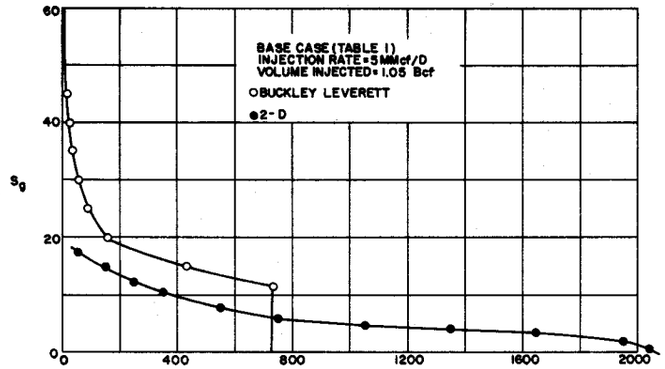

FIG. 4. COMPARISON OF SATURATION PROFILES CALCULATED BY BUCKLEY-LEVERETT AND 2-D METHODS - BASE CASE.

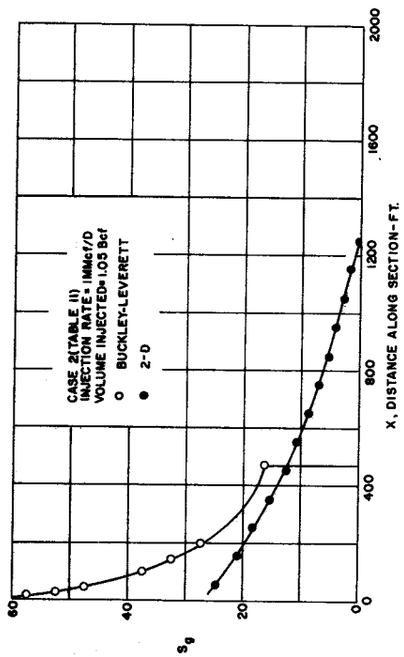

FIG. 5. COMPARISON OF SATURATION PROFILES CALCULATED BY BUCKLEY-LEVERETT AND 2-D METHODS - CASE 2.

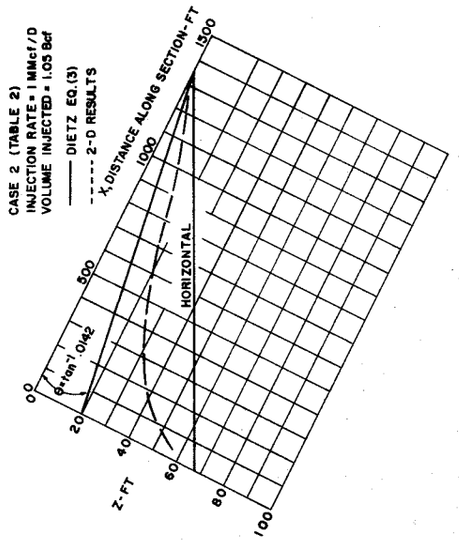

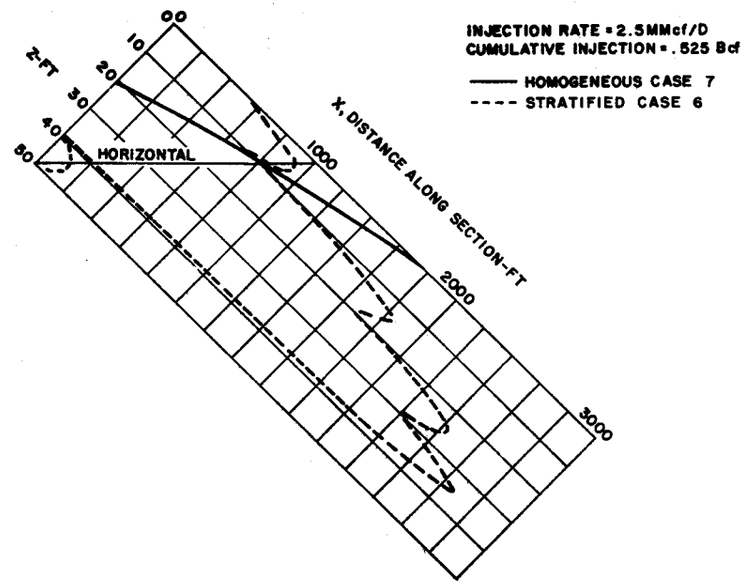

FIG. 7. COMPARISON OF GAS-WATER INTERFACE POSITIONS IN STRATIFIED AND HOMOGENEOUS AQUIFERS.

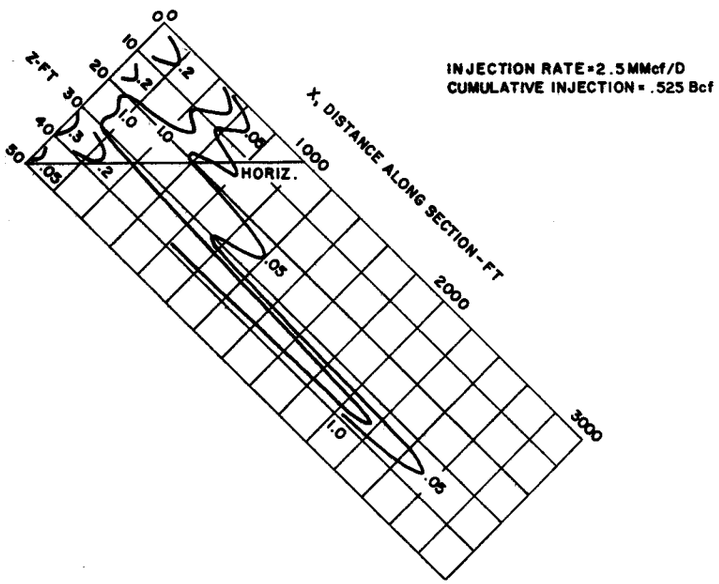

FIG. 8. CALCULATED GAS SATURATION CONTOURS IN STRATIFIED AQUIFER - CASE 6

A Study of Wellbore Heat Losses during the Injection of Superheated Steam

by C. J. Lingard

The Pennsylvania State University

1. INTRODUCTION

At present, steam injection operations are confined to the use of saturated steam. Thermal units now on the market can produce up to 80% quality steam with generator pressures up to 2500 psia, and capacities up to 20 MMBTU/hour. However, heat losses from surface lines and from the wellbore may considerably reduce the quality of steam at the formation, depending upon injection rate and formation depth. Recently, equipment companies have announced that they are capable of manufacturing thermal units which will deliver superheated steam. This study examines the advisability of using superheated steam, by consideration of the wellbore heat losses accompanying injection into a shallow formation.

Aside from an economic viewpoint, it is apparent that the greater the thermal energy that can be delivered to the formation during steam injection, the greater the benefits obtained through oil viscosity reduction, thermal expansion effects, steam distillation of light fractions, et cetera, in the reservoir. Although this energy can be increased, theoretically, by increasing injection rate alone, in practice low formation permeabilities may result in relatively low maximum injection rates. In such cases, we must resort to using steam at higher energy levels, either higher quality, or higher temperatures, possibly in the one-phase state, the latter possibility being dependent upon injection pressures. However it must be remembered that the prime objective of steam injection is not merely to deliver the maximum thermal energy to the formation, but is to obtain the maximum economic recovery. Thus the extra fuel costs for producing superheated steam must be carefully compared with any possible increase in oil recovery which may result. In this connection wellbore heat losses must be considered together with losses from surface lines and from the formation, and variations in bottom hole temperature are only important insofar as they affect temperature distributions in the reservoir.

2. LITERATURE REVIEW

Many recent papers have appeared in the literature on the various aspects of thermal effects in the wellbore during hot fluid injection, and a few of these will be mentioned for their relevance to this present study.

Squier et al. (1) considered temperature behavior of hot water injection wells, and used analytical techniques for calculating bottom hole temperature as a function of time. They regarded everything exterior to the tubing - annulus, casing, cement - as part of the formations, and obtained a solution in terms of Bessel functions by solving a system of differential equations, using various Laplace transforms.

Ramey (2) calculated heat losses to the casing and formation, in the case of hot water injection, by approximating the total energy equation for fluid flow. He introduced a time function to approximate transient heat conduction through the earth, and made use of an overall heat transfer coefficient for dealing with the different heat resistances in the wellbore. His solution was again analytic.

Leutwyler (3) presented a finite difference technique for studying casing temperature as a function of time during hot fluid, liquid or gas, injection. His results compared favorably with those of the analytical methods of Ramey, and Moss and White (4) and also with Caslaw and Jaegers' solution to the diffusivity equation for a line source (5). However he found that, for a constant tubing temperature, casing temperature did not stabilize as quickly as had been suggested by Ramey, and in one example, with a tubing temperature of 600°F, he calculated that the casing temperature still rose 1°F every 20 days, after 300 days of injection. He also examined the effect, on casing temperature, of a nitrogen filled annulus, special insulating cements, and aluminum coated tubing.

Satter (6) studied the effect of condensation during the injection of saturated steam, and by a numerical trial-and-error step method. He obtained a series of graphs applicable to calculation of heat losses for a wide variety of injection conditions. He developed useful correlations between injection pressure and temperature, injection rate, and heat loss per unit depth. He also examined the effect of downhole packers on heat losses to the casing and casing temperature.

3. ASSUMPTIONS

The following assumptions were made during the calculations. In this present study, the depth to the formation was 1000 feet, but it is felt that many of these assumptions would be extremely questionable in a similar study applied to greater depths.

1. The geothermal gradient is neglected. T_e, the initial earth temperature is assumed everywhere constant and is taken as the arithmetic average of the top and bottom hole temperature. To 1000 feet depth, the actual earth temperature increases approximately 15°F, and this variation is less than most fluctuations in surface temperature during the day.

2. Pressure is constant with depth. The effects of friction and gravity are in fact opposed during injection, and although unlikely to balance one another, their resultant effect is small in shallow wells.

3. Kinetic energy changes are negligible. This assumes fluid incompressibility, and is questionable.

4. The tubing hangs symmetrically inside the casing. Any variation from this position would have a marked effect on the shape factor for radiation in the Stefan Boltzman equation and consequently, heat losses to the casing would increase. If the tubing were to touch the casing, assumption 7 would not hold, and heat losses by continuous conduction to the earth would give locally high casing temperatures. However in shallow wells this assumption may well be true. It is also assumed that a downhold packer is used, and that the tubing is coated with aluminum.

5. The diffusivity and conductivity of the earth are constant with depth, and with temperature. This is at best a rough approximation, but lack of data makes it necessary for the calculation to assume average values of these properties. However it is possible that these average values are in error of 10% or more. If so, from a consideration of equation 13 it is apparent that we are calculating results applicable at some time t' instead of at time t, where $f(t')$ and $f(t)$ (Ramey's time function for transient conduction) may vary by 10%. This varying function may mean that, for example, when t is 3 months - the time we assume our calculated results apply - , t' is 12 months - the actual time that the results apply.

6. Conduction through the walls of the tubing and casing is neglected. Compared to the heat transfer coefficients for the annulus and the earth, the thermal resistance of steel is negligible.

7. Conduction and convection in the annulus are neglected. Conductivity of air is very low, and heat transfer by convection is difficult to estimate and probably overshadowed by radiant heat transfer.

8. The cement is taken as part of the earth. In fact thermal conductivity of cement is only slightly lower than that of earth.

9. Heat transfer in the wellbore is under steady-state conditions, whilst heat transfer from the casing to the earth is under unsteady state conditions. We assume that Ramey's graphical solution to this transient heat transfer is applicable at times greater than one month after the start of injection. The former assumption follows from a comparison of the overall heat transfer coefficients for the wellbore, with that of the earth.

10. Lastly, we assume, as was done in all previous work on this subject, that injection temperature and injection rate are both constant. However two interesting points arise in this connection.

Firstly, it may be deemed more economical to follow up a period of steam injection with a period of cold or hot water injection. In this case,of course, the results are only applicable to the former period. Injection temperatures may be increased to offset reduced injection rates, as the fill-up time in approached. This is the second point of interest. No work has as yet been done on injection behavior of steam injection wells, but undoubtedly the behavior will be similar to the case of behavior of cold water injection wells. In the latter case, injection rates may fall sharply during the fill-up time. Injection rate is one of the most important factors affecting percentage heat loss, and thus, for the initial period of injection heat losses will be somewhat greater than those calculated.

4. DERIVATION OF EQUATIONS

By consideration of an element of depth, dz, in the wellbore we can equate the following heat transfer rates.

dq = rate of heat transfer from tubing (heat loss of steam)
= rate of heat transfer to casing (radiation alone)
= rate of heat transfer to earth (transient thermal conductivity)

(a) The total energy equation for fluid movement through the tubing is

$$dH + \frac{g}{g_c}\frac{dZ}{J} + \frac{u\,du}{g_c\,J} = dQ - \frac{dW_f}{J} \qquad (1)$$

Assuming steady flow, $dW_f = 0$
Neglecting K.E. changes, $du = 0$
Neglecting P.E. changes, $dZ = 0$

And, since Q, the heat transferred per unit mass, is given as

$$dQ = -\frac{dq}{W} \qquad (2)$$

Hence

$$dq = -W\,dH \qquad (3)$$

In the case of a cooling gas in the tubing (superheated steam), the specific heat at constant pressure, C_p, is defined by

$$C_p = \frac{\partial H}{\partial T_1}_{p\ =\ \text{constant}} \qquad (4)$$

Furthermore, C_p is a function of temperature. But within any small step, dz in which the steam temperature falls by an amount dT_1, C_p is approximately constant, and

$$dH = C_p\,dT_1 \qquad (5)$$

where C_p is the specific heat at the average steam temperature in the interval. Equating (3) and (5)

$$dq = -W\,C_p\,dT_1 \qquad (6)$$

In the case of a condensing gas, specific enthalpy is a linear function of quality and so

$$H = Y \cdot h_{fg} + h_f \qquad (7)$$

or

$$dH = dy \cdot h_{fg} \qquad (8)$$

Equating (8) and (3) yields

$$dq = -h_{fg}\,W\,dy \qquad (9)$$

Thus equations (6) and (9) give the heat transfer rate from the tubing, for superheated and saturated steam, respecitvely.

(b) With the assumptions previously given, heat transfer from the tubing to the casing over the element dz is given by

$$dq = m\left(\frac{(T_1 + 460)^4}{100} - \frac{(T_2 + 460)^4}{100}\right) \qquad (10)$$

where

$$M = 0.172\,F_e\,F_a\,\frac{\pi}{12}\,D_t \qquad (11)$$

and $$Fe = \frac{1}{\frac{1}{e_t} + \frac{D_t}{d_c}\left(\frac{1}{e_c} - 1\right)} \qquad (12)$$

which is the Stefan Boltzman equation for radiant heat transfer, modified for emissivity and shape factors.

(c) Heat transfer to the earth over the element dz is given by

$$dq = \frac{2\pi K_e}{f(t)} (T_2 - T_e)dz \qquad (13)$$

which is Ramey's approximate solution to the radial transient conduction equation (diffusivity equation). The time function f(t) has the same relationship to transient heat conduction from a wellbore, that the Van-Everdingen & Hurst constant flux Q(t) function has to radial transient fluid flow. It is also dependent upon the diffusivity α and the outside casing diameter.

Hence by simultaneously solving equations (6), (10) and (13) we obtain T_1 (z,t) and T_2 (z,t) in the case of a condensing vapor. In both cases we also solve for dq and thus obtain the percentage heat loss in the tubing for each depth interval.

5. DATA FOR CALCULATIONS

(a) Earth Properties: Thermal Conductivity K_e = 1.40 BTU/hr.°F.ft
Thermal Diffusivity = 0.036 ft^2/hr
Average temperature to 1000 ft = 57°F

(b) Tubular Goods:

Casing (4 1/2" nominal)	I.D. 4.09"	O.D. 4.50"	e = 0.9
Tubing (2 1/2" nominal)	I.D. 2.441"	O.D. 2.875"	e = 0.3

Shape factor = 1.0 (concentric pipes)

(c) Steam Properties:

Injection Pressure 422.6 psia (saturation temperature 450°F)
Sensible heat of saturated water = 430.1 BTU/lb
Sensible heat of saturated steam = 1204.6 BTU/lb
Latent heat of steam = 774.5 BTU/lb

Specific heat (at constant pressure of 422.6 psia) is approximated by the following empirical equation.

$$C_p = 0.530 + 56.59\, e^{(-0.01172\, T_1)} \qquad (14)$$

where T_1 is steam temperature.

(d) Injection Conditions: The calculations were made for combinations of the following conditions:

1. Injection Temperatures: 450°F, 550°F, 650°F, 750°F, 850°F
2. Injection Rates: 2000 lbs/hour, 4000 lbs/hour, 8000 lbs/hour 16000 lbs/hour
3. Time after starting injection (months): 1, 4, 12, 24, 120

6. CALCULATION PROCEDURE

A computer program was written and executed as a means of obtaining a solution on a depth step basis at a given injection time. The required output consisted of steam temperature or quality, casing temperature and percentage heat loss, all as functions of depth, for different injection conditions. Depending upon the state of the fluid in the tubing, the program was in two parts. In part A, profiles were calculated for superheated steam, whilst part B was for saturated steam. Following execution of each step calculation, the steam temperature was tested, and if found to be 450° (saturation temperature) or below, control was transferred from part A to part B. The general computational technique for a given depth-step was as follows. The step size was ten feet depth.

Part A

1) The steam temperature and cumulative heat loss at the top of the interval were calculated from the previous step. This steam temperature is called TT.

2) A steam temperature at the bottom of the interval was assumed - TB.

3) The drop in temperature over the interval, TDIF, and the average steam temperature in the interval, TAV, (arithmetic mean of TT and TB) were calculated.

4) C_p was calculated by substitution of TAV into equation (14).

5) The heat loss over the interval was calculated using equation (6) - (PER).

6) The average casing temperature over the interval, TCAV was calculated from equation (13).

7) The values of TAV and TCAV, are entered into equation (10) and the value of the heat loss compared with that obtained from step (5) - PER.

8) If the values did not agree to the desired accuracy, a new value of TB was chosen, based upon the magnitude and sign of the discrepancy, and the computation was continued from step (3).

9) If the agreement was sufficiently accurate, the value of PER was added to the cumulative heat loss at the top of the interval, to obtain the heat loss at the bottom. TB, TCAV and the percent heat loss were printed.

10) TB was now set as the new TT and the computation was repeated from step (1).

Owing to the nature of equation (10), it was felt that individual step casing temperatures might be of a lower accuracy than the steam temperatures for the same interval. (This is because casing temperature appears to the fourth power in equation (10).) For this reason, casing temperatures of the previous steps were not used in the next steps, but steam temperatures alone were the basis for the solution. Calculated casing temperatures were therefore free of accumulated errors.

Part B

This part of the computation was relatively simple, since steam temperature is not a variable, and casing temperature is constant with depth. A trial-and-error solution for casing temperature is therefore performed only once for each profile. This is done by combining equations (10) and (13). Then the heat loss for each interval is calculated from (13) and the quality is calculated using equation (9) for each step. Quality and percent heat loss are printed out versus depth.

7. DISCUSSION OF RESULTS

The results obtained from the computer are given in a series of graphs. Most of these graphs show the results quite clearly, by themselves, but some of the main features of each one will be discussed below.

The program was such as to perform calculations for:

a) Steam temperature and/or quality
b) Casing temperature
c) Percent heat loss.

under different conditions of injection, for depths to 1000'.

The three variables were

a) Injection temperature (°F)
b) Injection rate (lbs/hr)
c) Time after the start of injection

The graphs, therefore, try to show the effect of these three variables on the calculated functions mentioned above. Injection pressure was kept constant at 422.6 psia (saturated steam at 450°F) but the program would need little altering to take into account injection pressure. At higher pressures, saturation temperature increases, and for a given injection rate and temperature, this merely means that condensation of superheated steam occurs higher in the wellbore. Pressure variation alone does not greatly affect percent heat loss or bottom hole steam temperature, but is perhaps of more interest from its effect on increasing injection rates in those cases where formation permeability, rather than generator output, set limits on injection rate. Pressure variation, of course, also affects enthalpy values at given temperatures and, to a lesser extent, it affects the enthalpy change for given temperature changes (superheated steam) - this being the specific heat property.

Whilst Satter, working with saturated steam, obtained interesting correlations between certain variables (injection rate, temperature and pressure) and percent heat loss per unit depth, in the case of superheated steam, there are too many extra variables, and relations between them are generally non-linear and hence similar correlations are far more complex.

Figure 1 - shows depth-steam temperature profiles under a given injection rate (2000 lbs/hr). Two cases are considered. During injection of saturated steam (450°), the steam temperature remains constant, and the quality decreases linearly with depth. At later times, the quality at a certain depth slowly increases. During injection of superheated steam (550°) the temperature of the steam falls, the profile being characteristically shaped concave-downwards. This concavity is due to the greater heat losses from the steam at the higher temperatures. When the steam has cooled to 450°F, it remains at that temperature whilst the steam quality decreases. At any given time, the slope of the quality-depth line is the same for both cases, i.e. heat loss at a given temperature is independent of whatever temperatures occur higher or lower in the well - this comes from the assumption that heat losses occur in a horizontal direction only, and the formations penetrated have zero vertical conductivity. Note the relatively small effect of time on both cases, once the 30 day stage is reached. (Ramey's function is valid after

this time.) During injection at 550°, the condensation point travels downward with time, but only 50' between 1 month and 10 years after injection.

Figure 2 - shows casing temperature profiles as functions of time and injection temperature. Notice:

a) The profiles are concave downward, as for steam temperature.

b) The temperatures become constant at certain depths, depending upon time and injection temperature. This corresponds to the steam being at and below saturation temperature.

c) The effect of time is more pronounced for casing temperatures than for the corresponding steam temperatures. Thus at 200' depth, 550° injection temperature, the casing temperature increases 34°F between 1 month and 12 months, whilst the steam temperature increases only 3°F.

d) This increase in casing temperature with time is more pronounced near the surface than at depths.

3) At higher injection temperatures, the profiles are more concave - indicating greater heat losses - but the casing temperature becomes constant at the same temperature as in the case of lower steam injection temperatures, the only difference being that this constant temperature is reached at greater depths in the former case. Thus casing temperature will only stabilize at a given injection temperature, providing the depth to the formation is greater than that coreesponding to steam condensation.

Figure 3 - shows casing temperature profiles under injection of higher temperature steam (850°F). Notice:

a) Temperatures continue to decrease with depth (steam temperature at formation above 450°F).

b) The effect of injection rate on temperature profiles (to be contrasted with injection of saturated steam, where casing temperature is independent of rate.) At low injection rates, heat losses are greater, when expressed as a percent of the input energy at the surface. Hence casing temperatures decrease more with depth, although, at a given time, the temperature at the surface is the same for all injection rates. Compare this divergence of casing temperature with depth for different injection

rates to the convergence shown in Figure 2, for different injection temperatures. At very high injection rates, the profiles become approximately linear with depth. (At infinite rates of injection, steam temperature becomes constant and percent heat losses become zero, hence casing temperature profiles approach vertical lines.)

c) Approximately, a four-fold increase in injection rate causes casing temperatures at 1000' to be doubled - for 850° steam injection.

Figure 4 - shows steam temperature profiles as functions of injection temperature at 4000 lbs/hr injection.

a) Higher injection temperatures suffer greater heat losses and consequently the temperatures are reduced more. The different profiles do not completely converge, however, since the saturation temperature is eventually reached whereupon heat losses become constant for all cases. This temperature is reached at greater depths, of course, in the case of high temperature injection.

Figures 5, 6 and 7 - all give percent heat loss profiles to 1000' showing the relative effects of time, injection temperature, and injection rate.

a) Note the small effect of time in Figure 5. Between 1 year and 10 years. Percent heat loss decreases only 0.2% at 1000' for 4000 lbs/hr injection at 750°F.

b) The curves are characteristically concave downwards, tending to linearity with depth, since steam temperature approaches saturation temperature. (Figure 5) For saturated steam injection the lines are straight.

c) Note the much more pronounced effect of injection temperature in Figure 6. A 300°F increase in injection temperature almost doubles the percent heat loss.

d) Again in Figure 6, note that percent heat loss is related to input energy at the surface. Although for higher injection temperatures, the total input energy is greater (at constant rates) the actual heat loss over any depth increment is greater still for higher injection temperatures. These two effects do not balance one another, with the result that percent heat loss increases with injection temperature.

e) Injection rate has a marked effect upon percent heat loss (contrasting with saturated steam injection) for the same reason as mentioned above. At higher rates, input energy is greater in BTU/hr, although at constant temperature

of injection, heat loss over any increment is a function only of the temperatures at the top and bottom of the increment. Hence higher injection rates yield lower percent heat losses at a given depth (Figure 7).

f) At very high rates of injection, the relationship becomes approximately linear (percent heat loss vs depth), for the same reasons as mentioned in discussing casing temperature profiles (Figure 3).

Figure 8 - shows percent heat loss as a function of time for various injection conditions. All the curves are typically shaped, dropping very steeply during the first month, then undergoing a more gradual decline up to 1 year and thereafter the curves flatten out, with very small changes in heat loss percent for further times. These curves, reflecting the use of Ramey's time function, f(t), could perhaps be slightly in error, according to Leutwyler's study (see Literature Review), although the basic shape would be the same. These curves further emphasize the fact, mentioned previously, that time plays little part in temperature (steam) profiles, compared to other factors such as injection rate and temperature. Comparison of the four curves in Figure 8 show this to be true. For example, injecting 2000 lbs/hr of 550°F superheated steam, the heat loss percent after 10 years is still more than after injecting the same rate of 450°F steam (saturated) for 2 months. Put another way, the percent decrease in percent heat loss (2000 lbs/hr) from 1 year to 10 years after injection 450° steam is 2 %, whilst the percent decrease in percent heat loss (at the same injection rate, after 1 year), between injected steam at 550° and 450° is 8%.

Notice the much lower heat loss incurred during injection of 450°F steam at 4000 lbs/hr as compared to 2000 lbs/hr (curves (A) and (B)).

It is apparent from the curves that the shape is very similar whether the injected steam is saturated or superheated.

Figure 9 - shows a similar set of curves, this time plotting steam temperature at the formation instead of percent heat loss. Again the curves are characteristically shaped, but now, in contrast to Figure 8, the shape of each curve can be seen to reflect the injection conditions. For example, two points are apparent.

a) At constant injection rate (4000 lbs/hr), the curved portions of the graphs become more pronounced at higher injection temperatures.

b) At constant injection temperature, the curved portions become more pronounced at lower injection rates. This

means that at lower injection rates and higher injection temperatures, it takes longer for the bottom-hole steam temperature to stabilize, whereas under the reverse conditions, bottom steam temperature increases very rapidly during the initial few months then levels off.

Figure 10 - constructed after one month of injection, shows clearly the relation between percent heat loss at the formation and injection temperature and rate.

a) Percent heat loss increases almost linearily with injection temperature.

b) Percent heat loss declines exponentially (approximately) with increasing injection rate. At very high rates, percent heat loss approaches zero whilst at very low rates, the percent heat loss climbs rapidly and approaches 100% (presuming enthalpy of water at initial earth temperature is zero) of course in the region of low injection rates, the water condenses completely before reaching the formation.

Figure 11 - constructed after one month of injection shows bottom hole steam temperature as a function of injection rate and temperature. Increased injection rate increases the steam temperature at the formation, but the limit is the injection temperature, i.e. whatever injection rate is used, the maximum possible steam temperature at the formation is governed by the injection temperature. This is a rather obvious point, but it is the basis for preferentially injecting higher temperature steam, possibly at lower rates. For example, if we wish to have steam entering the formation at, say, 525°F we can either inject 650°F steam at 5000 lbs/hour, or 550°F steam at a rate 5 times as large. And few formations to be flooded will accept 25000 lbs/hour of steam (1750 B/day equivalent condensate).

At sufficiently low rates, steam temperature at the formation becomes much less dependent upon injection temperature. For example at just less than 2000 lbs/hour any steam injected at 850° or below will have reached saturation temperature at the formation. The difference then between the various injection temperatures is one of steam quality.

Figure 12 - is a modification of Figure 11 and it brings cost into the picture. The cost of a steam injection operation is largely a matter of the cost of fuel to produce the steam, or since generator efficiencies are largely independent of throughput rate, the cost bears a direct relationship to the product (W.H) where W = injection rate (lbs/hour) and H is the specific enthalpy of the produced steam (BTU/lb). Neglecting heat losses between generator and well-head, therefore, the cost of injection is directly proportion to the (W.H) product at the well-head.

Figure 12 is constructed from Figures 10 and 11 as follows:

a) Select a certain injection temperature - say 750°F.

b) Select an injection rate - say 4000 lbs/hr.

c) From Figure 10 obtain percent heat loss at formation = 8.35%.

d) From steam tables obtain enthalpy of 750°F steam at injection pressure (422.6) = 1388 BTU/lb.

e) Calculate input heat (BTU/hr) = 1388 X 4000 = $(5.55)10^6$.

f) Calculate heat throughput at formation = $(5.55)10^6$ X (1 - 0.0835) = $(5.09)10^6$ BTU/hr.

g) From Figure 11 obtain bottom hole steam temperature at 750° injection and 4000 lbs/hr = 545°F.

h) Enter Figure 12 and at point

Temperature (steam) = 545°F
Formation throughput = $(5.09)10^6$ BTU/hr

plot point corresponding to injection temperature of 750° and surface throughput of $(5.55)10^6$ BTU/hr.

By repeating this technique for other injection temperatures and rates and by connecting lines of equal injection temperature (°F) and surface throughput (BTU/hr), Figure 12 is constructed.

One important consequence of Figure 12 is apparent. Since the lines of constant surface rate (BTU/hr), denoted by Q, are nearly vertical, and since Q is a direct measure of operational cost, it is seen that by injecting higher temperature superheated steam and maintaining the same heat throughput into the reservoir, a much greater steam temperature at the formation is obtained with quite a <u>small</u> increase in Q, or cost.

For example consider two alternatives, both costing the same for their operation, i.e. Q constant. In the first we inject 550° superheated steam at such a rate that the heat throughput into the formation at 1000' is 14.7 MM BTU/hr. From the graph which one we find Q = 15 MM BTU/hr and the formation steam temperature to be 512°F. In the second case, we inject 750° saturated steam at such a rate (lower than in case one) that the heat throughput into the reservoir is 14.35 MM BTU/hr. From the graph we again find Q to be 15 MM BTU/hr, but now the formation steam temperature is 653°F. Hence, at the same cost we have increased this temperature by 140°F whilst our heat throughput at the formation has decreased by only 2.4%.

At first these figures may seem either to reflect a mistake in the calculation, or else an increase in thermal efficiency to more than 100%! However the real reason for the high increase in bottom hole temperature at the expense of a low heat throughput rate, is due to the rather misleading scale of temperature, i.e. a 25% increase in temperature (°F) corresponds (in the realm of values discussed above) to less than a 5% increase in enthalpy. (BTU/lb) Hence a 140°F increase in bottom hole temperature is not as impressive from a B.T.U. point of view as it might seem.

Another point to be noted, therefore, is that the cost of injection is far more dependent upon injection <u>rate</u> than upon injection temperature.

To return to the above example, what we require is a knowledge of which combination of formation heat throughput, and formation steam temperature, will produce the best recovery. This is further than the scope of this present study, however, two points will be made.

a) In the latter case discussed above, with higher steam temperature and lower heat input to the formation heat losses will be more rapid in the reservoir than in the former case.

b) Since recovery by steam injection is primarily dependent upon viscosity ratio reduction (μ_o/μ_w) and the viscosity ratio is more a function of temperature than heat content of the fluids, it is possible that the higher steam temperatures at the reservoir in the latter case will help recovery, even at the expense of a lower heat throughput rate.

8. <u>SUMMARY</u>

The following are the more relevant and interesting of the results described in detail above.

1. Too many variables involved in the problem to obtain correlations between them.

2. Time is of little importance in steam profiles, compared to injection rate and temperature. It is more important in casing temperature profiles.

3. Casing temperatures are increased by increased steam injection temperatures at a constant injection rate, and by increased rates at constant injection temperature. These increases in casing temperature can be quite large.

4. Higher injection temperatures suffer greater heat losses as do lower injection rates.

5. At times greater than 1 year, percent heat loss and steam temperature at the formation become approximately constant.

6. At high injection rates, increased injection temperatures produce large increases in steam temperature at the formation. At low injection rates, increased temperatures of injection produce only small increases in steam temperature at the formation.

7. Percent heat loss at the formation is approximately linear with injection temperature in the range of pressures and rates used in this study. Percent heat loss is approximately exponential with injection rate (inverse exponential).

8. For the same cost of injection, marked increases in formation steam temperature can be obtained with relatively small corresponding decreases of heat input into the reservoir. The effect of this on recovery is questionable.

9. In formations where injection rate is limited by low permeabilities, the use of superheated steam as a means of getting increased formation steam temperature, and increased heat input to the formation, cannot be ignored and the effect on viscosity ratio of the higher temperatures achieved may justify the extra fuel costs involved.

9. ACKNOWLEGEMENT

This report was prepared as a term project in PNG 515 - a course on modern petroleum recovery methods, taught by Professor D. A. T. Donohue in the Spring of 1966. As such it was done as an educational endeavor, and the author is well aware of its basic resemblance to the pepers published earlier by Satter (6). The present paper gives a more detailed explanation of wellbore heat losses and injection behavior for injection of superheated steam into a shallow formation.

10. REFERENCES

1. Squier, D. P., Journal of Petroleum Technology, April 1962.

2. Ramey, H. J., Journal of Petroleum Technology, April 1962.

3. Leutwyler, K., 40th Annual Fall Meeting of the Soc. Pet. Eng. of AIME, Denver, October 3-6, 1965.

4. Moss, J. T. and White, R. D., Oil and Gas Journal No. 11, March 1959.

5. Caslaw, H. and Jaegers, J., "Conduction of Heat in Solids", Second Edition, Oxford University Press, 1960.

6. Satter, A., Journal of Petroleum Technology, July 1965.

11. NOMENCLATURE

C_p	Specific heat at constant pressure	BTU/lb°F
d_c	Inside casing diameter	Inches
D_c	Outside casing diameter	Inches
D_t	Outside tubing diameter	Inches
e_c	Emissivity of casing	------
e_t	Emissivity of tubing	------
F_a	Shape factor for radiation	------
F_e	Emissivity factor for radiation	------
g	Gravitational acceleration (32)	32 ft/sec^2
g_c	Conversion factor	32 ft lb mass/ sec^2 lb force
H	Enthalpy	BTU/lb
h_f	Sensible heat of saturated water	BTU/lb
h_{fg}	Latent heat of steam	BTU/lb
h_g	Sensible heat of saturated steam	BTU/lb
J	Mechanical equivalent of heat	778 ft lb force/BTU
Ke	Thermal conductivity of earth	BTU/ft-hour-°F
Q	Heat transferred from surroundings	BTU/lb mass
q	Heat transfer rate	BTU/hour
t	Time	Months

T_e	Average earth temperature	°F
$T_1(z,t)$	Steam temperature, function of depth and time	°F
$T_2(z,t)$	Casing temperature, function of depth and time	°F
u	Fluid velocity	ft/sec
W	Injection rate	lbs/hour
W_f	Flow work	ft lb force/lb
y	Steam quality	-----
z	Depth	ft
α	Thermal diffusivity of earth	ft^2/hour

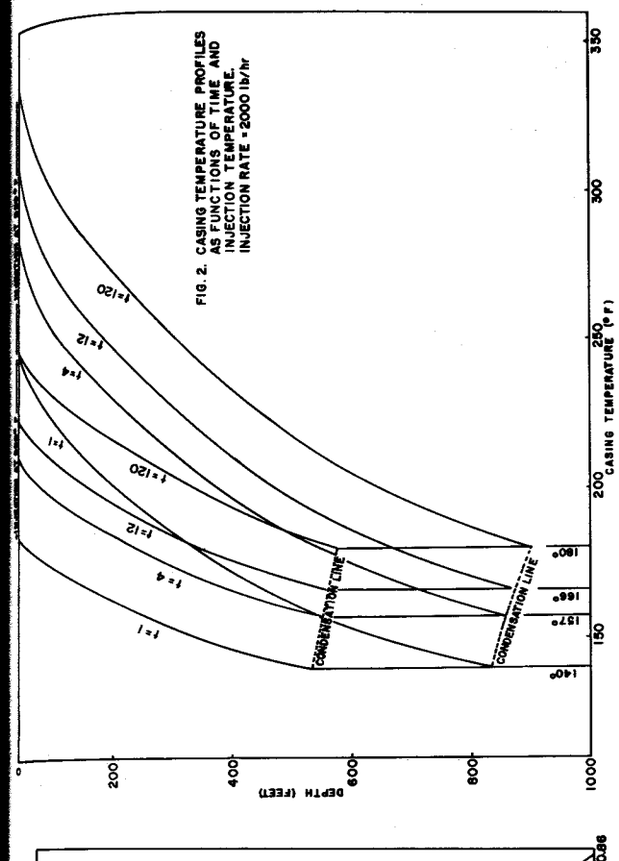

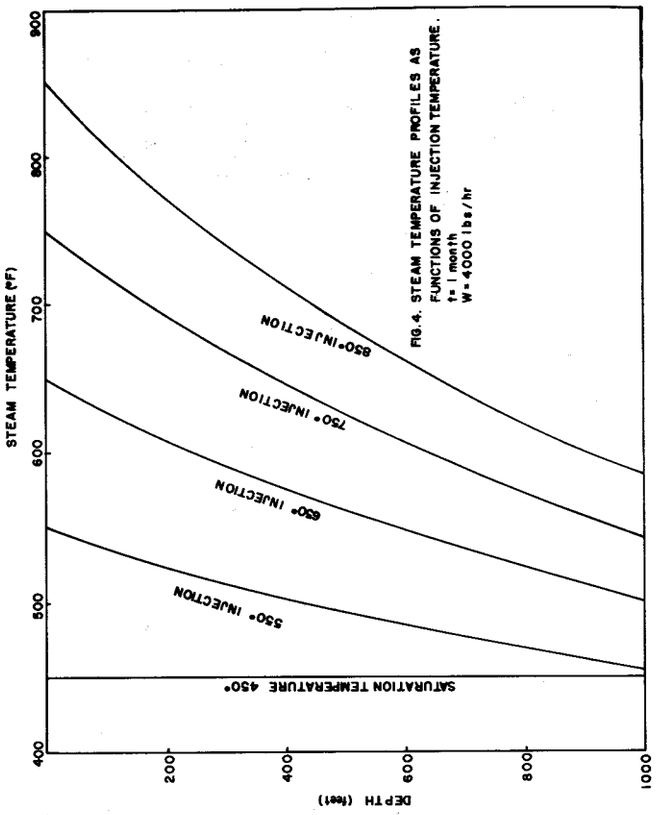

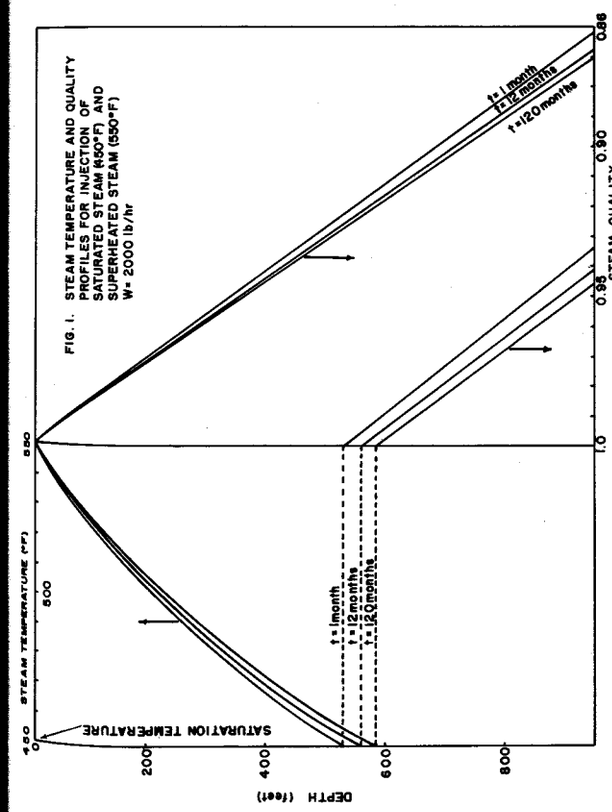

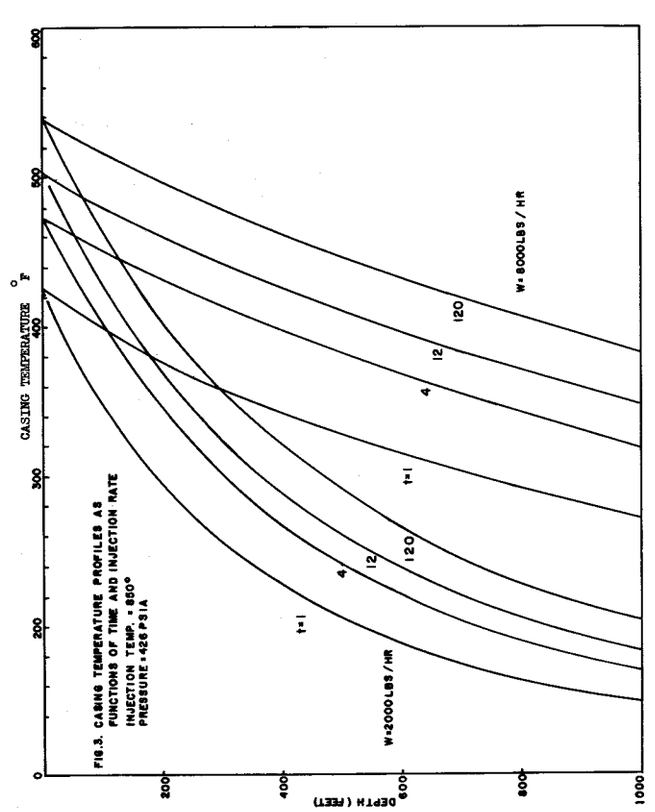

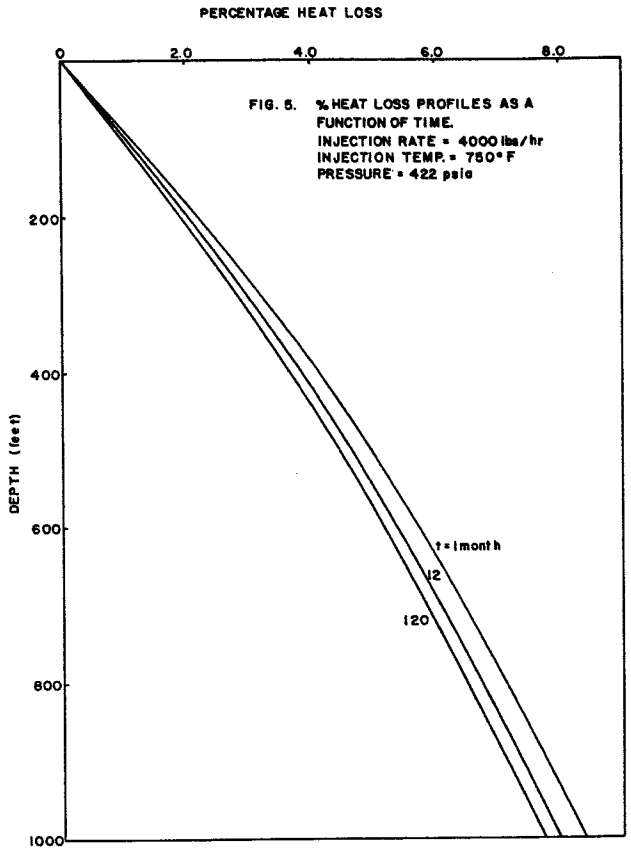

FIG. 5. % HEAT LOSS PROFILES AS A FUNCTION OF TIME.
INJECTION RATE = 4000 lbs/hr
INJECTION TEMP. = 750° F
PRESSURE = 422 psia

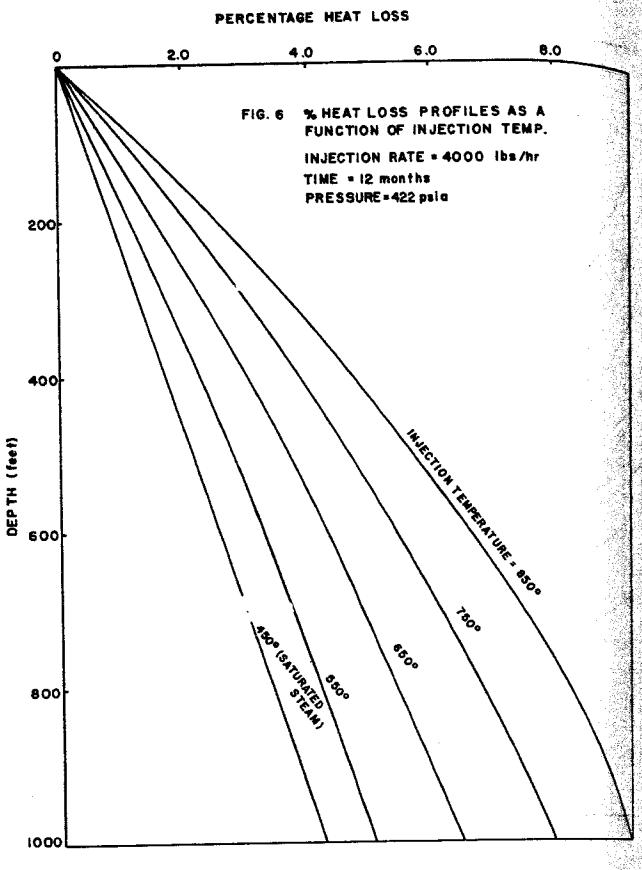

FIG. 6 % HEAT LOSS PROFILES AS A FUNCTION OF INJECTION TEMP.
INJECTION RATE = 4000 lbs/hr
TIME = 12 months
PRESSURE = 422 psia

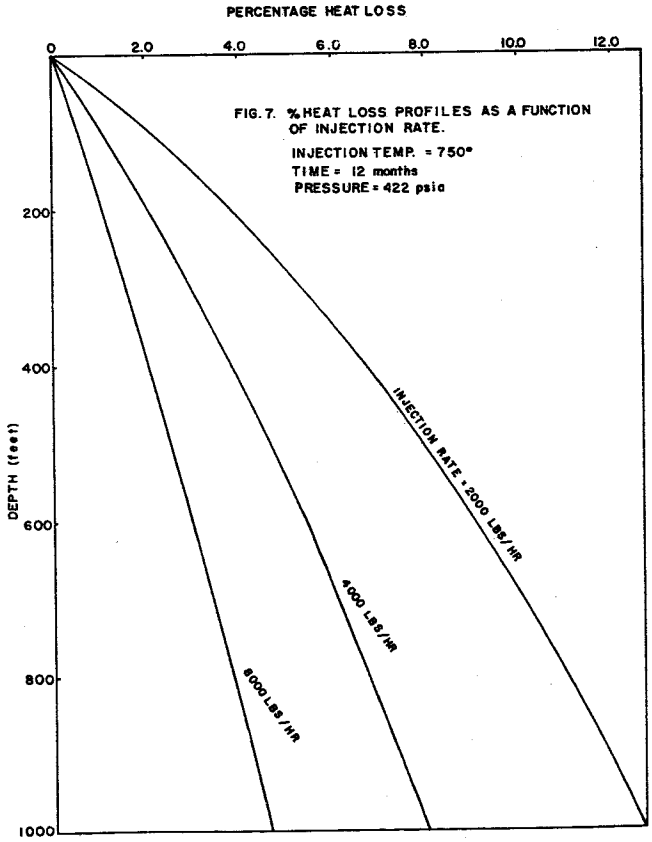

FIG. 7. % HEAT LOSS PROFILES AS A FUNCTION OF INJECTION RATE.
INJECTION TEMP. = 750°
TIME = 12 months
PRESSURE = 422 psia

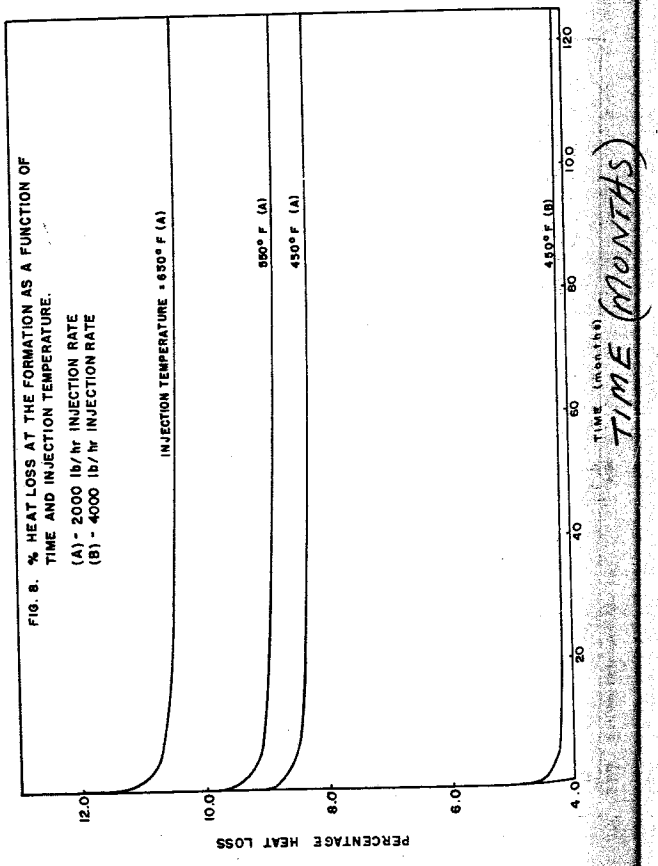

FIG. 8. % HEAT LOSS AT THE FORMATION AS A FUNCTION OF TIME AND INJECTION TEMPERATURE.
(A) - 2000 lb/hr INJECTION RATE
(B) - 4000 lb/hr INJECTION RATE

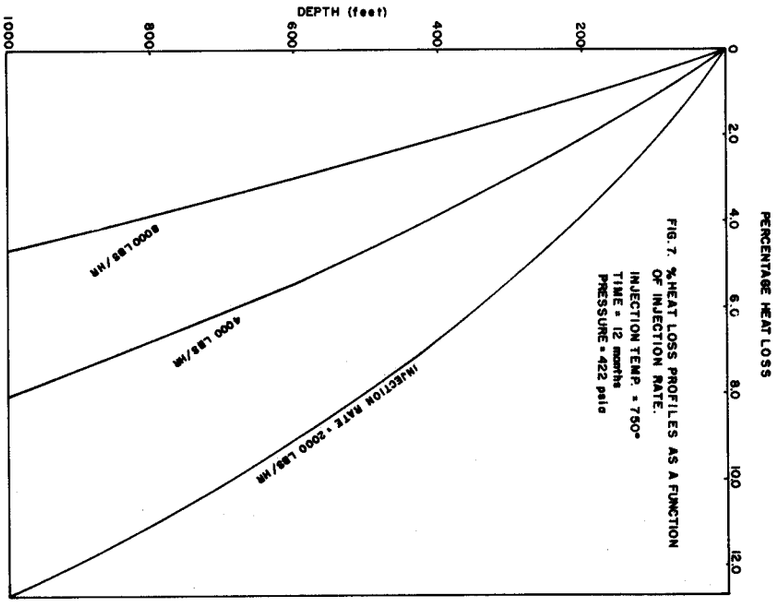

FIG. 7. % HEAT LOSS PROFILES AS A FUNCTION OF INJECTION RATE.
INJECTION TEMP. = 750°
TIME = 12 months
PRESSURE = 422 psia

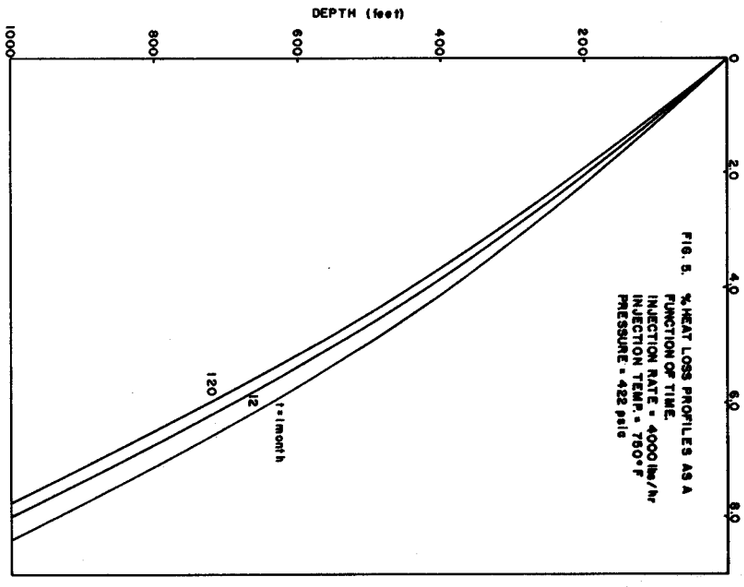

FIG. 5. % HEAT LOSS PROFILES AS A FUNCTION OF TIME.
INJECTION RATE = 4000 lbs/hr
INJECTION TEMP. = 750° F
PRESSURE = 422 psia

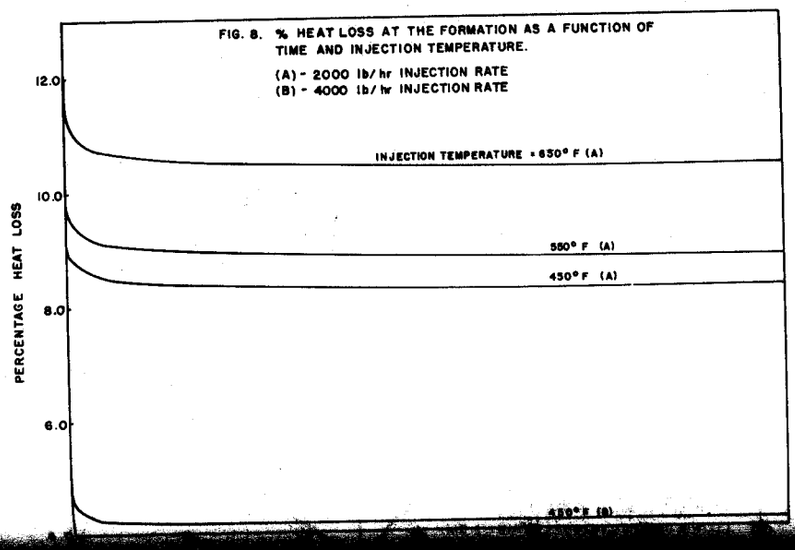

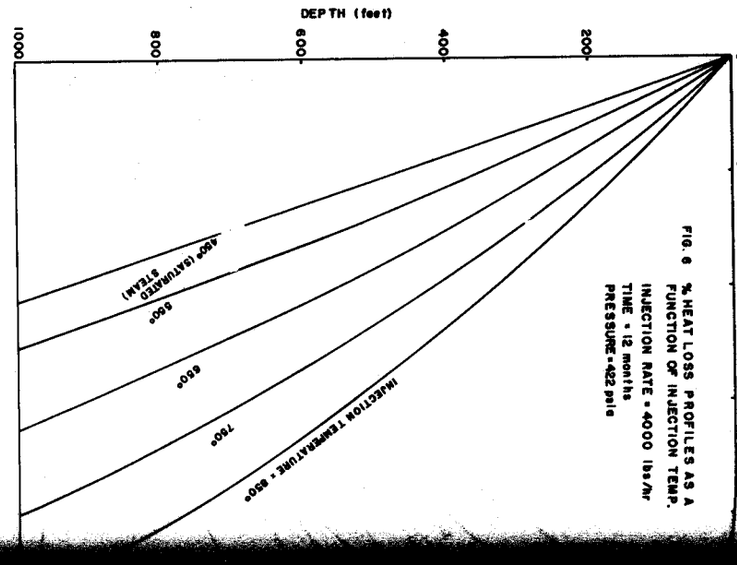

FIG. 6 % HEAT LOSS PROFILES AS A FUNCTION OF INJECTION TEMP.
INJECTION RATE = 4000 lbs/hr
TIME = 12 months
PRESSURE = 422 psia

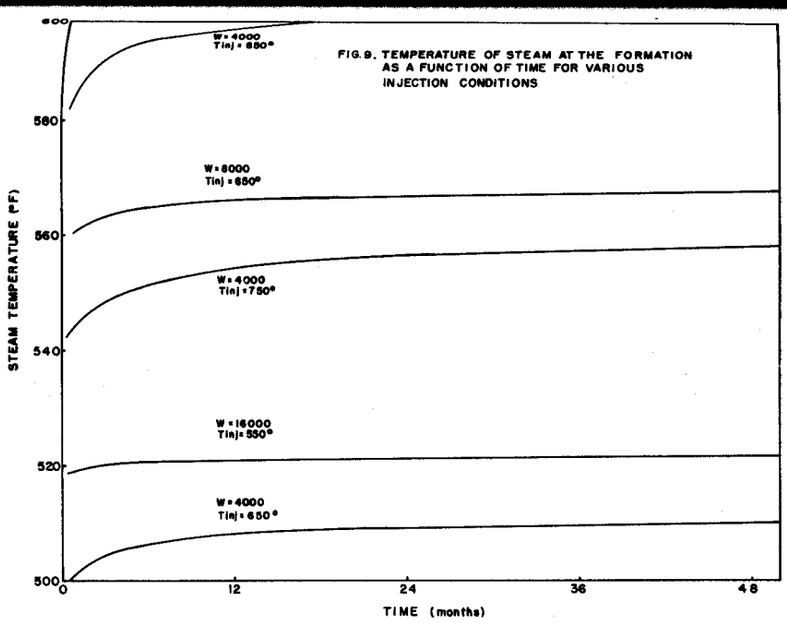

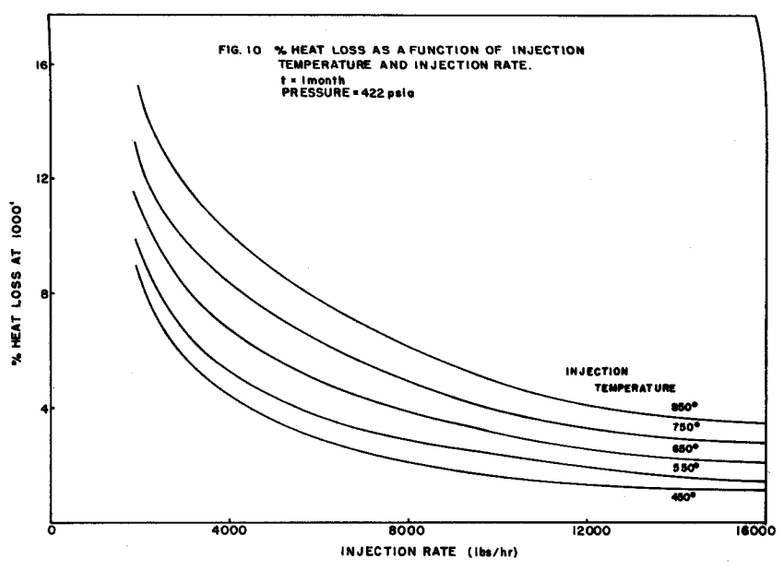

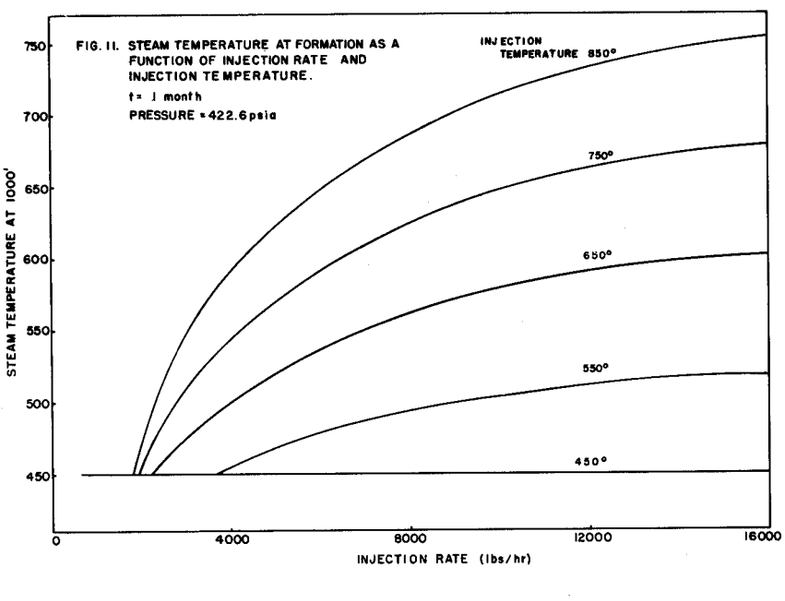

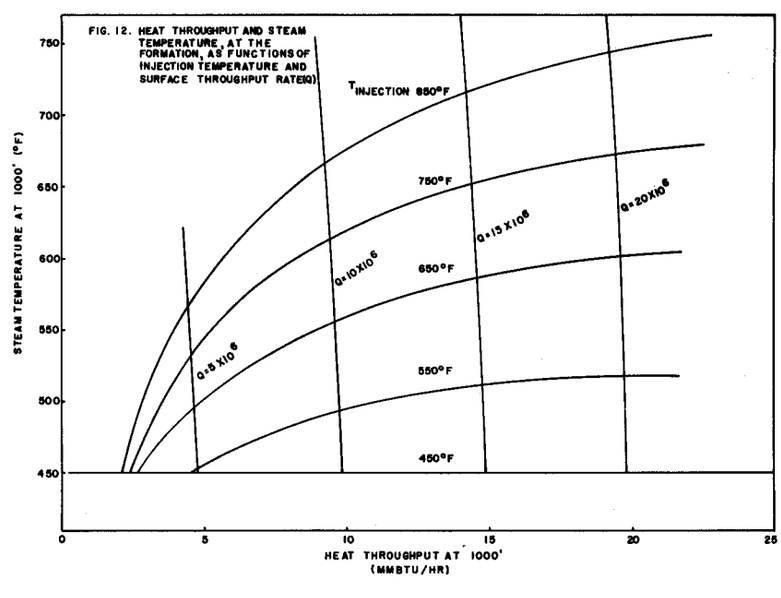

THERMAL EXPANSION OF CEMENTED CASING

By

F. M. Smith

Gulf Research & Development Company, Pittsburgh, Pa.

ABSTRACT

Increased use of thermal methods for oil-well stimulation, such as steam injection, prompted an investigation of the effects of heating cemented steel pipe. In this investigation, cemented steel pipe was repeatedly heated to a temperature of up to 670°F. Pipe elongation and cement bond strength were measured and thermal stresses determined. In addition, the effects of heating on three commonly used cement compositions were evaluated.

Steel pipe cemented with neat cement was found to elongate about 0.73×10^{-6} in./in.-°F when heated. Using a neat cement - 40 per cent silica flour slurry, the elongation was about 1.04×10^{-6} in./in.-°F; and, using a Lumnite - 40 per cent silica flour slurry, the elongation was negligible. Axial stress in the pipe caused by restrained thermal expansion exceeded the yield stress of the pipe after a temperature rise of about 200°F. Cooling after a temperature rise of more than 200°F resulted in cement bond failure at the cement top and pipe shrinkage. Repeated heating cycles resulted in progressive cement bond failure and additional pipe shrinkage.

At temperatures of 450°F and above, deterioration of the neat cement occurred, resulting in a decreased cement bond strength. Cement bond failure of the neat and Lumnite cement - 40 per cent silica flour slurries resulted from leakage through cracks

in the cement matrix. Neat cement appears to be the best material for cementing wells to be thermally stimulated, especially where casing temperatures are 450°F or less.

A qualified extension of the test results to oil-well conditions indicated that casing cemented with neat cement could be heated to about 430°F without adverse effects. To avoid possible casing and cement bond failure at higher temperatures, use of a down-hole thermal packer in conjunction with tubing injection is suggested. This investigation serves to emphasize the need for good cement jobs in wells to be thermally stimulated so that casing failure can be avoided.

INTRODUCTION

Production stimulation using thermal methods has become an increasingly popular oil-field practice. Two common thermal methods for production stimulation are in-situ combustion and steam injection. Steam injection is the most widespread thermal method used at the present time because of its low cost and simplicity of application. When steam injection from the surface is used for production stimulation, the temperature of the entire bore hole is raised. Research publications[1,2,3,4*] have presented methods for estimating the casing temperature during steam injection. Leutwyler and Bigelow[5] extended their research to include an analysis of the mechanical problems associated with this stimulation method. However, their analysis of the mechanical problems was confined to the free pipe in a well, excluding the cemented portion of the well casing. Since the cemented portion of the well casing encompasses the oil-productive interval, the possible effects of heating this region needed investigation. This paper presents the results of such an investigation. Steel pipe, cemented with one of three commonly used cement

* References given at end of paper.

mixtures, was heated to a temperature of up to 670°F for various numbers of times. The effect of heating the pipe and cement was evaluated.

The following discussion consists of (1) a description of the test apparatus and procedure, (2) a detailed discussion of the tests performed, and the implication of the test results when extended to actual oil wells, and (3) conclusions reached from the results of the tests.

TEST APPARATUS AND PROCEDURE

Apparatus

The test apparatus, shown in Figures 1 and 2, consists of a 10-ft length (two coupled 5-ft lengths) of 1/2-in. standard pipe centered inside of a 10-ft length of 7-in. OD, 20-lb/ft casing. The 1/2-in. pipe was rigidly attached at one end by threading it into a 1/2-in. thick steel plate welded to one end of the casing. All pipe surfaces were solvent-cleaned before assembly.

Temperature measurements were made using three tubular steel Chromel-Alumel thermocouples, as shown in Figure 1. These were located at the mid-length of the 7-in. casing. The first thermocouple was located in the outer wall of the 1/2-in. pipe; the second in the casing annulus at its mid-point; and the third, on the outer wall of the casing. The first thermocouple served as the heater temperature control point. The thermocouples were connected to a strip-chart temperature recorder-controller.

The electrical equipment used is shown in Figures 3 and 4. The electric heater was located inside the 1/2-in. pipe and extended through its entire length. The control circuit provided intermittent heater operation by use of the timer which actuated the solenoid switch.

Temperature control was very good. Excessive temperatures were prevented by the temperature-actuated limit switch.

Test Procedure

The test procedure consisted of testing, cementing, heating, cement bond testing, and sectioning. Each of these steps is discussed below.

Prior to cementing the pipe in the casing, the apparatus was assembled and measurements were made of the thermal elongation of the free pipe. The pipe temperature was raised to 200°F and dial gage values were recorded. Thermal elongation of the pipe was calculated and, if found to be 6.9×10^{-6} in./in.-°F (thermal elongation value for steel)[6], the next step in the procedure was followed. If the thermal elongation was in error, the apparatus was adjusted and the calibration heating cycle repeated.

1. Cementing

The casing annulus was cemented using three commonly used cement slurries. Data for these mixtures are given below:

Cement Data

Test No.	Cement Type	gal Water/Sack	Set Time (hr)
1-5	Neat	5.2	72
6	Neat w/40% Silica Flour	7.0	72
7	Lumnite* w/40% Silica Flour	6.5	72

The apparatus was then sealed and pressurized to 1000 psig with a hydraulic pump. The inside and outside of the 1/2-in. pipe were

* Calcium-aluminate refractory cement.

pressurized simultaneously to simulate actual well conditions during cementing operations.

2. Heating

After the dial gages and electric heater had been installed, the pipe was heated to the test temperatures for a prescribed length of time and then cooled to ambient temperature. The heating cycle was then repeated a various number of times. Dial gage and temperature readings were recorded throughout each heating cycle.

The temperature rise rate was controlled to approximate actual well conditions during steam injection and thus simulate the effect of transient thermal stresses. About a four-hour heating period was used to reach the maximum temperature in each test.

3. Cement Bond Testing

Eight 1/8-in. holes at a 90° spacing were drilled through the steel plate on the bottom of the casing. Four holes intersected the outer wall of the pipe while the other four holes intersected the inner wall of the casing. The apparatus was then filled with dyed water and pressurized simultaneously on the inside and outside of the 1/2-in. pipe in 100 psi increments until water flowed through the holes in the plate. The cement bond strength was considered to be the pressure which caused fluid communication through the apparatus at a flow rate of 1 cc/min.

4. Sectioning

The casing was saw-cut at 1- to 3-ft intervals and the cross-sections obtained were visually inspected for cracks, discolorations or other irregularities and then photographed. One-inch diameter cores were cut adjacent to both the 1/2-in. pipe and the inner wall of the 7-in. casing for compressive strength tests. Some sections were used for penetrometer tests, where the cement strength was further evaluated.

DISCUSSION OF RESULTS

Results of seven tests made to determine the linear thermal expansion of cemented casing are presented in Table I and a discussion of these results follows.

Net values for elongation of the cemented pipe were plotted versus temperature change as shown in Figure 5. For neat cement, with a temperature change of less than about 450°F, the plot has a slope of 0.73×10^{-6} in./in.-°F, which appears to be the linear thermal expansion of cemented steel pipe at a stress below its yield stress. For temperature differences above 450°F, pipe elongation increased considerably, indicating that pipe slippage had occurred and a cement bond was no longer effective over the entire length of the cemented pipe.

For neat cement with 40 per cent silica flour, at a temperature difference below 190°F, the linear thermal expansion of the pipe was about 1.04×10^{-6} in./in.-°F. At a temperature difference above 190°F, results similar to those for neat cement were had.

Tests with Lumnite cement containing 40 per cent silica flour resulted in a linear thermal expansion of about 1.04×10^{-6} in./in.-°F at temperature differences below 110°F. However, at temperature differences above 110°F, pipe elongation stopped. This phenomenon can be explained by the fact that Lumnite cement shrinks[7] when it is heated instead of expanding like neat cement. Therefore, the mechanical bond between the pipe and the cement would be expected to improve as the temperature increased.

Stress

Since the axial stresses created in the 1/2-in. pipe by the heating were almost completely absorbed by the cement and the casing,

the stresses were treated as if they had been created by rigidly confining the pipe at each end and then heating it. The axial stress was calculated using the following equation:

$$S = E \cdot e \cdot \Delta T$$

where: S = stress - psi

E = modulus of elasticity - 30×10^6 psi for steel

e = coefficient of thermal expansion - 6.9×10^{-6} in./in.

ΔT = temperature difference - °F

Since the linear thermal expansion for pipe cemented with neat cement was established at 0.73×10^{-6} in./in.-°F, the effective value for e used in the above equation was $(6.9 - 0.73) \times 10^{-6}$ or 6.17×10^{-6} in./in.-°F. A yield stress of 37,000 psi for the 1/2-in. pipe was experimentally determined. Substitution of this yield stress in the above equation resulted in a ΔT of 200°F. The test results show that, virtually every time the yield stress of the pipe was appreciably exceeded (a ΔT above 200°F), the pipe shortened after cooling.

Similar results were obtained with the other two cements tested. In the case of the neat cement - 40 per cent silica flour mixture, the pipe shortened after cooling when a temperature difference of about 190°F was reached. With the Lumnite - 40 per cent silica flour mixture, pipe shortening occurred after cooling from a 155°F temperature difference.

An explanation of pipe shortening is as follows: During the heating cycle, with the pipe restrained by the cement in the vertical direction, the internal stresses generated exceeded the yield stress

of the pipe. Pipe deformation occurred, therefore, resulting in a slight thickening of the pipe wall. During the cooling cycle, an opposite action took place. The pipe and cement both contracted but, since the elasticity of neat cement is but 1/15th that of steel, the cement did not contract quite as much as the pipe. Thus, the internal pipe stresses were relieved which resulted in pipe shortening and slippage along the pipe wall-cement interface. This phenomenon apparently took place at or near the cement top and progressed downward as the number of heating cycles increased.

In Test No. 7, an effort was made to determine the extent of the pipe wall thickening. A section at the mid-length of the pipe was machined and the ID and OD of the pipe carefully measured. After heating, this section of pipe was remeasured. It was found that the ID of the pipe had not changed but the OD had increased by 0.002 in. The volume of 1/2-i pipe lost to cumulative pipe shortening (0.586 in.) was then assumed to be distributed on the outer surface of the remaining pipe. The calculated increase in pipe OD to accommodate this volume was also 0.002 in. Althoug this result is not conclusive, it does indicate that pipe thickening takes place.

Cement Bond Strength

Results of the cement bond strength tests are shown in Table I.

The neat cement bond strength of unheated pipe was taken from published literature[8] and was about 1500 psig. Based on cement compressive strengths, the bond strength of the other two cements tested would give similar values. Cement-bond testing the cemented pipe prior to heating would have destroyed the test sample.

Test results indicate that the cement bond strength increases as a function of the cement curing pressure. For example, at a 0 psig

cure pressure, the cement bond failed at 50 psig; when the cement was cured at 1000 psig, the cement bond failed at 1500 psig. The temperature to which the cement is heated also affects the bond strength. For example, when neat cement was cured at 1000 psig and heated to 645°F, the cement bond failed at 500 psig. During Test No. 5, where the cement was cured at 1000 psig and heated to 500°F, the cement bond did not fail at a pressure of 2000 psig. The type of cement used had the greatest effect on the cement bond. Where 40 per cent silica flour was added to the neat cement and heated to 500°F, the cement bond failed at 300 psi. This was considerably below the >2000 psi bond strength of the neat cement heated to the same temperature.

In the case of the Lumnite - 40 per cent silica flour cement, the cement bond after heating to 650°F was only 40 psi.

Sectioning

After completing the cement bond tests, the cemented casing was sectioned to permit visual examination of the cement. Typical sections are shown in Figures 6, 7 and 8. With neat cement (Figure 6), the center portion showed several colored concentric rings around the pipe while radial cracks were observed at each end. Fluid leaked only along the pipe; no dye appeared in the cracks or at the 7-in. casing-cement interface.

Appearance of the neat cement - 40 per cent silica flour mixture, shown in Figure 7, was similar to that of the neat cement. In addition to the colored rings and end cracks, very slight radial cracks were noted throughout the total length of cement. Fluid leaked along the pipe and through the radial cracks in the cement.

Appearance of the Lumnite - 40 per cent silica flour cement was significantly different from the other cements as shown in Figure 8. Cement discoloration was slight, but three radial cracks were evident throughout the length of the cement. Cement shrinkage away from the casing wall was also apparent. Dye deposits showed that fluid leaked at the pipe and casing-cement interfaces and through the cement cracks.

Penetrometer and compressive strength tests were made on the cements at various radial distances from the 1/2-in. pipe, the results of which are given in Table II. Significant differences in compressive strength were noted between the neat cement cores taken close to the casing and those taken close to the pipe. With the other cements, no significant differences in strength were noted between core locations. However, addition of silica flour made the cements brittle and they fractured readily. The Lumnite cement was found to be especially brittle.

Penetrometer results confirm the core results for, with neat cement, they indicate an abrupt decrease in strength at a distance of about 3/4 in. from the pipe. Relating this distance to temperature, using Figure 9 where typical temperature profiles versus distance were plotted, the neat cement strength decreased at about 450°F. Similar results were found with the neat cement - 40 per cent silica flour mixture.

Where the Lumnite - 40 per cent silica flour cement was used, the penetrometer results showed only a slight decrease in cement strength near the pipe wall. The remainder of the cement appeared unaffected by heating.

EXTENSION OF RESULTS TO WELL CONDITIONS

The test results are believed to be fairly representative of actual well conditions. Although the geometry and materials in the two systems are different, calculations indicate that the yield stress of well casing would be reached at only a 16 per cent lower temperature difference. Other limitations to extending the test results are: First, cementing results were probably better than is realized in most wells since all metal surfaces were cleaned prior to cementing. Second, the test section represents only a very small segment of a length of cemented oil-well casing. Thus, end effects in the test apparatus may appear to be of greater significance than they actually are in a well-bore. With these limitations in mind, it is believed that some qualitative conclusions can be reached by extending the test results to actual oil-well conditions.

If a yield stress of 70,000 psi at 500°F is taken for commonly used J-55 oil-well casing, and neat cement is used, a ΔT of about 350°F can be reached before plastic deformation of the casing occurs. Assuming an 80°F starting temperature, a steam injection temperature of 430°F into the well casing would not be expected to cause any adverse results to the cemented casing. At higher steam injection temperatures, ranging from about 450°F to 670°F, cement bond deterioration and casing shrinkage might be expected with the possibly serious result of interzonal communication. This would be especially true if the well underwent several heating cycles. However, Satter[9] and others have shown that high casing temperatures can be avoided by injecting steam into the tubing alone in conjunction with a down-hole thermal packer. Under these conditions, casing temperatures

would be low enough that casing or cement bond failure would not be expected. These results emphasize the need for good cement jobs in wells to be thermally stimulated to avoid casing failure.

CONCLUSIONS

The following conclusions are made on the basis of the foregoing tests:

1. Steel pipe cemented with neat cement thermally expands linearly (below the yield stress of the pipe) with an elongation of about 0.73×10^{-6} in./in.-°F. Using a neat cement - 40 per cent silica flour slurry, the elongation was about 1.04×10^{-6} in./in.-°F; and, using a Lumnite cement - 40 per cent silica flour slurry, the elongation was negligible.
2. The bond strength of neat cement was higher than that of the other two cements tested at all temperatures up to 670°F. Above 500°F, neat cement bond failure resulted from cement degradation at the pipe-cement interface. Cement bond failure of the neat and Lumnite cement - 40 per cent silica flour slurries was caused by extensive cement cracking in the cement matrix.
3. When cemented steel pipe was heated to a temperature where the axial stress created in the pipe exceeded the yield stress (a ΔT of about 200°F) and then cooled, plastic deformation of the pipe occurred. Pipe shortening and cement bond failure resulted. Repeated heating cycles produced additional pipe shortening and progressive cement bond failure.
4. On the basis of these tests, neat cement appears to be the best material for cementing wells to be thermally stimulated - especially where casing temperatures are 450°F or less.

ACKNOWLEDGMENTS

The author gratefully acknowledges the valuable discussions with many of the personnel in the Production Division of Gulf Research & Development Company, especially Drs. H. H. A. Huygen and E. W. Gaylord.

REFERENCES

1. Bailey, H. R., and B. K. Larkin, "Heat Conduction in Underground Combustion", Trans. AIME (1959), 216, 123.
2. Ramey, H. T., Jr., "Wellbore Heat Transmission", Journal of Petroleum Technology, April, 1962, pp. 427-435.
3. Moss, J. T., P. D. White, and J. S. McNiel, "In-Situ Combustion Process - Results of a Five-Well Field Experiment in Southern Oklahoma", Trans. AIME (1959), 216, 55 (Journal of Petroleum Technology, April, 1959, 55.)
4. Huygen, H. H. A., "Steam Condensation in Wellbore and Casing Temperature During Steam Injection", GR&DCo. File Note, KR-63, January, 1965.
5. Leutwyler, K., Jr., and H. L. Bigelow, "Temperature Effects on Sub-Surface Equipment in Steam Injection Systems", Journal of Petroleum Technology, January, 1965, pp. 93-101.
6. Armco Steel Corporation, Engineering Data Book, pp. 10-051.
7. Universal Atlas Cement, Division of United States Steel, "Refractory Concrete Manual".

8. Bearden, W. G., J. W. Spurlock, and G. C. Howard, "Control and Prevention of Interzonal Flow", Journal of Petroleum Technology, May, 1965, pp. 579-584.

9. Satter, Abdus, "Heat Losses During Flow of Steam Down a Wellbore", Journal of Petroleum Technology, July, 1965, pp. 845-851.

TABLE I

Summary of Test Results

Test No.	Cement Type	Maximum Pipe Temp. (°F)	Pipe-Casing Temp. Difference (°F)	No. of Heating Cycles	No. of Heating Cycles Resulting in Pipe Yielding	Cumulative Pipe Shrinkage (in.)	Cement Cure Pressure (psig)	Cement Bond Strength (psig)
1	Neat	590	460	2	2	0.25	0	50
2	Neat	685	520	13	3	>0.25	1000-0	500
3	Neat	670	490	6	2	0.052	1000	1500
4	Neat	670	455	5	4	0.391	1000	500
5	Neat	500	302	8	4	0.076	1000	>2000
6	Neat with 40% silica flour	500	338	9	6	0.292	1000	300
7	Lumnite with 40% silica flour	650	470	19	13	0.586	1000	40

TABLE II

Strength of Heated Cement

Compressive Strength Tests

Test No.	Maximum Test Temp. °F	Approximate Core Location	Average Compressive Strength psi	Cement Type	Remarks
3	670°F	1/2-in. Pipe	2770	Neat	
	Short Time Test	1/2-in. Pipe	3075		
		7-in. Casing	5945		
4	645	1/2-in. Pipe	2200	Neat	
		7-in. Casing	3370		
5	500	1/2-in. Pipe	2050	Neat	
		1/2-in. Pipe	2355		
		7-in. Casing	3225		
6	500	1/2-in. Pipe	5570	Neat with 40% silica flour	Cores brittle - some fractured when coring
		7-in. Casing	4870		
7	650	1/2-in. Pipe	2985	Lumnite with 40% silica flour	Cores very brittle - many fractured when coring
		7-in. Casing	3510		

Penetrometer Tests

Test No.	Average Strength (psi) at Distance from 1/2-in. Pipe Wall 1/8"	1/4"	1/2"	3/4"	1"	1-1/2"	2"	2-1/2"
3	33,800	37,000	40,300	40,800	38,000	60,000	41,000	46,000
4	5,500	4,750	5,450	6,100	10,500	17,000	11,900	21,700
5	14,900	13,800	13,400	11,300	13,000	13,000	15,800	14,100
6	20,500	24,000	30,000	50,000	41,000	36,200	41,000	30,000
7	23,700	27,600	26,600	25,100	26,500	30,500	26,500	35,500

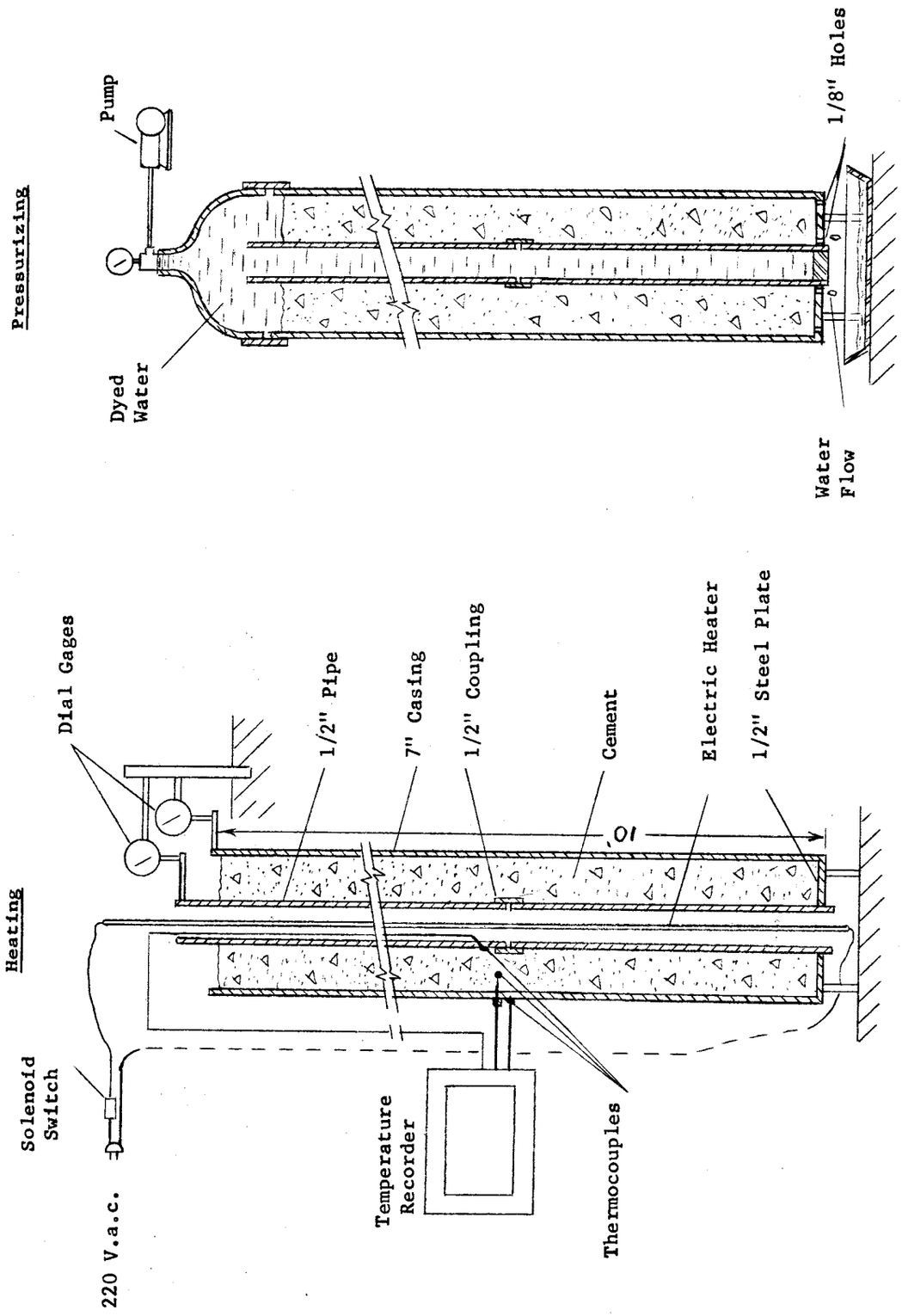

Test Apparatus for Thermal Expansion of Cemented Pipe

FIGURE 1

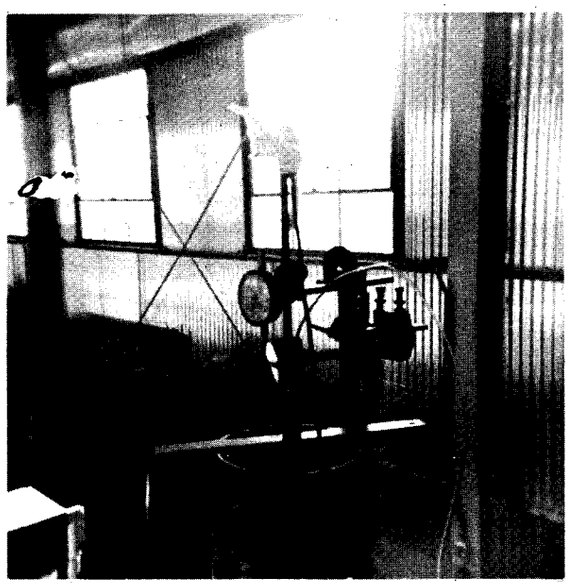

Dial Gages

Apparatus

Test Apparatus for Thermal Expansion
of
Cemented Pipe

FIGURE 2

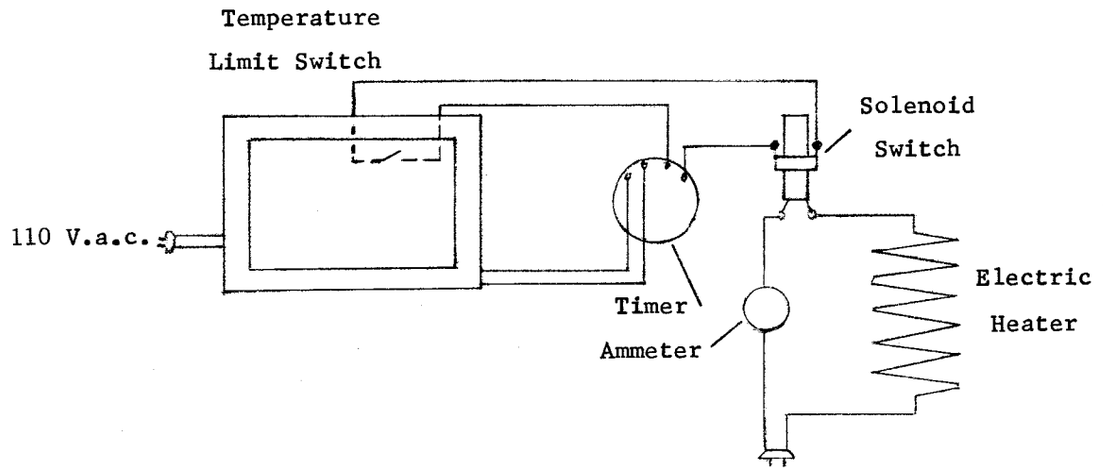

Electrical Control Circuit

FIGURE 3

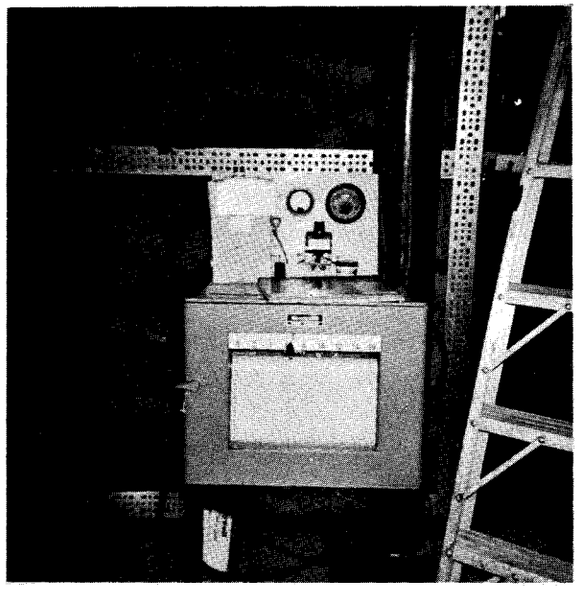

Electrical Control Circuit

FIGURE 4

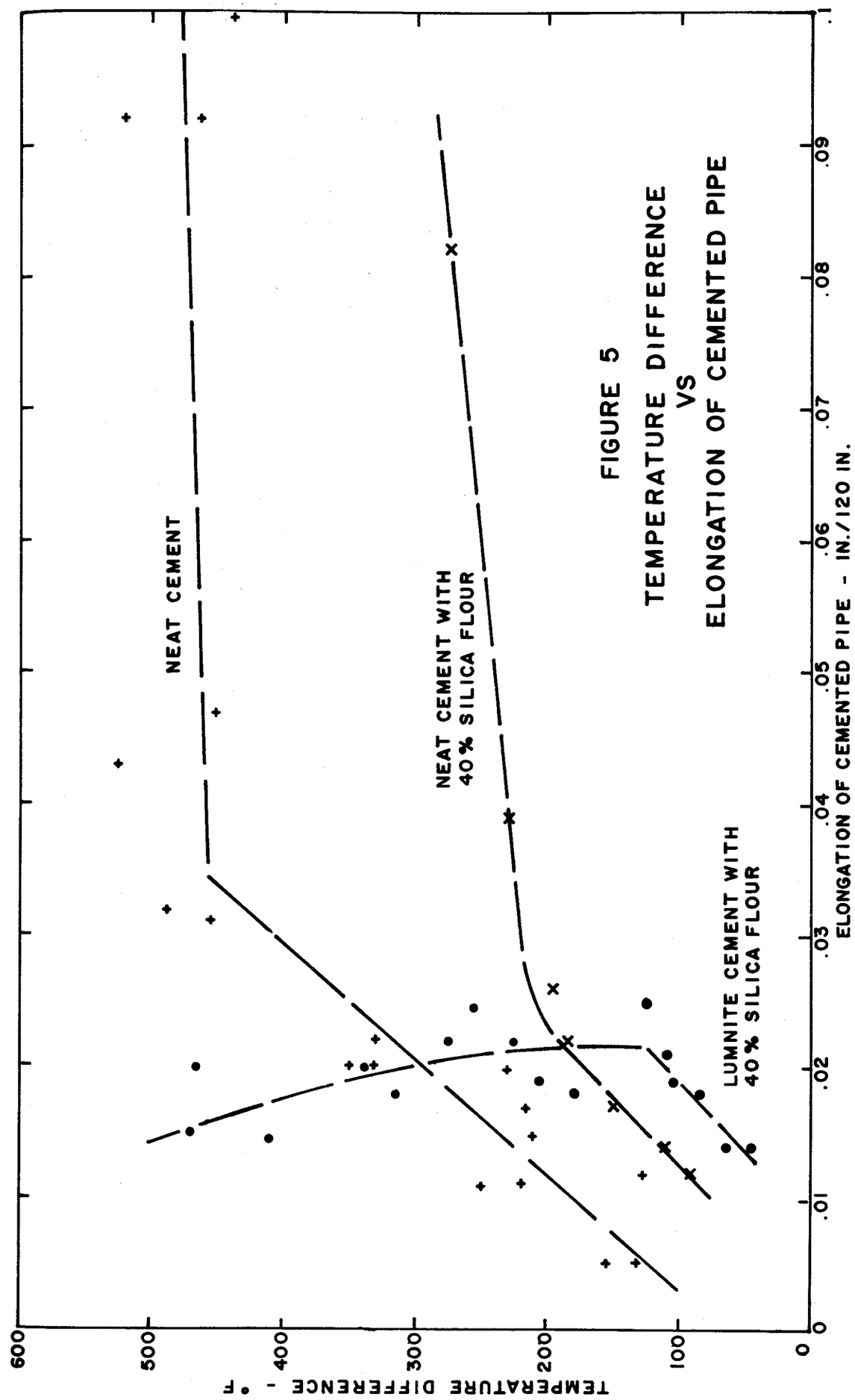

FIGURE 5
TEMPERATURE DIFFERENCE
VS
ELONGATION OF CEMENTED PIPE

One Foot from Top

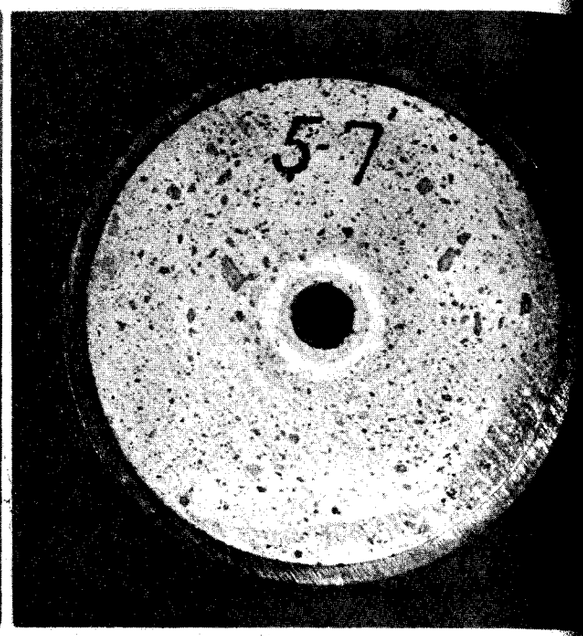

Near Mid-Length

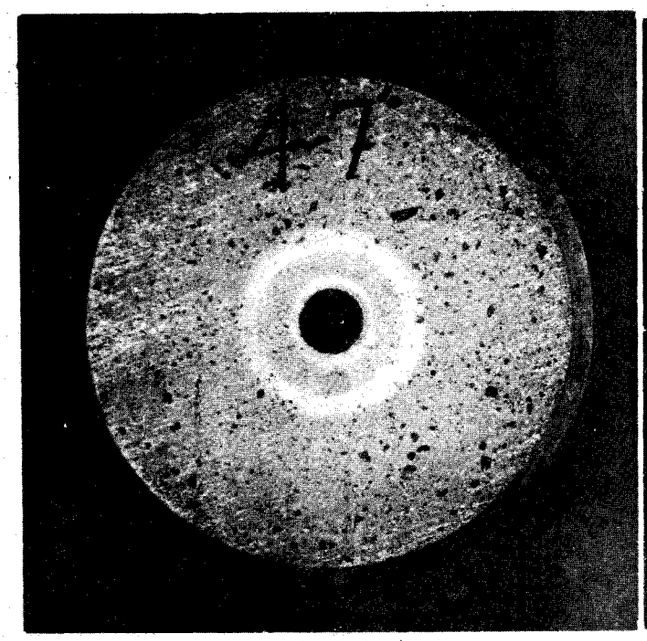

Near Mid-Length

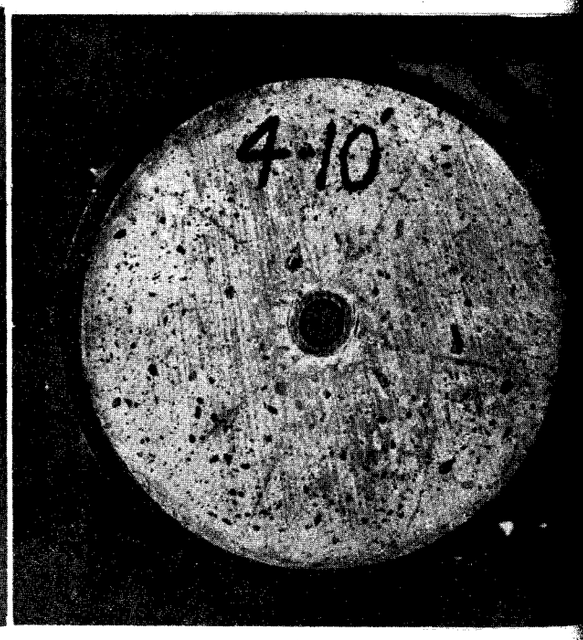

Bottom

Typical Cross Sections
of
Cemented Pipe
Neat Cement

FIGURE 6

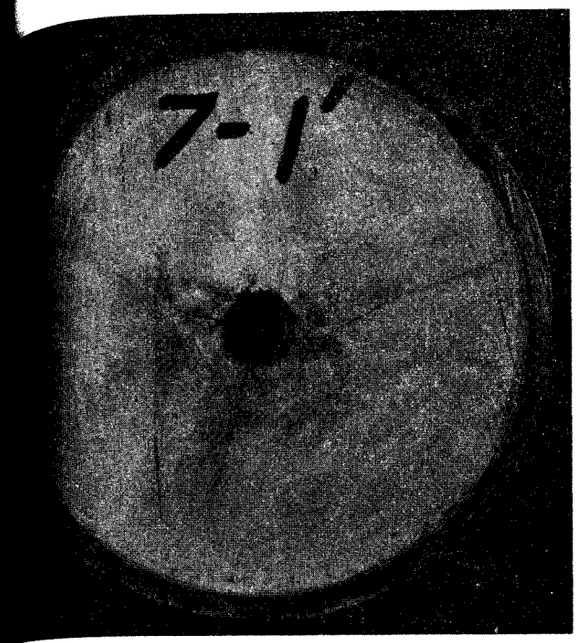

One Foot from Top

Near Mid-Length

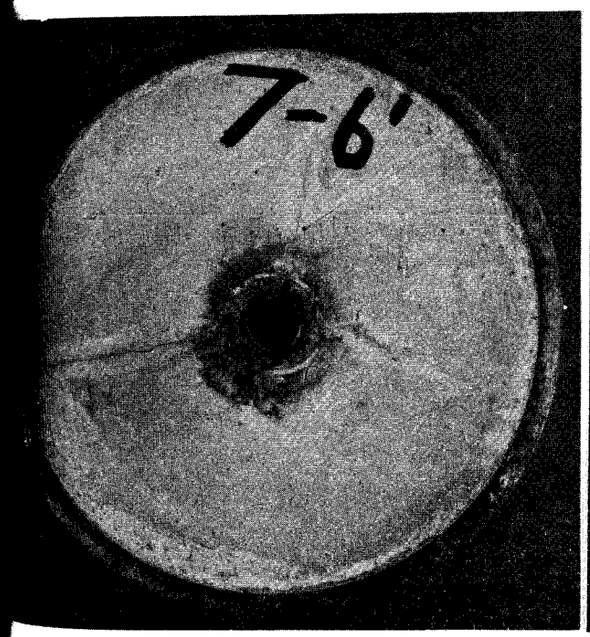

Near Mid-Length

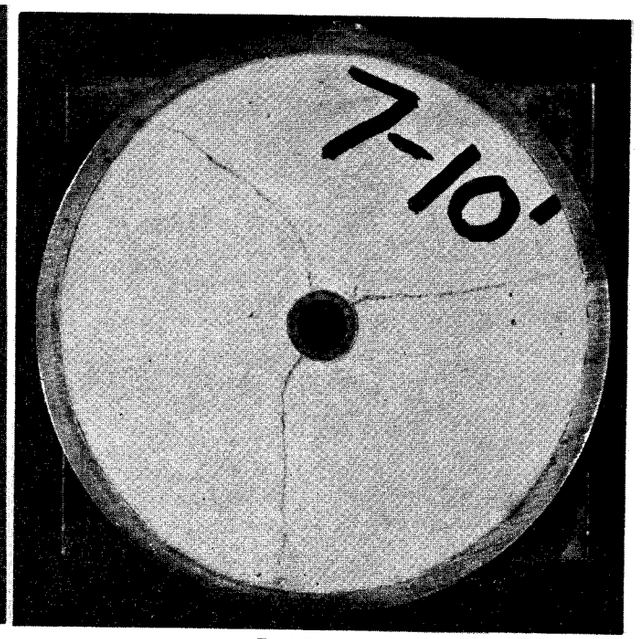

Bottom

Typical Cross Sections
of
Cemented Pipe
Lumnite Cement - 40% Silica Flour

FIGURE 8

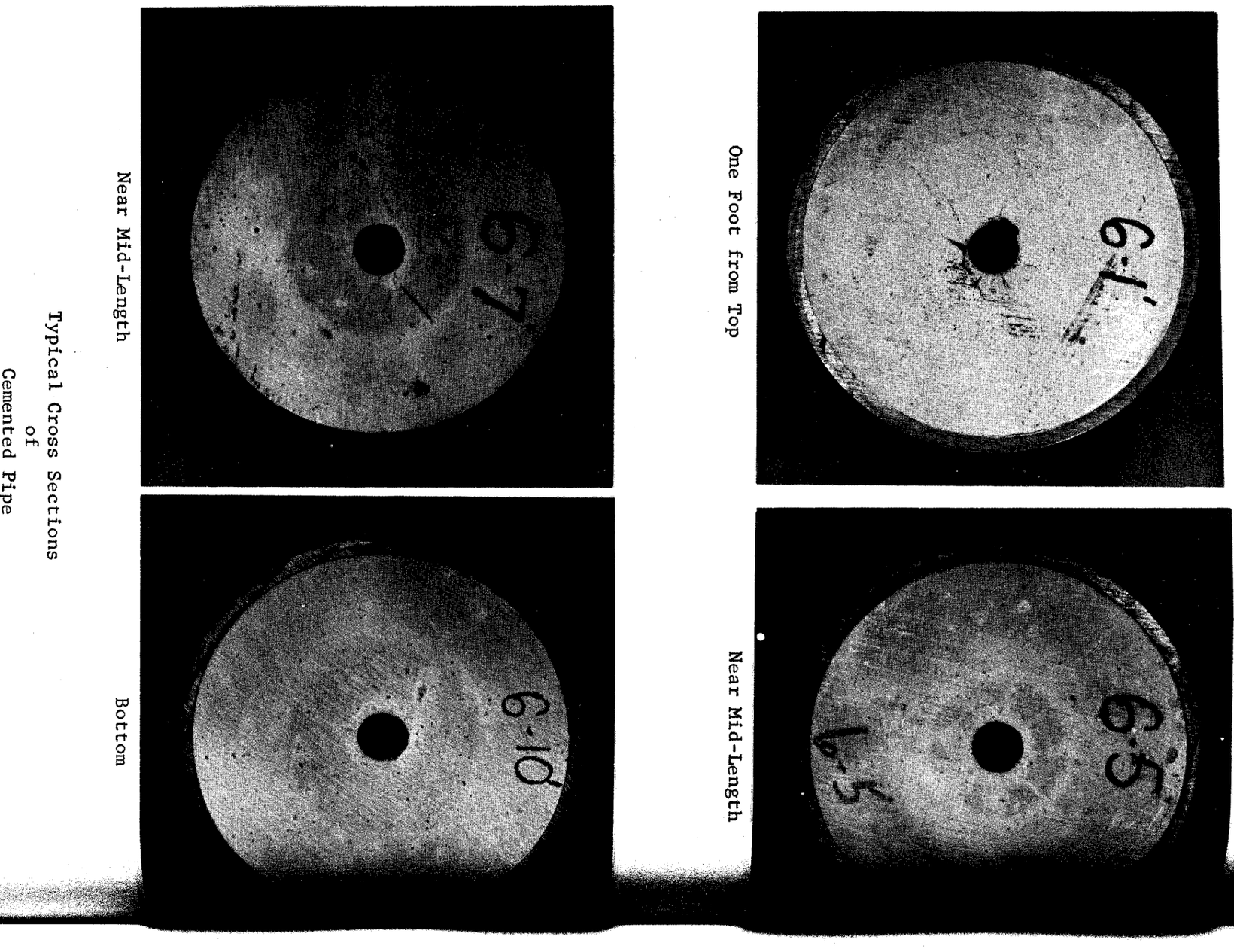

Typical Cross Sections
of
Cemented Pipe
Neat Cement - 40% Silica Flour

FIGURE 7

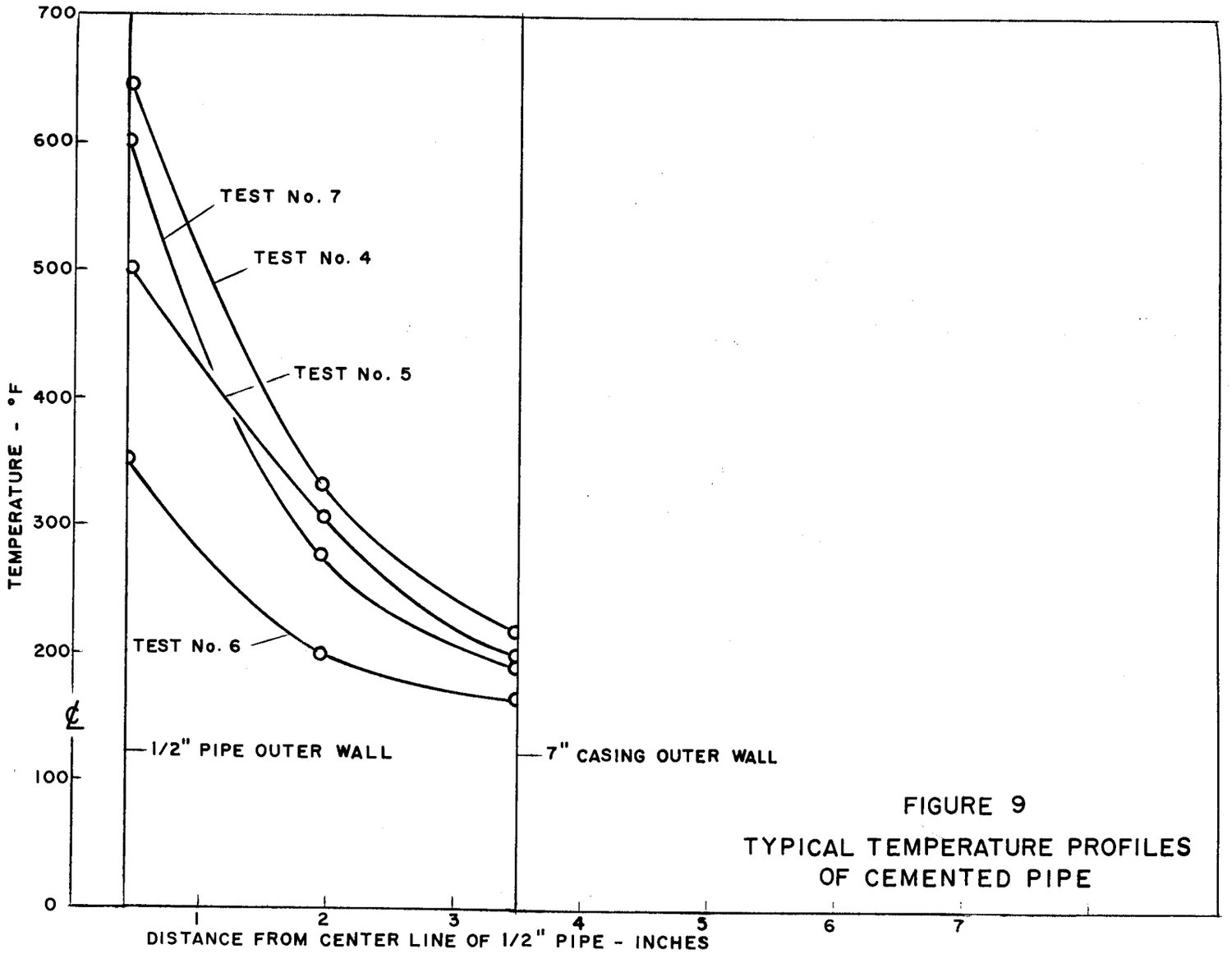

FIGURE 9

TYPICAL TEMPERATURE PROFILES
OF CEMENTED PIPE

A DOWN-HOLE BURNER - VERSATILE TOOL FOR WELL HEATING

By

F. M. Smith

Gulf Research & Development Company, Pittsburgh, Pa.

ABSTRACT

A versatile down-hole burner has been developed for supplying large amounts of heat to oil-producing formations. Although the burner is normally fueled with propane because of its availability, the burner can be operated with any hydrocarbon more volatile than gasoline. The device is unique in that it is capable of much greater heat-release rates than other down-hole burners despite its simpler and smaller combustion chamber. Destruction of the burner tube is prevented by a vortex of relatively cool air around the inner surface of the tube; the vortex is created by tangential slots on the side of the combustion chamber. A thermocouple, located in the burner exhaust pipe, measures the exhaust temperature.

In practice, the burner is lowered inside of well tubing, under pressure, on the end of a spooled 1/4-in. OD fuel tube containing a thermocouple lead wire. A pyrophoric liquid pumped into the fuel tube ahead of the fuel ignites the burner. Temperature is controlled by the fuel-air ratio.

This burner has been used in the field during the past six years for thermal stimulation, in-situ combustion ignition and warm air coking. It has been operated at (1) depths to 4400 ft, (2) pressures to 5000 psi, (3) temperatures from 150°F to 1500°F, (4) heat-release rates to 1,300,000 Btu/hr and (5) air rates ranging from 200 MCFD

to 3000 MCFD. The burner is simple to install and control, and it has proven to be a useful tool for well heating under a wide range of operating conditions.

INTRODUCTION

Before the recent interest in thermal stimulation and the recovery of oil by in-situ combustion, there was little use for a down-hole burner. However, such a device can be used today for an increasing number of purposes. At low operating temperatures (150-400°F), it can be used to consolidate sand by the warm air coking process. At higher operating temperatures (400-1200°F), it can be used to initiate in-situ combustion, provide thermal stimulation by lowering oil viscosity, and decrease wellbore damage caused by clay swelling, emulsion blockage, and paraffin deposition. Recognizing the need for a down-hole heating method capable of higher heat-release rates than is feasible with electric heaters, several oil companies have undertaken the development of down-hole burners.* Although many of these burner systems have enjoyed increasing use, all of the burners reported in the literature have rather limited capabilities.

This paper reports the development of a versatile down-hole burner which is capable of high heat-release rates. The burner is simple and relatively inexpensive to make, install, and operate; and it is capable of continuous operation on the inside of conventional oil-well tubing. The burner is normally fueled with propane but can be operated with any hydrocarbon more volatile than gasoline. It has been used in the field during the past six years for a variety of purposes and under a wide range of operating conditions.

DOWN-HOLE BURNER SYSTEM

The equipment used for down-hole burner operation includes surface equipment for installing the burner and for supplying metered

* References given at end of paper.

quantities of air and fuel, the thermocouple-fuel tubing, and the burner assembly itself. Installation, ignition, and dependable burner operation with excellent temperature control are easily accomplished.

Burner Assembly

The basic burner assembly is shown in Fig. 1 and consists of a (1) burner and burner stop, (2) fuel check valve, (3) "Y" block, and (4) thermocouple. In addition, a sinker bar is incorporated in the complete burner assembly (shown in Fig. 2). The assembly is designed for use inside tubing with a minimum ID of 2-3/8 in.

The burner shown in Fig. 1 consists of a 1-1/2-in. IPS stainless steel pipe that is tangentially slotted near the top end with one set of four slots spaced 90° apart. An open-ended fuel tube with a flame anchor on the end passes into the burner and terminates at a point above the tangential slots. A number of equally spaced sweep holes are located on the top end of the burner adjacent to the fuel tube. Attached to the open or lower end of the burner is the burner stop, a tapered steel nose containing asbestos seals. The burner stop ultimately makes a seal in a burner seating nipple, located at the bottom of the production tubing. Thus, with the burner landed in the seat, all air injected into the production tubing is forced through the burner with flow being divided between the sweep holes and tangential slots. The sweep holes provide a primary stream of air which mixes with fuel discharged from the flame anchor. Secondary air flow through the tangential slots results in a highly turbulent air stream inside the combustion chamber which (1) enhances fuel-air mixing, (2) promotes complete combustion of the fuel-air mixture, and (3) provides a vortex of relatively cool air around the inner wall of the burner. The resultant flame is stable within a

wide range of air velocities and is confined to an area close to the longitudinal axis of the pipe.

A fuel check valve, located immediately above the burner, prevents backflow of well fluids into the fuel tubing. Attached to the upper end of the check valve is a hollow sinker bar (see Fig. 2) which permits the burner assembly to be run into and out of a well under pressure. Both the burner and sinker bar are equipped with centralizers. The length of sinker bar used depends upon the wellhead pressure; a weight of about 50 lb per 1000 psi pressure is required to lower the assembly into a well.

The "Y" block is an "X" shaped block of stainless steel having one entrance passage and two exit passages. One exit passage, attached to the upper end of the sinker bar, is for fuel flow. The second exit provides a quick-disconnect junction for a thermocouple and lead wire. An Inconel-sheathed thermocouple is clamped along the outer wall of the sinker bar and burner with the hot junction being located inside the burner exhaust pipe.

The thermocouple-fuel tubing consists of a continuous length of 1/4-in. OD Monel tubing through the center of which extends a Teflon-insulated thermocouple lead wire. With a burner and 100-lb sinker bar attached, the maximum setting depth for this type assembly is about 5000 ft. The tubing size is such that it is (1) sufficiently large to allow a minimum restriction to fuel flow with the thermocouple wire installed, (2) flexible enough to be spooled, (3) strong enough to withstand high pressures and yet (4) small enough to require a minimum sinker bar weight for burner installation under elevated pressure. The fuel tubing is attached to the top of the "Y" block, with the thermocouple wire extending into the quick-disconnect thermocouple adapter.

Surface Equipment

The basic surface equipment is shown in Fig. 2 and includes (1) a simple wellhead installation and (2) a mast and hoist for installing the burner. In addition to that shown in Fig. 2, air and fuel supply, metering facilities, and temperature recording and safety control instruments are part of the installation.

The wellhead hookup is quite like that used for most wire-line operations, having a lubricator with a set of blowout preventers and a line wiper located at its upper end. The Christmas tree is equipped with wing valves to enable both tubing and casing to be used for either injection or production.

A mast, extending above the lubricator, is required for the installation of the burner assembly, and may be simply a light-weight gin pole or an "A" frame. A 3-ft diameter idler sheave is installed close to its peak.

The hoist equipment for spooling the burner fuel tube consists of a hydraulically operated spooling device which, again, is quite similar in operation to many wire-line units.

The air supply must be capable of uninterrupted operation at pressures up to 1 psi per foot of depth to the zone to be treated. Both air compressors and liquid air systems with capacities in the range 0.2-3 MMCFD have been used. The air supply is connected to the tubing and casing through a parallel set of control valves and orifice meter runs, thereby permitting the control and measurement of the air flow into each.

Fuel is metered to the burner with a diaphragm-type metering pump. Although the burner can operate on most paraffin hydrocarbons more volatile than gasoline, propane is the preferred and most widely

used fuel since it can be readily metered, is widely available, and is relatively inexpensive.

A continuous measurement of the burner exhaust temperature is had by connecting the upper end of the thermocouple lead wire to a temperature recorder. Automatic safety control during burner operation is primarily provided by a temperature limit switch which stops fuel injection to the burner should an excessive temperature develop as a result of an air supply failure, wellbore fire, etc. Supplementary shut-down mechanisms are also used.

Installation and Operation

Well preparations for burner installation are minimal in that a rig is required only to run production tubing with a burner seating nipple on bottom. Once the tubing has been landed, usually no more than 5 ft above the perforations, thorough cleaning of the well is necessary to prevent a down-hole fire or explosion. This is accomplished by circulating a solvent, such as diesel fuel, and a detergent solution until the returns are clean. Air injection into the formation is then begun. Meanwhile, the burner is installed in the lubricator, lowered inside of the well tubing, and landed in the seating nipple.

Although the bulk of the air is normally injected into the tubing during down-hole burner operation, a small air flow rate is maintained into the casing to keep the casing annulus purged and prevent the formation of an explosive mixture. In instances where a tubing packer is used, of course, all the air is injected into the tubing and through the burner.

Preparations for burner ignition are made by beginning fuel injection and adjusting the air and fuel rates for the desired temperature rise. Ignition is accomplished by injecting into the fuel tubing a small

volume of triethylborane, a liquid pyrophoric compound. When the igniter fluid enters the air stream passing through the burner, ignition occurs. The use of triethylborane has proven to be a safe, inexpensive, and extremely dependable method for igniting the burner.

Desired changes in burner exhaust temperature are made simply by adjustment of the air and fuel rates. The burner has proved to burn clean and operate efficiently at temperatures between 150 and 1500°F. Air requirements range from four to 10 times that of stoichiometric conditions at the foregoing temperatures, and, thus, complete combustion results. The only products of combustion entering the formation are CO_2 and water vapor with very little to no deposition of carbon on the burner itself.

Upon completion of the heat treatment or at any other time, the burner can be shut off and retrieved without stopping air injection or lowering the well pressure. If desired, the well can then be put on production without the services of a rig.

System Advantages

All of the burners reported in the literature are run in the well on either a single or dual string of large-diameter oil-well tubing or pipe; therefore, a rig is required to install and retrieve the burner. Most of these burners are large, elaborate, ceramic-lined, and gas-fired units which must be run inside the casing; furthermore, they are incapable of being run into and retrieved from a well under pressure. Few of the burners are equipped with thermocouples for continuously monitoring exhaust temperature. Despite the large size of these burners, their maximum heat-release rates are quite low -- of the order of 100-400,000 Btu/hr.

By way of comparison, the down-hole burner described in this paper operates on any fuel more volatile than gasoline and is run into and out of a well under pressure on a continuous length of flexible, small-diameter fuel tubing. A rig is required only to install and, eventually, remove the burner seat. In instances where a bottom-lock pump is to be used in the well, even this becomes unnecessary; the pump seating nipple can be used as a burner seat. The burner is made from ordinary stainless steel pipe, is simple in design and is relatively inexpensive; and, it is sufficiently small to be run inside commonly used sizes of production tubing. Owing to this feature, the burner can be operated in wells equipped either with or without a tubing packer. Finally, the thermocouple wire contained in the fuel tube and the thermocouple attached to the burner itself permit continuous observation of burner performance.

Full-scale laboratory tests and field applications have demonstrated a heat-release capability in excess of 1,300,000 Btu/hr. Further, this burner has been operated at (1) depths to 4400 ft, (2) pressure to over 5000 psi, (3) temperatures from 150°F to 1500°F, and (4) air rates ranging from 200 MCFD to 3000 MCFD. Field applications during the past six years include thermal stimulation, in-situ combustion, and warm air coking for sand control.

SUMMARY

A down-hole burner has been developed which is an improvement over other burner systems. Although installation and operation are simple, the burner is capable of releasing very large amounts of heat under a wide range of operating conditions. It has proven to be a useful tool for a variety of well heating applications.

ACKNOWLEDGMENT

The burner described in this paper is the result of efforts of many individuals at Gulf Research & Development Company over a period of about six years. The helpful suggestions and direction given by Messrs. R. J. Goodwin, J. W. Jennings and P. L. Terwilliger were instrumental to the development of this device. The contributions of J. F. Muirhead are gratefully acknowledged.

The author also expresses appreciation to the Management of Gulf Research & Development Company for permission to present this paper.

REFERENCES

1. DePriester, C. L., and A. J. Pantaleo, "Well Stimulation by Down-Hole Gas-Air Burner", Jour. Pet. Tech., December, 1963, pp. 1297-1302.
2. Strange, Lloyd K., "Ignition: Key Phase in Combustion Recovery", Petroleum Engineer, December, 1964, pp. 97-98.
3. Moss, Jon T., "Practical Notes on Ignition in Fire Flooding", Petroleum Engineer, May, 1965, pp. 74-75.
4. Brandt, H., W. G. Poynter, and J. D. Hummell, "Stimulating Heavy Oil Reservoirs with Down-Hole Air-Gas Burners", World Oil, September, 1965, pp. 91-95.

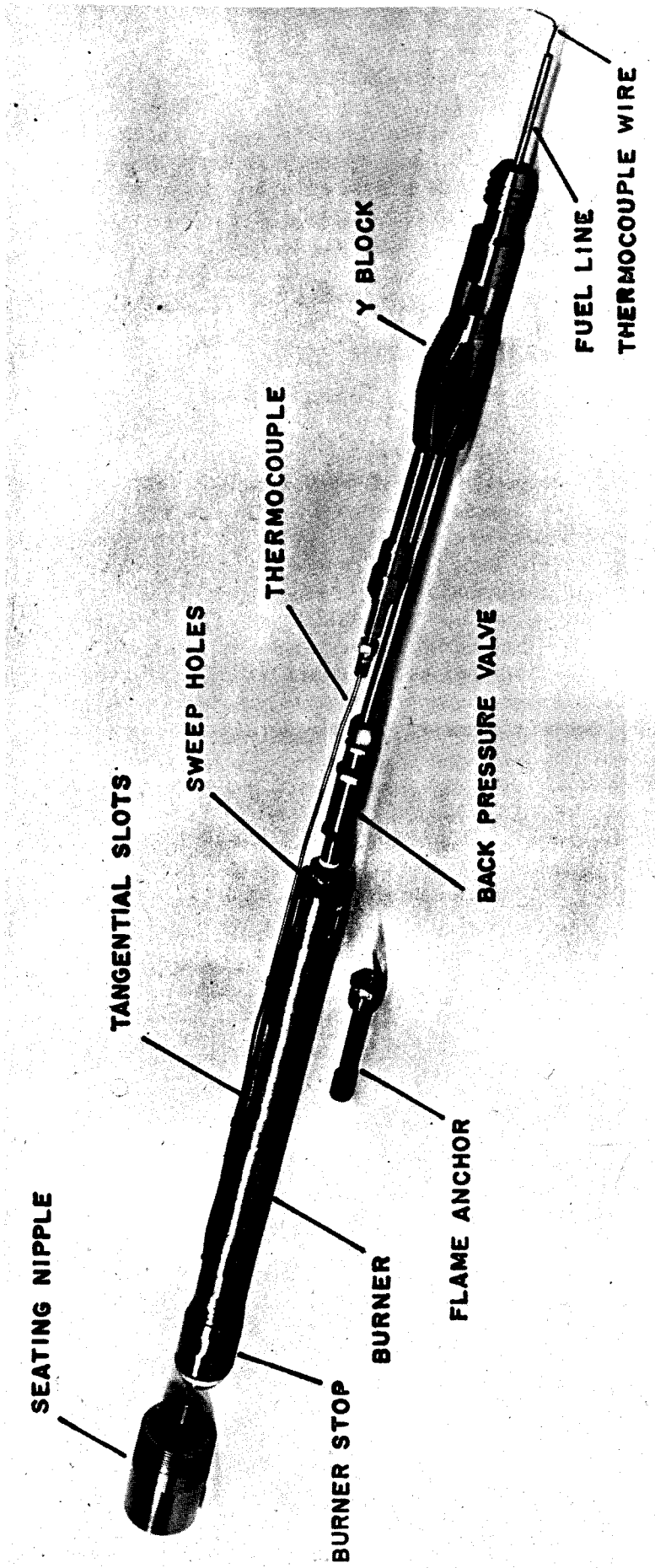

FIGURE 1

1-1/2" I.P.S. DOWN-HOLE BURNER ASSEMBLY

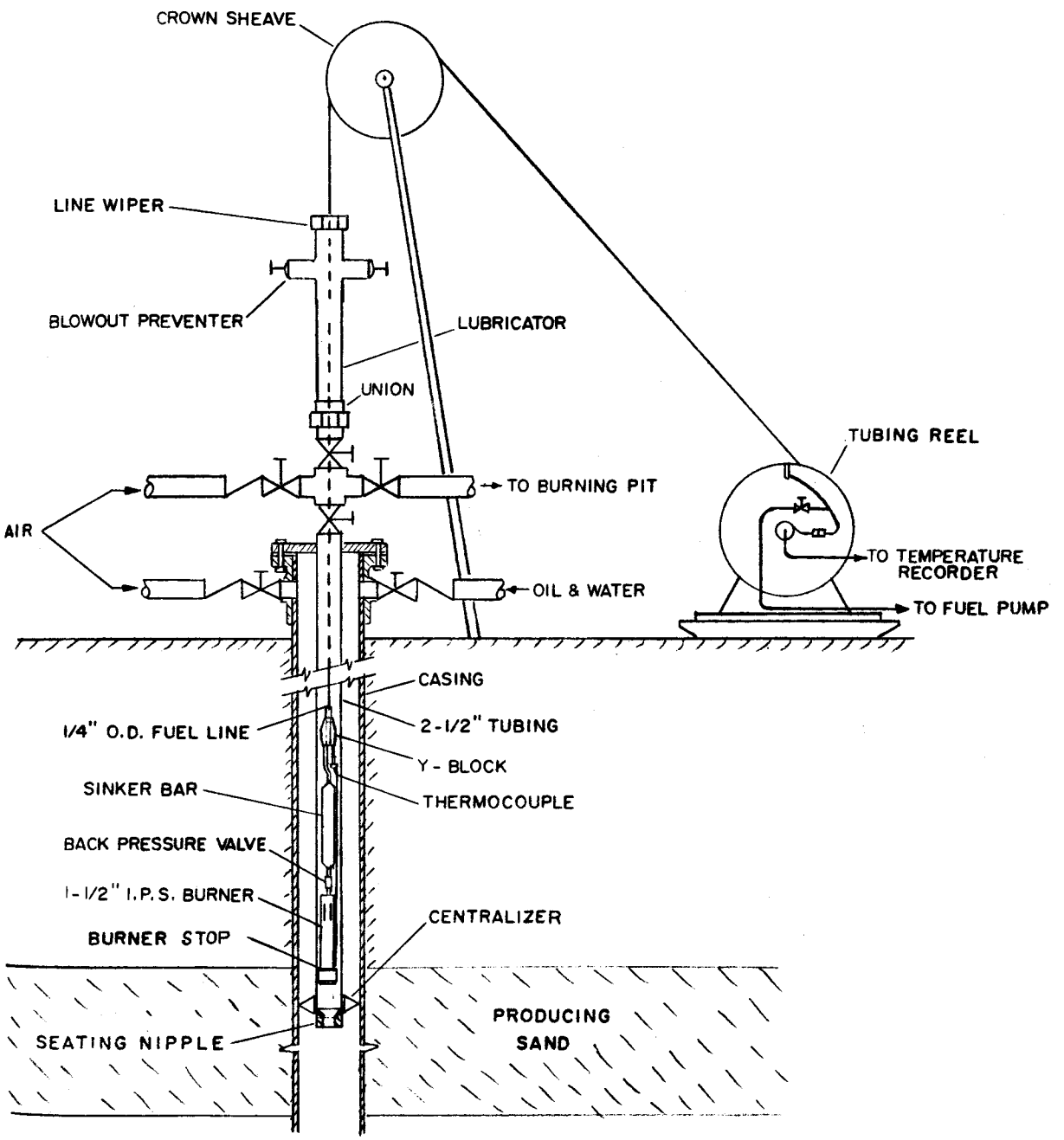

SCHEMATIC OF WELL COMPLETION

FIG. 2

THEORETICAL AND FIELD WATERFLOOD PERFORMANCE, KANE OILFIELD, ELK COUNTY, PA.

by

Leo A. Schrider,[1/] John R. Duda,[1/] and Harry R. Johnson[2/]

ABSTRACT

A prediction for oil recovery from a pilot waterflood in the Kane oilfield, which is located in Elk, Forest, and McKean counties, Pa., was made and compared with actual field performance.

The calculated behavior of the pilot waterflood, which was initiated in January 1963, was predicted using a modified Craig, Geffen, and Morse calculation technique. Maximum recovery from this low-permeability, preferentially oil-wet formation was predicted to be about 22,500 barrels of oil after 300,000 barrels of water had been injected into the pilot area. After additional field data were collected, it became necessary to reevaluate the pilot flood area. The gas saturation prior to the flood was estimated to have been 20 percent, based on an assumption regarding the required volume of water injected to initiate oil production. In view of the actual field performance, a gas saturation of 13 percent is indicated. When this gas saturation and the method originally proposed by Craig, and others, are used, the predicted results are more representative.

1/ Morgantown Petroleum Research Laboratory, Bureau of Mines, Morgantown, W. Va.

2/ Office of Director of Petroleum Research, Bureau of Mines, Washington, D. C.

In December 1965, field performance was further analyzed using a hyperbolic decline curve as presented by Arps. Based upon this evaluation method, the pilot waterflood in the Kane sand should produce 37,000 to 42,000 barrels of oil with the injection of 300,000 barrels of water. By continuing this secondary-recovery project to a reasonable economic limit, ultimate oil recovery may be as much as 50,000 to 55,000 barrels, or 129 to 142 barrels per acre-foot from 36.5 acres.

INTRODUCTION

The Bureau of Mines is studying selected Appalachian area reservoirs to determine their susceptibility to secondary recovery. The objective of this work is to increase the recovery of oil from known pressure-depleted reservoirs. The Kane oilfield was selected for study under the program, since it afforded the Bureau an opportunity to compare theoretical and field performances.

Two wells were cored in the pilot waterflood area; one by the operator, Fords Brook Drilling Company, and the other by the Bureau of Mines. The core analyses along with well logs and field-production data were used to predict the performance of this secondary-recovery waterflood project. Following three years of injection-production data, a comparison of the original prediction with the actual performance and subsequent reevaluation of the project was accomplished.

GEOLOGY AND HISTORY

The Kane oilfield, approximately 12 miles long and 1 mile wide, is located in parts of Elk, Forest, and McKean Counties, Pa., (fig. 1) along the northwestern flank (surface axis) of the Smethport anticline.

Initial oil production was from the Nansen, Sackett, and Duhring pools which were discovered about 1881. Subsequent development combined these into the Kane oilfield. Drillers in the area correlated the Kane sand of this field with the Kane sand found in the Bradford District, McKean County.

The Kane sand is in the Upper Devonian system at a depth of approximately 2,200 feet.

Published records (10) show that the first successful oil well in the Kane field was drilled in 1881. Nine years later, the first well was drilled on that portion of Land Warrant 3777 covered in this report. By January 1891, 17 wells had been drilled; and by October 1900, the development was completed with an additional 52 oil wells on an approximately 10-acre spacing.

Initial production rates in the Kane field were as high as 100 barrels per day per well (10). The average production rates for the 10-year period, prior to waterflooding, were less than 1 barrel per day per well in Land Warrant 3777 with producing gas-oil ratios ranging from 200 to 500 scf per barrel. Estimates of cumulative oil production range from 6,000 to 14,000 barrels per well. No water was produced before initiation of the pilot flood.

Original reservoir energy in this field is attributed to a combination solution-gas and gas-cap drive. Production of the gas cap and subsequent shrinkage has inactivated the gas-cap drive and permitted the oil to migrate updip into the original cap area. Oil production from wells that originally produced only gas is evidence of this migration. Not all of this up-structure oil is recoverable by natural means since a portion will become residual oil in the invaded gas sand.

DEVELOPMENT OF PILOT WATERFLOOD

The operator chose a location for the pilot waterflood where the wells, for the most part were already drilled. The spacing and location of the wells selected for the test are shown in figure 2. This area consists of nine injection and four producing wells enclosing an area of 36.5 acres. Old producing wells were converted to injection wells and new producing wells were drilled and completed, resulting in four normal five-spot patterns.

All wells in the pilot project were subsequently hydraulically fractured, using 300 to 500 barrels of water and 9,000 to 12,000 pounds of sand. Treating pressures in the four new wells were about 800 psig less than in the old wells owing to the use of 3-inch tubing in the new wells as opposed to 2-inch tubing in the old. The average breakdown and treating pressure was about 4,500 and 3,000 psig, respectively. Before fracturing, the wells produced only a few gallons of oil per day; after fracturing, they produced a few barrels per day. The major increase in production was not experienced until "fill-up" occurred.

In January 1963, surface water was injected into the Kane sand. This water was treated with a corrosion inhibitor and injected at a wellhead pressure which ranged from 1,500 to 1,700 psig.

An unusually large amount of water was produced in June and July of 1963. This large volume of water which broke through was attributed in part to fractures which the operator believed existed from injection to production wells. This was later confirmed in August 1963 when the operator slugged fluorescein dye into the injection wells. The extremely short time (1 to 3 days) required to produce the injected dye confirmed the existence of communicating or near-miss fractures.

Additional tracer tests conducted by the Bureau of Mines will be discussed later.

Producing wells E-1 and E-3 (fig. 2) were cored and logged. Well E-1 was cable-tool cored using dextrose water as the drilling fluid and well E-3 was rotary cored with air.

Electrical logs were run through the Kane sand in all the producing wells (E-1 through E-4) and were used to evaluate and correlate this sand throughout the pilot-flood area. The logs indicate that the Kane sand is approximately 36 feet thick. These electric logs and cores from wells E-1 and E-3 also show that the sand is heterogeneous with considerable shale interbedding. Consequently, all of the formation cannot be considered floodable or effective sand. Approximately 16 feet of the formation is shale and separates the 20 feet of sand into thin lenses.

RESERVOIR CHARACTERISTICS

Only 60 percent of the core was recovered from well E-3, therefore the sequence of formation characteristics is indistinguishable in this well. This core analysis, therefore, cannot be used to evaluate the sand with any degree of reliability. In well E-1, however, 95 percent of the core was recovered. Approximately 96 percent of the total injection capacity of well E-1 is contained in the sand interval with air permeabilities above 1 millidarcy. The total of these intervals (10.6 feet) is the effective sand thickness. The weighted-average air permeability of this effective sand is 4.4 millidarcys. Table 1 summarizes the core and log analyses of wells E-1 and E-3.

Representative core samples of the Kane sand were tested to determine preferential wettability. Five adjacent pairs of samples were chipped from

the fresh core obtained from well E-3. One sample of each pair was immersed in oil and the other in distilled water. The initial rate of water or oil imbibition into each sample (11) and the total amounts imbibed were determined. The results are given in table 2. The Kane sand samples imbibed both oil and water; however, oil was imbibed much faster than water and also in greater volume. In a preferentially oil-wet system, water will not enter the smaller pore channels because the capillary forces causing imbibition are greater for oil than for water. This behavior was exhibited by the samples taken in the Kane sand, indicating it to be a preferentially oil-wet system.

The relative-permeability characteristics of a reservoir also reflect the effect of wettability (8). The average relative permeability to water at residual oil saturation is 4.7 times greater in figure 3 than the relative permeability to oil at residual water saturation.

The average water saturation determined by log and core analysis of well E-1 and log analysis of well E-3 was 13.2 percent (table 1). This water is immobile since water is not produced from the Kane sand.

The journal article published in the August 1964 issue of Producers Monthly (3) predicted the oil recovery from the pilot-flood area using an assumed gas saturation of 20 percent. This prediction was necessarily based on several assumptions and the assumed gas saturation was apparently too high. The field data now indicate that an initial average gas saturation of about 13 percent existed in the Kane sand reservoir. Based on this current knowledge, the oil saturation prior to initiation of the flood would have been 73.8 percent. The residual oil saturation from relative-permeability tests is 46.3 percent (fig. 3). A stock-tank sample of oil was taken from well E-1 in November 1962. The measured viscosity and specific gravity of

the sample was 3.05 cp and 0.795, respectively, and the API gravity was 44.7°. All tests were made at the bottom-hole temperature of 80° F.

PREDICTION METHOD

The method originally employed to predict secondary recovery of oil from this area by waterflooding was that proposed by Craig, Geffen, and Morse with a modification in the injected volume of water required to initiate oil production (3). In the paper by Craig, and others (6), it was assumed that all of the free gas space within the confined area need be liquid filled before oil production begins. In preparing the Kane sand prediction, however, the authors assumed that only the gas space in the initially swept area need be liquid filled. Other authors (7, 13) state that all the gas space must be liquid filled. It was therefore necessary to reevaluate the pilot-flood prediction.

This reevaluation was made using a composite of the original Craig, and others, method and that proposed by Suder and Calhoun (14). The Suder-Calhoun technique, based on Darcy's radial flow equation and a material balance of the injected fluid, was applied up to water breakthrough. This results in a realistic profile of water-injection rates until the beginning of the steady-state flow. After water breakthrough, emphasis was placed on the method originally proposed by Craig, and others. This method accounts for continued oil production from the invaded region through the use of the frontal-advance equation proposed by Buckley and Leverett (4) and modified by Welge (15). Also considered is oil production from the newly invaded region as the areal sweep efficiency increases with continued water throughput. The data required to perform these calculations are presented in table 3.

PREDICTED AND ACTUAL WATERFLOOD PERFORMANCE

Figure 4 shows a plot of the dimensionless production rates as a function of the cumulative water injected into the pattern. The predicted performance for gas saturations prior to waterflooding of 13 and 20 percent is compared to the actual field performance of the waterflood.

It is readily apparent from figure 4 that the original estimated gas saturation of 20 percent (3) yields low production-rate values. This is further confirmed in figure 5 which indicates a low cumulative oil recovery as compared to the actual recovery.

The difference between the originally predicted results (using 20 percent gas saturation) and the actual field data is believed to be due to an assumption made in developing the original prediction. It was assumed that only the gas space in the initially swept portion of the reservoir need be liquid filled in order to initiate response at the producing wells. The theoretical minimum gas saturation that existed in the reservoir was then established by noting the volume of water injected until a response at the production wells was observed. The pilot flood indicated this response by June 1963, and a gas saturation of approximately 20 percent was calculate When these same field data are viewed under the assumption that all of the gas space within the confined area must be liquid filled, an initial gas saturation of about 13 percent was calculated. Although a gas saturation of 13 percent is now accepted as approximately correct, the results of prediction calculations using this figure still do not match actual performance. In making the calculations, the Kane sand was assumed, for purposes of simplification, to consists of a single, homogeneous layer. Such an assumption is weak for several obvious reasons. Because this sand is highly stratified, the injected water can move through the sand at varying rates

depending on the permeability of the individual strata and breakthrough will not occur simultaneously in all layers. Perhaps a more important factor in the discrepancy between actual and predicted results is the fact that the wells were hydraulically fractured during completion. Some of these fractures provided almost direct communication between injection and production wells. As a result, a very early water breakthrough was experienced and a percentage of the injected water has done little or no work in displacing oil. The sweep efficiency and displacement efficiency have improved with continued injection, and production rates have held up well. Ultimate recovery from the pilot flood may therefore approximate the predicted ultimate recovery.

PRODUCTION-DECLINE ANALYSIS

Oil production from the Kane sand pilot waterflood has declined since April 1964. Various methods and mathematical relationships were investigated to evaluate this decline. Exponential, hyperbolic, and harmonic declines were utilized for fitting the production data.

The hyperbolic or log-log type of decline can be recognized when the difference of the loss ratios is constant, or nearly so. Differences of consecutive initial values in the loss ratio are sometimes referred to as the b exponent (12) and can vary between 0 and 1. For the Kane sand production, the calculated loss ratios were not constant nor could a constant difference of loss ratios between 0 and 1 be found. Therefore, an alternate method was used (1), and a b exponent of 0.5 was found to best approximate a straight line. The hyperbolic-decline curve as presented by Arps was then derived. The result of this mathematical technique is shown graphically in figure 6.

The Kane sand, as for most waterfloods, consisted of first a period of fill-up and then a period during which the oil-production rate responded to water injection. After the peak oil-production rate was attained, the oil-production rate started to decline as the flood reached maturity. During this time, the water saturation and relative permeability to water increased, while the oil saturation and relative permeability to oil decreased. The oil-production decline, however, may or may not be a direct function of time (9); although at all times it is a function of the volume of water injected. Therefore, it should be emphasized that true decline for secondary waterfloods seldom exists since water injection and thus, oil production is subject to the control of the operator (9).

As indicated, a recovery of 37,000 to 42,000 barrels of oil is expected if 300,000 barrels of water is injected into the pattern. If the flood is continued to a production rate of 1 barrel per day per well, an additional 13,000 barrels of oil may be produced, or a total of 50,000 to 55,000 barrels (129 to 142 barrels per acre-foot), may be recovered. This compares to about 45,000 barrels of oil predicted by the technique described earlier.

Figure 6 can also be used to estimate the cumulative oil production at a particular time. Suppose, for example, that an estimate of cumulative oil production to January 1968 is needed. The first step is to estimate the production rate for that time from the rate-time curve using the scale on the left of figure 6. For January 1968, the rate indicated on the figure is an estimated 350 barrels per month. This rate value is then transferred to the right-hand scale on the figure and extrapolated to the rate-cumulative curve. As shown, the predicted cumulative production for January 1968 is 39,500 barrels. Inherent in any estimate from this figure is the

assumption that the operator will continue to inject water at about the current rate of 11,600 barrels per month.

Figure 7 illustrates the cumulative history of Kane sand oil production from Land Warrant 3777 in the Allegheny National Forest. Oil recovered through January 1966 by primary (2) and secondary-recovery methods is estimated to be 1,047,000 stock-tank barrels, and continued water injection into the pilot-flood area should give an additional 20,000 barrels.

DISCUSSION OF RESULTS

The likelihood that communicating fractures existed in the formation was confirmed by the operator in August 1963 when fluorescein dye tracers were injected. Further tracer work was initiated in January 1965 by the Bureau of Mines to reconfirm that fractures or near-miss fractures existed in the Kane sand reservoir. It was also hoped that if they did exist, the percentage of water going through the fractures could be determined. A paper presenting the results of these tests (5) will follow this presentation.

In preparing a study of this nature, the various parameters inherent to the method are very difficult to establish. When viewing the predicted results for the pilot flood it is quite evident that the originally assumed initial gas saturation of 20 percent was in error, whereas a saturation of 13 percent may be more realistic.

The favorable field response of the pilot waterflood has prompted the operator to expand his present project. The addition of 180 acres to the southwest of the current pilot flood was initiated in January 1966 and will add approximately 10 normal five-spots to the existing flood pattern. Orientation of the fracture system will also be attempted in order to establish communication between injection wells and thus create a linear-

flow system for the flood. The knowledge gained in fracture extent and orientation from the current flood will, if successful, lead to a more efficient waterflood pattern in the Kane field.

CONCLUSIONS

The assumed gas saturation of 20 percent used in the original prediction was incorrect. The maximum oil recovery predicted at the time the assumption was made is considerably less than the actual field performance. Furthermore, the field performance indicates that an initial gas saturation of 13 percent existed in the reservoir. When this gas saturation is used, predicted results for ultimate recovery agree with calculated values derived by decline-curve analysis. Based upon the latter calculations, the pilot waterflood in the Kane sand should ultimately produce 50,000 to 55,000 barrels of oil, or 129 to 142 barrels per acre-foot.

ACKNOWLEDGMENTS

The authors acknowledge the suggestions of Dr. E. T. Heck, consultant and vice president, Minard Run Oil Company, Bradford, Pa., and the cooperation of Mr. Knight Thornton, Thornton Producing Company, Wellsville, N. Y., who generously provided much of the data for this report. The writers also acknowledge the assistance of Dean W. Boley, petroleum engineer, formerly on the staff of the Morgantown Petroleum Research Laboratory. Recognition is also given to the Bureau of Mines Industry Technical Advisory Committee for their suggestions concerning this study.

REFERENCES

1. Arps, J. J. Analysis of Decline Curves. Trans. AIME, v. 160, 1945, pp. 228-247.
2. Arps, J. J., and T. G. Roberts. The Effect of the Relative Permeability Ratio, the Oil Gravity, and the Solution Gas-Oil Ratio on the Primary Recovery from a Depletion Type Reservoir. Trans. AIME, v. 204, 1955, pp. 120-127.
3. Boley, Dean W., Harry R. Johnson, and John R. Duda. Predicted Oil Recovery from a Pilot Waterflood in the Kane Oilfield, Elk County, Pa. Producers Monthly, v. 28, No. 8, August 1964, pp. 10-16.
4. Buckley, S. E., and M. C. Leverett. Mechanism of Fluid Displacement in Sands. Trans. AIME, v. 146, 1942, pp. 107-116.
5. Burwell, E. L. Multiple Tracers Aid Evaluation of a Pilot Waterflood. To be pres. at 25th Tech. Conf. on Petrol. Production, Oct. 19-21, 1966, The Pennsylvania State Univ., University Park, Pa.
6. Craig, F. F., Jr., T. M. Geffen, and R. A. Morse. Oil Recovery Performance of Pattern Gas or Water Injection Operations from Model Tests. Trans. AIME, v. 204, 1955, pp. 7-14.
7. Dyes, A. B., and Philip H. Braun. Sweepout Patterns in Depleted and in Stratified Reservoirs. Producers Monthly, v. 19, No. 2, December, 1954, pp. 24-30.
8. Higgins, R. V. Applications of Buckley-Leverett Techniques in Oil-Reservoir Analysis. BuMines Rept. of Inv. 5568, 1960, 21 pp.
9. Jordan, J. K. Reliable Interpretation of Waterflood Production Data. Trans. AIME, No. 2, Waterflooding reprint series, 1959, pp. 70-76.
10. Lytle, W. S. Crude Oil Reserves of Pennsylvania. Pennsylvania Topographic and Geol. Survey, Bull. M32, 1950, 256 pp.

11. Moore, T. F., and R. L. Slobod. The Effect of Viscosity and Capillarity on the Displacement of Oil by Water. Producers Monthly, v. 20, No. 10, August 1956, pp. 20-30.

12. Pirson, S. J. Production Decline Curve of Oil Well May be Extrapolated by Loss-Ratio. Oil and Gas J., v. 34, No. 26, Nov. 14, 1935, pp. 34-35.

13. Prats, M., C. S. Matthews, R. L. Jewett, and J. D. Baker. Prediction of Injection Rate and Production History for Multifluid Five-Spot Floods. Trans. AIME, v. 216, 1959, pp. 98-105.

14. Suder, Floyd E., and John C. Calhoun, Jr. Water-Flood Calculations. API Drilling and Production Practices, 1949, pp. 260-270.

15. Welge, H. J. A Simplified Method for Computing Oil Recoveries by Gas or Water Drive. Trans. AIME, v. 195, 1952, pp. 91-98.

TABLE 1. - Results of core and log analyses, Kane sand

	Well E-1		Well E-3		
	Core	Log	Core	Log	Average
Oil saturation.....pct pore vol	30.4	-	27.0	-	28.7
Water saturation.....pct pore vol	11.9	14.0	8.9	13.4	1/13.2
Porosity.....pct	10.8	10.3	12.1	11.0	1/10.8
Air permeability.....md	4.4	-	5.7	-	2/ 4.4
Effective sand thickness.....ft	10.6	-	-	-	10.6

1/ Based on the average of core and log analyses of well E-1 and log analysis of well E-3.
2/ Based on results of core analysis of well E-1.

TABLE 2. - Results of imbibition tests

Sample number	Oil imbibed		Water imbibed	
	Initial rate, pore vol/hr	Total fraction of pore vol	Initial rate, pore vol/hr	Total fraction of pore vol
1.....	0.59	0.30	0.34	0.07
2.....	.73	.48	.64	.15
3.....	.95	.66	.52	.25
4.....	1.39	.76	.20	.15
5.....	1.35	.54	.81	.37
Average	1.00	.55	.50	.20

TABLE 3. - Data required to perform waterflood calculations, Kane sand, Highland Township, Elk County, Pa.

Oil viscosity	3.05 cp
Water viscosity at reservoir conditions	1.0 cp
Relative permeability characteristics	figure 3
Interstitial water saturation	13.2 pct pore vol
Gas saturation before water injection	13 and 20 pct pore vol
Total area flooded	36.5 acres
Thickness	10.6 ft
Porosity	10.8 pct
Absolute permeability	3.2 md
Injection well to injection well distance	635 ft
Wellbore radius	approximately 10 ft
Pressure at the sandface	2,500 psig
Pore volume of confined area	324,000 bbl
Oil formation - volume factor	1.05
Assumed water-injection rate after January 31, 1966	11,600 bbl/month

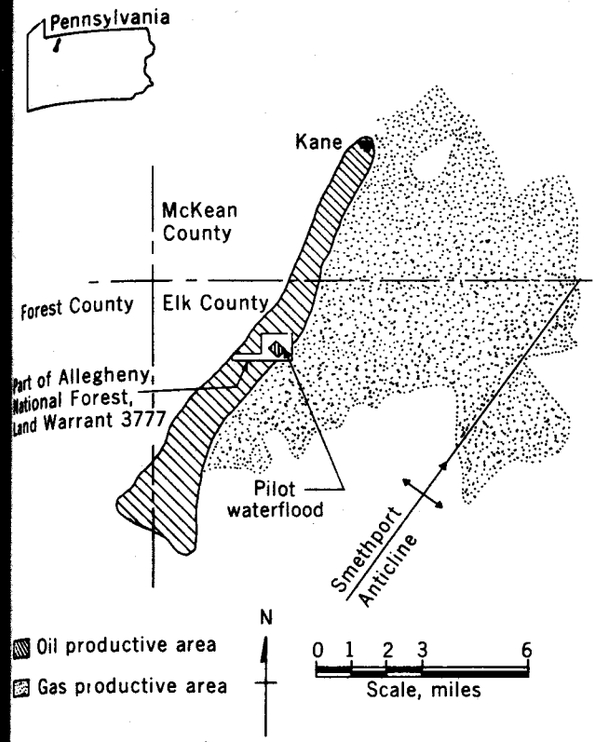

FIGURE 1. - Kane oilfield, Highland Township, Elk County, Pa.

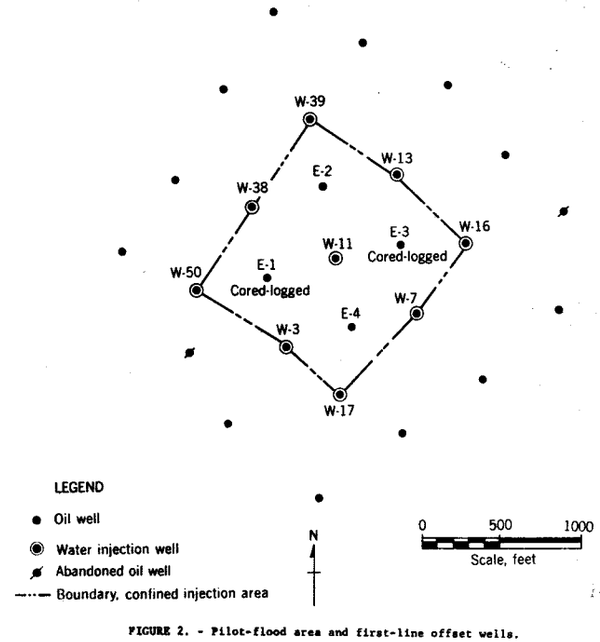

FIGURE 2. - Pilot-flood area and first-line offset wells.

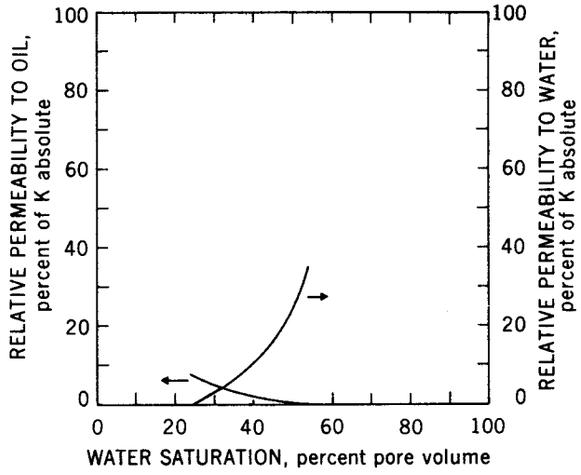

syn
3203

FIGURE 3. - Average water and oil relative-permeability curves for the Kane sand, well E-3.

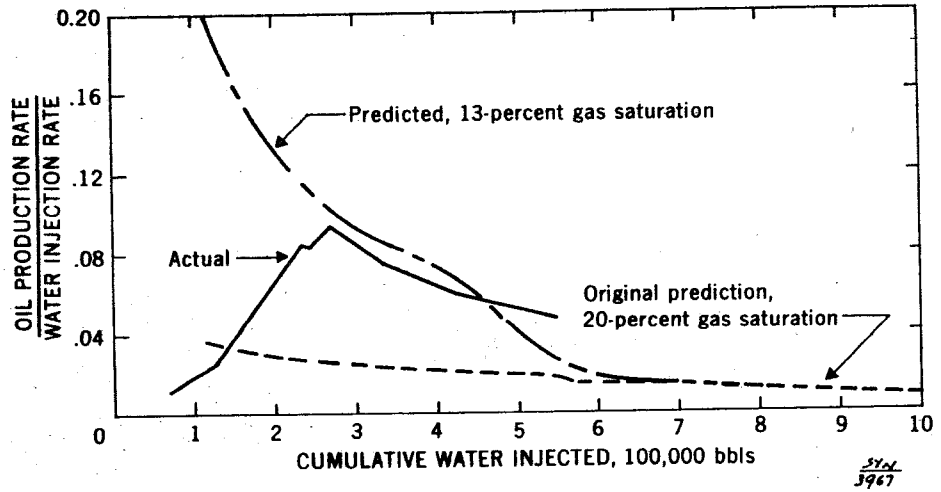

FIGURE 4. - Predicted and actual field performances, pilot waterflood, Kane oilfield, Elk County, Pa.

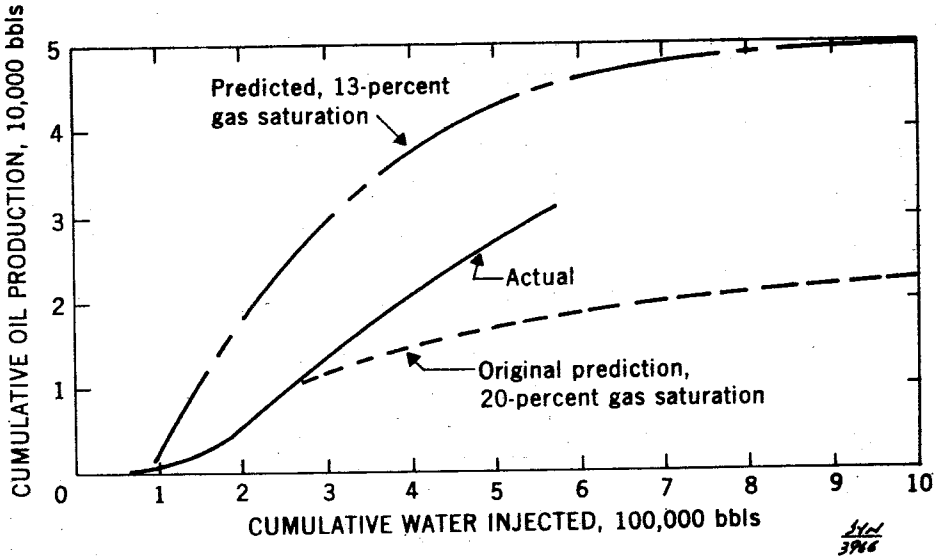

FIGURE 5. - Cumulative oil recovery using predicted and actual field results, pilot waterflood, Kane oilfield, Elk County, Pa.

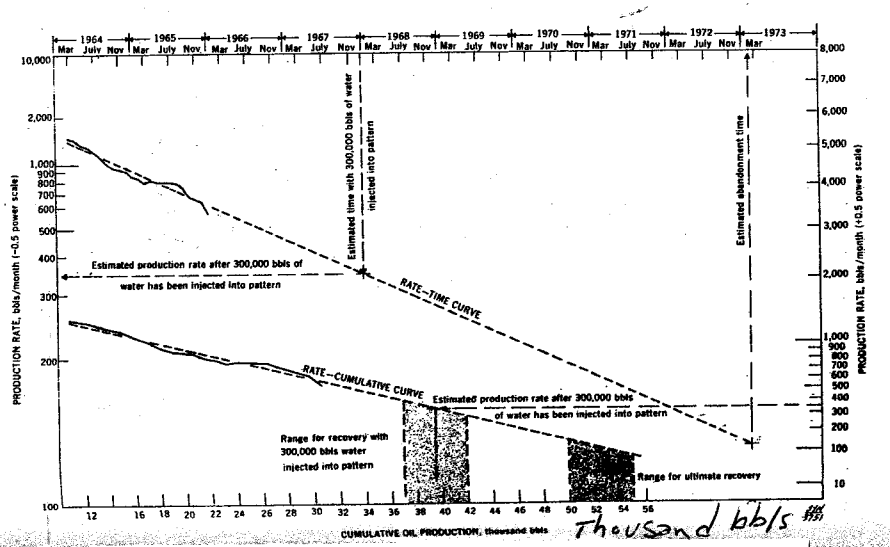

Figure 6. – Straight-line projection of hyperbolic decline (exponent b=0.5), pilot waterflood, Kane oilfield, Elk County, Pa.

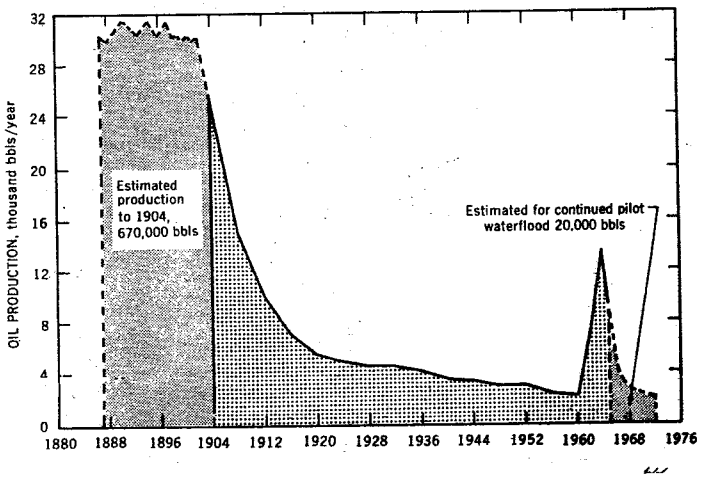

Figure 7. – Production history and prediction of future performance, pilot waterflood, Kane oilfield, Elk County, Pa.

MULTIPLE TRACERS AID EVALUATION OF A PILOT WATERFLOOD

by

Edward L. Burwell

Morgantown Petroleum Research Laboratory, Bureau of Mines
Morgantown, West Virginia

ABSTRACT

Many materials have been used to trace fluid flow in porous media. This report describes the use of five different tracers to help define the orientation and flow capacity of a fracture system believed to be present in a reservoir during a pilot waterflood project on the Fords Brook Drilling Company lease, in the Kane oilfield, Elk County, Pa. The presence and nature of the fractures were established, the preferential flow direction was indicated, and the approximate volume of injected water being produced through the fracture system was measured.

INTRODUCTION

The search for a suitable material to trace fluid flow in porous media has included such diverse substances as sugar, boron, ammonia, fluorescein, iodine, and probably many others (2, 3, 5, 6, 7, 9). This report concerns the use of five tracers in a pilot waterflood on the Fords Brook Drilling Company lease, in the Kane oilfield, Elk County, Pa. Three series of tests, each lasting 1 to 2 months, were conducted during a 2-year period to help

define the presence, orientation, and flow capacity of a fracture system believed to be present in the reservoir. To avoid confusion, each series will be discussed separately.

The injection pattern (fig. 1) consisted of four normal five-spots with nine injection and four producing wells. All injection lines were connected to a common header on which the pressure was maintained at approximately 1,600 psig. Water injection began in January 1963, and by June 1963 the injection rate had stabilized at 330 barrels per day at a wellhead pressure between 1,650 and 1,700 psig. During June 1963, cumulative water production increased from 37 to 1,330 barrels. The first series of tracer tests was performed to help explain the source of this water production.

First Series of Tracer Tests

A series of seven tracer injections into all wells, except for W-39 and W-16 (fig. 1), of about 75 grams of fluorescein each was begun in August 1963. During this series, the wellhead pressure was between 1,490 and 1,630 psig. The injections were scheduled to prevent interference between tests. Previous calculations, based on core data for wells in the pattern, indicate that injected tracer should travel through the formation to a producing well in not less than 40 days. This is an absolute minimum figure derived by assuming that all injected water travels through the most permeable 1 foot of formation. The injected dye was produced within 1 to 3 days from three of the four offset producing wells (fig. 2). This proved the existence of a fracture system, but subsequent oil production demonstrated that the fracture system was not extensive enough to prevent economic operation of the waterflood (4).

Second Series of Tracer Tests

As has been previously presented (8), during 1963 and 1964 this pilot waterflood was the subject of a thorough reservoir engineering study (1, 4) and a second series of tracer tests was planned to help explain an apparent lack of correlation between the predicted and actual performance of the waterflood.

The second series was designed to determine the amount of injected water that was bypassing the sand body through fractures. Prior to actual testing, the nine injection wells were equipped with recording flow meters so that accurate records of volumes injected into each well could be obtained. The following five tracers were used: Boron as boric acid, Rhodamine B and fluorescein as fluorescent dyes, gold-198 as gold chloride, and hydrogen-3 as tritiated water (table 1). The conditions for the six tests in this series are shown in table 2.

Analysis for the Rhodamine B was performed both visually with a ratio fluorometer having a sensitivity to this dye of about 10 parts per billion. As this dye is adsorbed to some degree on sandstone, an open fracture would be necessary for the dye to be produced; and as no Rhodamine B was produced, it was concluded that such a fracture was not present.

The boron analysis was sensitive to boron concentrations of about 2 parts per million which we later found to be the background boron concentration in the brine in this area. The injected boron was not detected at any time although samples were collected for 8 to 10 weeks at regular intervals.

On January 14, 5 curies of tritium as tritiated water were injected. Produced water samples were collected and analyzed using a liquid scintillation counter. Tracer was found to be present in one well (E-3) in less

than 4 hours and was present in all four producing wells within 48 hours. The percentage of tagged injection water produced daily from the four producing wells during the 28 days following injection is shown in figure 3. About 5 percent of the amount injected during the 15.5-hour injection period was produced from the four wells within the project boundary during this 28-day interval.

In an attempt to correlate this test series with the 1963 work, a slug of 200 grams of Rhodamine B was injected into well W-11 (fig. 4) on January 27, 1965, followed on January 28 by 320 millicuries of gold-198 slug-injected into the same well. Neither of these was produced nor was fluorescein which was slug-injected into well W-11 on February 2. The gold-198 was not produced because it tended to plate out of solution on metal surfaces with which it came into contact. However, the failure of the fluorescein to be produced definitely established that there had been a change in the performance and response of the reservoir to injection.

Third Series of Tracer Tests

The third series of tracer tests in the summer of 1965 was accompanied by injection pressure increases and designed to investigate the (1) variation in performance data between the 1963 and 1965 tests, (2) flow pattern of injected fluids, and (3) effect of injection-pressure fluctuation on the fractures in the reservoir.

Before the tests were started, the reservoir was conditioned by maintaining a constant pressure on the common header serving the nine injection wells and establishing a stable injection rate. Accurate pressure and injection volume data were recorded for the entire series. As soon as reasonably stable conditions were reached, a dye tracer was slug-injected and

the pressure was increased 60 to 90 psig. The individual injections and conditions are shown in figure 5. Using this test procedure, tracer injection into three of the injection wells was followed within 1 to 3 days by tracer production in a well in an easterly direction from the injection well. At no time was there indication of tracer flow in any direction other than east. This easterly flow may reflect the existence of pressure gradients effected by earlier, relatively rapid depletion of the gas cap to the east.

Water-injection rates and pressures were recorded continuously during the entire third series. The pressure-volume relationship for three of these wells (fig. 6) shows an almost linear increase of intake rate with injection-pressure increases, but the other wells (fig. 7) show a sharp, nonlinear increase in intake rates between 1,630 and 1,640 psig wellhead pressure. Evaluation of these data explains the pilot waterflood performance and the performance of each series of tracer tests; namely, that there is an east-west oriented fracture system of low-flow capacity present in the reservoir which can be opened and closed when differential pressure is varied in the reservoir.

When the first tests were performed in 1963, water injection into the pattern had been underway for only a few months and there undoubtedly existed a high differential pressure in the reservoir close to the injection wellbore. Injection pressures during the 1963 dye tests were 1,490 to 1,630 psig. The fracture system--later proved to be present in the reservoir--should have opened under these conditions, and this explains the short time required to produce the dye injected during the 1963 tests. At that time, the dye was injected in small amounts (approximately 75 grams) and was produced in high concentrations. At the time of the second series, early in 1965, the

waterflood had been in progress for over 2 years and condition of equilibrium had been more nearly established in the reservoir. If no appreciable differential pressure existed in the reservoir immediately surrounding the wellbore, the fractures may have partially closed. However, they must have remained open wide enough to permit the short travel time of the tritium tracer which would not be adsorbed or absorbed in any appreciable amount. An adsorbable dye would have been removed from the water because the fractures were nearly closed, thus causing more intimate contact with the sand body.

The third series of dye tests was designed to detect such a fracture system and determine its response. Dye injections were accompanied by injection pressure increases. Under these conditions, dye was produced in such a short time that it could not have traveled through a sand body but rather through a fracture. The easterly flow of tracer observed from these tests indicates that the fractures are oriented in an east-west direction and confirms the results of the earlier (1963) injection tests.

CONCLUSIONS

The 2-year multiple-tracer study demonstrated the problems involved in finding a suitable material for use in tracing waterflow. The selection of the tracer must be governed by the information desired. Tracer production through a sand body over a long distance (300 to 1,000 feet) requires a chemical not easily adsorbed and which can be detected in extremely minute quantities. For these purposes, tritium is excellent and may be the only practical tracer. If a fracture system is present, information may be obtained as conveniently and more economically by use of a suitable dye.

All test data should be correlated with any other available information such as intake volume, pressure fluctuations, production volumes, and changes in chemical content of brine produced. During this particular tracer study, the following information was indicated or proven:

1. Production of large volumes (in the range of thousands of barrels per month) of water during the early stages of a waterflood should not be taken, by itself, as an indication that the flood will be unsuccessful.

2. A fracture system with an east-west orientation is present in the reservoir described in this report.

3. The fracture system in this reservoir may be opened or closed by control of the injection pressure.

4. Approximately 5 percent of the injected water produced from the four wells in the pattern is bypassing the sand body through a fracture system when a condition of equilibrium exists in the reservoir.

ACKNOWLEDGMENTS

The technical guidance of Dr. E. T. Heck, Minard Run Oil Company; the assistance of Mr. John Burkhart of the Kendall Oil Refining Company; and the cooperation and assistance of Mr. Evan E. Christy and lease personnel of the Fords Brook Drilling Company, who conducted the first series of tests and assisted with the second and third series, is gratefully acknowledged.

REFERENCES

1. Boley, Dean W., Harry R. Johnson, and John R. Duda. Predicted Oil Recovery from a Pilot Waterflood in the Kane Oilfield, Elk County, Pa. Producers Monthly, v. 28, No. 8, August 1964, pp. 10-16.
2. Carter, Ralf C., W. J. Kaufman, G. T. Orlob, and David K. Todd. Helium as a Ground-Water Tracer. J. Geophysical Res., v. 64, No. 12, pp. 2433-2439.
3. Champion, C. A., H. E. Schaller, and B. R. Jackson. Some Recent Applications of Radioactive Tracers in Determining Subsurface Flow Behavior. Soc. Petrol. Eng., AIME, Dallas, Tex., Paper No. SPE-1246; presented at 40th ann. fall meeting, SPE, Denver, Colo., Oct. 3-6, 1965, 12 pp.
4. Duda, J. R., L. A. Schrider, and H. R. Johnson. Field Performance of a Pilot Waterflood, Kane Oilfield, Elk County, Pa.--A Progress Report. Producers Monthly, v. 29, No. 12, December 1965, pp. 8-10.
5. Edwards, J. M., and E. L. Holter. Applications of a Subsurface Solid-State Isotope Injector to Nuclear-Tracer Survey Methods. J. Petrol. Technol., v. 19, No. 2, February 1962, pp. 121-124.
6. Heck, E. T. Tracing Fluids Between Wells. Producers Monthly, v. 18, No. 9, July 1954, pp. 31-33.
7. Jenkins, R. E., and E. H. Koepf. New Tools and Methods Improve Fluid Tracing. Oil and Gas J., v. 61, No. 13, Apr. 1, 1963, pp. 102-104.

8. Schrider, Leo A., John R. Duda, and Harry R. Johnson. Theoretical and Field Waterflood Performance, Kane Oilfield, Elk County, Pa. (Presented at 25th Tech. Conf., The Pennsylvania State Univ., University Park, Pa., Oct. 19-21, 1966.)
9. Welge, H. J. Super Sleuths Trace Flow of Injected Gas. Oil and Gas J. v. 54, No. 17, August 29, 1955, pp. 77-79.

Boron as Boric Acid

Rhodamine B as a Fluorescent Dye

Fluorescein as a Fluorescent Dye

Gold-198 as Gold Chloride

Hydrogen-3 as Tritiated Water

TABLE 1 - Tracers Used for Pilot Waterflood Flow Studies.

Date	Injection well	Tracer	Method of injection	Results
1-13-65	All wells	Rhodamine B	Continuous for 8 hours at 19.2 ppm	No show
1-13-65	All wells	Boron	Continuous for 5 hours at 99 ppm	No show
1-14-65	All wells	Tritium	Continuous for 15.5 hours at 0.150 μc/ml	E-1,2,3,4
1-27-65	W-11	Rhodamine B	Slug-200 grams	No show
1-28-65	W-11	Gold-198	Slug-320 millicuries	No show
2-2-65	W-11	Fluorescein	Slug-55 grams	No show

TABLE 2. - Second Series of Tracer Tests.

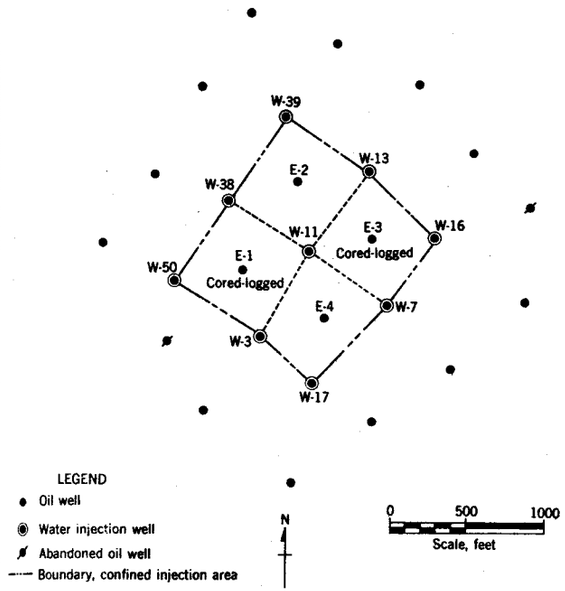

FIGURE 1. - Five-spot pattern of pilot waterflood.

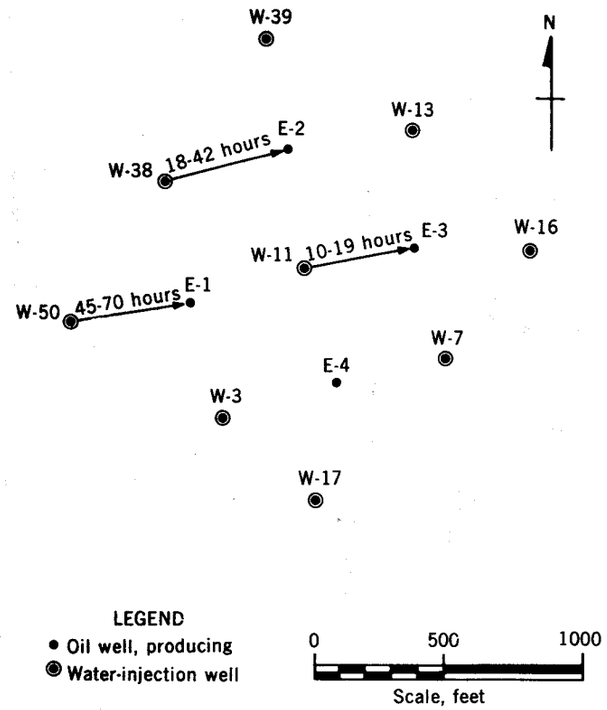

FIGURE 2. - First Series of Tracer Tests.

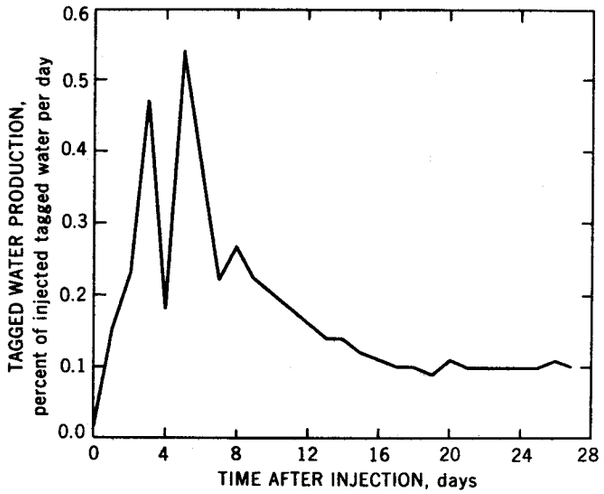

FIGURE 3. - Tagged water production rate from wells E-1, 2, 3, and 4 1965 tracer test.

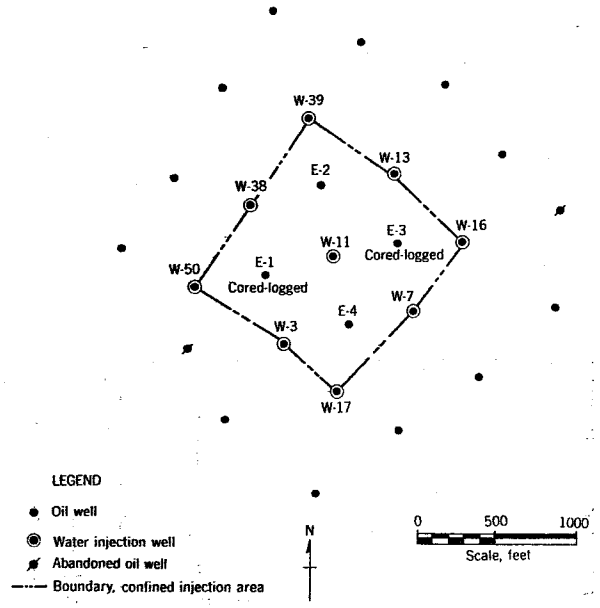

FIGURE 4. - Well pattern of pilot waterflood.

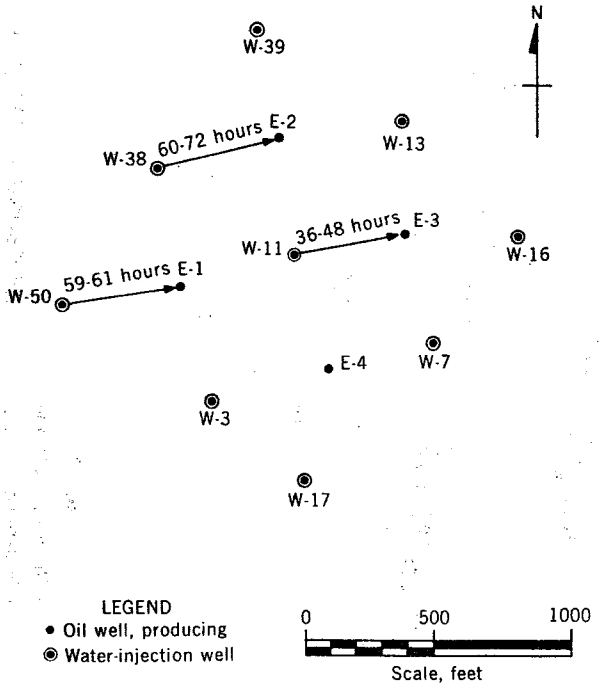

FIGURE 5. - Fluorescein Injections During Third Series.

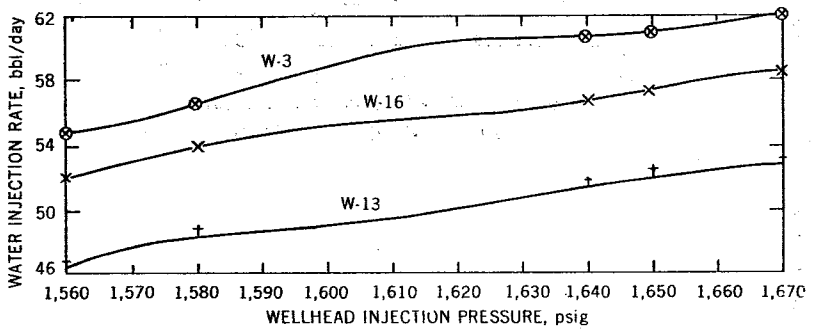

FIGURE 6. - Pressure-volume relationship for wells W-3, 13, and 16.

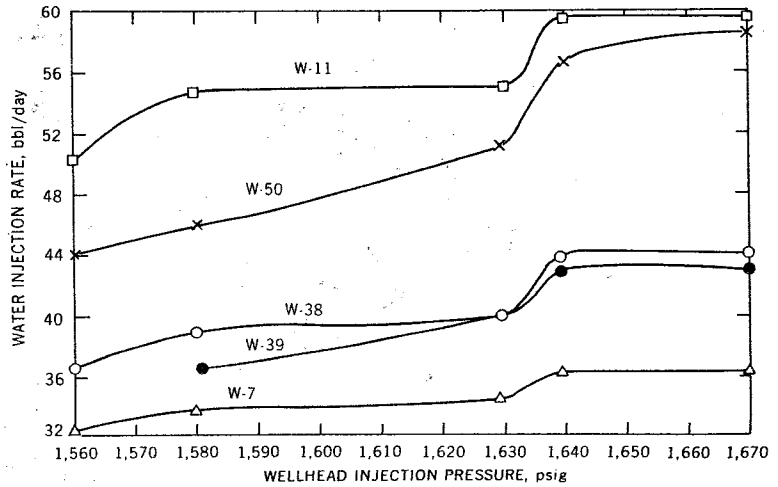

Figure 7. – Pressure-volume relationship for wells W-7, 11, 38, 39, and 50.

EFFECT OF ADDITIVES ON PHASE DIAGRAMS: NORMAL BUTANE ADDED TO CONDENSATE-NATURAL GAS SYSTEM

By

Byron A. Baker and C. Kenneth Eilerts*

ABSTRACT

The effect on phase-boundary pressures of a related series of condensate mixtures of additions of normal butane was determined with a windowed P-V-T cell. The investigation was conducted at pressures up to 5,000 psia and at temperatures in the range 70° to 310° F. Relationship of the critical state to changing compositions was evaluated. The fluids were a mixture of intermediate hydrocarbons and selected distillation cuts from a field condensate combined with mole fractions of natural gas in the range 0.800 to 0.933.

The data were subjected to statistical analysis using a computing program that provided a polynomial for interpreting the results. The polynomial yields phase-boundary pressures, and independent variables are temperature, natural gas content, and mole fractions of normal butane additive. A method is described for approximating such a polynomial before measurements are complete using a mathematical model that requires more measurements than are available.

---

*Bartlesville Petroleum Research Laboratory, Bureau of Mines, Bartlesville, Oklahoma

INTRODUCTION

Processes used in recent years to increase the recovery of oil from reservoirs have involved injection into the reservoir such additives as enriched natural gas and mixtures of hydrocarbon components including ethane, propane, butane, and pentane. These additives combine with reservoir hydrocarbons to form a miscible front (3, 5, 7)[1/] which can be forced through the reservoir with a lean gas or perhaps water. Ideally this front is a single, gas-like phase that does not bypass oil in place but in the course of the process converts it to a gas also. Thus retention of oil in the reservoir as "irreducible" liquid saturation during the recovery process is minimized. This paper is concerning the quantity of an additive needed to lower phase-boundary pressure of a reservoir material a required amount to comprise the front.

The authors have reported (2) results of a computing investigation using published correlations of phase relationships to determine relative effectiveness of various materials as additives. This report is of a laboratory investigation made to determine the effect of one such additive, normal butane, upon the phase-boundary pressures of a related series of prepared condensate mixtures with liquid gravities in the range 41° to

1/ Underscored numbers in parentheses refer to items in references at the end of this report. Page and section citations are included in some instances.

65° API. Dew-point, bubble-point, and critical pressures were measured in the temperature range 70° to 280° F. Normal butane was added to the condensate fluid in amounts up to 0.2 mole per mole of fluid. A digital computing program was used to analyze the data by statistical methods, and measured pressures of the phase boundary were represented by a polynomial with temperature, natural gas content, and additive concentrations the independent variables.

EXPERIMENTAL INVESTIGATIONS

Apparatus

The phase-boundary pressures of condensate mixtures studied were measured using a windowed cell (4, sections A7e through A7k). The volume of this cell is varied by use of mercury, and phase equilibrium is achieved by rocking the cell.

Phase volumes are determined to the nearest 0.5 ml by measuring the angle the axis of the cell makes with the horizontal when the mercury-liquid or the liquid-gas meniscus is opposite the center of the window. This angle is related by calibration to the volume of the phase or phases being viewed. Pressures of phase equilibrium achieved in the windowed cell were measured with a piston gage. It is estimated that the overall accuracy of these measurements was $\pm$ 25 psi, including the uncertainty of attaining equilibrium and control of temperature.

The windowed cell was operated in a bath of 50-weight motor oil. Temperatures in the range 40° to 310° F were obtained by using electrical

heaters and a portable cooling coil for 70° F and lower temperatures. A selected temperature was maintained constant to ± 0.2° F.

Gas for a sample was measured in the windowed cell. The quantity of liquid required for mixing with the gas was measured into the cell under pressure from a cylinder fitted with a movable piston which will hereinafter be referred to as the piston displacement meter. The piston has attached to it an external stem calibrated in milliliters to indicate volume displaced by the piston.

Fluid Constituents

The fluids investigated were mixtures of 3 constituents, a natural gas, a mixture of 6 hydrocarbons, and distillation cuts of a gulf coast condensate. The respective terms used for these constituents in this paper are "Natural Gas", "Intermediates", and "Distillation Cuts 3 through 10".

Composition of the natural gas used is shown in column 2 of table 1. Values of the compressibility factor needed to measure the natural gas were available from an unrelated investigation in progress (1).

The Intermediates mixture was prepared by combining weighed quantities of technical grade hydrocarbons. The lightest of these components including normal butane was cooled to 25° F to reduce evaporation during the weighing and mixing operation. Composition of the Intermediates mixture is given in column 3 of table 1. The isomer

2, 2 dimethylbutane represented the group of components designated 135-56 C_6, normal hexane represented 56-35 C_6, 2, 4 dimethylpentane represented 35-17 C_7, and normal heptane represented 17-11 C_7.

The fluid constituent designated Distillation Cuts 3 through 10 was prepared using fractions obtained by distillation of a gulf coast condensate in a 4-foot, screen-packed, Stedman column. Amounts of distillation fraction thus obtained are listed in column 3 of table 2. Only that distillate recovered in the boiling range 167° to 347° F comprised the constituent. Higher boiling cuts were not used because they could contain high-molecular weight waxes or asphaltic material which could coat the high-pressure glass windows of the P-V-T cell and make volume measurements difficult or impossible. Cuts 1 and 2 were not used because they were volatile, and hydrocarbons in them could be provided for the fluid under better control as Intermediates. The specific gravity of each fraction was used to determine relative weights of the fractions and weight percents distilled. Mole fraction composition of the fractions, as given in column 4 of table 1, was computed from the weight percent distilled using a method that has been described (4, Sec. A9f). The component designation nC_8, for example, represents all hydrocarbons in the boiling-point range of the isomers of octane.

Based on a consideration of separator gas and liquid compositions of

7 field condensates the composition of an average gas-condensate fluid was defined as shown in the following table for the purpose of this investigation.

Average gas-condensate fluid

Constituent	Mole fraction
Natural Gas	0.98007
Intermediates	.00751
Distillation Cuts 3 through 10	.01242
Total	1.00000

Based on this information the ratio of Distillation Cuts to Intermediates for an average condensate was calculated as follows on a mole fraction basis

$$\frac{\text{Distillation Cuts}}{\text{Intermediates}} = \frac{0.01242}{0.00751} = 1.654 .$$

This ratio was used throughout the study. In effect the number of constituents became 2; Natural Gas in a range of concentrations and a mixture of Distillation Cuts 3 through 10 and Intermediates in a constant ratio. Density of Distillation Cuts was 0.761 gm/cc at 75° F. Density of Intermediates was 0.637 gm/cc at 75° F.

Preparation of Test Fluids

The first step in preparation of one of the original fluids was to

charge the windowed cell at a selected volume with the natural gas. With temperature maintained constant, pressure of the gas in the cell was measured. The molal quantity of gas contained in the cell was calculated (4, equation 2.11) using the gas equation N = PV/ZRT. Because compressibility factors for this natural gas had been measured at 100° F, this temperature was cell temperature for the mixing operation.

Volume of the mixture of Distillation Cuts and Intermediates required for injection into the cell to mix with the contained gas was calculated from density of the liquid and the mole fraction of gas required in the test fluid. Table 3 contains compositions of 5 original condensate mixtures prepared in this manner. These are fluids GI800, GI840, GI876, GI910, and GI933 containing 0.800, 0.840, 0.876, 0.910, and 0.933 mole fraction natural gas, respectively.

Fluids with Additive

After phase-boundary pressures of a fluid had been determined for the range of temperatures of the investigation, normal butane was added to it in the amount of 0.1 moles per mole of the fluid. The addition was accomplished by means of the piston displacement meter. Volume of the butane was measured to 0.001 ml at room temperature and cell pressure. The volume of normal butane to be injected was calculated from its density under the conditions of transfer. Table 4 shows compositions of the 5 original fluids modified by the first addition of normal butane. In

the text, tables, and figures that follow these fluids are identified by constituents of the original fluid and the molal proportion of added butane. For example, the identification GI840 + 0.1 nC_4 implies that an amount of the original fluid which would contain 0.840 moles of natural gas had added to it 0.1 moles of normal butane.

After phase-boundary pressures were measured on a modified fluid containing the first addition of normal butane, a second addition was made in the proportion of 0.1 moles of butane to 1.1 mole of the modified fluid. A resulting fluid is identified by the total content of additive, for example, GI840 + 0.2 nC_4. Compositions of all such fluids are given in table 5.

Measurement of Phase-Boundary Pressures and Temperatures

Phase equilibrium was attained in the windowed cell by rocking it at constant temperature and pressure perhaps for as much as 30 minutes. Equilibrium was indicated to have been attained when successively measured volumes of the sample differed by no more than 0.5 ml and there was not a monotonic drift in this property. Examples of typical dew-point and bubble-point pressure determinations are shown in figure 1. Attainment of equilibrium at the bubblepoint took less time than attainment of equilibrium at the dewpoint. Normal procedure is to attain equilibrium at the highest pressures first. Pressures for the attainment of equilibrium usually were selected in increments of about 200 psi.

As shown in figure 1 two separate straight lines of pressures were obtained for each phase-boundary pressure determination. The upper line in each instance represents pressures of the single phase. The lower line represents pressures of the two-phase region which is predominately liquid for bubble-point determinations and predominately gas for dew-point determinations. Intersection of the two lines is the phase-boundary pressure sought.

The critical pressure is a phase-boundary pressure but is unique because phases at temperatures and pressures closely approximating those of the critical state are identical in properties. On the phase-boundary curve the critical temperature represents the division between dew-point and bubble-point states.

Determination of the critical state requires measurement of the relative liquid volume L/F. This relative volume is a ratio of liquid-phase volume to total-fluid volume and is determined with the aid of observations made through windows of the cell. The interpretation of relative volume data to determine unique states on the phase-boundary curve has been described (4, Sec. 2.4e).

EXPERIMENTAL RESULTS

Only original fluid GI840 had a critical temperature within the temperature range of the investigation. The configuration of relative liquid volumes, measured to determine the critical state, and pressures

and temperatures of those volumes is shown in figure 2. As indicated, bubblepoints and related states were measured at temperatures as high as 170° F, and dewpoints and related states were measured at temperatures as low as 175° F to bracket the critical temperature 172.5° F.

Figures 3 and 4, respectively, indicate the change in critical state properties of fluid GI840 that occurred when normal butane was added to it in the proportions 0.1 and 0.2 moles of butane per mole of original fluid. The critical temperature of normal butane is 306.0° F, and added butane had the effect of increasing critical temperature of the original fluid to 207.5° and 232.5° F, respectively.

Figure 5 shows the phase-boundary pressures of fluid GI840 including the critical pressure. As it happens the critical pressure is an approximation of the cricondenbar pressure or maximum pressure for coexistence of gas and liquid phases of the fluid. The curves for fluid GI840 modified by added butane show that temperature of the cricondenbar state was increased more by the addition of butane than the critical temperature was increased by the same addition.

Phase-boundary pressures (dew-point and bubble-point pressures) for the 5 original fluids and their respective mixtures formed by the addition of normal butane are given in figures 6, 7, 8, 9, and 10. Smooth curves fitted to the data points were obtained by statistical means and computing that will be described. Because of the computing it was

possible to estimate curves of phase-boundary pressure for temperatures and compositions not actually explored experimentally. In figure 6, for example, pressures were measured only for the original fluid.

These figures show that the overall effect of adding normal butane to a related series of condensate mixtures is to lower the phase-boundary pressure in every instance. The maximum pressure lowering for given amounts of additive occurs at the lowest temperatures and for those fluids for which the concentration of natural gas is the highest. For example, at a natural gas concentration corresponding to 0.933 mole fraction and at 70° F the phase-boundary pressure is lowered about 1,100 psi by the addition of 0.1 moles of normal butane per mole of fluid. At the same concentration of natural gas (0.933 mole fraction) but at 310° F, the phase-boundary pressure is lowered only about 600 psi by the addition of 0.1 moles of normal butane per mole of fluid. Now at a natural gas mole fraction of 0.800 and at a temperature of 310° F, 0.1 moles of additive per mole of fluid lowered the phase-boundary pressure only about 350 psi. However, if the temperature is 70° F with the natural gas mole fraction 0.800, 0.1 moles of butane added to 1.0 mole of fluid will lower the phase-boundary pressure 900 psi.

Critical pressure as measured for fluid GI840 was lowered 765 psi by the addition of 0.1 mole fraction of normal butane per mole of

condensate. When the second 0.1 mole of normal butane per mole of fluid GI840 was added the critical pressure as measured on fluid GI840 + 0.1 nC_4 was lowered 480 psi. The overall effect of normal butane on the critical pressure was to lower it but at a diminishing rate.

STATISTICAL ANALYSIS

A mathematical model was devised to represent the experimental data. This model is a polynomial with powdered transforms as arguments Y (X_1, X_2, X_3). Here Y is phase-boundary pressure, and X_1, X_2, and X_3 are, respectively, transforms representing natural gas content of the fluids, temperature, and concentration of the additive used to modify the fluids. In the beginning the X matrix to represent arguments and response values was 15 x 75 in size, but this size was reduced as terms originally conceived were found to lack significance.

Inversion of the X matrix was accomplished using standard techniques. Methods described by Mendenhall (6) were followed in solving for and testing coefficients β to represent the test results. The computing program was applied to the problem before it was experimentally complete, and less than 75 measured values of Y were available. For the first analysis estimates of Y were used where measured values of Y were not available. After the coefficients β had been obtained values for all responses were computed using the matric multiplication $Y_{c,i} = X\beta_i$. The estimates of

Y then were replaced with computed values $Y_{c,i}$ and coefficients β_{i+1} were computed. This step followed by the computation $Y_{c,i+1} = X\beta_{i+1}$ constituted an iteration. Each time the iteration was repeated $Y_{c,i+1}$ used in the place of a Y that had not been measured contributed less and less to the values of resulting coefficients, because

$$\lim_{i \longrightarrow \infty} \Sigma(Y_{c,i+1} - Y_{c,i})^2 = 0 \quad ,$$

and, as shown in Appendix A, at the limit only measured values of Y determined the values of computed coefficients.

The transforms X_1, X_2, and X_3 devised to represent variables for the model were as follows:

Variable	Transform	Range
Natural Gas concentration	$X_1 = \frac{NG - 0.88}{0.1}$	$0.80 \leq NG \leq 0.933$
Temperature, t °F	$X_2 = \frac{t, ^\circ F - 190^\circ}{120^\circ}$	$70^\circ \leq t, ^\circ F \leq 310^\circ$
Moles nC_4 added per mole fluid, m	$X_3 = \frac{m - 0.1}{0.1}$	$0.0 \leq m \leq 0.2$
Pressure, psia	Y	

Before selecting a mathematical model to represent the phase-boundary pressures as determined from laboratory measurements, these pressures were plotted against natural gas concentration on glass plates to provide relationships similar to those illustrated in figure 11.

These glass plates were mounted vertically in special metal holders and arranged in the order of descending temperature. Three distinct surfaces were thus defined by the three-dimensional array of plotted data. Each of these surfaces of pressure was convex within the experimental range of the independent variables.

Because data were available for 5 gas concentrations, the original mathematical model was made fourth degree in X_1. Because data were available for 5 temperatures, the original model was made fourth degree in X_2, but term by term the higher powers were found unnecessary until only powers up to and including the second remained. Data for 3 concentrations of the additive were available, so X_3 was represented to the second degree. The final model had the form,

$$Y = \beta_0 X_0 + \beta_1 X_1 + \beta_2 X_1^2 + \beta_3 X_1^3 + \beta_4 X_2 + \beta_5 X_2^2 + \beta_6 X_3 + \beta_7 X_3^2 + \beta_8 X_1 X_2 + \beta_9 X_1 X_3 + \beta_{10} X_2 X_3 \ .$$

Elimination of terms to arrive at the above equation was not conducted solely on the basis of computed relative size of the Student's t for each coefficient and the Student's t according to the 95-percent confidence interval elected and the degrees of freedom available. When representation of the transform X_2 seemed excessive, as indicated by low values of Student's t for certain of its terms, the term with the highest power was eliminated first. All lower powers of X_2 were retained, if values of Student's t for these terms found in a subsequent computation of

coefficients were acceptable.

Coefficients of the final model and data pertaining to them are given in table 6. The column of Student's t indicates that all coefficients except the one for X_1^3 met the requirements for the confidence interval. Because this term does contribute in a substantial way to the value of Y, and because the X_1^3 argument may be more significant in other systems that may be studied than in this one, the term was retained for the purpose of later comparisons.

The curves in figures 6, 7, 8, 9, 10, 11, and 12 represent values of Y computed with coefficients of table 6. Surfaces for each of the 3 concentrations are convex within the range shown for the independent variables.

Table 7 shows significant items of output from the last 3 iterations of the model of table 6. The sum of squares of errors contributed by those pressures Y_e that were not measured is subtracted from the sum of squares of errors SSE for all pressures and divided by degrees of freedom for the measured pressures to provide the variance s^2. The standard deviation s is 69.2 psi. If additional iterations were performed, SSE and s both would be lowered but by decrements which are diminishing in size.

Square-Root Model

The mathematical model in table 6 provides single values of the pressure for all values of the arguments. Because the phase diagram of gas-condensate fluids is such that phase-boundary pressure can have two values at high gas concentrations and also at relatively high temperatures, a model that would provide more than one pressure might afford an especially good fit for pressures representing the convex surface. The following set of transforms was designed and used in a model to provide more than one pressure for given argument values.

Variable	Transform	Range
Natural Gas concentration	$X_1 = \frac{\sqrt{NG} - \sqrt{0.880}}{\sqrt{0.880} - \sqrt{0.800}}$	$0.800 \leq NG \leq .933$
Temperature, T °F abs.	$X_2 = \frac{\sqrt{T} - \sqrt{649.7}}{\sqrt{649.7} - \sqrt{529.7}}$	$529.7 \leq T \leq 769.7$
Moles nC_4 added per mole fluid, m	$X_3 = \frac{m - 0.1}{0.1}$	$0.0 \leq m \leq 0.2$
Pressure	Y	

Only positive roots were used in interpreting these transforms to fill the X matrix in preparation for a computation of coefficients.

The device of using estimated pressures in the Y matrix where measured pressures were not available was used with this model also. Results of the second iteration to find coefficients are given in table 8. The sum of squares of errors SSE did not indicate that this model would have any marked advantage over the one represented in table 6. Some

other model which would provide representation of more than one pressure for given values of arguments might afford an advantage, but the one of table 8 apparently did not. Because this model to provide more than one pressure for given arguments seemed to provide no better fit than the one defined in table 8, when all argument roots were interpreted as being positive, it was abandoned. Interpretations with various possible combinations of negative roots did not yield a helpful result.

Utilization of Statistical Results

Phase-boundary pressures computed by means of coefficients in table 6 are plotted in figure 11. The three curves in any one of the 5 sections of this figure represent phase-boundary pressures for the original fluids and for the two modified fluids obtained by butane additions. Temperatures identifying sections of the figure are parameters, so that each section shows the effect of gas concentration on phase-boundary pressure at selected temperatures.

Comparison of curves in the sections will reveal that lowering the phase-boundary pressure by additions of normal butane is the most effective when temperature is low and concentration of natural gas is high.

Phase-boundary pressures of figure 11 are shown in figure 12 as contours with mole percent natural gas and temperature as variables. Three plots representing the original fluids and the two modified fluids

obtained by additions of normal butane represent three convex surfaces. Configurations of the contour curves at 250-psi intervals show how cricondenbar temperatures are changed by the additive. Both cricondenbar and critical state temperatures are increased when the concentration of butane is increased. Pressures of these states are lowered.

CONCLUSIONS

1. Phase-boundary pressures of gas-condensate fluids with liquid gravities in the range 41° to 65° API are lowered when normal butane in concentrations up to 0.2 moles per mole of the original fluid is added to them. The maximum reduction in pressure for a given amount of additive occurs at relatively low temperatures for fluids containing relatively high concentrations of natural gas. At the most favorable conditions studied, 70° F and a natural gas concentration amounting to 0.933 mole fraction, butane added in the proportion 0.1 moles per mole of original fluid lowered phase-boundary pressure 1,100 psi.

2. Addition of normal butane to a gas-condensate fluid that contained 0.840 mole fraction of natural gas lowered the critical pressure, increased the critical temperature, and increased the cricondenbar temperature. However, this finding is not a basis for a generalization pertaining to all gas-condensate fluids in either a qualitative or a quantitative sense.

3. A mathematical model taking account of the independent variables natural gas concentration, temperature, and proportions of butane additive

can be devised to represent measured phase-boundary pressures of gas-condensate fluids with a standard deviation of the magnitude 70 psi. For applications to gas-condensate fluids, in general, such a model is expected to be more accurate for estimating the effect of changes in the independent variables than for providing absolute phase-boundary pressures.

ACKNOWLEDGMENT

Eudora Sumner gave assistance in the preparation of tables and figures for this report.

REFERENCES

1. Archer, F. G., and Eilerts, C. Kenneth. Piston-Fitted Cell for Measuring Compressibility Factor of Two-Phase Fluids. Research in progress, Bartlesville Petroleum Research Center, BuMines, Bartlesville, Okla.

2. Burman, L. M., Baker, Byron A., and Eilerts, C. Kenneth. Effect on Cricondenbar and Other Phase-Boundary Pressures of Adding Light Hydrocarbons, Nitrogen, and Carbon Dioxide to Oils and Gas-Condensate Fluids. BuMines Rept. of Inv. 5920, 1962, 41 pp.

3. Clark, Norman J., Shearin, H. M., Schultz, W. P., Garms, Kenneth, and Moore, J. L. Miscible Drive - Its Theory and Application. Jour. Petrol. Technol., vol. 10, June 1958, pp. 11-20.

4. Eilerts, C. Kenneth, and Others. Monograph 10, Phase Relations of Gas-Condensate Fluids, Amer. Gas Assoc., New York, N. Y., 1959, 362 pp.

5. Kieschnick, W. F., Jr. What is Miscible Displacement? Petrol. Eng., vol. 31, Part 2, August 1959, p. B-56.

6. Mendenhall, William. Introduction to Statistics. Wadsworth Publishing Co., Inc., Belmont, California, 1964, 305 pp.

7. Moses, D. L., Thomas, C. E., and Koepf, E. H. Applications of Miscible Phase Displacement Processes. Producers Monthly, vol. 23, No. 12, October 1959, pp. 14, 16-21.

APPENDIX A

EFFECT OF ESTIMATED RESPONSES

In matrix notation the sum of the errors SSE is given by

$$SSE = Y'Y - \beta'X'Y \quad . \tag{A1}$$

An equivalent expression in algebraic notation, assuming certain of the Y's to be estimated or computed values Y_c, is

$$(SSE)_m + (SSE)_c = \{\Sigma YY + \Sigma Y_c Y_c\} - \Sigma \beta \{XY + \Sigma XY_c\} \tag{A2}$$

where m designates that part of SSE due to measured Y's and c designates the part due to computed values Y_c. The term of equation A2 representing

$-\beta'X'Y$ may be manipulated to provide the steps,

$$-\Sigma\beta\{\Sigma XY + \Sigma XY_c\},$$

$$-\Sigma\beta\Sigma XY - \Sigma\beta\Sigma XY_c,$$

$$-\Sigma\beta\Sigma XY - \Sigma\Sigma Y_c X\beta,$$

$$-\Sigma\beta\Sigma XY - \Sigma Y_c \Sigma X\beta \quad . \tag{A3}$$

Now if iterations progress to a limit condition such that Y_c's used provide coefficients that will yield these Y_c's exactly then $Y_c = \Sigma X\beta$ and a final step for the terms A3 is

$$-\Sigma\beta\Sigma XY - \Sigma Y_c Y_c \quad .$$

Thus for the limit condition equation A2 may be written

$$(SSE)_m + (SSE)_c = \Sigma YY + \Sigma Y_c Y_c - \Sigma\beta\Sigma XY - \Sigma Y_c Y_c$$

or, because $(SSE)_c = 0$,

$$(SSE)_m = \Sigma YY - \Sigma\beta\Sigma XY \quad . \tag{A4}$$

Thus for an iteration representing a close approximation of the limit condition, coefficients β calculated depend for their values only on measured values of Y.

For this method to be helpful there should be enough measured Y's, compared to the number of estimated or calculated Y's, so that the iterations will not only converge but converge at a satisfactory rate.

Table 1. - Compositions of liquid and gas constituents used to prepare fluids

1	2	3	4
Component	Natural Gas, mole fraction	Intermediates Mixture 1/, mole fraction	Distillation Cuts (3-10) 2/, mole fraction
N_2	0.002,820	--	--
CO_2	.010,000	--	--
nC_1	.893,310	--	--
nC_2	.063,980	--	--
nC_3	.016,250	--	--
iC_4	.002,520	--	--
nC_4	.003,680	0.160,000	--
iC_5	.001,130	.160,000	--
nC_5	.000,960	.150,000	--
135-56 C_6	.000,050	.170,000	--
56-35 C_6	.002,325	.190,000	--
35-17 C_7	.000,775	.170,000	--
17-11 C_7	.000,775	--	0.159,100
nC_8	.000,775	--	.185,200
nC_9	.000,650	--	.149,200
nC_{10}	--	--	.119,100
nC_{11}	--	--	.090,000
nC_{12}	--	--	.074,900
nC_{13}	--	--	.069,100
nC_{14}	--	--	.058,400
nC_{15}	--	--	.066,200
nC_{16+}	--	--	.028,800
Total	1.000,000	1.000,000	1.000,000

1/ Actually used 2,2 dimethylbutane for iC_6 and 2,4 dimethylpentane for iC_7.
2/ Values listed were calculated from values taken off of distillation curve.

Table 2. - Distillation analysis of gulf coast condensate 61069

1	2	3	4	5	6	7	8
Fraction number	Cut temp., °F	Volume percent by analysis	Sum volume percent 1/ adjusted	Specific gravity, 60°/60°F	Relative weight of fractions	Weight percent	Sum weight percent
			Distillation pressure, 740 mm.				
1	122	4.3	6.4	0.626	4.01	5.18	5.18
2	167	6.9	13.3	.672	4.64	5.99	11.17
3	212	8.9	22.2	.720	6.41	8.28	19.45
4	257	8.9	31.1	.733	6.52	8.42	27.87
5	302	6.6	37.7	.747	4.93	6.37	34.24
6	347	9.7	47.4	.760	7.37	9.52	43.76
7	392	7.0	54.4	.771	5.40	6.98	50.74
8	437	6.7	61.1	.784	5.25	6.78	57.52
			Distillation pressure, 40 mm.				
9	302	6.4	67.5	.802	5.13	6.63	64.15
10	347	9.7	77.2	.819	7.94	10.26	74.41
11	392	7.5	84.7	.823	6.17	7.97	82.38
12	437 2/	5.0	89.7	.833	4.16	5.37	87.75
Residuum	--	10.3	100.0	.920	9.48	12.25	100.00
Loss	--	2.1	--	--	--	--	--
					77.41	100.00	

1/ Distillation loss of 2.1 percent assumed to be all in fraction number 1.
2/ Distillation discontinued here.

Table 3. - Compositions of original fluids

Component	Mole fraction composition of indicated mixtures				
	GI800	GI840	GI876	GI910	GI933
N_2	0.002,256	0.002,370	0.002,470	0.002,566	0.002,630
C_1	.714,648	.750,380	.782,240	.812,911	.833,770
CO_2	.008,000	.008,400	.008,760	.009,100	.009,330
C_2	.051,184	.053,740	.056,030	.058,222	.059,720
C_3	.013,000	.013,650	.014,230	.014,788	.015,170
iC_4	.002,016	.002,120	.002,210	.002,293	.002,350
nC_4	.015,002	.012,740	.010,720	.008,775	.007,450
iC_5	.012,962	.010,600	.008,480	.006,454	.005,070
nC_5	.012,072	.009,850	.007,870	.005,961	.004,670
135-56 C_6	.012,851	.010,290	.008,000	.005,811	.004,320
56-35 C_6	.016,178	.013,400	.010,940	.008,561	.006,940
35-17 C_7	.013,431	.010,900	.008,640	.006,470	.004,990
17-11 C_7	.020,450	.016,510	.013,010	.009,628	.007,330
C_8	.023,703	.019,120	.015,040	.011,092	.008,400
C_9	.019,116	.015,430	.012,130	.008,960	.006,810
C_{10}	.014,845	.011,880	.009,230	.006,680	.004,950
C_{11}	.011,218	.008,970	.006,970	.005,048	.003,740
C_{12}	.009,336	.007,470	.005,800	.004,201	.003,110
C_{13}	.008,613	.006,890	.005,350	.003,876	.002,870
C_{14}	.007,279	.005,820	.004,520	.003,275	.002,430
C_{15}	.008,251	.006,600	.005,130	.003,713	.002,750
C_{16+}	.003,589	.002,870	.002,230	.001,615	.001,200
Total	1.000,000	1.000,000	1.000,000	1.000,000	1.000,000

Table 4. - Compositions of fluids modified with normal butane (0.1 moles of nC_4 per mole of fluid)

Component	Mole fraction composition of indicated mixtures				
	GI800 + 0.1 nC_4	GI840 + 0.1 nC_4	GI876 + 0.1 nC_4	GI910 + 0.1 nC_4	GI933 + 0.1 nC_4
N_2	0.002,051	0.002,155	0.002,250	0.002,333	0.002,390
C_1	.649,680	.682,164	.711,130	.739,009	.757,960
CO_2	.007,273	.007,636	.007,960	.008,273	.008,480
C_2	.046,531	.048,855	.050,940	.052,929	.054,290
C_3	.011,818	.012,409	.012,940	.013,444	.013,790
iC_4	.001,833	.001,927	.002,010	.002,085	.002,140
nC_4	.104,547	.102,489	.100,650	.098,886	.097,680
iC_5	.011,784	.009,636	.007,710	.005,867	.004,610
nC_5	.010,975	.008,955	.007,150	.005,419	.004,250
135-56 C_6	.011,683	.009,355	.007,270	.005,283	.003,930
56-35 C_6	.014,707	.012,182	.009,950	.007,783	.006,310
35-17 C_7	.012,210	.009,909	.007,850	.005,882	.004,540
17-11 C_7	.018,591	.015,009	.011,830	.008,753	.006,660
C_8	.021,548	.017,382	.013,670	.010,084	.007,640
C_9	.017,378	.014,027	.011,030	.008,145	.006,190
C_{10}	.013,495	.010,800	.008,390	.006,073	.004,500
C_{11}	.010,198	.008,155	.006,340	.004,589	.003,400
C_{12}	.008,487	.006,791	.005,270	.003,819	.002,830
C_{13}	.007,830	.006,264	.004,860	.003,524	.002,610
C_{14}	.006,617	.005,291	.004,110	.002,977	.002,210
C_{15}	.007,501	.006,000	.004,660	.003,375	.002,500
C_{16+}	.003,263	.002,609	.002,030	.001,468	.001,090
Total	1.000,000	1.000,000	1.000,000	1.000,000	1.000,000

Table 5. - Composition of fluids with additive (0.2 moles of nC_4 per mole of fluid)

Component	Mole fraction composition of indicated mixtures				
	GI800 + 0.2 nC_4	GI840 + 0.2 nC_4	GI876 + 0.2 nC_4	GI910 + 0.2 nC_4	GI933 + 0.2 nC_4
N_2	0.001,880	0.001,975	0.002,060	0.002,138	0.002,190
C_1	.595,540	.625,317	.651,850	.677,427	.694,810
CO_2	.006,667	.007,000	.007,300	.007,583	.007,780
C_2	.042,653	.044,783	.046,690	.048,518	.049,770
C_3	.010,833	.011,375	.011,860	.012,323	.012,640
iC_4	.001,680	.001,767	.001,840	.001,911	.001,960
nC_4	.179,168	.177,284	.175,600	.173,979	.172,880
iC_5	.010,802	.008,833	.007,070	.005,378	.004,220
nC_5	.010,060	.008,208	.006,560	.004,968	.003,890
135-56 C_6	.010,709	.008,575	.006,670	.004,842	.003,600
56-35 C_6	.013,482	.011,167	.009,120	.007,134	.005,780
35-17 C_7	.011,192	.009,083	.007,200	.005,392	.004,160
17-11 C_7	.017,042	.013,758	.010,840	.008,023	.006,110
C_8	.019,752	.015,933	.012,530	.009,243	.007,000
C_9	.015,930	.012,858	.010,110	.007,467	.005,680
C_{10}	.012,371	.009,900	.007,690	.005,567	.004,120
C_{11}	.009,348	.007,475	.005,810	.004,207	.003,120
C_{12}	.007,780	.006,225	.004,830	.003,501	.002,590
C_{13}	.007,178	.005,742	.004,460	.003,230	.002,390
C_{14}	.006,066	.004,850	.003,770	.002,729	.002,020
C_{15}	.006,876	.005,500	.004,280	.003,094	.002,290
C_{16+}	.002,991	.002,392	.001,860	001,346	.001,000
Total	1.000,000	1.000,000	1.000,000	1.000,000	1.000,000

Table 6. - Coefficients of mathematical model and related statistical data

Argument	Coefficient, β	Student's t
X_0	4,025.83	299.8
X_1	-77.84	2.4
X_1^2	-629.92	13.5
X_1^3	-20.29	.2
X_2	73.91	9.6
X_2^2	-316.43	24.8
X_3	-703.17	106.1
X_3^2	33.44	2.9
X_1X_2	-393.86	24.9
X_1X_3	-155.40	11.3
X_2X_3	276.07	29.8

Degrees of freedom	28
Confidence interval	.95
Table Student's t	2.05
SSE basis last iteration	133,900
Standard deviation	69.2

Table 7. - Convergence of iterations

Sequence	Sum of squares of errors: All pressures	Sum of squares of errors: Estimated pressures	Standard deviation, psi: Basis all pressures	Standard deviation, psi: Basis measured pressures
i + 1	159,200	4,500	49.9	74.3
i + 2	146,200	3,200	47.8	71.5
i + 3	136,400	2,500	46.1	69.2

Table 8. - Coefficients of mathematical model to provide more than one pressure for given arguments

Argument	Coefficient, β	Student's t
X_0	4,022.69	256.5
X_1	-56.89	1.9
X_1^2	-430.22	11.3
X_1^3	-100.30	1.8
X_2	37.28	3.9
X_2^2	-342.72	21.1
X_3	-699.41	90.3
X_3^2	34.32	2.6
$X_1 X_2$	-328.05	21.0
$X_1 X_3$	-139.70	10.8
$X_2 X_3$	270.35	24.0

Degrees of freedom basis all pressures	64
Confidence interval	.95
Table Student's t	2.00
SSE basis last iteration	185,100
Standard deviation basis all pressures	53.8

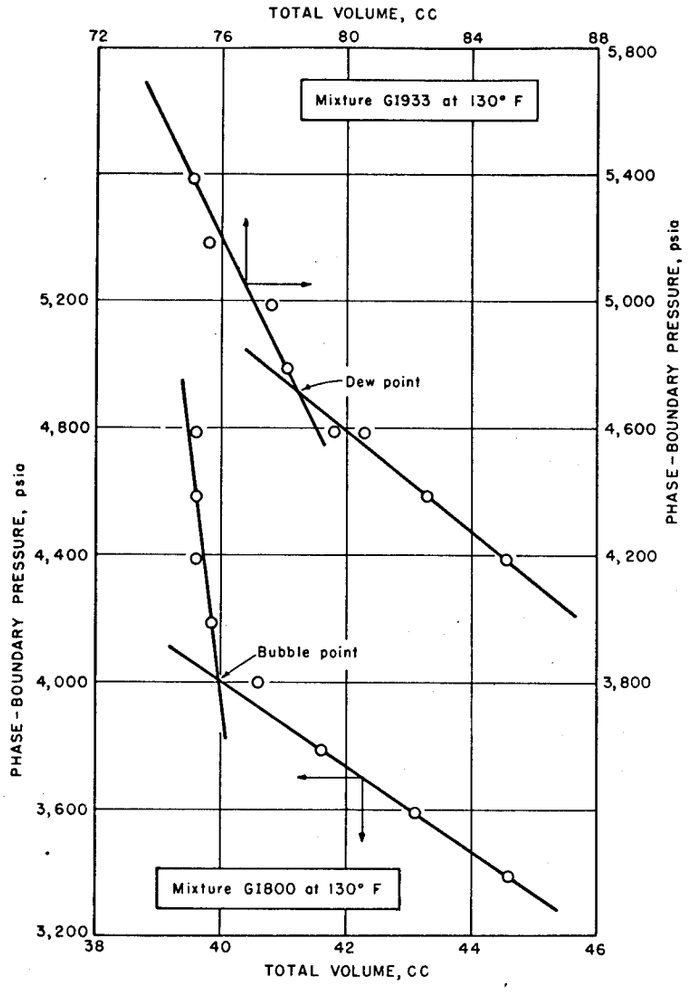

FIGURE 1 .— Determination of Dew-Point and Bubble-Point Pressure of Condensate Mixtures.

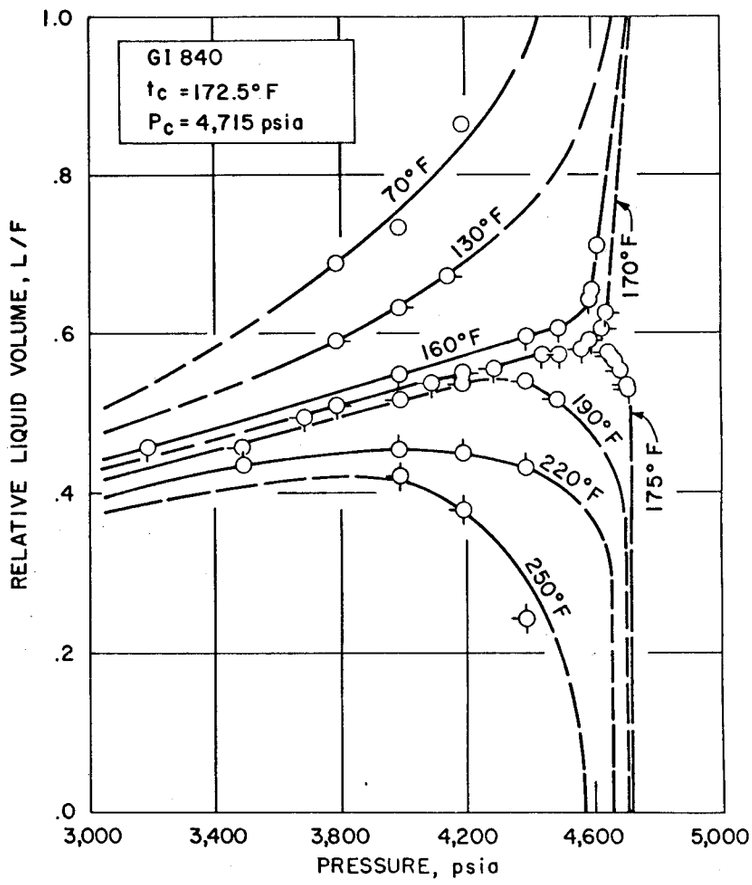

FIGURE 2.-Determination of Critical State of Condensate Fluid GI 840 .

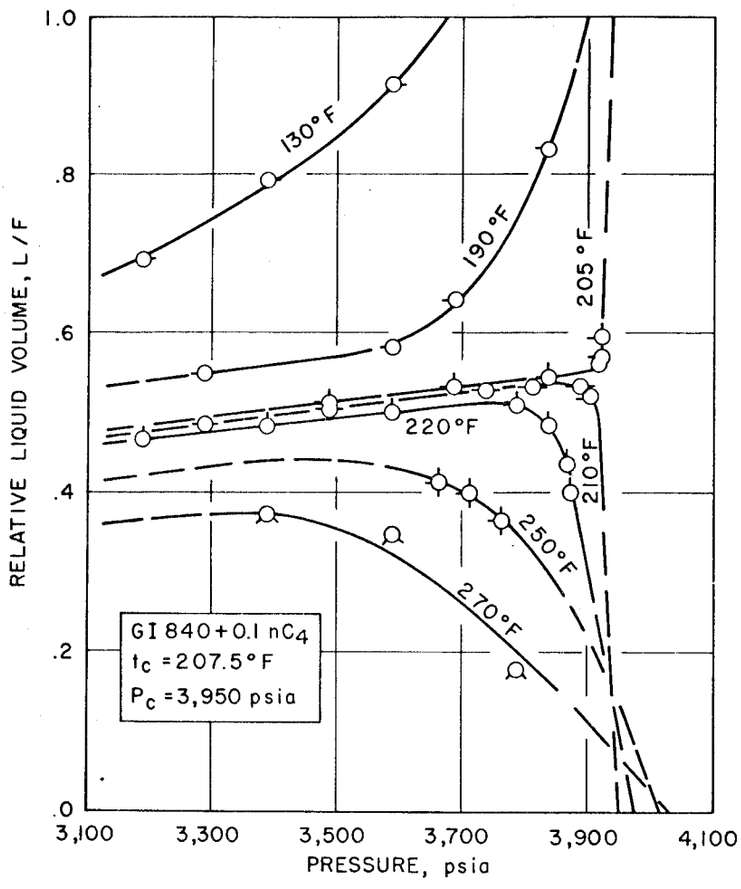

FIGURE 3.-Determination of Critical State of Condensate Mixture GI 840+0.1 nC_4.

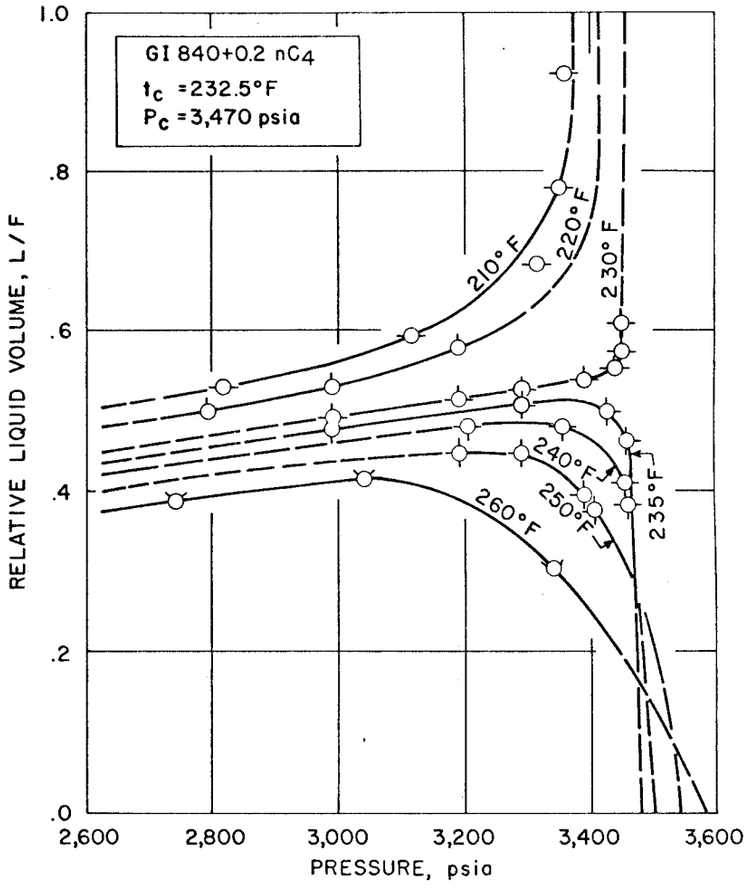

FIGURE 4.-Determination of Critical State of Condensate Mixture GI 840+0.2 nC_4.

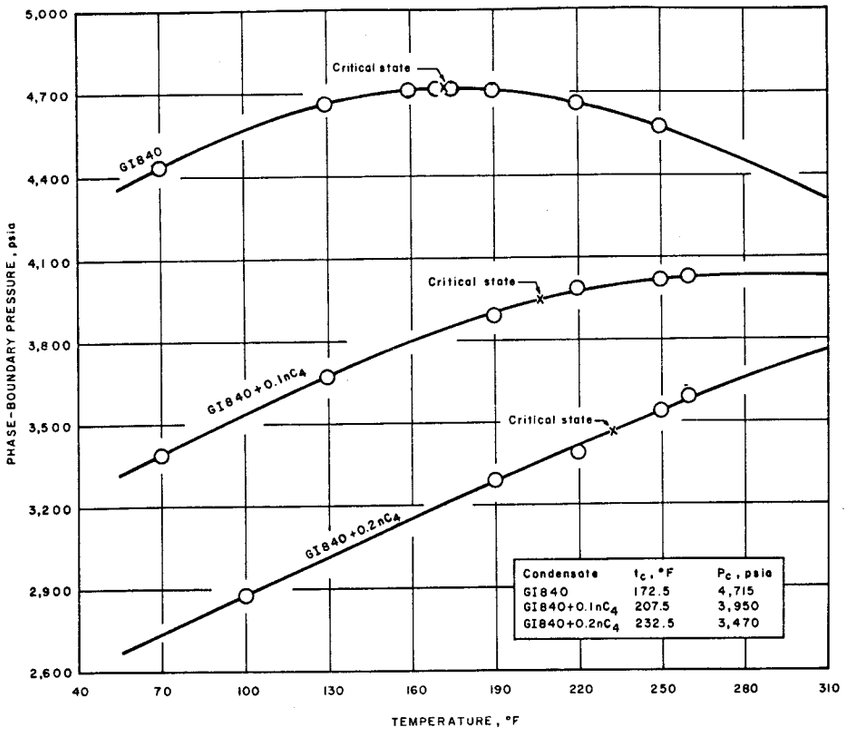

FIGURE 5.—Phase-Boundary Curves of Condensate Mixtures GI840, GI840+0.1nC_4, and GI840+0.2nC_4.

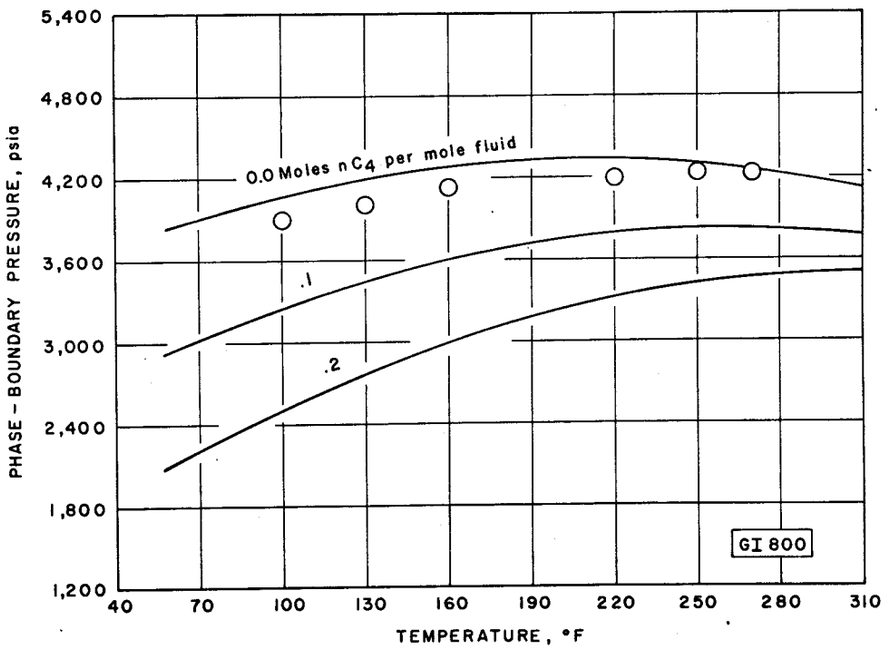

FIGURE 6.-Effect of Normal Butane on Phase-Boundary Pressure of Condensate Fluid GI 800.

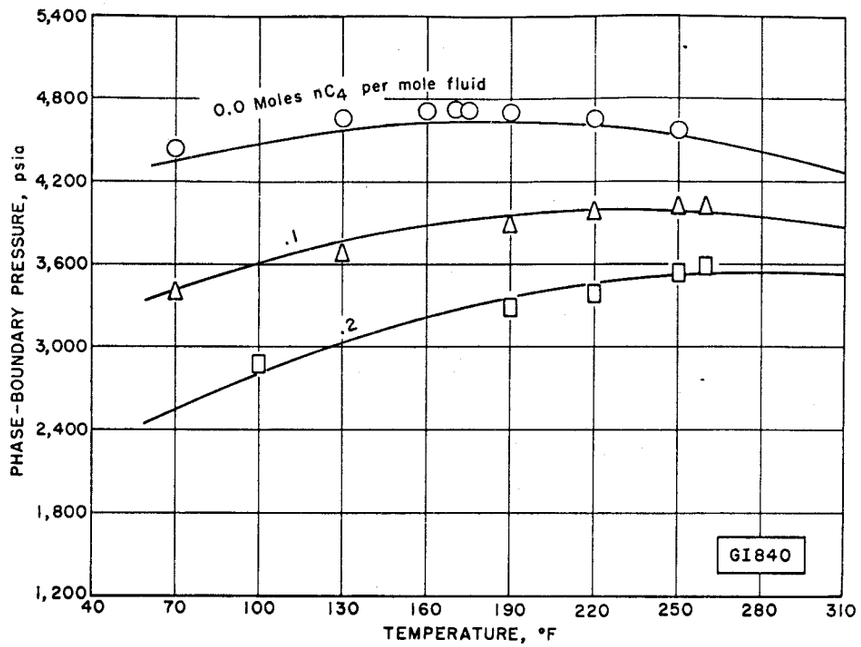

FIGURE 7.—Effect of Normal Butane on Phase-Boundary Pressure of Condensate Fluid GI840.

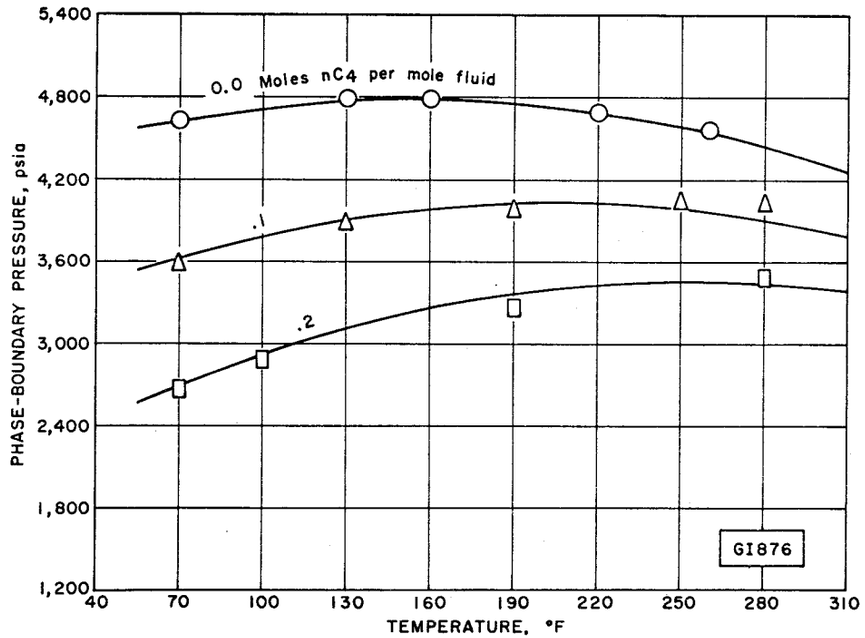

FIGURE 8.—Effect of Normal Butane on Phase-Boundary Pressure of Condensate Fluid GI876.

akr 9-28-66

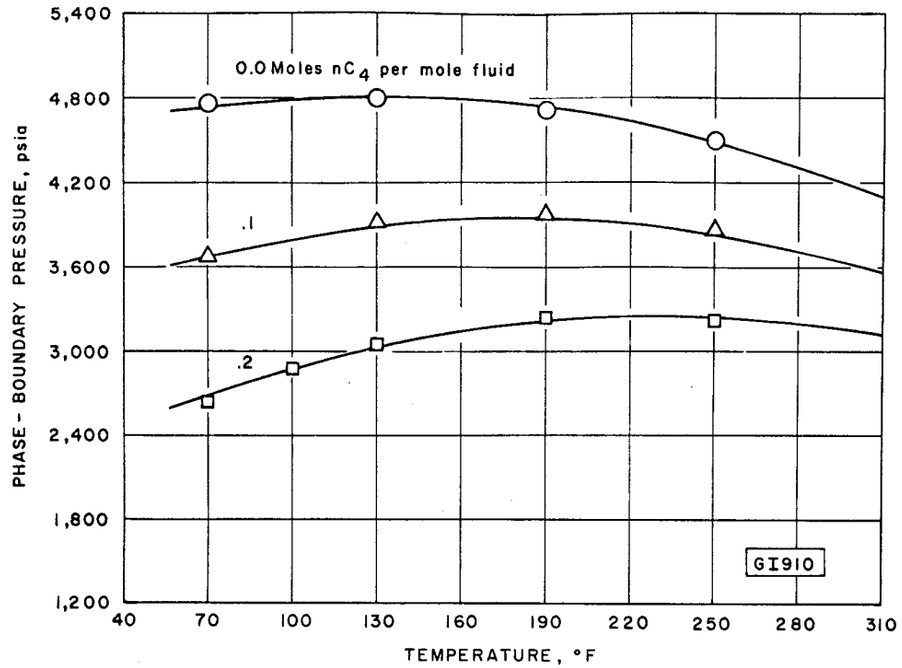

FIGURE 9 .-Effect of Normal Butane on Phase-Boundary Pressure of Condensate Fluid GI 910.

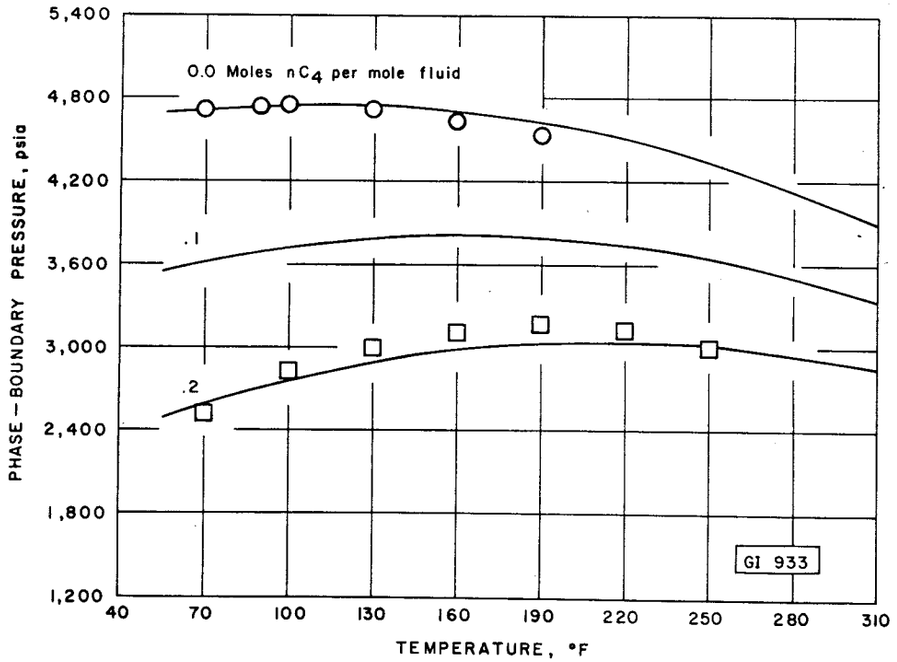

FIGURE 10.- Effect of Normal Butane on Phase-Boundary Pressure of Condensate Fluid GI 933 .

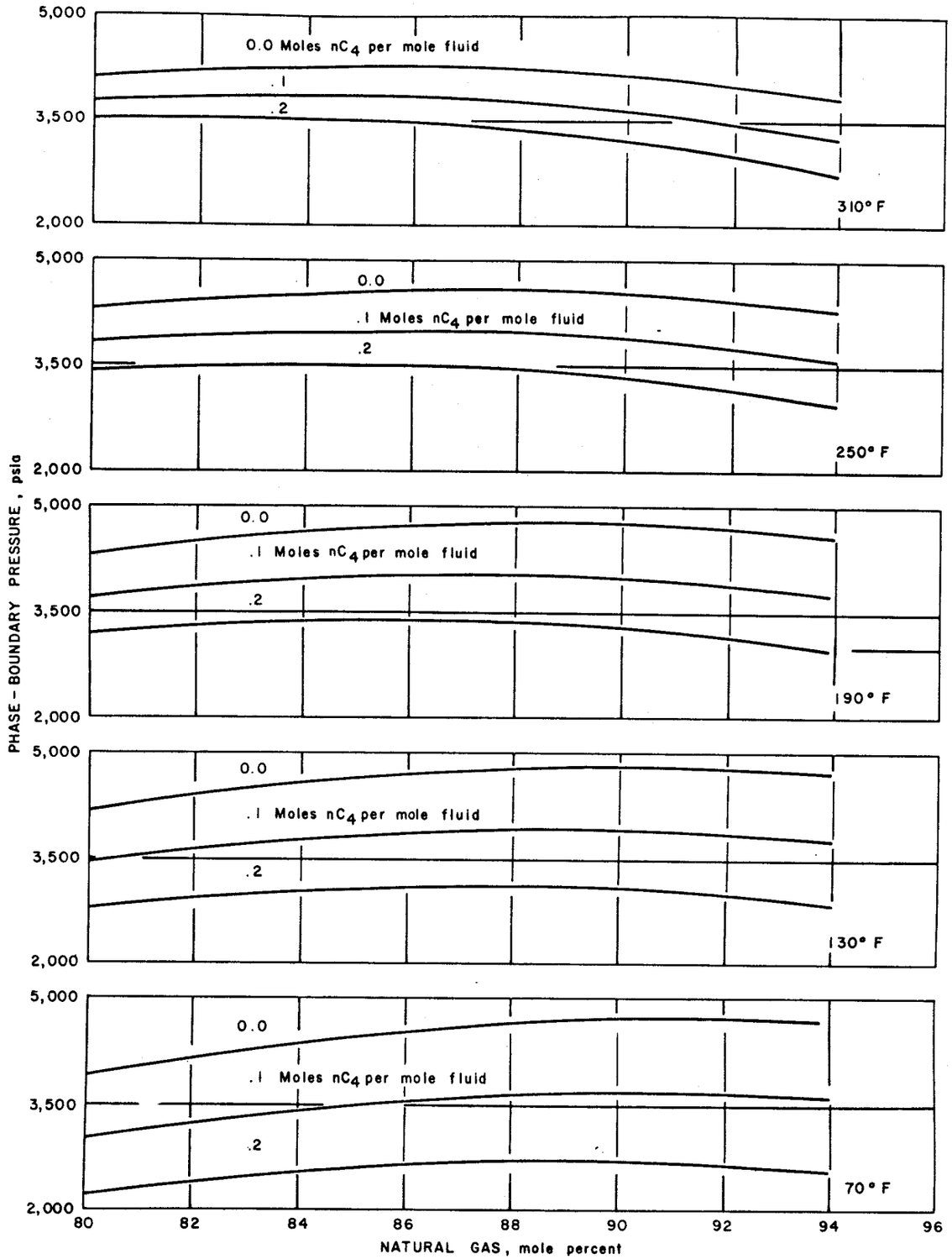

FIGURE 11.- Effect of Natural Gas Content on Phase-Boundary Pressure of Butane-Condensate Mixtures .

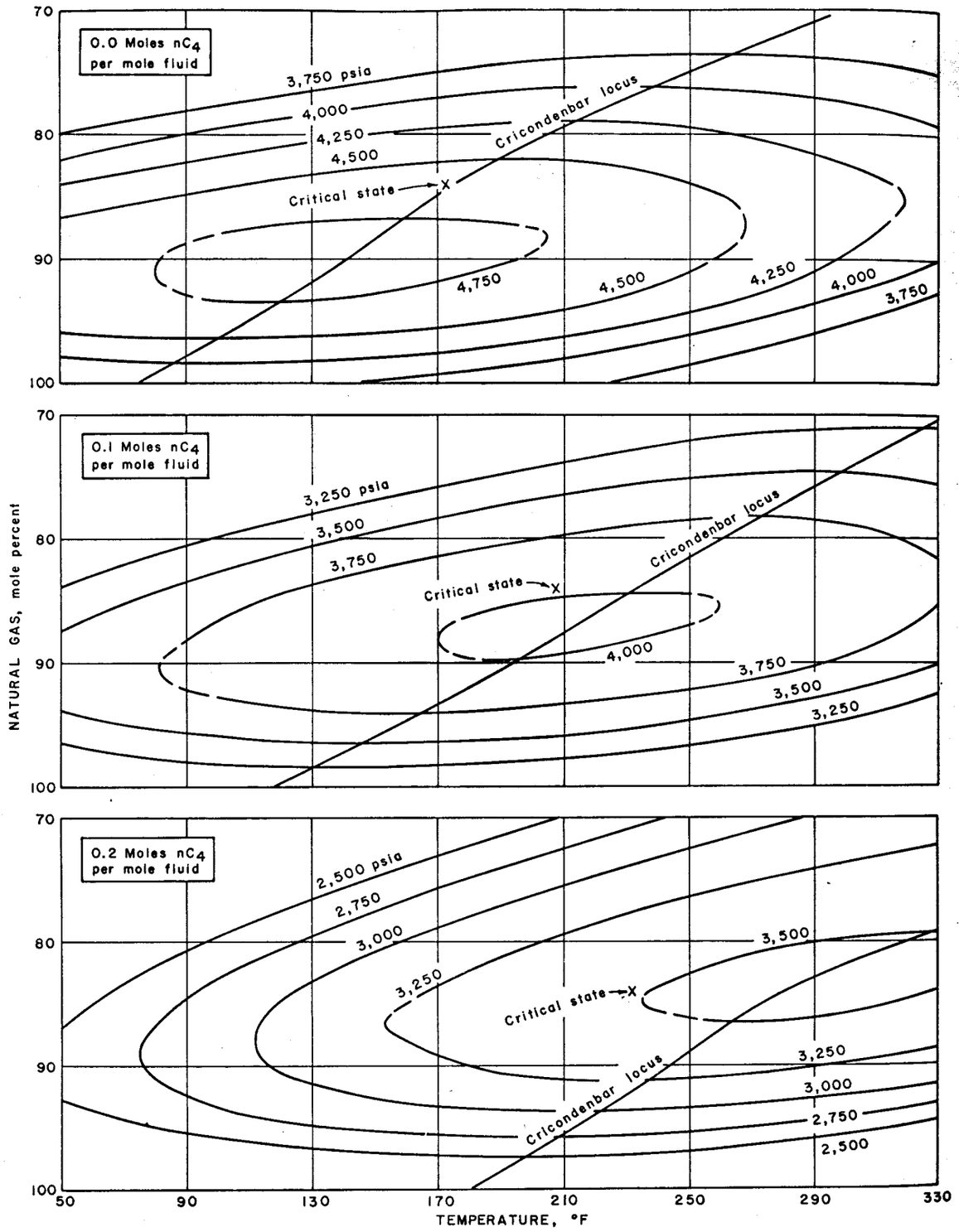

FIGURE 12.— Effect of Normal Butane on Phase-Boundary Surfaces of Condensate Mixtures.

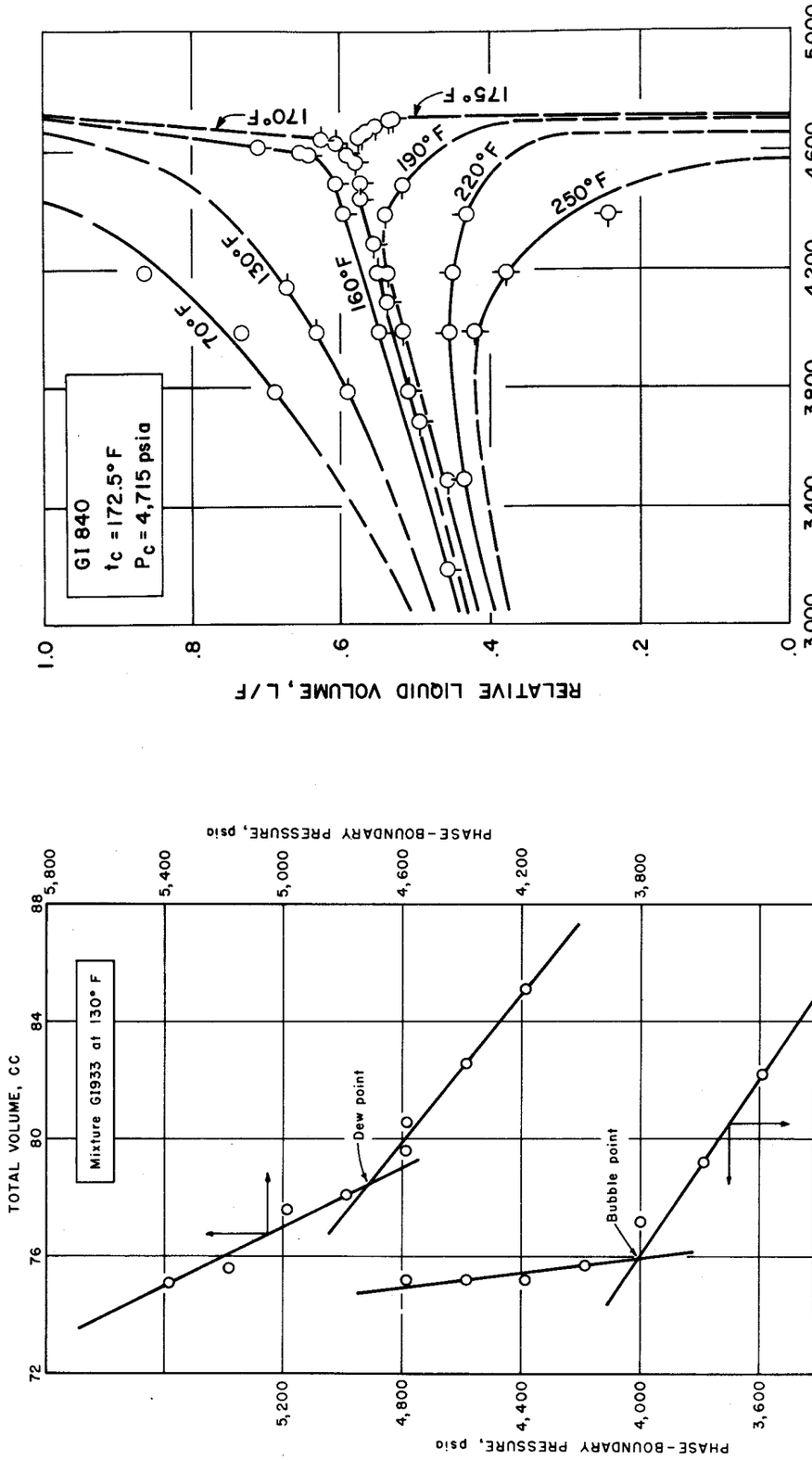

FIGURE 1.— Determination of Critical State of Condensate Fluid GI 840 .

FIGURE 1 .— Determination of Dew-Point and Bubble-Point Pressure of Condensate Mixtures.

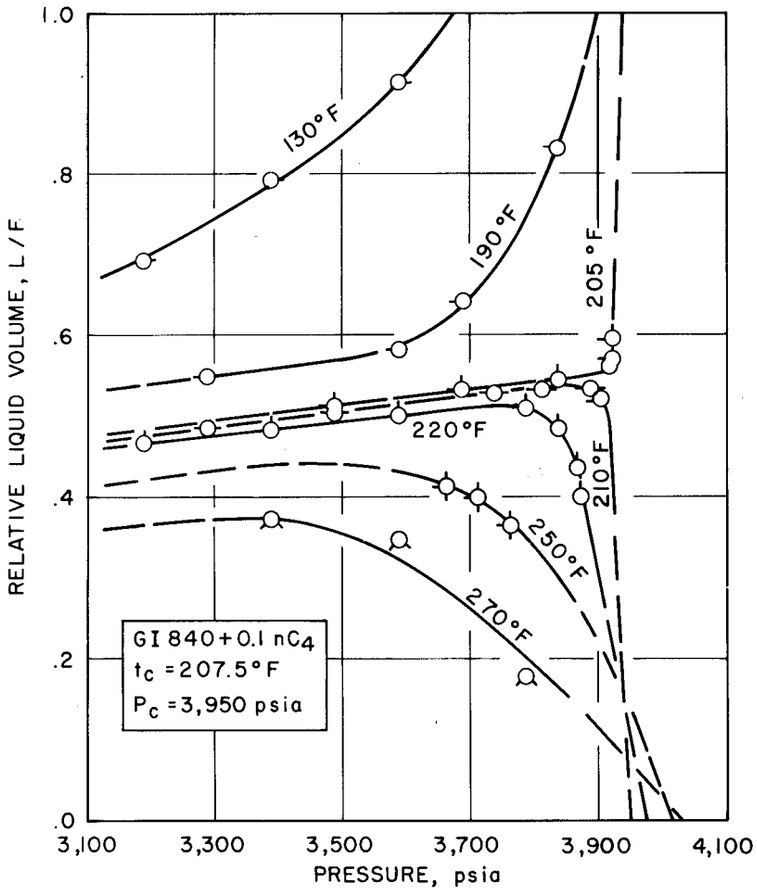

FIGURE 3.-Determination of Critical State of Condensate Mixture GI 840+0.1 nC_4.

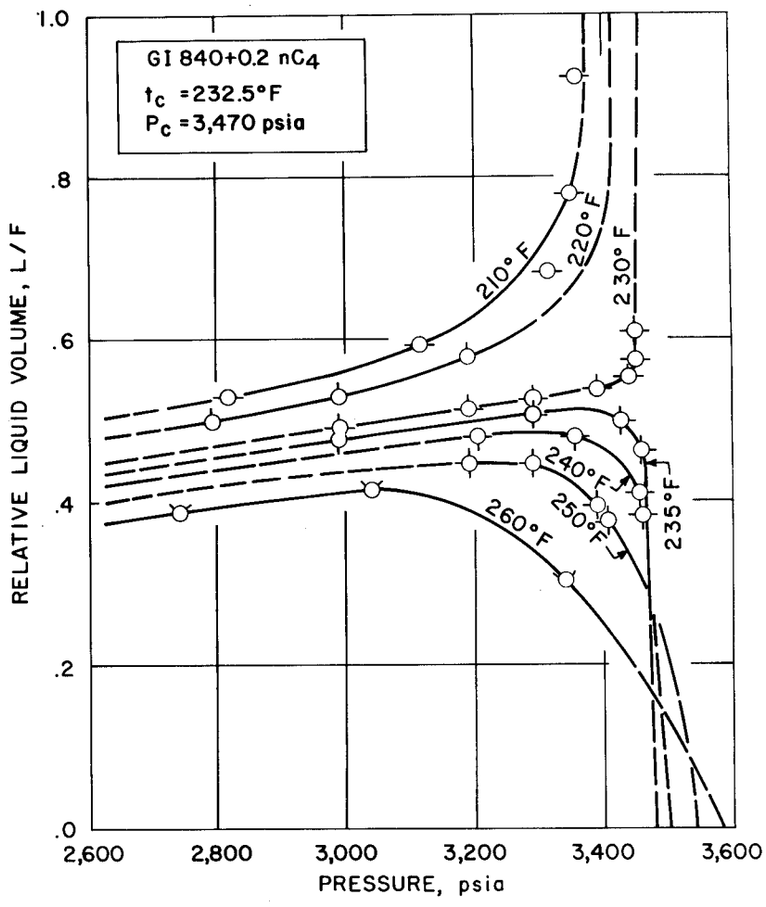

FIGURE 4.-Determination of Critical State of Condensate Mixture GI 840+0.2 nC_4.

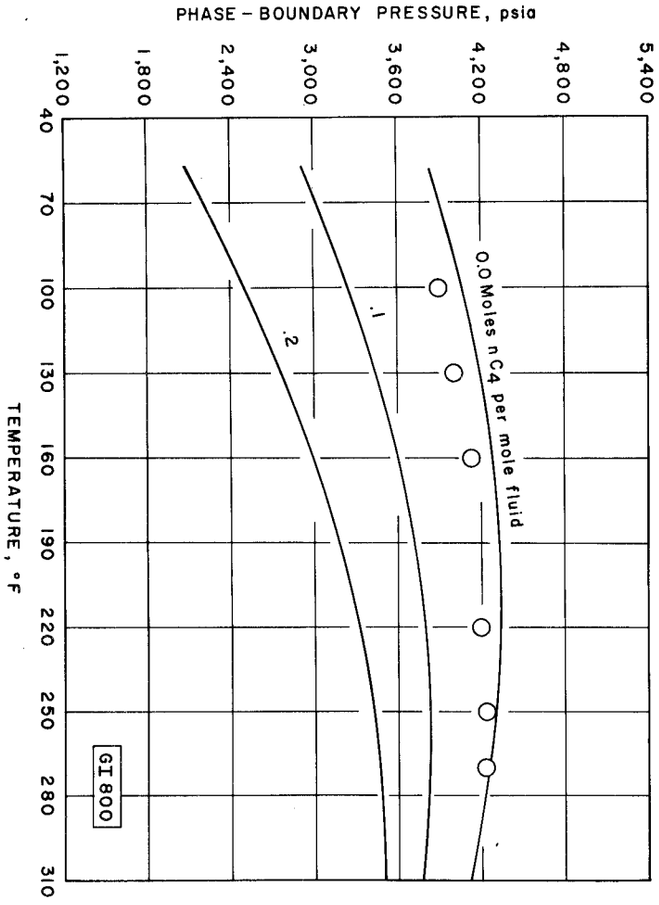

FIGURE 6.-Effect of Normal Butane on Phase-Boundary Pressure of Condensate Fluid GI 800.

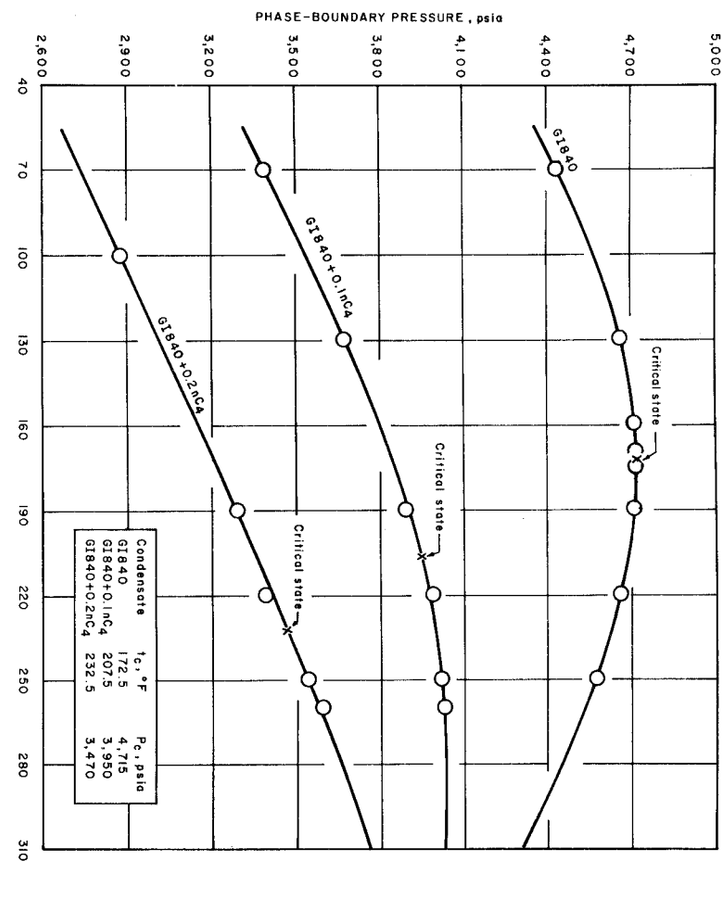

FIGURE 5.-Phase-Boundary Curves of Condensate Mixtures GI 840, GI 840+0.1 nC_4, and GI 840+0.2 nC_4.

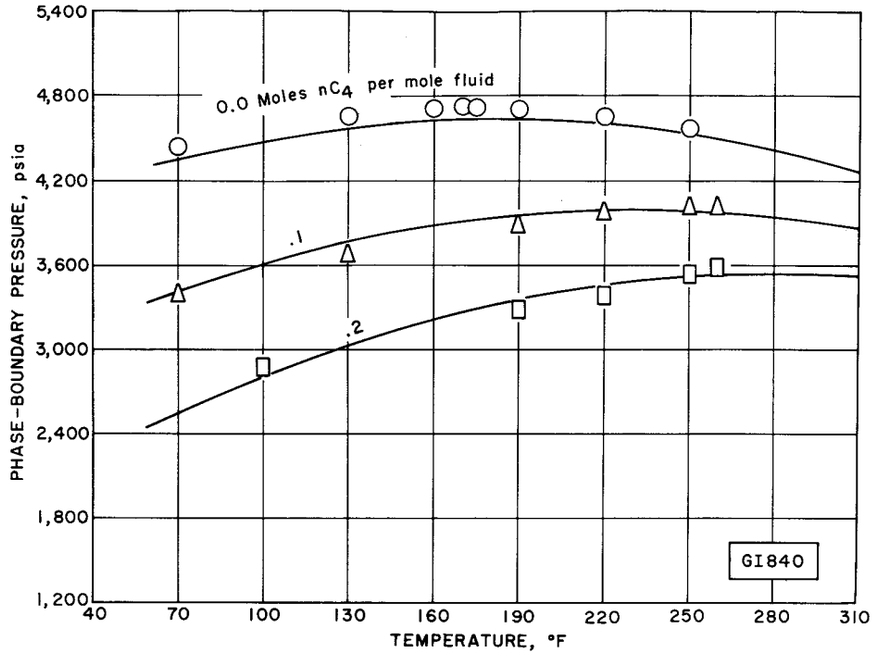

FIGURE 7.–Effect of Normal Butane on Phase-Boundary Pressure of Condensate Fluid GI840.

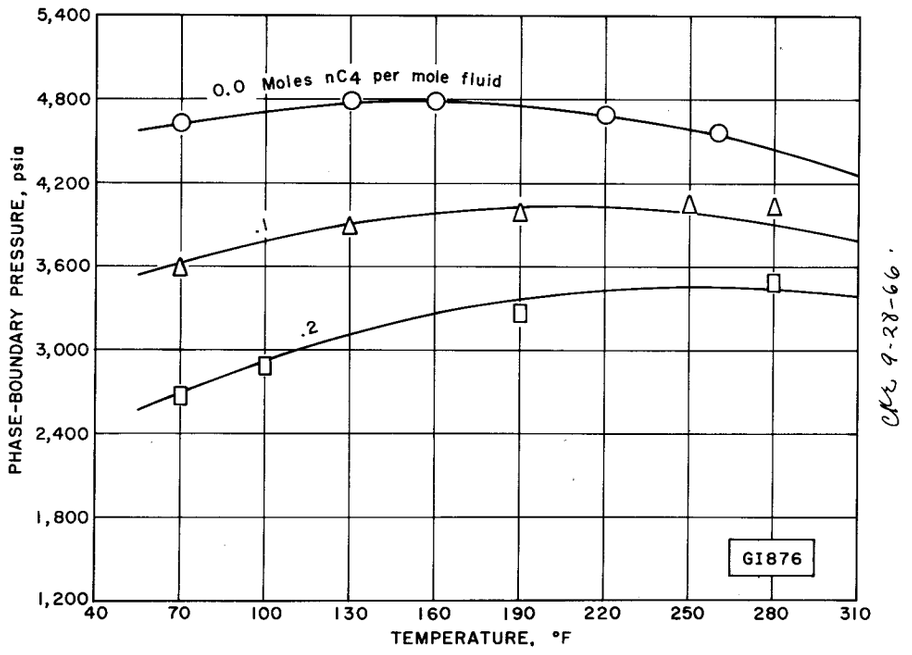

FIGURE 8.– Effect of Normal Butane on Phase-Boundary Pressure of Condensate Fluid GI876.

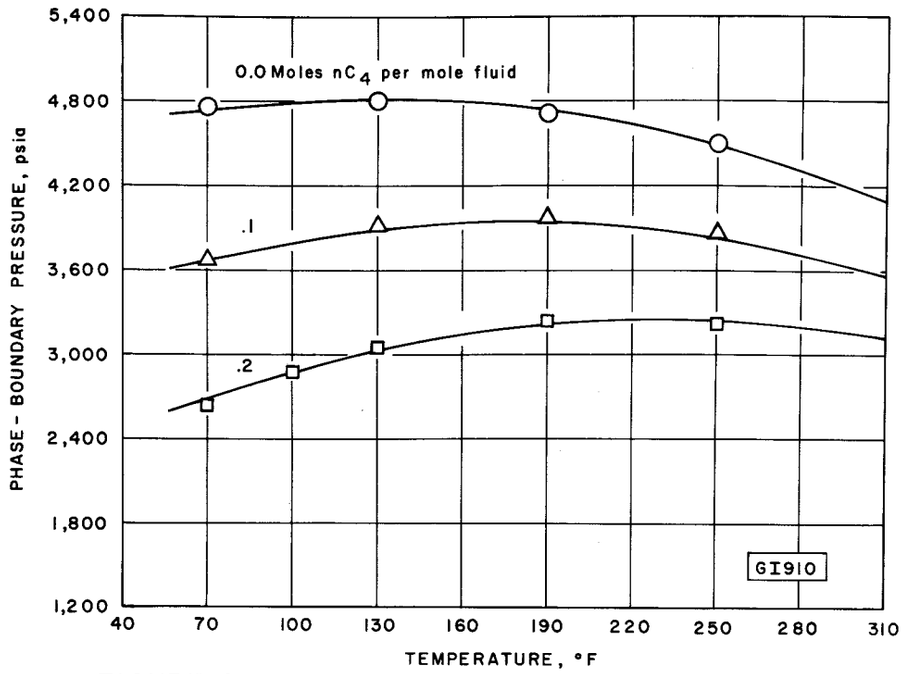

FIGURE 9 .-Effect of Normal Butane on Phase-Boundary Pressure of Condensate Fluid GI910.

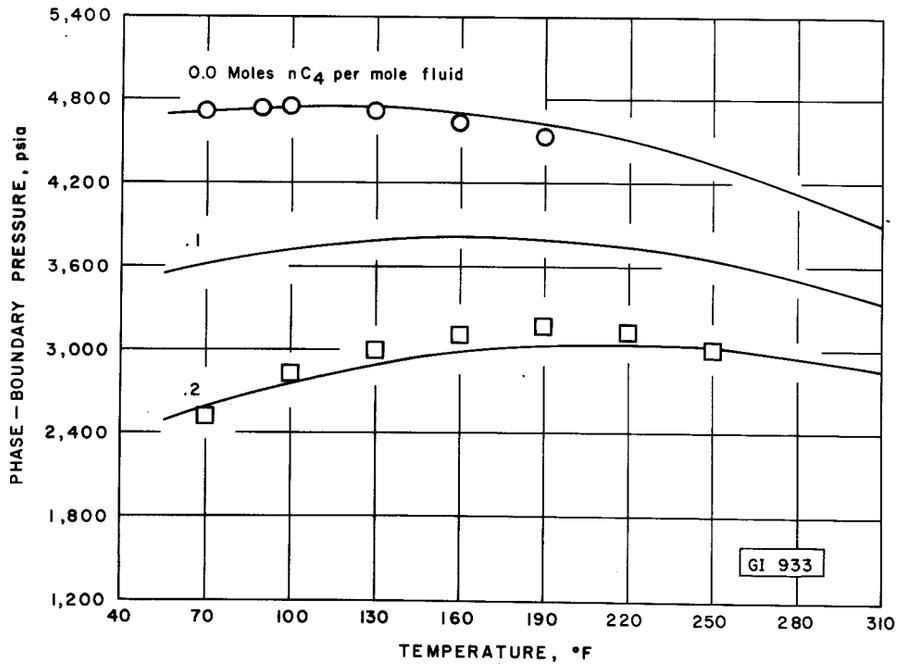

FIGURE 10.– Effect of Normal Butane on Phase-Boundary Pressure of Condensate Fluid GI 933 .

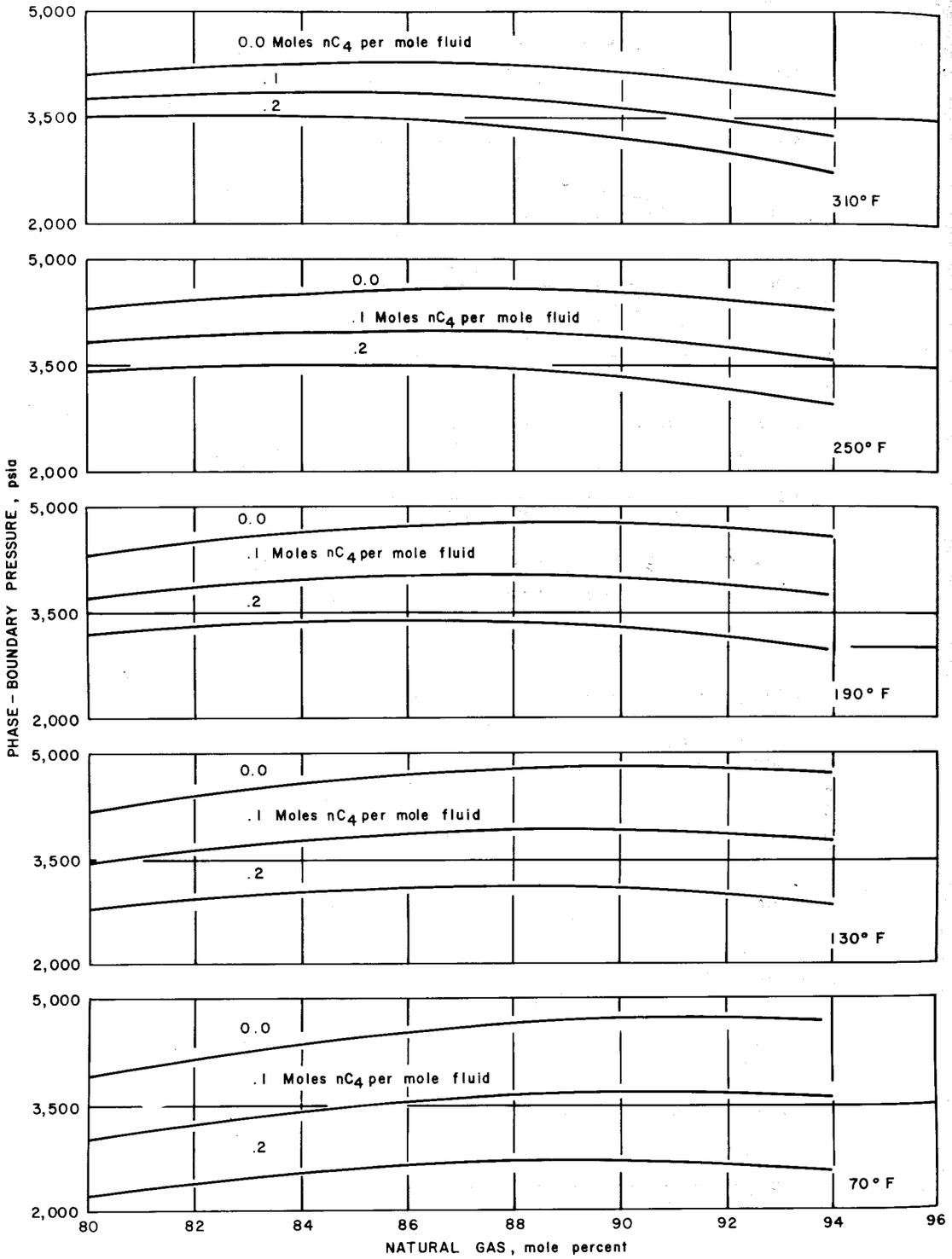

FIGURE 11.– Effect of Natural Gas Content on Phase–Boundary Pressure of Butane–Condensate Mixtures.

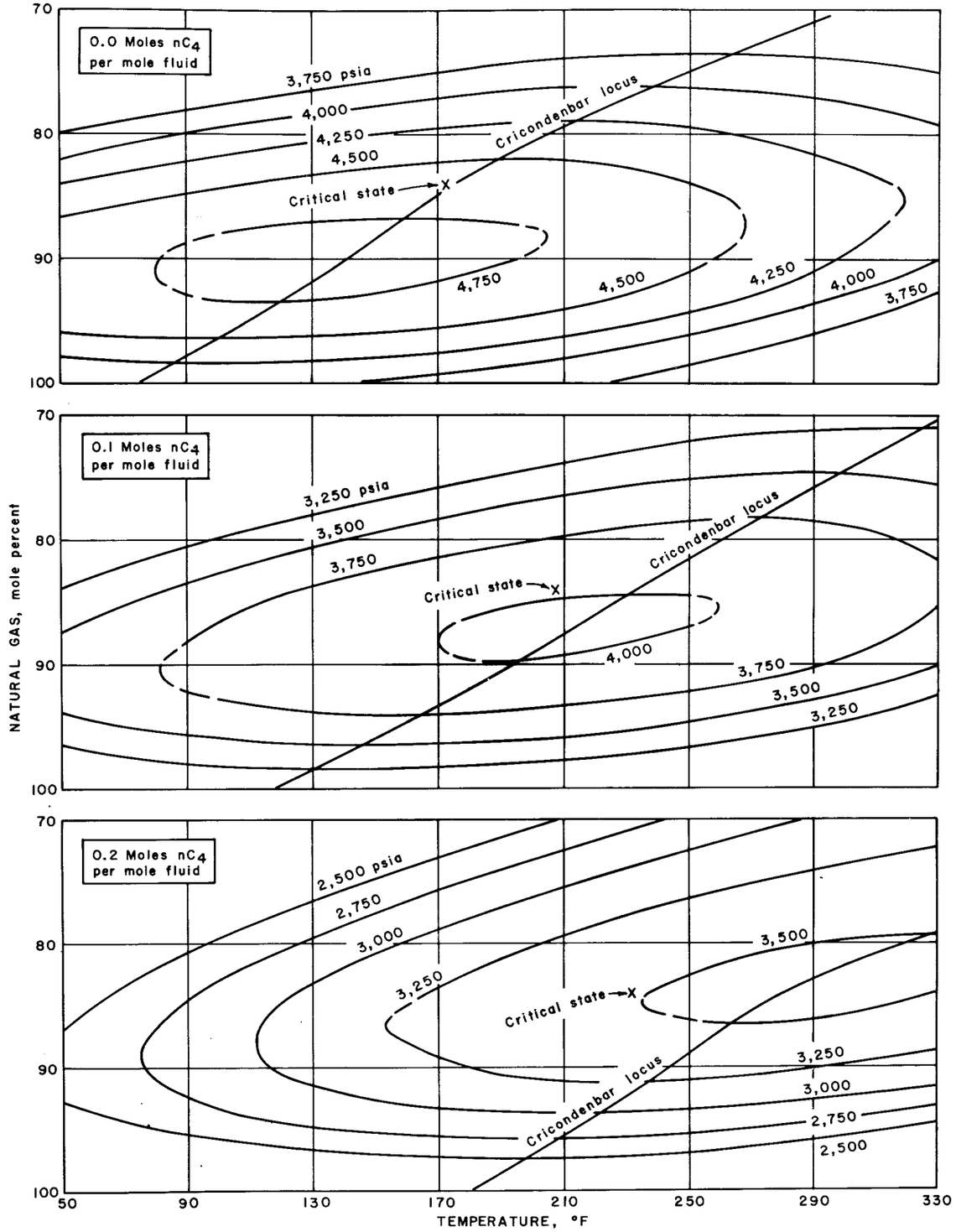

FIGURE 12.– Effect of Normal Butane on Phase–Boundary Surfaces of Condensate Mixtures.

ON THE RELATION OF MULTI-WELL VERTICAL FRACTURES TO FIVE-SPOT SWEEP EFFICIENCY

by

J. T. Hansford and D.A.T. Donohue
The Pennsylvania State University

INTRODUCTION

Several recovery stimulation processes have been developed by the petroleum industry, some having widespread application to a variety of producing conditions and other, more exotic, techniques requiring special conditions in order to be beneficial. Of the former, two important recovery aids have proven especially successful: hydraulic fracturing and waterflooding. In some cases, these two techniques can be combined to take advantage of the benefits of both. However, the effects of such a combination on fluid flow patterns and pressure distributions must be examined. A common measure of the effectiveness of a particular flow pattern in displacing oil with water is areal sweep efficiency, a factor dependent upon fluid flow patterns and pressure distributions.

An extensive review of literature (see Reference 1) concerning hydraulic fracturing establishes the fact that vertical fractures do occur in many cases and that, at least in some cases, these fractures have a preferred, azimuthal orientation. For optimal operation of a fractured reservoir undergoing pattern waterflooding, knowledge of fluid flow behavior for any existing set of fracture conditions is essential. The object of this investigation was to determine the effects of vertical fractures of various lengths and orientations on the sweep efficiency of a normal five-spot waterflood pattern having all wells fractured along a particular azimuth. A potentiometric model and a numerical technique were employed to obtain values of sweep efficiency.

PROCEDURE OF INVESTIGATION

Experimental Model

A potentiometric model geometrically scaled to simulate a completely developed reservoir was constructed using Teledeltos paper, an electrically conductive paper, as the conductive medium. A potentiometric plotter connected to a network of sources and sinks was used to obtain potential distributions in the center five-spot,

a pattern surrounded by five-spots to represent a completely confined pattern (see Figure 1). Fractures of the desired length and orientation were simulated by painting lines with conductive silver paint radiating from each well location, represented by a brass screw. By virtue of the analogy between Ohm's law and Darcy's law, the resultant potential distributions determined with the experimental model are identical to the pressure distributions in the reservoir prototype.

A series of runs was made to determine potential distributions for the confined five-spot with vertical fractures at all wells oriented at angles of 10°, 20°, 30°, 40°, and 45° as shown in Figure 2. For all of these runs, half-fracture length L was 20 percent of the spacing between like wells, W. An example of the resulting potential distribution is shown in Figure 3 for an angle of orientation of 10°. Construction of a network of curvilinear squares yielded the lines of force orthogonal to the equipotential lines, or streamlines. Flood front position at breakthrough was calculated for each case (see Figures 4 through 8) and sweep efficiencies were obtained by planimetering the swept areas.

Numerical Technique

This investigation concerned a two-dimensional, steady-state, incompressible fluid flow problem described by Laplace's equation:

$$\frac{\partial^2 p}{\partial x^2} + \frac{\partial^2 p}{\partial y^2} = 0 \qquad (1)$$

Such behavior governs problems investigated using the potentiometric model. The solution to Equation 1 with appropriate boundary conditions gives the pressure distribution of the system. Since boundary conditions for a fractured five-spot are a function of the fracture geometry, an explicit expression for values of potential at the boundaries is required. For fractures parallel to the boundary of a five-spot element (0° orientation), empirical correlations of boundary potential (pressure) as a function of L/W were obtained to explicitly define these conditions. Runs were made with the potentiometric model for L/W values of 0.0 (unfractured), .20, and .30 for which values of potential on the boundaries of the center five-spot were recorded. These data were correlated using standard techniques for obtaining empirical equations such as are presented by Davis (2). The resultant analytical expressions giving boundary potentials for any L/W value may be found in Appendix A.

A numerical approximation to Laplace's equation was calculated for various values of L/W using these empirically determined boundary conditions with an iterative process, Liebmann's extrapolated technique, which is first order correct. Pressure values were calculated for model points of a grid superimposed on the five-spot.

These values were then used in a particle-tracking scheme similar to that described by McCarty and Barfield (3). A velocity field is calculated and particles are moved through the field from injection fracture to producing fracture by integrating at chosen time intervals to obtain new particle location:

$$x_{t+1} = x_t + v_x \Delta t$$
$$y_{t+1} = y_t + v_y \Delta t \qquad (2)$$

where the velocities v_x and v_y are given by Darcy's equation:

$$v_x = \frac{dx}{dt} = -\frac{k}{\mu}\frac{\partial p}{\partial x} \quad ; \quad v_y = \frac{dy}{dt} = -\frac{k}{\mu}\frac{\partial p}{\partial y} \qquad (3)$$

Flood front positions at breakthrough (or earlier) were calculated for the chosen L/W values, and sweep efficiencies were obtained by measuring the swept areas. The entire procedure lended itself readily to programming for a high-speed digital computer. A proper choice of the time interval, Δt, allowed execution of the program on the IBM 7074 in 2-3 minutes for each run.

Throughout this study, the following assumptions governing fluid flow behavior apply:

(1) The fluids are ideal, incompressible, and immiscible with a mobility ratio of unity.

(2) The porous medium is horizontal, of constant thickness and uniform permeability. Effects of gravity are negligible.

(3) The fractures are symmetrical with respect to the wellbore, completely penetrate the producing zone, and have an infinite capacity compared to that of the reservoir.

RESULTS

Computer simulations of the runs involving fractures oriented at 0° produced the data shown in Figure 14. Sweep efficiencies are given for various values of L/W. Values of L/W ranged from 0.0 (unfractured) to .4, with L/W = .5 known intuitively to give 100 percent sweep efficiency. The same calculations yielded the flood front location at breakthrough for each of these cases. Results are shown in Figures 9 to 13.

Obtained from potential distributions of the experimental model, flood fronts in patterns having oriented fractures, all with L/W = .20, are shown in Figures 4 to 8. The calculated sweep efficiencies are given in Figure 15, with angle of fracture orientation as the parameter. Sweep efficiencies for the interior fracture pattern, the exterior fracture pattern, and the total flood pattern are presented.

DISCUSSION OF RESULTS

Fractures at 0°

Sweep efficiency is increased by increasing the L/W value of the well fractures. Values of sweep efficiency range from 73 percent for L/W = 0.0 (unfractured) to 100 percent for L/W = .50. Only a slight increase in sweep efficiency over the unfractured case is obtained for L/W values of .20 and less. For values of L/W greater than .20, sweep efficiency markedly increases. In general, the shape of the flood front is altered by both the injection fracture and the producing fracture. The first determines initial partical location, and therefore, influences the early stages in the front movement. The second affects the shape of the front as it nears the producing fracture. The longer the producing fracture, the greater is the degree of linearity, desirable for sweep efficiency, finally approached by the flood front. This degree of linearity may be described as the extent to which the flood front is uniformly flat. A line-drive flood would yield a front of the highest degree of linearity, completely linear.

For L/W = .10, the flood pattern resembles the unfractured five-spot flood and the 74 percent sweep efficiency is close to the 73 percent given by the latter. Effects of the short injection fracture are seen on early shape of the front, but the producing fracture induces little linearity in the front and "cusping" is evident at breakthrough. For L/W = .20, cusping has been reduced by the longer fracture and the sweep efficiency increases to 76 percent. Sweep efficiency is increased to 85 percent for a value of L/W = .30. The flood front is flattened somewhat by the longer producing fracture. For L/W = .40, the flood front is highly linear at breakthrough and a sweep efficiency of 93 percent is achieved. Completely fractured boundaries, given by L/W = .50, would intuitively give 100 percent sweep efficiency.

The orientation of fractures is the most favorable for waterflooding since it is perpendicular to the flooding direction. Previous investigators (4-6) have studied some aspects of this case but with only one type of well fractured, never both injection and producing wells. The results of these past studies show sweep efficiency to decrease when only one type of well is fractured. A more complete discussion of these findings may be found in Reference 1. The present investigation clearly shows the advantage of fracturing both injection and producing wells located such that 0° orientation exists.

Oriented Fractures

Sweep efficiency increases as the angle of fracture orientation decreases. The limiting factor for the case of oriented fractures is the length of the shortest streamline in the system, i.e. the path along which breakthrough occurs. As the fractures are oriented at greater angles, the limiting streamline from injection well (or fracture) to producing well (or fracture) decreases in length and allows earlier breakthrough. Earlier breakthrough, in turn, limits the growth of the flood pattern and yields lower sweep efficiencies.

For all orientations, two distinct flood patterns are observed. The first, and larger, pattern is in the vicinity of the "interior" injection fracture, that fracture which lies partially within the five-spot. The second flood pattern originates at the "exterior" injection fracture, that fracture lying completely without the five-spot. In all cases, the flood pattern surrounding the interior fracture is the larger. It is noted that the term "breakthrough" used in conjunction with oriented fractures refers to earliest breakthrough, from the interior injection fracture, and not for breakthrough of both of the two distinct flood patterns. As the angle of fracture orientation increases, the ratio of the exterior fracture pattern area to that of the interior fracture pattern diminishes.

Due to the relation between lengths of limiting streamlines and relative sweep efficiencies, the 45° fracture orientation yields the lowest sweep efficiency, 26 percent. Breakthrough occurs along the linear flowpath connecting the interior injection fracture to the producing fracture. The short time to breakthrough allows the flood front to advance only a small distance from the exterior injection fracture. Breakthrough occurs at the tip of the producing well fracture. An immediate deduction from the above data is that increased sweep efficiency is possible by eliminating the fracture in the producing well. A five-spot pattern having only injection wells fractured should gain in sweep efficiency by virtue of the delay in time to breakthrough. This deduction is verified by past investigations of patterns having only injection wells fractured. Dyes et al (5) obtained a sweep efficiency of 45 percent for fracture that would be slightly shorter (L/W = .18 rather than .20) when adopting the basis for L/W measurements used in this study and a mobility ratio of 1.1. A potentiometric study by Simmons et al (4) for a similar case (mobility ratio of one, L/W = .15) yielded 50 percent

sweep efficiency. This smaller L/W value indicates another method for increasing sweep efficiency when fracture orientations are near 45°: limit the length of the injection well fractures to delay time to breakthrough but still obtain benefits from the fracturing such as increased injectivity. Eliminating the fracture in the producing well would, of course, reduce the productivity for a given well-to-well pressure drop.

Several practical applications result from these investigations of oriented fractures. By setting proper five-spot boundaries such that the fractures are oriented at 0°, the operator will obtain maximum recovery. For such an orientation, the longest possible fracture length in both the injection and producing wells is desirable, giving higher sweep efficiency and thus greater recovery to breakthrough. In case knowledge of the fracturing plane of the reservoir is either inconclusive or not obtainable, it is advisable to: (1) limit the length of fractures through suitable planning of fracturing treatments; and, (2) avoid completely the fracturing of the producing wells.

CONCLUSIONS

From this study of the flow behavior of a pattern displacement process in which all wells are fractured, the following conclusions can be drawn:

1. With several limiting conditions, the potentiometric model described herein was found to satisfactorily simulate the field-size prototype and yielded data that, when empirically correlated, supplied the necessary boundary conditions for computational calculations of sweep efficiency. The potentiometric model also directly provided equipotential distributions from which flood front locations and resulting sweep efficiencies were determined.

2. For a given fracture length, breakthrough sweep efficiency of a normal five-spot having all wells fractured decreases as angle of fracture orientation increases. The greatest sweep efficiency results from a fracture orientation of 0°, and the manner in which it decreases as the fracture angle increases to 45° is illustrated.

3. For the most favorable fracture orientation of 0°, sweep efficiency at breakthrough increases as fracture length is increased, the greatest increases occurring at values of L/W greater than .20 in nearly uniform increments. Sweep efficiency is slightly increased at L/W values equal to, or less than, .20.

ACKNOWLEDGEMENT

The authors would like to acknowledge the original suggestion of E. T. Heck, Minard Run Oil Company, Bradford, Pennsylvania that this particular investigation be carried out. Dr. Heck has been a strong proponent of the concept of directionally oriented fractures and has used this concept to advantage in field operations in the Penn Grade Area.

BIBLIOGRAPHY

1. Hansford, J. T., "Effect of Multi-Well Vertical Fractures on Pattern Fluid Displacement Behavior," M.S. Thesis, The Pennsylvania State University (1966).

2. Davis, D. S., Nomography and Empirical Equations, Reinhold, New York (1962).

3. McCarty, D. G. and Barfield, E. C., "The Use of High Speed Computers for Predicting Flood Out Patterns," Trans. AIME (1958) 213, 139.

4. Simmons, J., Landrum, B. L., Pinson, J. M. and Crawford, P. B., "Swept Areas After Breakthrough in Vertically Fractured Five-Spot Patterns," Trans. AIME (1959) 216, 73.

5. Dyes, A. B., Kemp, C. E. and Caudle, B. H., "Effect of Fractures on Sweep-Out Pattern," Trans. AIME (1958) 213, 245.

6. Hartsock, J. H., "Effect of Vertical Fractures on Sweep Efficiency of a Normal Five-Spot Pattern," M.S. Thesis, The Pennsylvania State University (1959).

APPENDIX A

Empirical Correlations of Boundary Pressure Values

0° Fracture Orientation (see Figure 2)

Sides A-B and C-D:

$$P = A + (.05 + 0.1\ L/W)\left[\cosh\left(\frac{3.6\ x}{6 - 10\ L/W}\right) - 1\right]$$

where

$$A = .52 + .0021 \cosh(15.5\ L/W) - .004 \exp(31\ L/W - 0.93)$$

Sides A-D and B-C:

$$P = A + .05 \left[\cosh (.6 |x|) - 1\right] \text{ for unfractured case}$$

$$P = .2x + A \left[1.10 \exp (-.471 |x|) - .10\right] \text{ for fractured case}$$

where

$$A = .53 - \left[\cosh (3 L/W) - 1\right]\left[.282 \exp (.66 L/W)\right] \text{ for both cases.}$$

For the above:

P = value of pressure on boundary

x = distance toward injection well from center of side

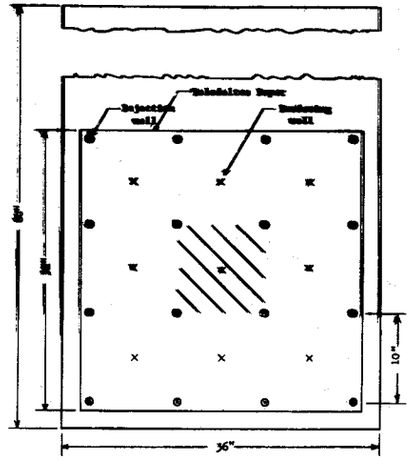

Figure 1 - Experimental Reservoir Model
(Confined Five-Spot of Investigation
Shown by Shaded Area)

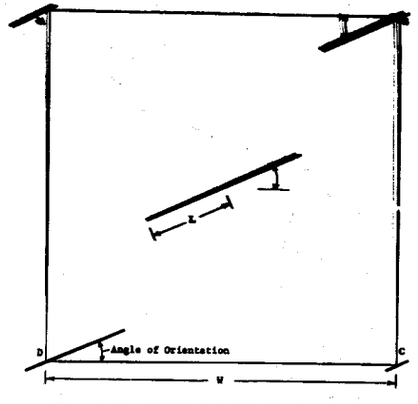

Figure 2 - Geometric Model of a Five-Spot Pattern

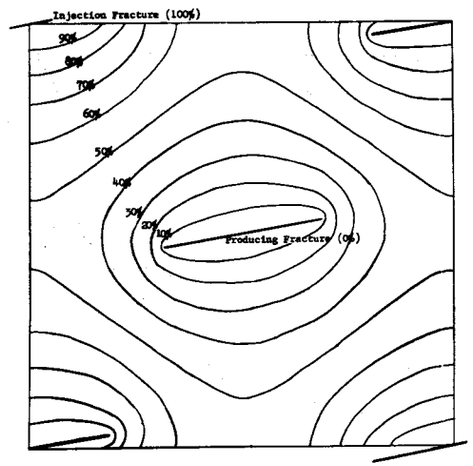

Figure 3 - Equipotential Distribution for a Fractured
Five-Spot, Angle of Orientation = 10°
(L/W = .20)

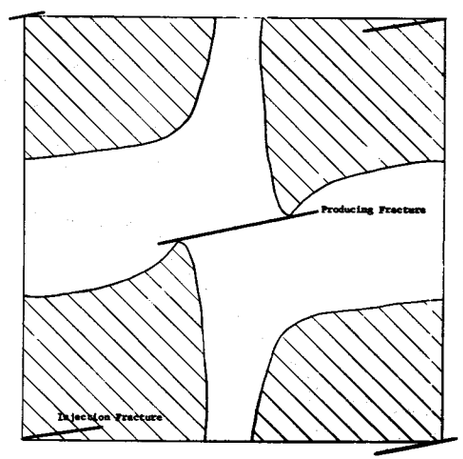

Figure 4 - Location of Flood Front at Breakthrough for a
Fractured Five-Spot, Angle of Orientation = 10°
Sweep Efficiency = 39%
(L/W = .20)

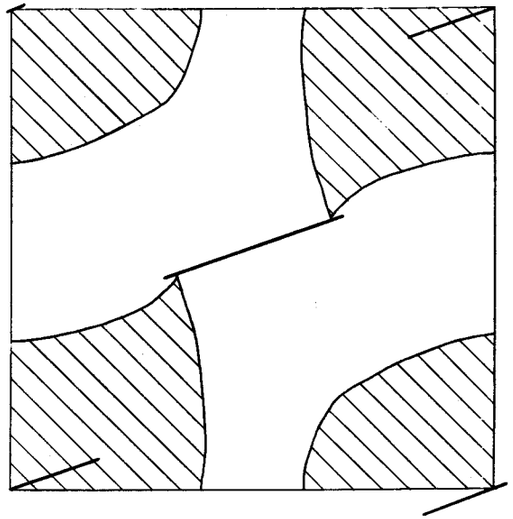

Figure 5 - Location of Flood Front at Breakthrough for a Fractured Five-Spot, Angle of Orientation = 20° Sweep Efficiency = 46% (L/W = .20)

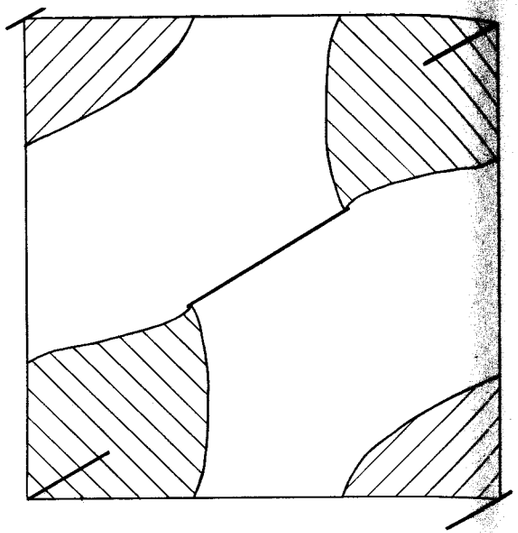

Figure 6 - Location of Flood Front at Breakthrough for a Fractured Five-Spot, Angle of Orientation = 30° Sweep Efficiency = 35% (L/W = .20)

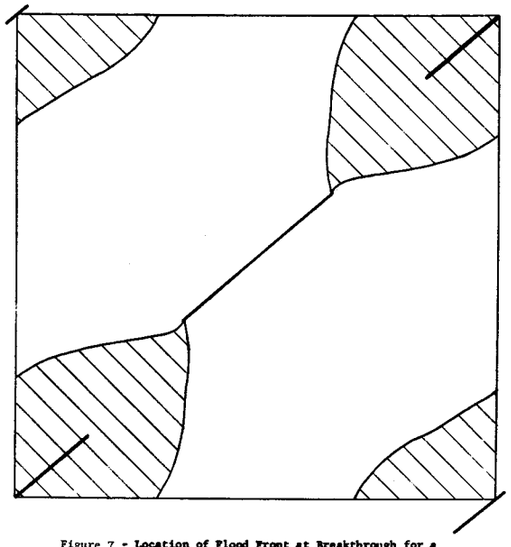

Figure 7 - Location of Flood Front at Breakthrough for a Fractured Five-Spot, Angle of Orientation = 40° Sweep Efficiency = 28% (L/W = .20)

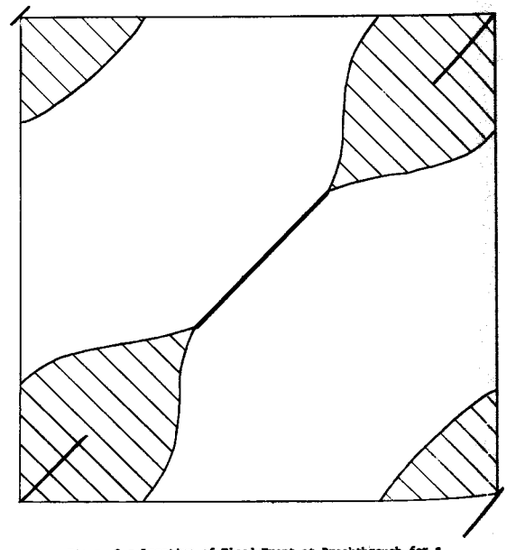

Figure 8 - Location of Flood Front at Breakthrough for a Fractured Five-Spot, Angle of Orientation = 45° Sweep Efficiency = 26% (L/W = .20)

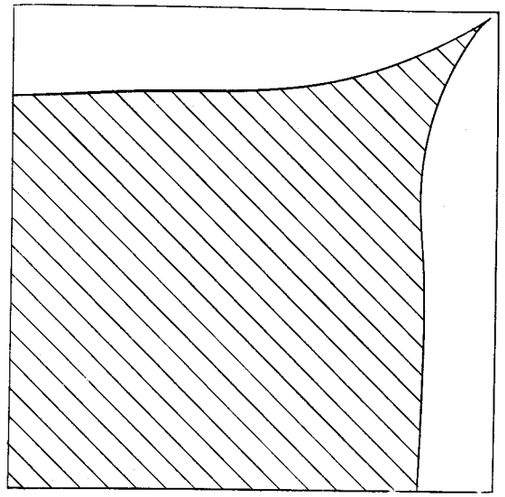

Figure 9 - Location of Flood Front at Breakthrough for a Fractured Five-Spot Quadrant, L/W = 0.0 Breakthrough Sweep Efficiency = 75%

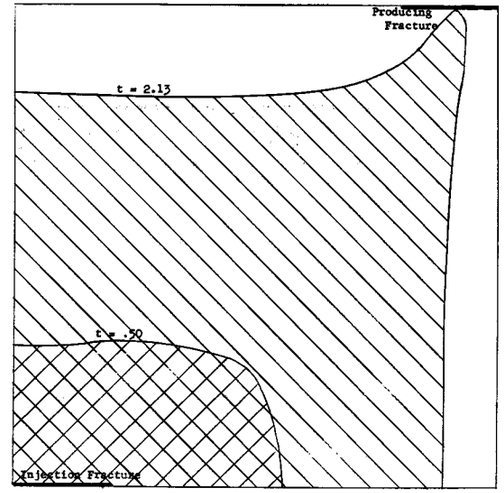

Figure 10 - Location of Flood Front at Relative Times for a Fractured Five-Spot Quadrant, L/W = .10 Breakthrough Sweep Efficiency = 74% (Angle of Orientation = 0°)

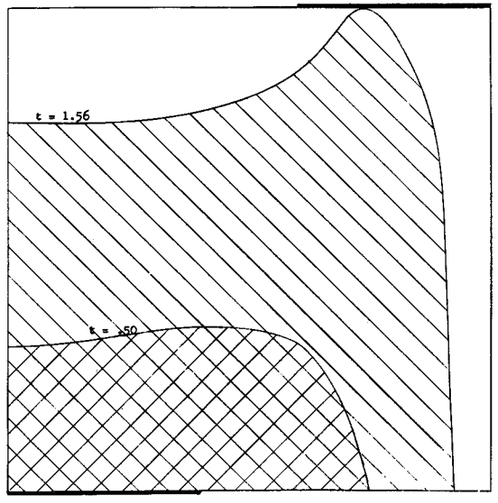

Figure 11 - Location of Flood Front at Relative Times for a Fractured Five-Spot Quadrant, L/W = .20 Breakthrough Sweep Efficiency = 76% (Angle of Orientation = 0°)

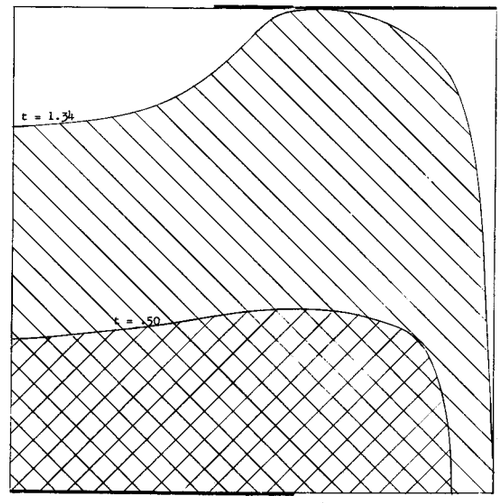

Figure 12 - Location of Flood Front at Relative Times for a Fractured Five-Spot Quadrant, L/W = .30 Breakthrough Sweep Efficiency = 85% (Angle of Orientation = 0°)

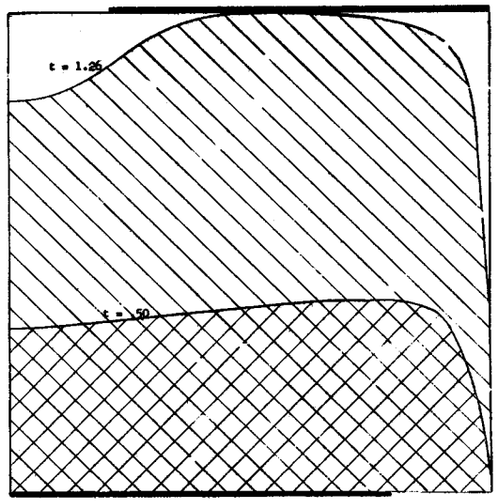

Figure 13 - Location of Flood Front at Relative Times for a Fractured Five-Spot Quadrant, L/W = .40 Breakthrough Sweep Efficiency = 93% (Angle of Orientation = 0°)

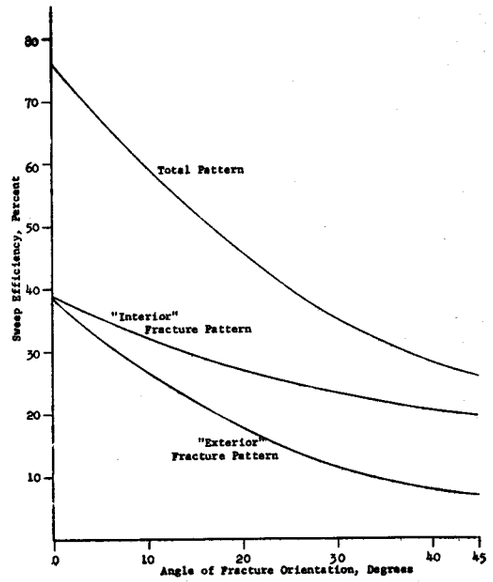

Figure 15 - Effect of Fracture Orientation on Sweep Efficiency of a Five-Spot Pattern, L/W = .20 (Flux Plot Results)

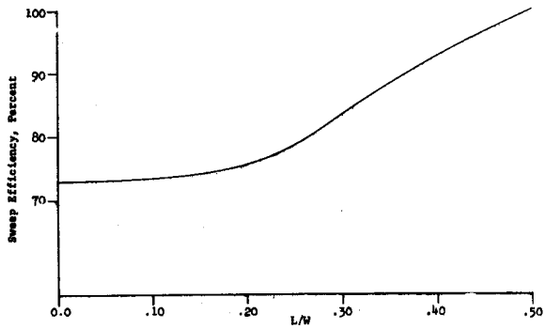

Figure 14 - Effect of Fracture Length on Sweep Efficiency of a Five-Spot Pattern, Angle of Orientation = 0° (Computer Results)

COMPUTATION OF SWEEP EFFICIENCY IN ALCOHOL FLOODING

Y. C. Chiao, S. M. Farouq Ali and C. D. Stahl

Abstract

A simple technique is described for calculating the sweep efficiency obtained in alcohol flooding in a five-spot flow pattern. The method is applicable to other areal flow problems involving direct line drive, seven-spot flow etc.

The technique described herein utilizes two simplifying approaches. The first of these is division of a flow pattern into channels, and the subsequent division of channels into cells of equal volume. The second feature is the use of the cell model to simulate alcohol slug displacement. The combination can be used for predicting the sweep efficiency, fluid production history, and the distribution of the unrecovered oil in a miscible displacement process such as alcohol flooding.

Computations were carried out to predict the sweep efficiency and displacement behavior in a five-spot flow pattern. The computed results were compared with the experimental and field data reported in the literature by various investigators. The agreement was generally good, thus indicating that the assumptions of constant boundary channels and of negligible material transport across the channels constitute good approximation of the physical situation.

Introduction

During the past decade numerous papers[1-5] have appeared on field and laboratory studies of miscible displacement for oil recovery. Several of these have dealt specifically with "alcohol displacement" or the "alcohol slug process", introduced by Gatlin and Slobod[1].

Alcohol displacement or alcohol flooding, as generally understood, involves the injection into the reservoir of a small volume or "slug" of a solvent (generally, a suitable alcohol), which is miscible with both the oil and water in the reservoir. Subsequently, the slug is driven by injection of water. The injected solvent slug, by virtue of its miscibility characteristics, effectively removes the capillary forces, responsible for the retention of the residual oil in a conventional waterflood. In this manner, the solvent slug displaces the oil and water in the reservoir more or less like a piston, and theoretically, 100% oil recovery can be obtained. In practice, however, the solvent tends to dissipate in the formation through convective mixing or dispersion. That is to say, there is no clearly defined solvent front. Rather, there is a "transition zone" within which the solvent concentration varies from 0 to 100%. Since the transition zone grows with time and distance traversed, the displacement efficiency is greatly impaired, and the oil recovery is low. Both laboratory[1-5] and field investigations[6] have confirmed the presence of this sort of behavior.

All investigations of alcohol flooding reported to date have been concerned with displacements in linear models of porous media. A few studies[7-10] of miscible displacement in areal patterns of various types have been conducted. Miscible displacement involves the use of two mutually soluble liquids, and thus bears only a limited similarity to alcohol flooding, in which two phase flow and phase equilibria must be considered.

The present paper outlines a simplified approach for determining the sweep efficiency in alcohol flooding. The computations included here are concerned with the displacement of a hydrocarbon and water by two different types of alcohols in a five-spot pattern. The technique is, however, equally applicable to other flow patterns. The computed results for the miscible regime are compared with experimental and field results of various investigators. The agreement is found to be good.

Mechanism of Alcohol Displacement

The mechanism of alcohol displacement, for the case where the alcohol is injected continuously, rather than in small amounts, has been discussed by Gatlin and Slobod[1], Taber, Kamath and Reed[2] and Holm and Csaszar[3]. Taber et al[2], in particular, presented a clear picture of the mechanism involved in the displacement process. They noted that the actual displacement mechanism is closely related to the phase behavior characteristics of the alcohol-hydrocarbon-brine system involved. Such ternary systems show a small region of mis-

cibility (i.e. compositions for which all three component systems are completely miscible) and a large region of immiscibility, wherein two phases, each containing all three components, coexist. Depending on the phase behavior involved, either of these phases would diminish in volume as increasing amounts of the liquid common to the two miscible pairs, i.e. the alcohol, are added. Taber et al[1] showed that if the oil-rich (oleic) phase decreases in volume, the alcohol displacement involved would be governed by a residual oil type mechanism. In this case, a certain proportion of the oil in place is left in the porous medium, which could be recovered only by a process of solution by the advancing alcohol as opposed to displacement. If a small alcohol slug is used, this quantity of oil would be unrecoverable. On the other hand, if the water-rich (aqueous) phase decreases in volume, the oleic phase remains continuous, and piston-like displacement of oil is ensured. The above theory neglects dispersion of alcohol in the oil and water, which would be present in both cases. Recent work by El-Saleh[11] has shown that in a slug type process, dispersion or convective mixing would largely modify the displacement mechanism outlined above, since the oil remaining in the porous medium would greatly accelerate the loss of miscibility of the slug material.

Examples of two typical alcohol-hydrocarbon-water systems, showing opposite phase behavior as far as displacement of oil in a porous medium is concerned, are presented in Figures 1 and 2.

Figure 1 shows the isopropyl alcohol-Soltrol-brine system, characterized by a plait point on the oil side. The displacement of oil in this case would be incomplete due to the deposition of an immobile oleic phase in the porous medium. Figure 2 shows the tertiary butyl alcohol-Soltrol-brine system, having the plait point on the water side. The displacement of oil in this case would be "piston-like". It should be noted that a brine is substituted for water in order to prevent the swelling of clays in the porous medium used. However, as shown by Farouq Ali[5], the use of brine (2% $CaCl_2$ by weight) rather than water is indispensable in the second ternary system to obtain the desired phase behavior.

Both of the systems depicted by Figures 1 and 2 were employed in the calculations of sweep efficiency discussed in the present article.

Sweep Efficiency in Miscible Displacement

Before discussing the calculation of sweep efficiency in alcohol flooding, it is instructive to consider the previous investigations of sweep efficiency in miscible displacement (involving two mutually soluble liquids), since the two processes, though different, are closely related.

Some of the earlier laboratory investigations of sweep efficiency in waterflooding involved the use of miscible liquids. Within limitations, these would more appropriately represent sweep efficiency in miscible displacement. Some caution must be exercised

in judging the results, however, since the models were not dimensionally scaled for miscible displacement. The early work of Dyes, Caudle and Erickson[7] among others falls into this category. Their findings regarding the influence of the mobility ratio on waterflooding are equally applicable to miscible displacement. They found that the sweep efficiency showed a sharp decrease with an increase in the mobility ratio, which, in this case equalled the ratio of the viscosity of the displaced liquid to that of the displacing liquid.

Habermann[8] studied the efficiency of miscible displacement, using artificially consolidated sand models. He found a decrease in sweep efficiency, both on the bases of the area contacted and the volume injected, with an increase in the mobility ratio. Moreover, he found that changes in the model size, rate and direction of flow, and permeability did not produce any significant changes in the sweep efficiency.

Blackwell, Rayne and Terry[12] found that oil recoveries at breakthrough decreased from values of over 96%, for a mobility ratio of unity, to values as low as 13%, for a mobility ratio of 383. They observed excessive viscous fingering at the higher mobility ratios.

A field investigation of sweep efficiency in miscible displacement has been reported by Greenkorn, Johnson and Haring[9]. Mobility ratios of 0.1, 1 and 10 were employed in this test. They concluded that the sweep efficiency was a pronounced function of the mobility ratio, thus indicating that the viscous fingering as observed

in simple laboratory models, occurred in the field as well.

An additional complication in miscible displacement is introduced through vertical sweep efficiency arising from the segregation of the solvent and the in-place fluids, due to the differences in the densities of the fluids. Very little information is available on this effect. Enright[13] has considered vertical sweep in LPG injection.

Computation of Sweep Efficiency in Alcohol Flooding

The present scheme for calculating sweep efficiency in alcohol flooding in an areal pattern involves two basic concepts. The first of these is the distribution of a flow pattern into flow channels, and the subsequent division of the flow channels into cells of equal volumes. This type of scheme has been utilized by Higgins and Leighton[14] for calculating sweep efficiency in waterflooding. The flow of the fluids is then assumed to be confined to the various channels, proceeding from cell to cell, in a step-wise manner. Since the choice of the channels is based upon the streamline pattern involved, the latter must be obtained by an experimental or analytical technique, for the given mobility ratio. Following the procedure of Craig, Geffen and Morse[15], the mobility ratio in a waterflood can be taken to be constant. However, in an alcohol displacement it varies from point to point, due to the presence of a transition zone. In this case mobility ratio is defined as

$$M = \frac{k_{ro}/\mu_{ol}}{k_{rw}/\mu_{aq}}$$

where k_{ro} and k_{rw} are the relative permeabilities to oil and water, respectively, while μ_{ol} and μ_{aq} are the viscosities of the oleic and the aqueous phases, respectively. It is tacitly assumed that the relative permeabilities to the conjugate phases are the same as those for the corresponding oil-water system.

Therefore, it follows that, strictly speaking, the flow channels in an alcohol displacement are time-dependent. However, the shape of the streamline pattern, though depending upon the mobility ratio, changes rather slowly with an increase in the mobility ratio. In fact, Higgins and Leighton[14] successfully used the same streamline pattern for mobility ratios ranging from 0.083 to 754. The agreement between their calculations and those conducted on the basis of a mathematical model was excellent. In view of the above considerations, the streamline pattern employed by Higgins and Leighton was used for all alcohol flood computations conducted in this study. In this way it was possible to utilize the geometrical shape factors for the individual cells as reported by Higgins and Leighton[16] in a more recent publication.

The second concept employed in the present calculations is that of the "cell model" for simulating an alcohol displacement. Such a model has been successfully employed by Farouq Ali and Stahl[17,18] to simulate alcohol flooding. El-Saleh[11] used the same model for simulating the alcohol slug process, and investigated the slug breakdown behavior. A brief description of the cell model used will be given in the next section.

Cell Model for Simulating Alcohol Displacement

Representation of a flow process in a porous medium by means of a cell model is equivalent to dividing the process into a number of discrete stages. Aris and Amundsen[19] utilized the concept of a number of cells connected in series to simulate diffusion. Deans[20] proposed a three-parameter cell model of miscible displacement in a porous medium, and showed analytically that, if certain conditions were met, the model simulated miscible displacement. Donohue[21] used a similar model for simulating alcohol displacement. A more general model has been proposed by Farouq Ali and Stahl[17,18]. A brief description of this model will be given below, since it was used in the present computations.

It is assumed in the cell model of Farouq Ali and Stahl, that the porous medium can be represented by means of N cells connected in series. The number of cells, N, is the only unknown involved. However, it can be chosen on the basis of the length of the porous medium. Next, each cell is assumed to contain immovable oil and water fractions, being equal to the residual oil and irreducible water saturations, respectively, characteristic of the porous medium under consideration. This is a logical assumption, considering that the same fractional volumes represent the immovable saturations in a porous medium. If the volume of each cell is taken as unity, the remaining cell volume is termed the movable volume.

In simulating alcohol displacement, one movable cell volume of alcohol is initially injected into the first cell, while the displaced

material is transferred into the next cell, and the process is continued until an equal volume is produced from the last cell. The injected alcohol is now allowed to reach phase equilibrium with the resident fluids. A second movable volume of alcohol is then injected into the first cell, and the whole procedure is repeated. This process is continued until a desired volume of alcohol is injected, following which, injection of water may be initiated, if so desired.

The above cell model has been tested for different types of alcohol displacements, and has been found to simulate the formation of a stabilized bank, as well as other typical features of experimental data.

The application of the above model requires the representation of ternary phase behavior data by means of mathematical equations. This can be accomplished by the simple technique developed by Farouq Ali and Stahl[22]. Similarly, the relative permeability data as well as the three-component viscosity data must also be represented by means of mathematical equations. All of the information thus formulated is employed in a computer program for conducting alcohol displacement calculations.

Mathematical Representation of Phase Equilibrium, Permeability and Viscosity Data

The ternary systems employed in the present investigation are depicted in Figures 1 and 2, which also give the equations of the segments of the binodal curves and the tie lines. Details of such representation have been reported elsewhere[22].

The relative permeability data used in the present computations were taken from Leverett[23] and Muskat[24] for typical unconsolidated and consolidated porous media, respectively. The respective curves are shown in Figures 3 and 4. The curves were fitted by equations of the following type:

$$k_{rw} = a_1(S_w - S_{wir}) + b_1(S_w - S_{wir})^2 + c_1(S_w - S_{wir})^3$$

$$k_{ro} = a_2(S_o - S_{or}) + b_2(S_o - S_{or})^2 + c_2(S_o - S_{or})^3$$

where

k_{rw} = relative permeability to water (or aqueous phase), fraction.

k_{ro} = relative permeability to oil (or oleic phase), fraction.

S_w = water (or aqueous phase) saturation, fraction.

S_o = oil (or oleic phase) saturation, fraction.

S_{wir} = irreducible water (or aqueous phase) saturation.

S_{or} = residual oil (or oleic phase) saturation.

and the constants a_1, b_1, c_1, a_2, b_2 and c_2 were as follows:

	Unconsolidated Sand	Consolidated Sandstone
a_1	-0.129	0.0156
b_1	1.800	-0.917
c_1	-0.125	3.000
a_2	0.083	0.993
b_2	1.000	-4.900
c_2	0.417	32.600
S_{or}	0.100	0.420
S_{wir}	0.200	0.280

For saturations of the aqueous or the oleic phase below the respective critical saturation (S_{wir} or S_{or}), the relative permeability to the particular phase involved was taken to be zero.

The viscosities of the two-phase, three-component mixtures were taken from the data presented by Farouq Ali[17], for the two alcohol-hydrocarbon-brine systems studied. The viscosities of a number of miscible, three-component mixtures were measured and the data filled by a simple relationship of the following type:

$$\mu_m = A + Bx + Cy$$

where,

μ_m = viscosity of a miscible mixture, centipose.

x = fraction of oil in the mixture.

y = fraction of alcohol in the mixture.

The experimental data as well as the mathematical approximations of the same are presented in Figures 5 and 6 for isopropyl alcohol-Soltrol-brine and tertiary butyl alcohol-Soltrol-brine systems, respectively. While more complicated schemes can be devised for representing the viscosity data involved, the mathematical expressions given in Figures 5 and 6 were considered to be sufficiently accurate for the computer program, over the variable ranges involved.

Calculation of the Resistance of a Flow Channel

The present scheme for computing the sweep efficiency in alcohol flooding essentially considers an octant of a five-spot pattern,

because of the eight-fold symmetry. Figure 7 shows a quadrant of a five-spot, divided into two sets of four flow channels. Each of the flow channels is divided into 40 equal volume cells. It is assumed that a constant pressure differential is maintained between the injection and the production wells. Under these circumstances, the flow rate in a given channel will depend on the saturations and viscosities of the fluids in each cell within the channel, in addition to the geometrical shapes of the individual cells. This means that, as alcohol displacement calculations are carried out for a given channel, a complete account must be kept of the compositions and the viscosities of the fluids occupying each cell of the channel. Given the relative permeabilities and viscosities of the two phases, the geometrical shape factors would determine the rate of flow. The geometrical shape factor, G, introduced by Higgins and Leighton[14,16], is defined as the ratio of the average length, L, of the cell, to its average width, W. It is tacitly assumed that the porous medium involved has a uniform thickness. Then, the flow rate q_i at time step i, in cubic feet per day, is given by

$$q_i = \frac{6.33\ HK\ \Delta P}{N \sum_{n=1} \frac{G_n}{\frac{k_{rw}}{\mu_w} + \frac{k_{ro}}{\mu_o}}}$$

where

K = absolute permeability of the porous medium, millidarcy.

ΔP = pressure differential between the injection and production wells, psi.

Subscripts i and n refer to the number of time step and the cell no., respectively.

Computational Procedure

Having expressed all the data in mathematical form, the computational procedure essentially consisted in conducting alcohol displacement in each channel, and then combining the individual production histories, after normalizing the data on the basis of equal times.

Since the cell model approach requires that the same volume (the movable volume), or its multiples, be injected at any time step, it was necessary to calculate the flow rate at a given time, and then compute the time needed to inject the movable volume. This time was added to the previous figure for the cumulative time, and the new flow rate was calculated for the next time step. In this manner, four different fluid production histories were obtained for the four representative flow channels. These data were then reprocessed through interpolation so that all production figures referred to a common time scale. Finally the data were combined, allowing for the fraction of the total five-spot area represented by channels of each type, to obtain the overall production behavior.

The sweep efficiency was computed on the bases of the first appearance of the injected alcohol (2% alcohol in the invaded cell) and the first appearance of a zone of miscibility. Furthermore, the cumulative production of the fluids in place was also determined for various times.

At the end of each run, a material balance check was performed, and the areal distribution of the oil left in the formation was determined.

A lengthy computer program was written for performing the computations described above on an IBM 7074 digital computer. On account of severe storage limitations, six tape unite had to be employed for loading the core storage at the appropriate moment. A typical computer run took 500 seconds. The computational procedure is described schematically in Figure 8.

Results of Computations

In waterflood operations, there is a distinct front (neglecting the variable zone due to capillary effects), and therefore, sweep efficiency can be defined on the basis of the area invaded by the water front at any given time. For unit mobility ratio, the sweep efficiency at breakthrough is known to be about 72%.

In alcohol flooding, there is no distinct front, and as mentioned in the previous section, it was necessary to define the sweep efficiency on an arbitrary basis. Two criteria were employed - one on the basis of the presence of a trace of alcohol (2% by volume), and the other on the basis of the first appearance of a single miscible phase in a cell. In addition, an indirect measure of the sweep efficiency was provided by the plots of cumulative oil production as functions of cumulative fluid injection.

All computations were based upon a five-spot pattern having a side of 400 feet and a formation thickness of 50 feet. Porosity and permeability were assumed to be 20% and 200 md, respectively. The pressure differential was maintained constant at a value of 50 psi.

Figure 9 shows the computed oil and alcohol production curves for the individual channels. It is seen that alcohol breakthrough occurred earliest in channel 1 (containing the shortest path between the injection and production wells), and successively later in the other channels. This type of behavior was observed in all of the 100 or so computer runs conducted.

Figures 10 and 11 depict plots of sweep efficiency vs pore volumes injected, for a number of slug sizes, for the isopropyl alcohol-Soltrol-brine and tertiary butyl alcohol-Soltrol-brine systems, respectively. The sweep efficiency at breakthrough, both on the basis of 2% alcohol concentration and the miscible zone front, was found to be 77% in the case of isopropyl alcohol, and 78% in the case of tertiary butyl alcohol. The anomalously large sweep efficiency, when the 2% alcohol concentration is used as a basis, is attributed to the excessive dispersion of alcohol. On the basis of Figures 10 and 11, it can be concluded that the areal sweep efficiency in alcohol flooding does not depend on the phase behavior of the alcohol-hydrocarbon-brine system involved. One might expect the sweep efficiency to be much higher in the case of the tertiary butyl alcohol on account of its higher viscosity. However, the attainment of miscibility in this

system requires a higher alcohol concentration than in the corresponding isopropyl alcohol system, so that the advance of the miscible front is slower.

Figure 12 shows plots of sweep efficiency vs pore volumes injected, based upon the miscible zone front, for the isopropyl and tertiary butyl alcohol systems. Also shown is an experimental curve for miscible displacement at a mobility ratio of unity, as reported by Habermann[8]. The dashed curve shows the approximate values of sweep efficiency as obtained experimentally in a displacement study, employing isopropyl alcohol. The agreement between the computed and the experimental values is seen to be reasonably good.

Oil Recovery Behavior

Figures 13 to 18 show computed cumulative oil recoveries for the two ternary systems studied. Figures 13 and 14 show plots of the cumulative oil recovery vs pore volumes injected, for the isopropyl and tertiary butyl alcohol systems, respectively. A comparision of the curves shows that oil recovery in the case of the tertiary butyl alcohol is always higher. In fact, a 29.5% slug of isopropyl alcohol recovered as much oil as a 14.1% slug of tertiary butyl alcohol. It should be made clear that although the areal sweep efficiencies in the case of the two alcohols were almost identical, the more favorable phase behavior of the tertiary butyl alcohol led to greater recovery from the area contacted.

The oil recovery behavior is better seen from Figure 15, which compares the data for the two ternary systems. It is interesting to note that, unlike a linear system, continued injection of either alcohol led to an increase in the cumulative oil recovery at a slow pace, for slug sizes ranging from 40 to 100%. The reason for such behavior is that most of the slug material continues to flow through the low-resistance channels, while the outer two channels are affected only to a limited extent. This is evident from Figures 16 and 17, which show the distribution of the residual oil at the breakthrough of the miscible zone in the production well, for isopropyl alcohol and tertiary butyl alcohol, respectively. In particular, the amount of oil present in outer channels, in the case of isopropyl alcohol, is much greater.

Figure 18 compares the computed behavior of the total production of in-place fluids with the field data reported by Greenkorn et al[9]. The computed data are for the tertiary butyl alcohol system, for a slug size in excess of one pore volume. Thus, the alcohol displacement may be looked upon as miscible displacement of oil and water by tertiary butyl alcohol. The resulting curve (solid line) is seen to fall close to the field test curve for a mobility ratio of 0.1. The mobility ratio in the alcohol displacement was approximately 0.3 with respect to the oil, and 0.2 with respect to water. Thus, the computed behavior follows the expected trend. It should be noted, however, that the computed behavior is not as favorable as it seems to be,

because macroscopic permeability heterogeneities were present in the field. It is conceivable, then, that the agreement would not have been as good if the field test were conducted in a homogeneous formation.

Conclusions and General Comments

The technique presented above for the computation of sweep efficiency in an alcohol flood seems to be reliable and sufficiently accurate, on the basis of comparison of the computed results with rather limited experimental data. The agreement between the computed and experimental data can be improved considerably by use of a variable cell model, representing a varying rate of mass transfer, as proposed by Farouq Ali[17]. Such a model has been shown to simulate experimental tests in a linear system with good accuracy.

The number of cells used in the above computations was taken as 40, since in this way it was possible to use the geometrical shape factors presented by Higgins and Leighton[16]. Work is presently in progress for generating the shape factor data for any number of cells. This would permit the use of the variable cell model, and allow greater flexibility in the choice of the number of cells.

One of the advantages of the present computational scheme is that the areal distribution of the formational permeability can be varied in any desired manner. As shown by Greenkorn et al[9], permeability variations must be incorporated in the model, in order that the model predictions may simulate the field situation.

The limitations of the cell model, as discussed in detail by Farouq Ali[17], apply to all the computed data discussed. In particular, it should be noted that in a field test of alcohol flooding excessive fingering would be present, so that the sweep efficiency and oil recovery would be lower than those predicted by the model.

References

1. Gatlin, C. and Slobod, R. L.: "The Alcohol Slug Process for Increasing Oil Recovery", Trans. AIME (1960) 219, 46.

2. Taber, J. J., Kamath, I. S. K. and Reed, R. L.: "Mechanism of Alcohol Displacement of Oil from Porous Media", Trans. AIME (1961) 222, 195.

3. Holm, L. W. and Csaszar, A. K.: "Oil Recovery by Solvents Mutually Soluble in Oil and Water", Trans. AIME (1962) 225, II-129.

4. Houshmand, P.: "A Study of Effect of Rate and Slug Size on Fluid Displacement by Alcohol in a Consolidated Core", M.S. Thesis, The Pennsylvania State University, 1962.

5. Farouq Ali, S. M.: "A Study of Some Ternary Systems - Alcohol-Water-Hydrocarbon", M.S. Thesis, The Pennsylvania State University, 1962.

6. Nielsen, R. F., Danielson, H. H. and Paynter, W. T., "Calculations on Alcohol Field Trial", Presented at the 24th Technical Conference on Petroleum Production, The Pennsylvania State University, October 23-25, 1963, 243.

7. Dyes, A. B., Caudle, B. H. and Erickson, R. A.: "Oil Production after Breakthrough as Influenced by Mobility Ratio", Trans. AIME (1954) 201, 81.

8. Habermann, B.: "The Efficiency of Miscible Displacement as a Function of Mobility Ratio", Trans. AIME (1960) 219, 264.

9. Greenkorn, R. A., Johnson, C. R. and Haring, R. E.: "Miscible Displacement in a Controlled Natural System", Paper of 1965 Fall Meeting of AIME, Paper No. SPE 1232.

10. Mahaffey, J. L., Rutherford, W. M. and Matthews, C. S.: "Sweep Efficiency by Miscible Displacement in a Five-Spot", Paper SPE 1233, Presented at the 40th Annual Fall Meeting of SPE, Denver, Colorado, October 3-6, 1965.

11. El-Saleh, M. M.: "A Theoretical and Experimental Study of the Alcohol Slug Process", M.S. Thesis, The Pennsylvania State University, 1965.

12. Blackwell, R. J., Rayne, J. R. and Terry. W. M.: "Factors Influencing the Efficiency of Miscible Displacement", Trans. AIME (1959) 216, 1.

13. Enright, R. J.: "Are Miscible Floods Worth the Cost?", O.G.J., Dec. 11, 1961, 43.

14. Higgins, R. V. and Leighton, A. J.: "A Computer Method to Calculate Two-Phase Flow in any Irregularly Bounded Porous Medium", J.P.T., June, 1962, 679.

15. Craig, F. F., Jr., Geffen, T. M. and Morse, R. A., "Oil Recovery Performance of Pattern Gas or Water Injection Operations from Model Tests", Trans. AIME (1955) 204, 7.

16. Higgins, R. V., Boley, D. W. and Leighton, A. J.: "Aids to Forecasting the Performance of Water Floods", J.P.T., Sept., 1964, 1077.

17. Farouq Ali, S.M.: "Simulation of Alcohol Displacement in Porous Media by Use of Digital Computer Program", Ph.D. Thesis, The Pennsylvania State University, 1964.

18. Farouq Ali, S. M. and Stahl, C. D.: "Computer Models for Simulating Alcohol Displacement in Porous Media", SPE Journal, 1965, 5, 89.

19. Aris, R. and Amundson, N. R.: "Some Remarks on Longitudinal Mixing or Diffusion in Fixed Beds", AIChE. Jr. (1957) 3, 280.

20. Deans, H. A.: "A Mathematical Model for Dispersion in the Direction of Flow in Porous Media", S.P.E.J.; Vol. 3, No. 1, March, 1963, 49.

21. Donohue, D. A. T.: "A Mathematical Model to Simulate the Recovery of Oil and Water from Porous Media by the Injection of Solvents", Ph.D. Thesis, The Pennsylvania State University, 1963.

22. Farouq Ali, S. M. and Stahl, C. D.: "Mathematical Representation of Ternary Systems", Producers Monthly, Vol. 29, No. 6 (June, 1965) 17-18.

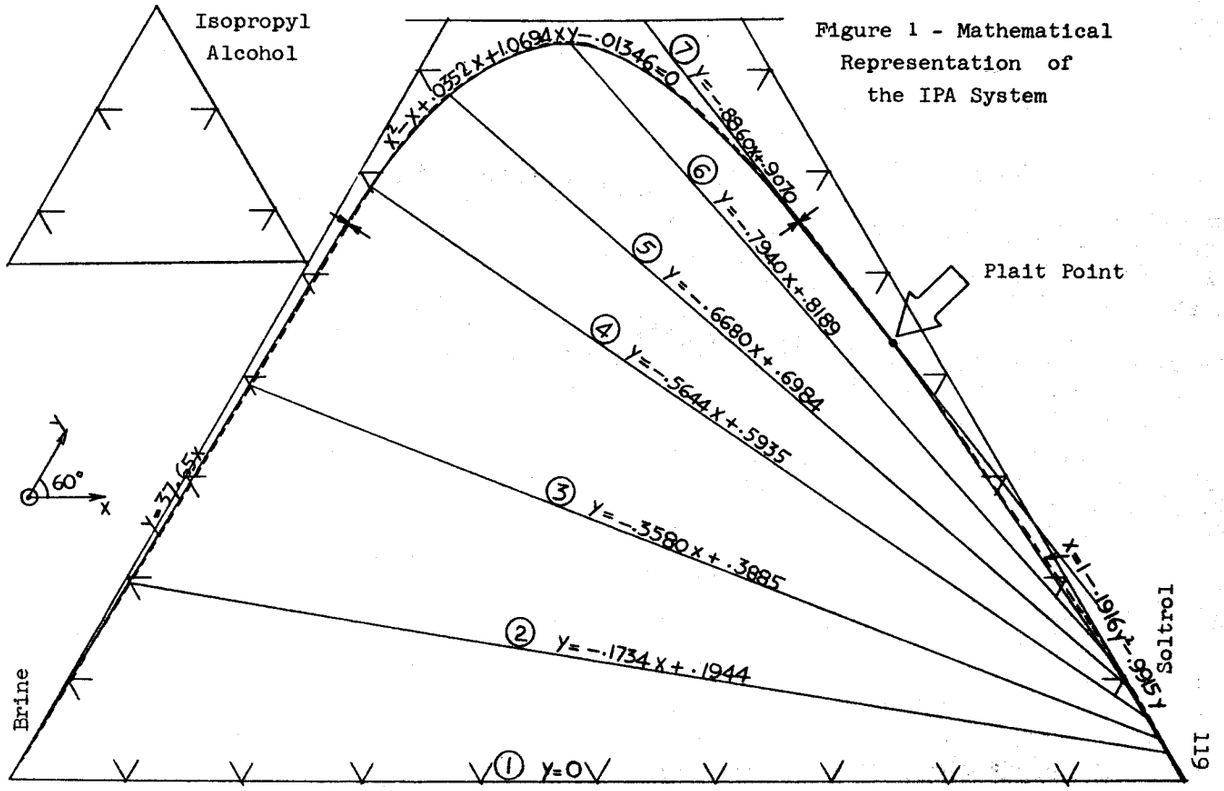

Figure 1 - Mathematical Representation of the IPA System

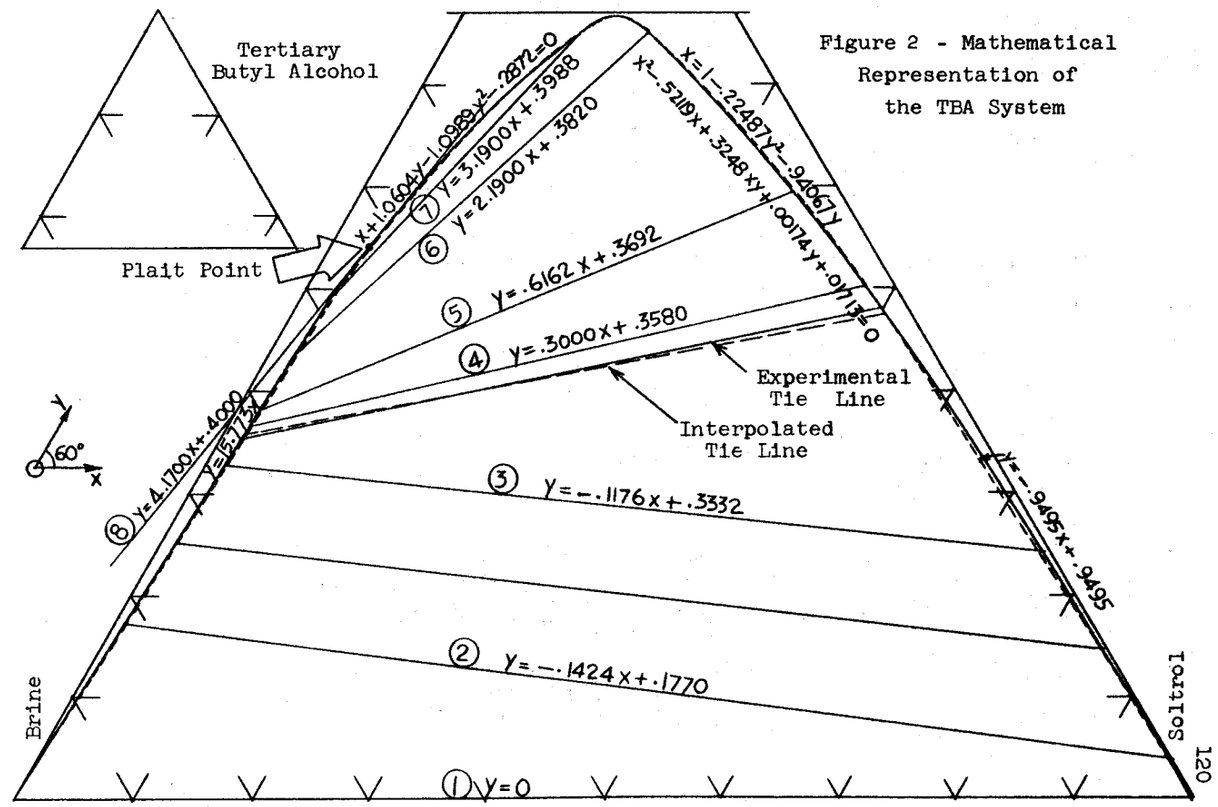

Figure 2 - Mathematical Representation of the TBA System

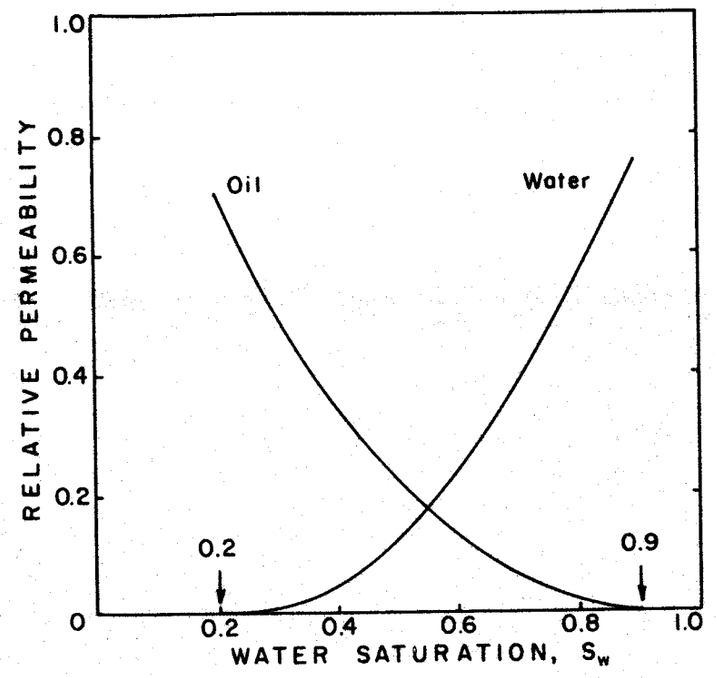

Figure 3

Relative Permeability Curve for Unconsolidated Sand, 100 to 200 Mesh Size (after Leverett)

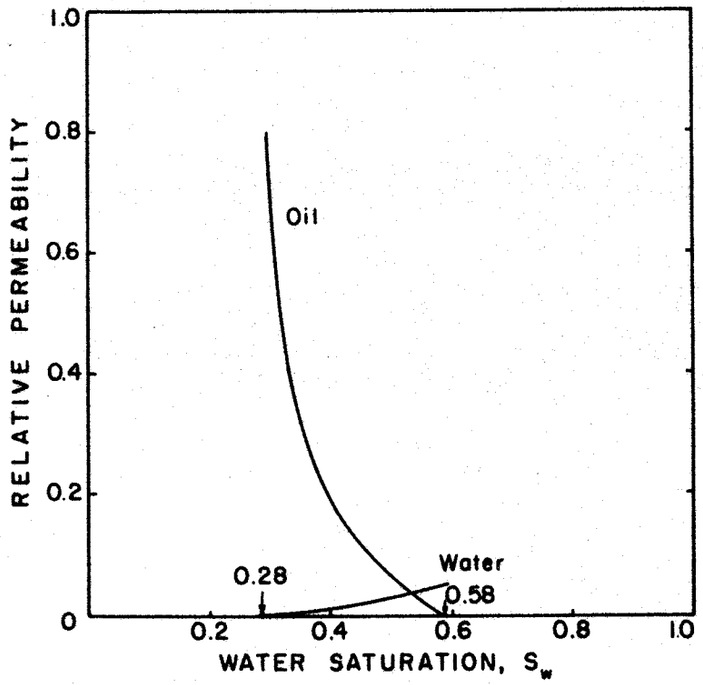

Figure 4

Relative Permeability Curve for a Second Venango Sandstone (after Muskat)

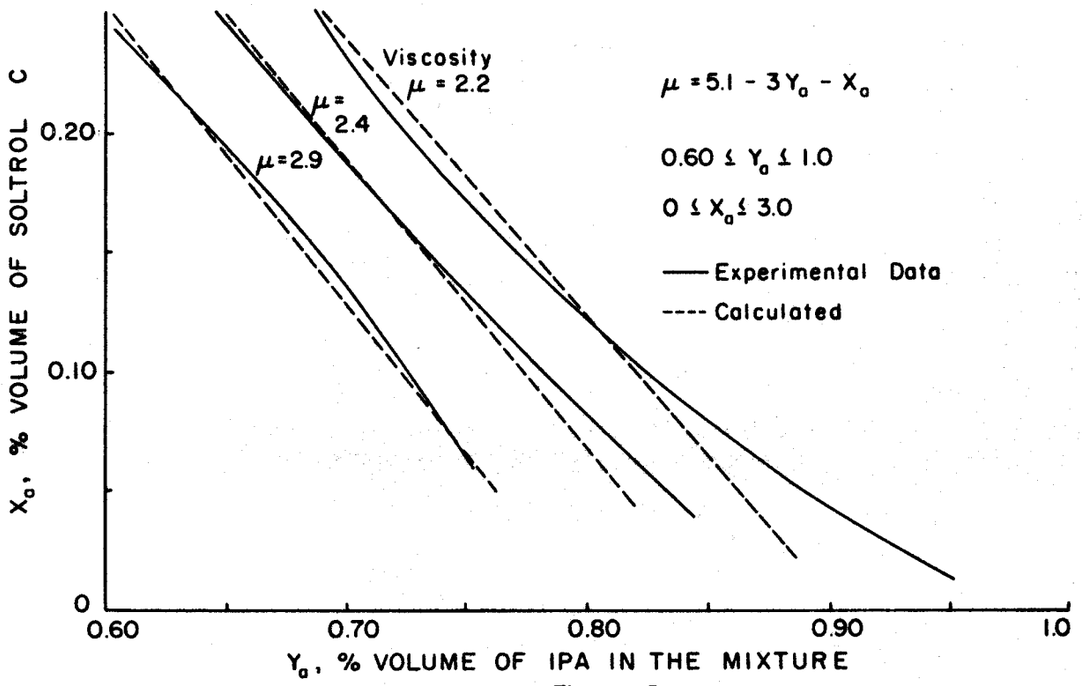

Figure 5

Correlation of Viscosities of Miscible Mixtures for the IPA-Soltrol-Brine System

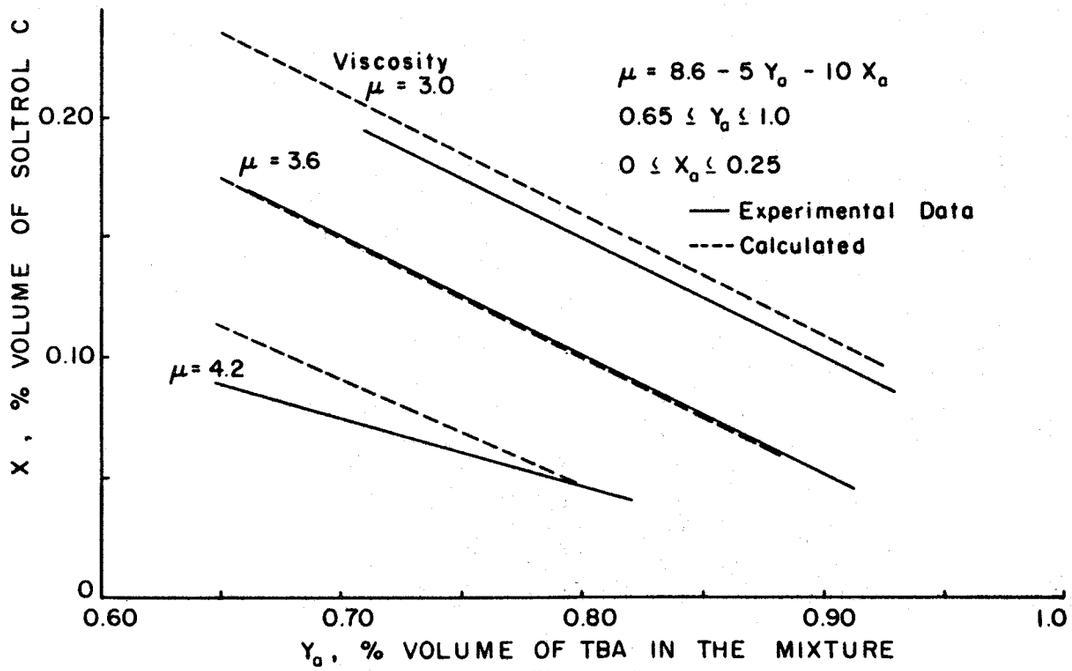

Figure 6

Correlation of Viscosities of Miscible Mixtures for the TBA-Soltrol-Brine System

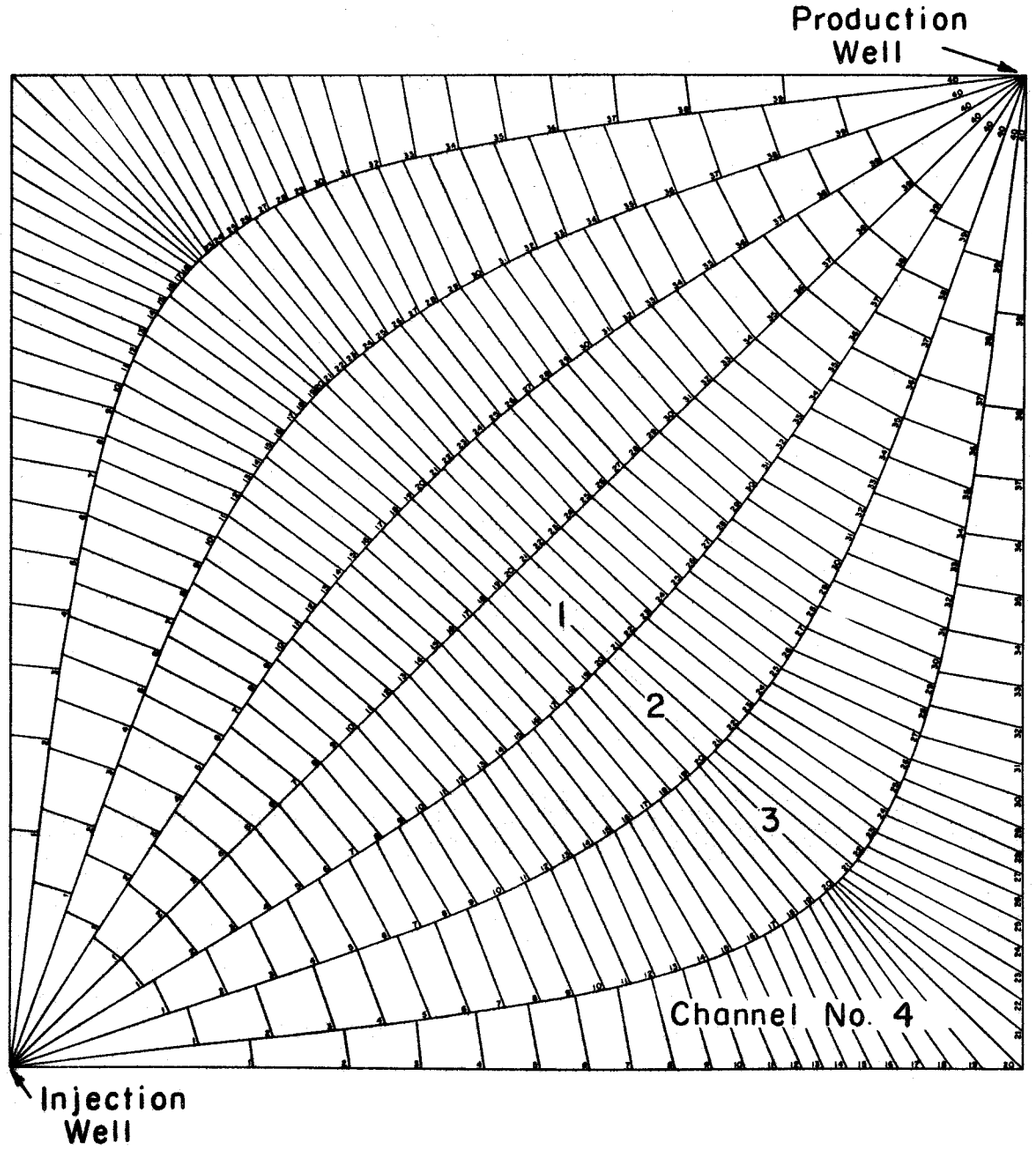

Figure 7

Quadrant of a Five-spot Flow Pattern Divided into Channels and Cells.

Figure 8

Scheme Employed for Calculating the Sweep Efficiency and Production History for Alcohol Displacement in a Five-Spot Pattern

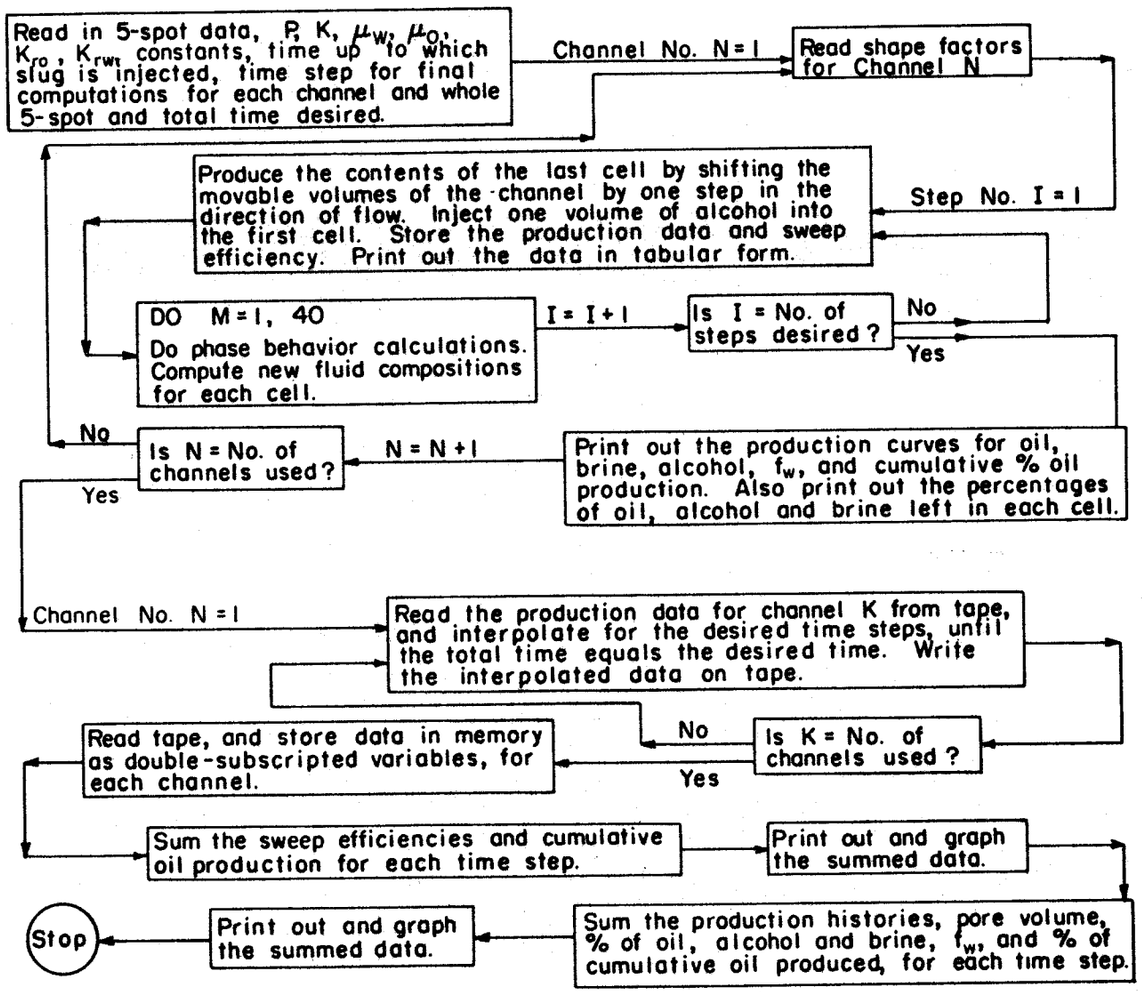

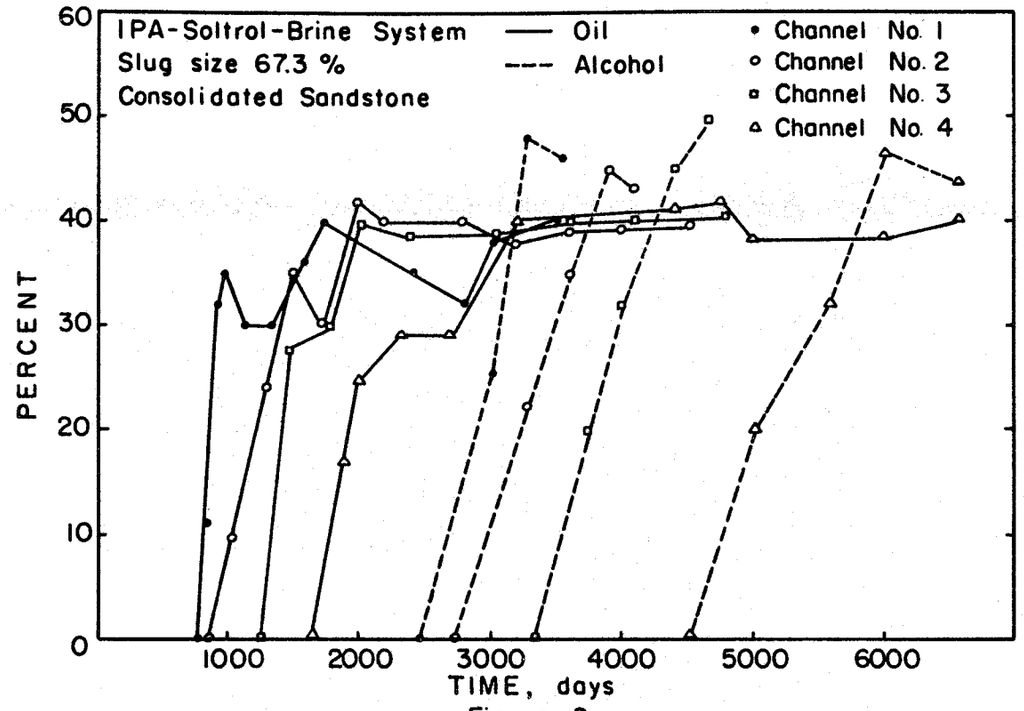

Figure 9

Computed Production Histories for the Four Channels of a Five-spot Pattern

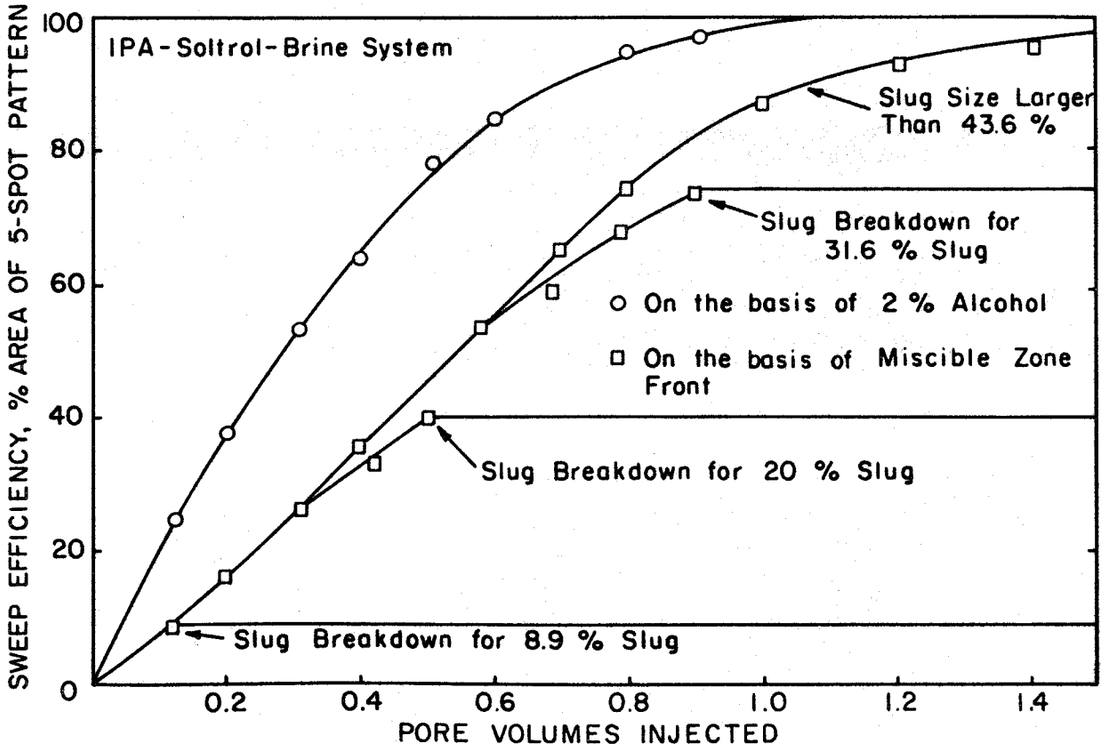

Figure 10

Computed Sweep Efficiency for a Five-spot Pattern (Consolidated Sandstone)

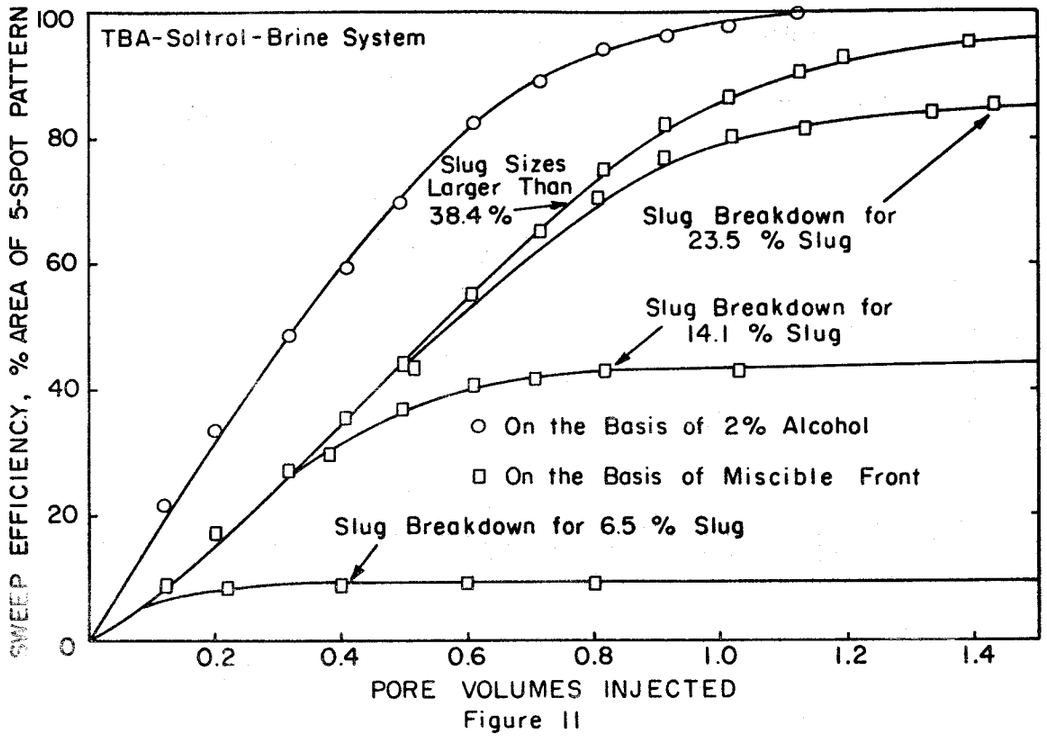

Figure 11

Computed Sweep Efficiency for a Five-spot Pattern (Consolidated Sandstone)

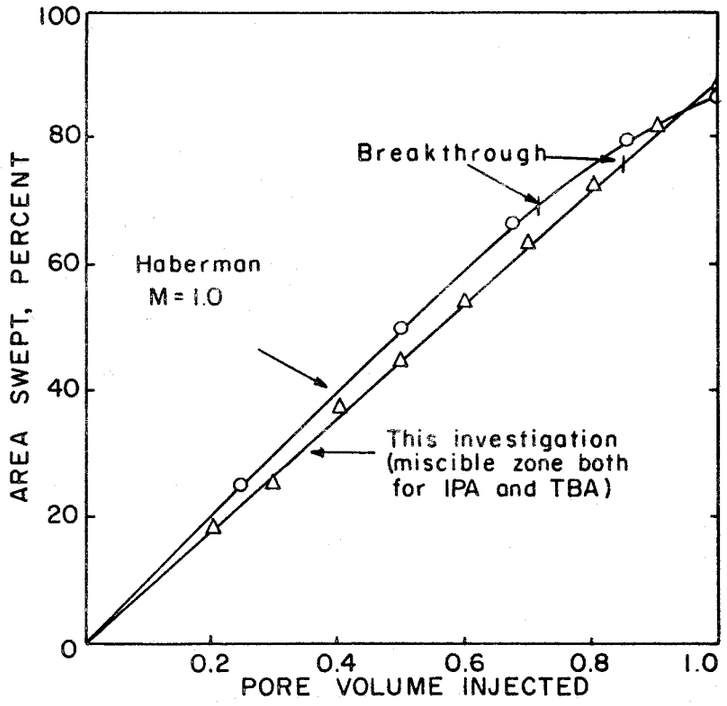

Figure 12

Comparison of the Computed Areal Sweep Efficiency for the IPA and TBA Systems with that for Miscible Displacement at a Mobility Ratio of 1.0.

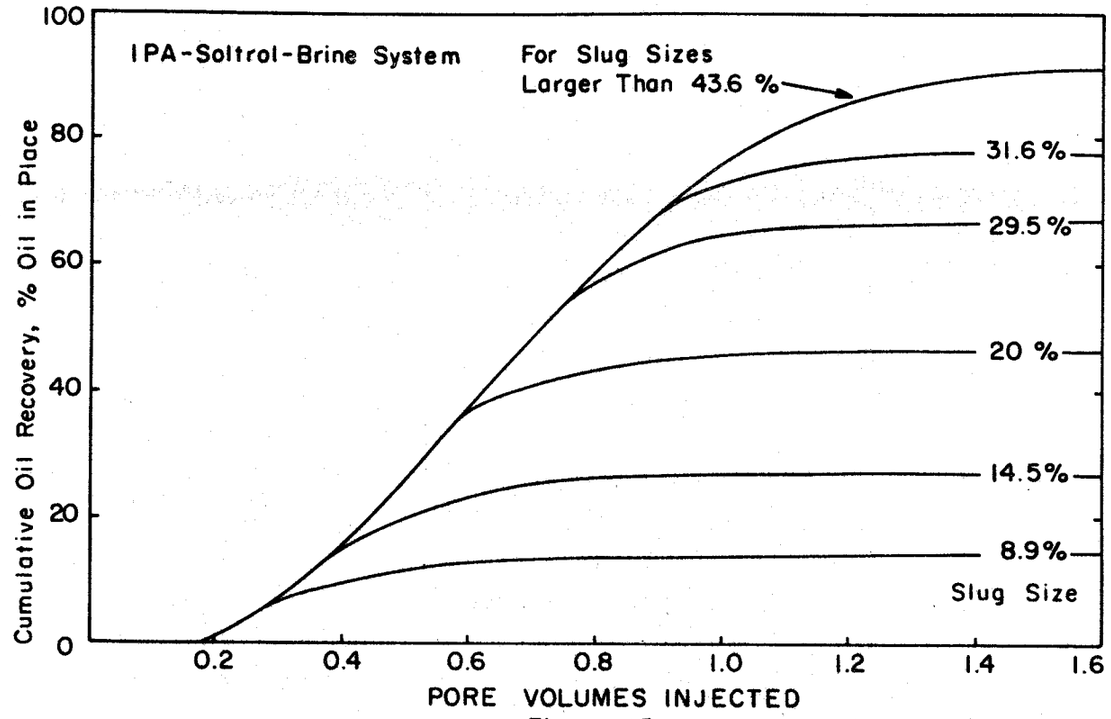

Figure 13

Computed Cumulated Oil Recovery as a Function of Pore Volumes Injected for a Five-Spot Pattern

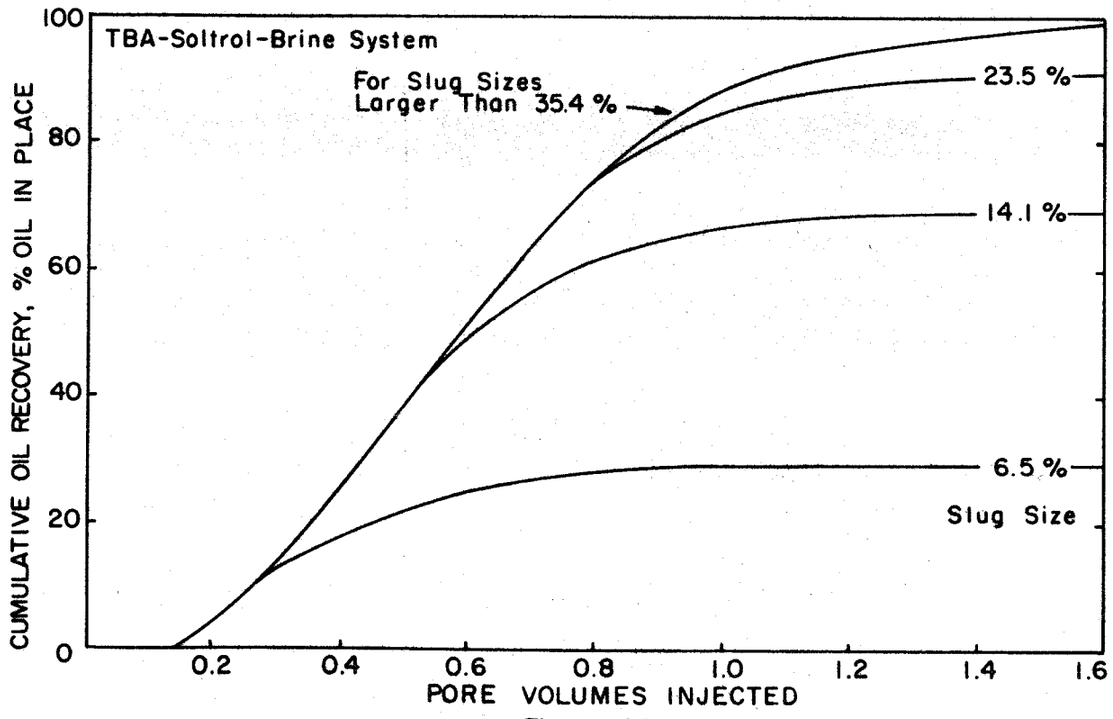

Figure 14

Computed Cumulative Oil Recovery as a Function of Pore Volumes Injected for a Five-Spot Pattern

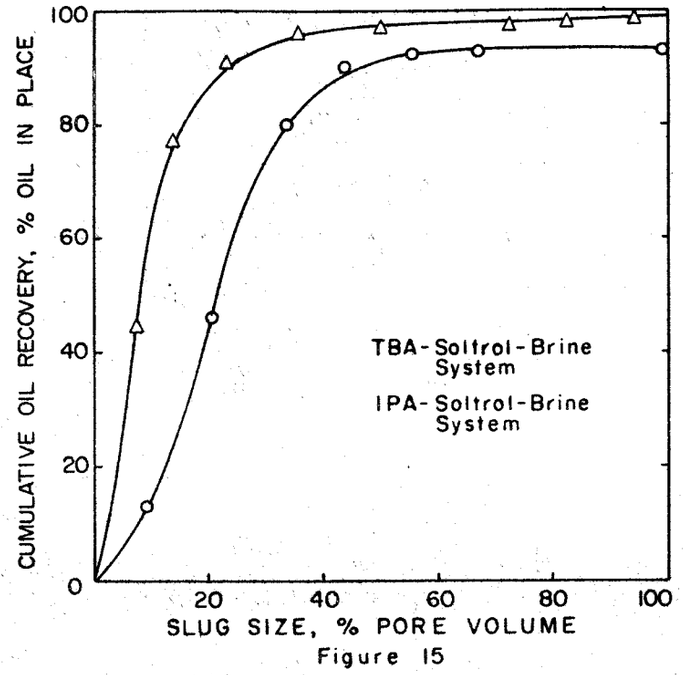

Figure 15

Computed Cumulative Oil Recovery as a Function of Slug Sizes (For 1.5 Pore Volumes Injected), for a Five-Spot Pattern

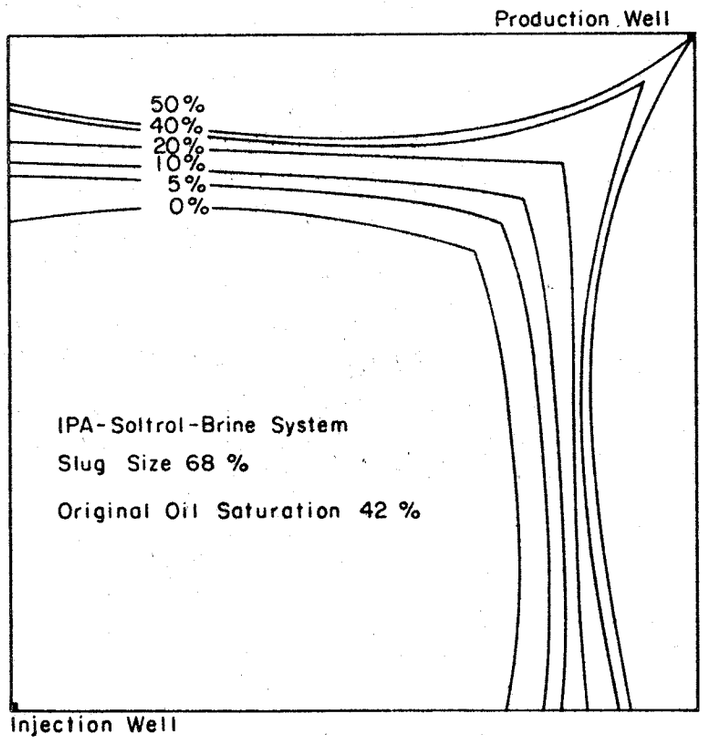

Figure 16

Computed Residual Oil Saturation at Miscible Zone Breakthrough (Consolidated Sandstone)

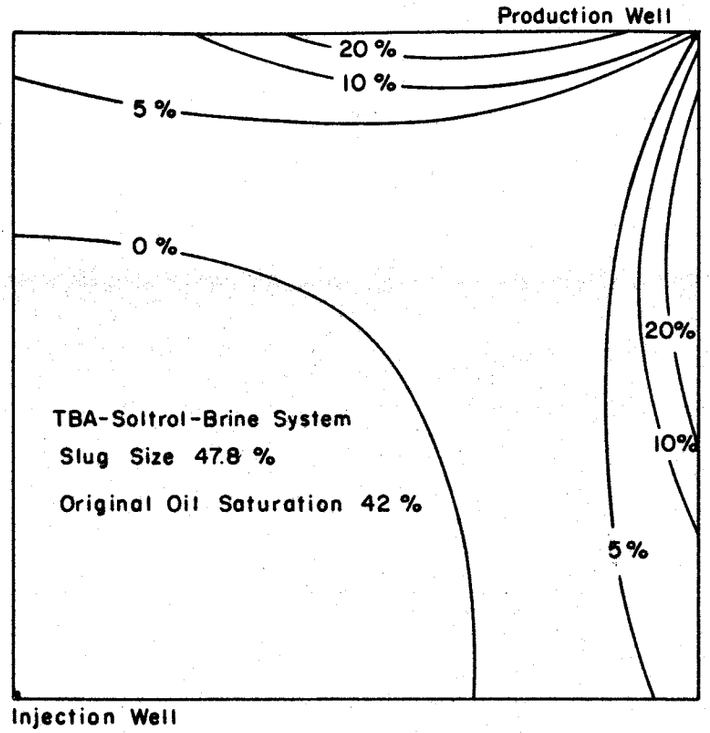

Figure 17

Computed Residual Oil Saturation at Miscible Zone Breakthrough (Consolidated Sandstone)

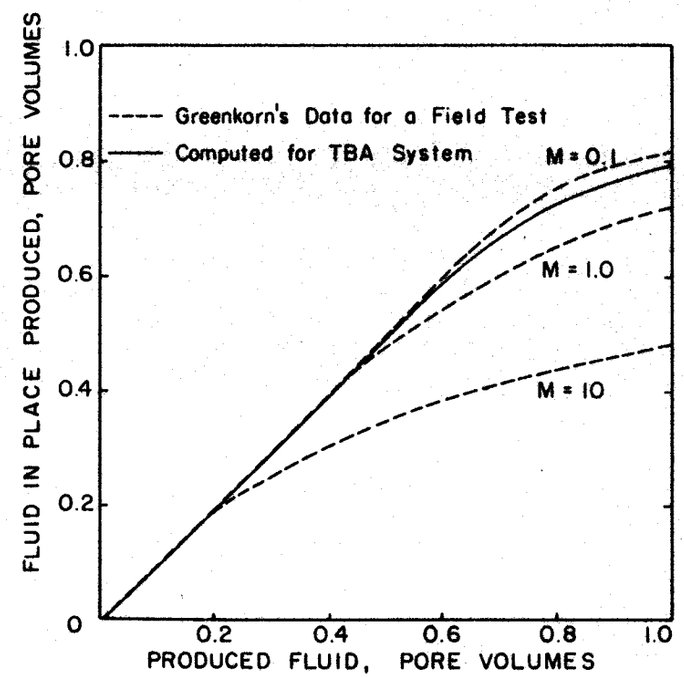

Figure 18

Comparison of the Fluid in Place Production Curve with Field Data

Petroleum Production Research at Penn State in Retrospect

R. F. Nielsen
L. T. Bissey

Introduction

At this Twenty-Fifth Technical Conference it seems appropriate to review some of the highlights of previous conferences and the research which has been done since the beginning of sponsorship by Pennsylvania producers. Also it seems appropriate to recall the names of certain people most actively concerned with the early work, and to mention certain incidents involving some of these people. The chief purpose of the review, however, is not to write a "human interest story" but to tell what has been done and, particularly, where details can be found. Useful ideas can often be obtained from early work, or one may wish to trace back a certain subject. The numbers refer to bulletins or theses listed at the end of the paper. These, or copies thereof, can be obtained from the Department of Petroleum and Natural Gas or through the University Library. Tables of contents of the bulletins and titles of all theses from the Department will be prepared soon and distributed.

A brief but excellent review of events leading up to the research program may be found in the Tenth Anniversary Bulletin, 1943, published as Bulletin 38 of the Mineral Industries Experiment Station[12] and in the June Producers Monthly of that year. Steps were taken by Dean Steidle and C. A. Bonine about 1928 to work with Pennsylvania producers in setting up research and teaching programs in oil production. In 1929

the Legislature granted $50,000 for the biennium, to be divided between refining and production research, the former having been carried on for some time already in the School of Chemistry. The cooperative program with Bradford District began in 1933. Some familiar names were associated with the program in the early years (1929-34) including Kenneth Barnes, George Fancher, James Lewis, C. A. Bonine, Clark Barb, Arthur Honess and, of course, "Doc" Gauger who was director of the newly organized M. I. Experiment Station. It was in those years of the great depression that hundreds of cores were collected, tested, and filed in Room 1 of the Mineral Industries Building, this room being labelled Pennsylvania Core Depository. Penn State pioneered in porosity and permeability measurements and the development of "flood pots" for measuring water flood efficiencies by radial flow in cylindrical cores. "Bulletin 12", containing the article "Some Physical Characteristics of Oil Sands", by Fancher, Lewis, and Barnes, has become a classic.

Sam Yuster joined the staff in 1934. The progress of the research program under his direction is common knowledge. Others whom some of you remember on the research staff up to 1940 include Luther Bissey, "Beech" Charmbury, Kurt Andresen, Joe Levine, and John Calhoun. Ralph Nielsen replaced Kurt Andresen in 1940. Francis Todd was on the research staff on "state funds".

A program sponsored by Penn Grade and connected primarily with the Middle District and air-gas drive research was started in 1936.

Gerald Hassler and Harry Krutter were appointed to the project and, in 1938, Bob Day. The famous "Hassler sleeve" was devised at that time. The air-gas and water flood research were combined under Yuster's direction when Krutter left in 1944.

The results of the programs were presented in periodic reports, at meetings with the advisory committees, and at annual conferences. The first Bradford District Technical Conference was in 1936. Another series of annual Petroleum and Natural Gas conferences began in 1930, under the auspices of the PNG department, headed in the early days by Bonine (geology and PNG) and later by Pirson. The proceedings were published in bulletins of the MI Experiment Station and contained mostly papers from outside the PNG department, although some important Penn State research was included. The famous Bulletin 12 was the Proceedings of the Third PNG Conference. There were ten of these conferences, the fourth to tenth being called Penn. Min. Ind. Conferences, PNG Section. Some well known "outside" contributors include Paul Torrey, Ralph Zook, George Hanks, Harry Ryder, Per Frolich, Merril Fenske, Gustav Egloff, Art Simmons, Charles Fettke, Ed Heck, F. W. Laverty, and William Brundred. A number of other people who worked closely with the Penn State research in the early days might be mentioned. These include members and officers of sponsoring groups and advisory committees. Such names as Joe Moorhead, Jerry Bauer, Cliff Martin, Cornell Pfohl, Coy Hogg, Tony Saxe, Ed Booth, "Dick" Jones, Bob Bossler, "Tex" Young, John DePetro, and George Holbrook come to mind.

Although established about ten years later than "early times", the Bradford District-Penn Grade Laboratory should be mentioned because of its close association with Penn State. The names of Rudy Pfister, Dick Hughes, Bob Bossler, and Joe Breston will be recalled in connection with its direction.

Now it seems to be in order to review some of the work done over the years. This will be grouped by subject matter rather than by time increments. Names will not in general be mentioned, but the references may be traced to show the people associated with various projects.

Porosity, Permeability, and Pore Structure

Bulletin 12 (1933) still stands as a monument to the systematic determination of the properties of porous media. One wonders how so few people could turn out so much work in so short a time. The determination of porosity and permeability and the relation of the latter to Reynold's number and turbulence were put on a scientific basis. Previously[1] (Barb and Honess, 1930) relations between porosity and permeability had been presented, and microscopic pore structures studied. The relation of permeability to Poiseuille's law for flow in capillaries was mentioned in 1934[11]. An empirical equation for calculating permeability from sieve analysis was suggested by Ryder[5] in 1936. The concept of relative permeability and its relation to fluid saturation was presented in 1936-37 without, however, using the word "relative".[10,14] Krynine's work on pore structure and petrology appeared over the years 1933-48[9, 15, 16, 23, 24, 38]. The effect of pressure on gas permeability was noticed in the late 1930's[16] and later became the subject of Calhoun's doctoral thesis. During the course of his thesis research, Calhoun, with Yuster and Nielsen, visited Muskat at the Gulf Laboratories to get an opinion. By a strange coincidence, Muskat had just then finished reviewing the manuscript of the famous Klinkenberg paper. This is just one of those cases where someone else "got there first".

Air drives on long cores[20, 21] from the Ranney "mine" yielded characteristic gas-oil ratio curves which Muskat showed to be due to the trend in the relative permeability ratio with saturation. The "Penn State Method"[24] of determining relative permeabilities, a major pioneering accomplishment, was developed in 1946-47.

Capillary Pressure, Pore Size Distribution, and "End Effect"

The concepts of interfacial tension forces in porous media, threshold pressure, and its relation to permeability were mentioned in reports as early as 1936[10, 13]. Jamin action, contact angles, and adhesion tension in two phase flow were mentioned in 1935[10, 11] and visual observance of these phenomena under a microscope was reported[11, 12]. Distribution of phases in the pores and the relation of pore structure and interfacial tension to displacement was discussed at the First Technical Conference (1936)[13].

The effect of pressureon oil recoveries from laboratory cores was apparent in some of the earliest work, but the relation of this effect to the capillary "end effect" was not recognized until the work on capillary pressure-saturation curves was under way, about 1946[22, 24, 27]. Strangely enough, the first mathematical derivation of

the end effect for displacement by the non-wetting phase (e.g. oil or water by gas) seen by the writers was a private communication from Lincoln Elkins to Sylvain Pirson. The end effect had been anticipated and measured some years earlier by Francis Todd, about 1938. He had sealed concentric rings to a core to determine brine saturations by electrical conductivity. But nobody would believe him at the time. In anger he destroyed all his data and disassembled the apparatus. One of the cores with the concentric rings was found several years later in a scrap drawer.

Penn State pioneered on many aspects of determining capillary pressure curves. For a while these determinations were on a real high speed mass production basis. A little incident in the laboratory illustrates this. Drew Stahl was making measurements in a cabinet containing 36 capillary pressure cells. One of these had been disconnected for repair. Sam Yuster happened to pass by and remarked "Drew, there are 36 capillary pressure cells in that cabinet! Why are only 35 of them running?" Later experiments included determination of pore size distribution by mercury injection[25] (with a view toward permeability calculations), hysteresis, and imbibition capillary pressure curves[29].

Application of the Flow Laws to Field Operations

The first Penn Grade Report (1936) says, regarding Darcy's Law, "This law has no direct quantitative application to the problem of flow in actual oil bearing sands". However, applications of Darcy's Law and its modifications to "actual oil bearing sands" have been made

by the Penn State staff and others from that time to the present. Muskat's papers on the conductivity and "sweep efficiency" of idealized well configurations and flooding patterns were being published in the 1930's and his book appeared in 1938. In those days, when most petroleum engineers were frightened by Muskat's mathematics, we had the good fortune of Harry Krutter's presence on the staff. Harry taught a course which took most of the mystery out of equations which previously seemed so formidable.

Methods of calculating secondary water flood histories, allowing for permeability profiles, were developed about 1944 and tested against actual field histories[20, 21]. These methods are still being used in modified forms. Pattern rearrangements, and intermittent injection in air-gas drive were suggested about 1942[18, 19, 20]. Delayed drilling[16] and other factors in developing a water flood were examined on the basis of the flow laws.

Jack Tarner published his well known "Tarner's Method" in 1944 while at Penn State. It was to have been his M. S. thesis, but a rule that a thesis may not be published prior to commencement was discovered, and Jack had to write a second thesis.

Selective Plugging

The use of air (or gas) in connection with water injection was a means of selective plugging by "Jamin action" was suggested[11, 14, 15] in 1934, and some field experiments were tried soon after that[16]. About 1938 experiments with suspensions and emulsions were under way[11, 16, 18, 19]. Bulletin 55 mentions an analysis of data from one

Pennsylvania oil company indicating a saving of over two million dollars due to selective plugging alone. Experiments on selective plugging with smokes were in progress for a while. Various methods of generating smokes, such as atomization, condensation, and chemical means, were tried, but the main difficulty was getting the smoke down the tubing.[20] Alternate injection of dry ammonia and dry hydrogen chloride gave "plugs" that lasted several months.[23] However, selective plugging with smokes was given up as impractical.

Miscible Displacement in Porous Media

The fact that a fluid may be displaced completely from a porous medium by one miscible with it has been known since research on porous media first began. Systematic study at Penn State was started[10] about 1952. The "equilibrium cell" theory for calculating transition (mixing or dispersion) zone compositions was proposed at that time, but the basic equations were not suited for hand computation. Later (1962)[35, 36] the method was programmed, and about this time algebraic solutions appeared in the production research literature. Experiments with long cores, using liquids and gases, were made[31] and relations to viscosity ratios and diffusion constants studied[31, 34, 36]. Further experiments included testing of equations for radial miscible displacement in porous media,[36] for gravity effects in vertical miscible displacement[35, 36], and for transition zone in long cylindrical capillaries[40, 41]. Fingering was studied by the method of x-ray shadowgraphs[42, 43] and other studies on fingering have been made and are

continuing. Experiments in which a liquid was displaced by the same liquid at a different temperature have been described[28, 29, 31] but the conduction and mixing effects were not separated in the mathematical developments. The effect of a second phase was studied[44] and also the effect of interphase material transfer.[45]

The Alcohol Slug and Other Miscible Slug Processes

The experimental work on the alcohol slug process was first reported[33] in 1959. Modified and combination slugs, and effects of slug sizes, velocities, sand type, and fluid properties have been studied over a period of years, as have numerous water-alcohol-hydrocarbon phase relations[34, 35, 36]. The Penn State staff worked closely with the oil producers in a field trial.[36] Theoretical and computational procedures have been developed[36, 46, 47] for linear and radial alcohol floods.

Studies have been made of oil recoveries from water flooded cores by the use of light hydrocarbons[36, 48] and liquid carbon dioxide[48]. In some of these studies water was injected with the solvent, and the core was tilted, to avoid fingering and overriding.

Flooding Models and Sweep Efficiency

A. Developed Floods

Electric models using metal foil and electrolytic models using solutions or gels have been employed here since the late 1930's. These have been limited to unit mobility ratio. Conductivities, flow lines[14, 15, 16] and sweep efficiencies for unusual patterns have been

studied by this method. Recently[49] the effect of vertical fractures and the effect of barriers[61] were studied with paper of high but uniform electrical resistance, using a "field plotter".

A sand-packed lucite model was used in 1941[19] to produce a motion picture showing the displacement of crude oil by water. Sweep efficiencies and water-oil ratios after breakthrough were obtained.

B. Pilot Floods (Closed Edge)

Sweep efficiencies for small groups of wells in which the total production from wells was equal to the injection have been studied with sand-packed models[50, 51] (miscible fluids) and "mathematical models"[51]. These included "bounded" and "unbounded" systems.

C. Pilot Floods (Open Edge)

Displacements in open edge models have been studied to simulate a pilot water flood in a field with an initial gas saturation. Artificially consolidated slabs[52] and Hele-Shaw (parallel glass plates) models[53, 54] were used. The large effect of rates and importance of rate control in such models were demonstrated. This has apparently not been emphasized in the literature in, for instance, the case of an inverted five-spot pilot. (See the paper by Bernard and Caudle presented at the October, 1966 SPE meeting).

Phase Equilibria

Certain measurements of a purely physico-chemical nature dealing with phase equilibria have been made. These include solubilities of methane and ethane[27] and equilibria in carbon dioxide-hydrocaron systems[29, 30, 36, 62].

Interfacial Tension Measurements

Measurements of water-gas interfacial tensions in the presence of a high pressure hydrocarbon gas phase were made by the pendant drop method[63]. Spreading coefficients were made on a hydrophile balance[15]. The rate of attainment of surface tension equilibrium[28] and the nature of viscous films[64] were studied.

Immiscible Displacement

Early experiments on displacement were aimed directly at increasing oil recovery by water or air-gas drive. Effect of pressure[12, 14, 19, 20, 26, 30], intermittent gas injection[20, 29], injection of both water and gas[12, 22, 23], and effect of viscosity[2, 12], interfacial tension[30], and wettability[25, 31] were among the factors studied. As displacement theory (Buckley-Leverett etc.) developed, such things as input[30] and outlet[29] transients, capillarity zones[29], saturation distributions and their rate of change, and gravity counterflow were investigated[65].

Surfactants and Other Additives

The addition of various materials to injection water in order to increase oil recovery was probably considered when water flooding began. Bulletin 11 (1932) describes laboratory experiments with soap, sodium carbonate, and other materials[2, 10]. Later numerous surfactants were tried[19, 22, 27, 28, 29] and the possibility of a chromatographic wave[27] suggested. Certain materials (e. g. carboxy-methyl-cellulose) which impart a high viscosity to water were tried in the early 1940's. Very recently other polymers such as acryl-amides have come

into the limelight as "pushers"[66, 67]. Some measurements of adsorption were made.[11 (1937)]

Well Shooting

The technique of "shooting" wells with nitroglycerine or similar explosives seems to have been well developed by the early 1930's. (The booklet "Oil Well Shooting Theory and Practice" by Paul F. Lewis, published by American Glycerine Co., was published in 1935). Articles dealing with corrective shooting appeared in reports and bulletins from 1937 to 1948[6, 11, 17, 18, 24]. Such concepts as "quarts per foot", "response", and "best shot", based on collected field information, were used in equations.

Well Problems

Certain well problems, such as corrosion and the deposition of "gypsum" ("gyp") and wax were reported in the early days of the research program. The relation of gas content to paraffin point[15], the prevention of calcium sulfate precipitation[16], and the use of amines and chromates for corrosion prevention[16] were studied in 1938-9. Simmons[4] reported on problems of flood water in 1935.

Microscopic Observations

Observations under a microscope have been made of fluid movements between sand grains. Some of these have involved oil displacement by air or water, using either small sand-filled cylindrical glass capillaries[55] or sand grains sealed between microscope slides[11, 12].

A color motion picture was made of the former and is in the Visual Aids Library files. Color films have also been made of alcohols displacing oil and water, with the fluids shown by various colors[39].

Miscellaneous Investigations and Reports

Many types of investigation not mentioned above can be named. Some of the topics are: electric logging[24, 25, 28, 29, 30], radioactive tracers[30], use of semipermeable diaphragms to lower water-oil and gas-oil ratios[22], tracers to detect drilling water invasion in cores[12], economics of well spacing[23], clay swelling[19], oxidation of crudes[56], use of foam[11(1935), 57, 58, 59, 60], magnetometer surveys[23], and determination of oil and water saturations by extraction[4, 12] and by matched refractive indices[31].

An article by Paul Torrey[1] (1930) gives an interesting account of "mining" oil in 1735 in the Pechelbronn field (Alsace) and the vertical gravity drainage from that field in 1917-24. Bulletin 20 contains several articles on the results and problems of the St. Patrick's day (1936) flood and storm.

References

Bulletins and Reports

1. Min. Ind. Exp. Sta. Bull. 9, Proc. 1st Petr. and Nat. Gas Conf., 1930.
2. Bull. 11, 2nd PNG Conf., 1932
3. Bull. 12, 34d PNG Conf., 1933
4. Bull. 19, 5th PNG Conf., 1935
5. Bull. 20, 6th PNG Conf., 1936
6. Bull. 21, 7th PNG Conf., 1937
7. Bull. 25, 8th PNG Conf., 1938
8. Bull. 30, 9th PNG Conf., 1940
9. Bull. 33, 10th PNG Conf. 1941
10. Penn Grade Repts. 1936-1944
11. Water Flood Repts. 1933-1950
12. Bull. 38, 10 Anniv. 1943
13. Proc. 1st Tech. Conf. on Petroleum Production 1936
14. Proc. 2nd Tech. Conf. 1937
15. Proc. 3rd Tech. Conf. 1938
16. Proc. 4th Tech. Conf. 1939
17. Proc. 5th Tech. Conf. 1940
18. Proc. 6th Tech. Conf. 1941
19. Proc. 7th Tech. Conf. 1942

20. Bull. 39, Proc. 8th TC 1944
21. Bull. 41, Proc. 9th TC 1945
22. Bull. 45, Proc. 10th TC 1946
23. Bull. 48, Proc. 11th TC 1947
24. Bull. 52, Proc. 12th TC 1948
25. Bull. 54, Proc. 13th TC 1949
26. Bull. 56, Proc. 14th TC 1950
27. Bull. 59, Proc. 15th TC 1951
28. Bull. 60, Proc. 16th TC 1952
29. Bull. 62, Proc. 17th TC 1953
30. Bull. 64, Proc. 18th TC 1954
31. Bull. 68, Proc. 19th TC 1955
32. Papers read at 20th TC 1957
33. Circ. 56, Proc. 21st TC 1959
34. Circ. 61, Proc. 22nd TC 1961
35. Circ. 63, Proc. 23rd TC 1962
36. Circ. 66, Proc. 24th TC 1963
37. Bull. 55, Progress in Research, M.I.Exp. Sta. 1949-51
38. Bull. 29, Petrology and Genesis of 3rd Bradford Sand, by P. D. Krynine 1940

Theses (MS unless PhD indicated)

39. C. Cronquist 1961
40. A. K. Csaszar 1960
41. R. E. McWilliams 1958
42. S. J. Lestz 1959
43. R. Thomas 1960
44. A. Khan, PhD 1961
45. R. E. Gilchrist, PhD 1958
46. Y. C. Chiao 1966
47. M. El-Saleh 1965
48. T. E. Ashton 1966
49. J. Hansford 1966
50. B. L. Paulsell 1958
51. J. J. Cosgrove, PhD 1963
52. D. S. Paxman 1959
53. R. N. Beamer 1960
54. H. A. Schueltz 1961
55. Q. J. Lowman 1950
56. J. V. Howard 1959
56. G. W. Spaid 1961
57. G. S. Bennett 1964
58. J. R. Deming 1964
59. R. Iden 1965
60. G. E. Kolb 1964
61. R. J. Sandrea, PhD 1966
62. C. Lara 1943
63. M. E. Hassan, PhD 1953
64. J. W. Edwards 1961
65. E. E. Templeton 1961
66. S. Y. Chain 1965
67. J. M. Spitzel 1965

TREATMENT OF EQUILIBRIA BETWEEN TWO LIQUID PHASES IN HYDROCARBON-CARBOND DIOXIDE SYSTEM

by

V. S. Gupta
R. F. Nielsen

The Pennsylvania State University
University Park, Pennsylvania

ABSTRACT

For better understanding of the behavior of liquid carbon dioxide as a secondary or tertiary recovery agent, it is desirable to have a wide range of equilibrium data for various liquid carbon dioxide-hydrocarbon mixtures. A lack of sufficient number of experimental investigations do not permit an exact quantitative analysis of this problem. Whatever tentative information has been reported by previous workers, has been accepted as a basis for our present qualitative investigation. Equilibrium calculations for two liquid phases in carbon dioxide-hydrocarbon systems were performed on the basis of previously reported observations. These calculations are similar to those for vapor-liquid equilibria.

This problem has also been treated from a theoretical angle. One of the simiempirical thermodynamic equations is used to predict the whole binodal curve of a ternary system on the basis of just one set of liquid-liquid equilibrium data. For want of more experimental observations, a comparison between theoretical and experimental curves is not possible at this stage.

INTRODUCTION

The possibility of using liquid carbon dioxide as a secondary or tertiary recovery agent for hydrocarbons has been recognized for some years. The wide abudnance of carbon dioxide and relative cheapness of its liquification makes this idea seem feasible. There is a good possibility that under favorable circumstances, liquid carbon dioxide may be an effective agent in miscible flooding.[1] This possibility was recognized at least fifteen years ago by Pirson[1], Weber[2], Martin[3] and Saxon et al[4]. Currently at least one field test is under way and some are being planned.

At room temperature (70°F), liquid carbon dioxide is miscible in all proportions with the pure normal paraffinic hydrocarbons below tetradecane. For tetradecane and higher, the miscibility range gradually becomes less with increasing molecular weight. For mixtures of hydrocarbons, complete miscibility depends on the average molecular

weight of the hydrocarbon mixture. In the absence of very heavy (waxy or asphaltic) constituents, complete miscibility is generally obtained if the average molecular weight is 180 or less.

While the critical temperature of carbon dioxide is low (88°F), the solvent properties extend above this temperature, if the pressure is sufficient. For instance, "the single phase region" may include the entire composition range with a light hydrocarbon at a temperature considerably above the critical. This property indicates the possibility of using carbon dioxide as a "pusher" in a graded miscible slug process.

A number of laboratory tests have been conducted[1,2,3,4] to study the effect of liquid carbon dioxide as a secondary or tertiary recovery agent. One such test was just conducted by Ashton[5] in this laboratory. Ashton observed that liquid carbon dioxide alone is less efficient than liquid propane alone in a simple miscible slug process. However these results do not exclude the use of carbon dioxide in a miscible process which must include the recovery of solvent or limit the amount of solvents.

It therefore seems desirable to have phase diagrams and phase data pertaining to equilibria in liquid carbon dioxide - hydrocarbon systems. Unfortunately nothing very systematic is available in this regard. Vapor-liquid equilibria involving carbon dioxide and light hydrocarbons have been studied by Kuenen[6], Olds et al[7], Poettman and Katz[8], Lara[9] and Stewert[10]. While vapor-liquid equilibria are related to liquid-liquid equilibria, the information from the farmer does not allow direct prediction of the latter for multicomponent systems.

Francis[11] and Meldrum and Nielsen[12] observed the miscibility relations mentioned previously. Francis' work, though quite extensive, does not cover the liquid-liquid equilibria involving carbon dioxide and two or more paraffinic hydrocarbons. Meldrum and Nielsen have reported a somewhat systematic treatment of liquid-liquid equilibria between carbon dioxide and some light and intermediate paraffinic hydrocarbons. Their work though limited to a few components, was a study of the compositions of the vapor phase and the one or two liquid phases in equilibrium with the vapor. One lighter phase, due to relative abundance of carbon dioxide, was called the carbon dioxide-rich phase and the other, due to a somewhat higher fraction of hydrocarbons, was called the hydrocarbon-rich phase. Meldrum and Nielsen also observed that the distribution coefficients (equivalent to equilibrium constants for vapor-liquid systems) of paraffinic components are dependent upon their respective molecular weights. One of their figures illustrating this dependence, drawn from very meager data, is reproduced here as Figure 1. For want of anything better, this figure will

be used here to illustrate some trends in the liquid-liquid equilibria.

It has been thought that some of the well known semi-empirical equations for departure from Raoult's might be applicable. If so, this can considerably cut down the number of lengthy and tiresome experimental investigations. Such equations are those of van Laar and those of Margules, as reported by Bendict et al[13] and applied by Wohl[14]. These equations, based on thermodynamics of solutions, are expressions for activity coefficients which measure the degree of departure from ideality, that is, from Raoult's law. The application of these equations to two liquid phases will be shown below. As an example, the Margules' two-suffix equation is used to predict the whole binodal curve on a ternary diagram on the basis of just one set of two phase equilibrium data, reported by Meldrum and Nielsen. However due to the lack of a sufficient number of experimental observations, a comparison between the theoretical and experimental curves cannot be made at this time.

Some attempts have been made to use ternary diagrams for liquid-liquid equilibria between carbon dioxide and complex hydrocarbon mixtures such as a crude oil. Horstman[15] used such diagrams but, as he pointed out, the curves were based on the first appearance of a second liquid phase and therefore gave incomplete information. The three components on his diagrams were crude oil, liquid carbon dioxide and a light hydrocarbon. The significance and location of such curves in relation to the order in which the components are mixed will be shown by some calculations making use of Meldrum's distribution coefficients.

THEORETICAL AND EMPIRICAL CONSIDERATIONS

1. Calculation of Liquid-Liquid Equilibria in Carbon dioxide - Hydrocarbon System:

Liquid-liquid equilibria can be treated in the same way as is commonly used for vapor-liquid system. The basic relations in this case are,

$$C_i^* = y_i/x_i \qquad \text{----------(1)}$$

The distribution coefficients of hydrocarbons as a function of their molecular weights are shown in Figure 1. An empirical relation for the distribution coefficient of liquid carbon-dioxide in carbon dioxide-hydrocarbon systems is given by Meldrum and Nielsen as,

$$C_{co_2} = 1+0.00\,6\ (M-180) \qquad \text{----------(2)}$$

*See the glossary of symbols.

Now consider a known mixture of hydrocarbons to which liquid carbon dioxide is continuously added under appropriate pressure and temperature so as to maintain the liquid state, until the first drop of carbon dioxide-rich phase appears. In this case the composition of hydrocarbon-rich phase is same as the total composition of the mixture. The mathematical relationship for this is,

$$(\sum x_i C_i)\ (1-X_{co_2}) + C_{co_2} = 1 \text{ ----------(3)}$$

Similarly starting with a fixed amount of liquid carbon dioxide and continuously adding a known mixture of hydrocarbons until the first drop of the hydrocarbon-rich phase appears, the composition of carbon-dioxide-rich phase in this case is same as the total composition, and the mathematical relationship will be,

$$(\sum {}^{yi}/_{ci})\ (1-y_{co_2}) + \frac{y_{co_2}}{C_{co_2}} = 1 \text{ ----------(4)}$$

When we have substantial amounts of both phases under equilibrium, i.e. when the total composition is well within the two phase region of the phase diagram, the mathematical relationship would be,

$$\sum \frac{Z_i\ (C_i - 1)}{v(C_1-1) + 1} = 0 \text{ ----------(5a.)}$$

$$x_i = \frac{Z_i}{(C_i-1)\ v + 1} \text{ ----------(5b.)}$$

The use of equations 1-5 will be illustrated below.

2. Margules' Two Suffix Equation:

Both Margules and van Laar have given a series of empirical equations for activity coefficients. These equations relate the activity coefficient of a particular component with the mole or volume fractions of other components. The higher the number of suffixes in such an equation, the more constants it contains and the greater are the chances of accuracy. However, the higher the number of suffixes, the greater is the number of experimental data required to solve the equations. As a first step, for ternary systems, the two-suffix Margules' equation was selected. This is the simplest of all such equations and its solution requires only one set of equilibrium data. The Margules two-suffix equation is as shown. If x_1, x_2, x_3 are the mole fractions of the components 1, 2 and 3 in a particular phase and their corresponding activity coefficients are γ_1, γ_2, γ_3 then

$$\log \gamma_1 = A_{12} x_2^2 + A_{13} x_3^2 + x_2 x_3 (A_{12} + A_{13} - A_{23}) \text{ ----------6a.}$$

$$\log \gamma_2 = A_{12} x_1^2 + A_{23} x_3^2 + x_1 x_3 (A_{12} + A_{23} - A_{13}) \text{ ----------6b.}$$

$$\log \gamma_3 = A_{13} x_1^2 + A_{23} x_2^2 + x_1 x_2 (A_{13} + A_{23} - A_{12}) \text{ ----------6c.}$$

where

$$\text{limit } \log \gamma_1 \ (x_1 \to o,\ x_2 \to 1) = \text{limit } \log \gamma_2 \ (x_2 \to o,\ x_1 \to 1) = A_{12} \text{--7a.}$$

$$\text{limit } \log \gamma_1 \ (x_1 \to o,\ x_3 \to 1) = \text{limit } \log \gamma_3 \ (x_3 \to o,\ x_1 \to 1) = A_{13} \text{--7b.}$$

$$\text{limit } \log \gamma_2 \ (x_2 \to o,\ x_3 \to 1) = \text{limit } \log \gamma_3 \ (x_3 \to o,\ x_2 \to 1) = A_{23} \text{--7c.}$$

When the two phases are at equilibrium i.e. carbon dioxide-rich and hydrocarbon-rich phases in our case, then we have

$$(x_j \gamma_j)_{co_2\text{-rich}} = (x_j \gamma_j)_{\text{HC-rich}};\ j = 1, 2, 3$$

$$\text{hence } (\log x_j + \log \gamma_j)_{co_2\text{-rich}} = (\log x_j + \log \gamma_j)_{\text{HC-rich}};\ j = 1,2,3$$

Substituting for $\log \gamma_j$ from 6a, 6b & 6c

$$\left[\log x_1 + A_{12} x_2^2 + A_{13} x_3^2 + x_2 x_3 (A_{12} + A_{13} - A_{23})\right]_{co_2\text{-rich}}$$

$$= \left[\log x_1 + A_{12} x_2^2 + A_{13} x_3^2 + x_2 x_3 (A_{12} + A_{13} - A_{23})\right]_{\text{HC-rich}} \text{--8a.}$$

$$\left[\log x_2 + A_{12} x_1^2 + A_{23} x_3^2 + x_1 x_3 (A_{12} + A_{23} - A_{13})\right]_{co_2\text{-rich}}$$

$$= \left[\log x_2 + A_{12} x_1^2 + A_{23} x_3^2 + x_1 x_3 (A_{12} + A_{23} - A_{13})\right]_{\text{HC-rich}} \text{--8b.}$$

$$\left[\log x_3 + A_{13} x_1^2 + A_{23} x_2^2 + x_1 x_2 (A_{13} + A_{23} - A_{12})\right]_{co_2\text{-rich}}$$

$$= \left[\log x_3 + A_{13} x_1^2 + A_{23} x_2^2 + x_1 x_2 (A_{13} + A_{23} - A_{12})\right]_{\text{HC-rich}} \text{--8c.}$$

Later in this paper it is shown that how Equations 8a, 8b, and 8c are applied to predict the whole phase diagram with just one set of equilibrium data for a ternary system.

CALCULATION PROCEDURE

1. Calculation of Liquid-Liquid Equilibria:

Equilibrium calculations were performed assuming one component as "crude oil," second component as carbon dioxide and third component as another hydrocarbon, in this case hexane or pentadecane. The assumed composition of the "crude oil" used in such calculations is as shown in Table 1.

Table 1

Assumed Composition of "Crude Oil"

Components	Mole Fraction
C_4	0.15
C_8	0.15
C_{12}	0.15
C_{16}	0.15
C_{20}	0.15
C_{24}	0.15
C_{30}	0.10

Making use of Equations 1-5, equilibrium calculations were performed for Crude oil - Carbon dioxide - Hexane and Crude oil - Carbon dioxide - Pentadecane systems for all three cases mentioned above, namely, when there is an infintesimal amount of carbon dioxide-rich phase, when there is an infitesimal amount of hydrocarbon-rich phase, and when both the phases in question are in substantial amounts. Results of these calculations are presented in Figures 2-9.

It should be noted that in representing these complex mixtures on a ternary diagram, the "crude" does not have the composition of the original "crude" except in a phase which is in equilibrium with only an infitisimal amount of the other phase. Note that the position of the

curves, with these restrictions, depend on the relative amounts of the starting components.

2. Applying Margules' two-suffix equation for predicting a phase diagram:

Modified forms of Margules' two-suffix equations, as represented by 8a, 8b and 8c, were used for the carbon dioxide - propane - hexadecane system. One set of equilibrium data for such a system was taken from Meldrum as a starting point. This set of equilibrium data is reproduced in Table 2.

Table 2

Component	Mole fraction in CO_2-rich phase	Mole fraction in hydrocarbon-rich phase
CO_2	0.960	0.740
C_3	0.023	0.033
C_{16}	0.017	0.227

The above values were substituted for x_1, x_2, x_3 in Equations 8a, 8b and 8c to obtain the values of A_{12}, A_{13} and A_{23}. Since these equations are linear with respect to A_{12}, A_{13} and A_{23}, solving these equations for A_{12}, A_{13} and A_{23} presents no problem. These values were then used in Equations 8a, 8b and 8c to compute other sets of points on the binodal curve. Since the sum of the mole fractions of all three components in both of the phases is unity, the mole fraction of any one of the components can be substituted in terms of the other two. Hence we are left with only four unknowns and three equations, so, theoretically it is possible to solve for any three of the unkowns in terms of the remainder. However it is to be noted that 8a, 8b and 8c are transcendental equations in terms of the mole fractions and therefore it is rather difficult to solve for mole fractions by any simple mathematical procedure. For this reason they were numerically solved on an I.B.M. 7074 digital computer, using trial and error technique.

It is also to be noted that these are second order equations and hence there is more than one solution for each unknown. This difficulty was noticed while solving these equations for mole fractions. To avoid this discrepancy, only those points out of the several possible solutions which more or less lie on a closed binodal curve were selected. The phase diagram thus obtained is presented in Figure 10.

DISCUSSION AND CONCLUSION

It is to be pointed out that the distribution coefficients presented in Figure 1 are tentative and extremely approximate and were drawn without enough experimental data. They represent a general trend rather than actual numerical values. For this reason the results presented in Figures 2-9 are not to be taken at their face values. Apart from this, the distribution coefficient of liquid carbon dioxide, represented as a linear function of the apparent molecular weight of the hydrocarbon mixture is questionable. Though this equation was empirically obtained by Meldrum and Nielsen, it is not founded on many experimental observations and hence its validity may be questioned over a wider range of hydrocarbon compositions. It is felt that the distribution coefficient of carbon dioxide may also vary with the total amount of hydrocarbon in the system. However this variation is not believed to be large enough to affect the qualitative trend in our results.

It is true that the results presented in Figures 2-9 are not backed by experimental observations, however as a first step to our long range undertaking, it does give us an idea as to what one might expect the phase diagrams for such mixtures to look like.

At this stage it cannot be said whether the predicted phase diagram for carbondioxide - propane - hexadecane system as shown in Figure 10 is correct or not. Margules' two-suffix equation was selected only to see if it gives us some kind of plot. The exact shape of such a phase diagram can be determined when more experimental data would be forthcoming. The fact that this approach does give us some kind of binodal curve, gives enough encouragement for solving other more accurate equations suggested by Margules and van Laar in order to find the most accurate mathematical fit for a particular system.

GLOSSARY OF SYMBOLS

Z_i - mole fraction of ith component in whole system.

X_i - mole fraction of ith component in hydrocarbon-rich phase

Y_i - mole fraction of ith component in carbon dioxide-rich phase

v - mole fraction of carbon dioxide-rich phase

C - distribution coefficient

M - average molecular weight of hydrocarbons

γ - activity coefficient

SUBSCRIPTS

i - refers to the properties of ith component. In Equations 3 and 4, i refers to hydrocarbons only.

CO_2 - refers to the properties of carbon dioxide

CO_2-rich - refers to carbon dioxide-rich phase

HC-rich - refers to hydrocarbon-rich phase

REFERENCES

1. Pirson, S. J., "Tertiary Recovery of Oil," paper presented before the Central Appalachian Section, AIME, June 26, 1951.

2. Weber, George, "New Recovery Technique," Oil and Gas Journal, Vol. 49, No. 38, p. 171, Jan. 25, 1951.

3. Martin, James W., "Field Data on Operation of the Orco Process Near Richburg, New York," Oil and Gas Journal, Vol. 50, No. 32, pp. 82-86, December 13, 1951.

4. Saxom, J.; Breston, J. N.; and MacFarlane, R. M., Laboratory Experiments with Carbon Dioxide and Carbonated Water as Flooding Mediums", The Pennsylvania State University, Mineral Industries Experiment Station Bulletin No. 59, 1951; Producers Monthly, Vol. 16, No. 1, pp. 8-14, Nov. 1951.

5. Ashton, T. E., "An Evaluation of Carbon Dioxide and Propane for the Recovery of Bradford Crude Oil from Previously Waterflooded Cores," M.S. Thesis, The Pennsylvania State University, University Park, Pennsylvania, 1966.

6. Kuenen, J. P., "Experiments on the Condensation and Critical Phenomena of Some Substances and Mixtures," Philosophical Magazine, Series V, Vol. 44, pp. 174-199, 1897.

7. Olds, R. H.; Reamer, H. H.; Sage, B. H.; and Lacey, W. N., "Phase Equilibria in Hydrocarbon Systems. The n-Butane - Carbon Dioxide System," Fundamental Research on Occurrence and Recovery of Petroleum 1948-1949, pp. 9-16, 1950.

8. Poettmann, F. H., and Katz, D. L., "Phase Behavior of Binary Carbon Dioxide - Paraffin Systems," Industrial Engineering Chemistry, Vol. 37, pp. 847-853, 1945.

9. Lara, C., "Phase Diagram for n-Heptane - Carbon Dioxide System," M.S. Thesis, The Pennsylvania State University, University Park, Pennsylvania, 1943.

10. Stewart, W. C., "Phase Equilibria for Mixtures of Carbon Dioxide and Several Normal Saturated Hydrocarbons," M.S. Thesis, The Pennsylvania State University, University Park, Pennsylvania, 1953.

11. Francis, A. W., "Ternary Systems of Liquid Carbon Dioxide," Journal of Physical Chemistry, Vol. 58, pp. 1099-1114, 1954.

12. Meldrum, A. H., and Nielsen, R. F., "A Study of Three-phase Equilibria for Carbon Dioxide - Hydrocarbon Mixtures," Producers Monthly, Vol. 19, No. 10, pp. 22-35, August 1955.

13. Bendict, M.; Johnson, C. A.; Solomon, E.; and Rubin, L. C., "Extractive and Azeotropic Distillation", Transactions American Institute of Chemical Engineers, Vol. 41, pp. 371-391, 1945.

14. Wohl, Kurt, "Thermodynamic Evaluation of Binary and Ternary Liquid Systems," Transactions American Institute of Chemical Engineers, Vol. 42, pp. 215-249, 1946.

15. Horstman, P. T., "Ternary Diagrams for Bradford Crude Oil - Liquid Carbon Dioxide - Light Hydrocarbon Systems," M.S. Thesis, The Pennsylvania State University, University Park, Pennsylvania, 1962.

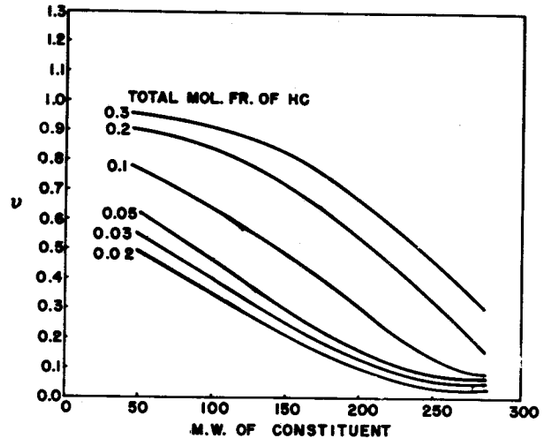

FIGURE 1: TENATIVE DISTRIBUTION COEFFICIENTS OF HYDROCARBONS. REPRODUCED FROM MELDRUM AND NIELSEN.

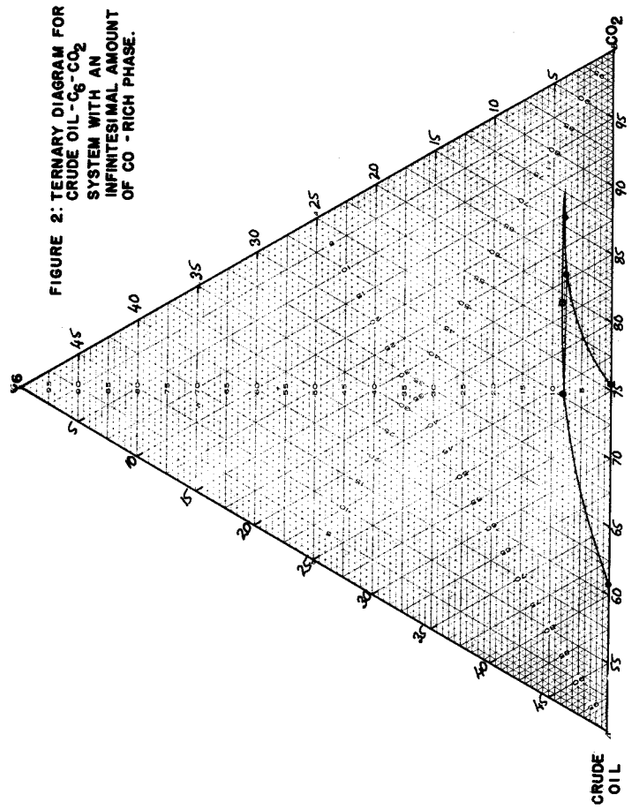

FIGURE 2: TERNARY DIAGRAM FOR CRUDE OIL-C_6-CO_2 SYSTEM WITH AN INFINITESIMAL AMOUNT OF CO_2 - RICH PHASE.

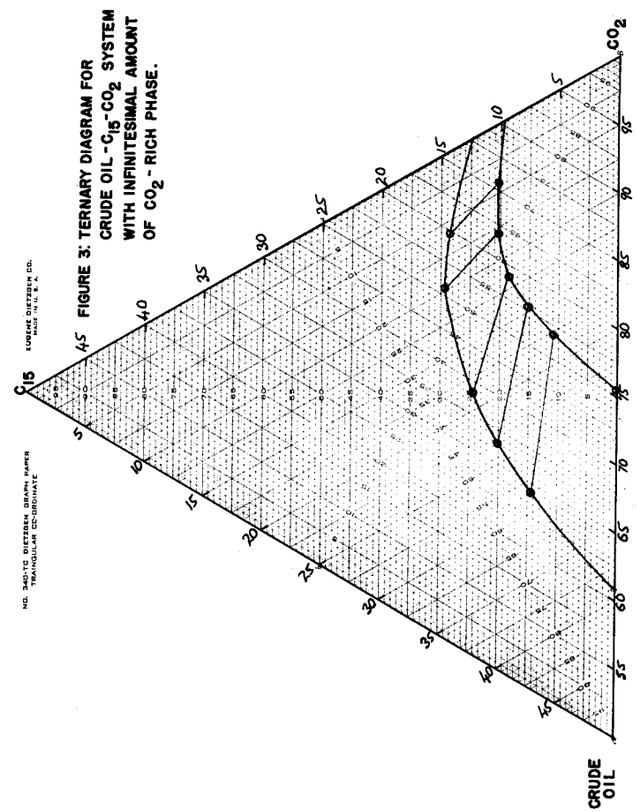

FIGURE 3: TERNARY DIAGRAM FOR CRUDE OIL-C_{15}-CO_2 SYSTEM WITH INFINITESIMAL AMOUNT OF CO_2 - RICH PHASE.

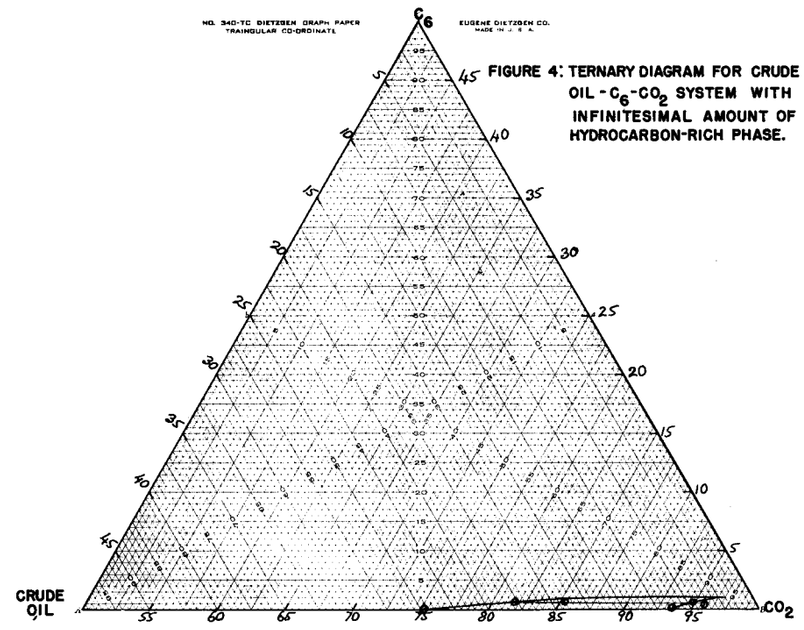

FIGURE 4: TERNARY DIAGRAM FOR CRUDE OIL - C_6 - CO_2 SYSTEM WITH INFINITESIMAL AMOUNT OF HYDROCARBON-RICH PHASE.

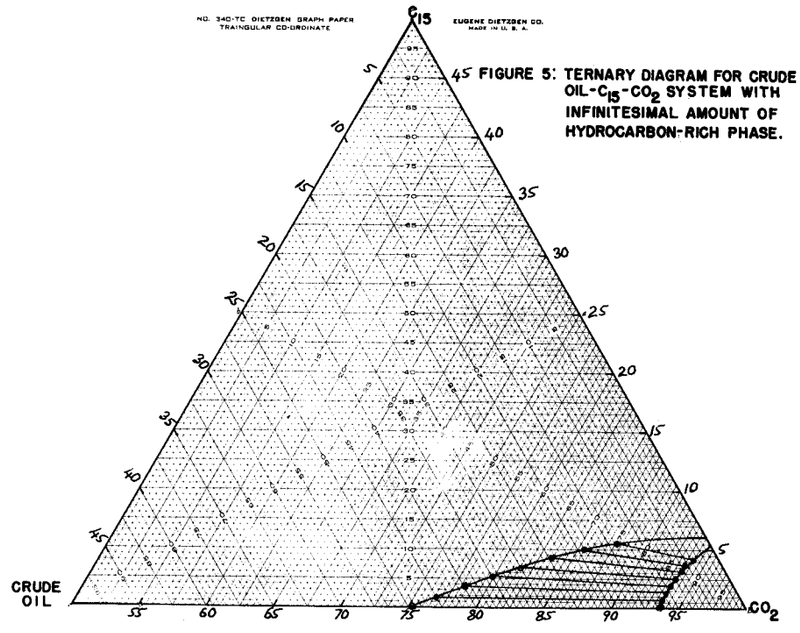

FIGURE 5: TERNARY DIAGRAM FOR CRUDE OIL - C_{15} - CO_2 SYSTEM WITH INFINITESIMAL AMOUNT OF HYDROCARBON-RICH PHASE.

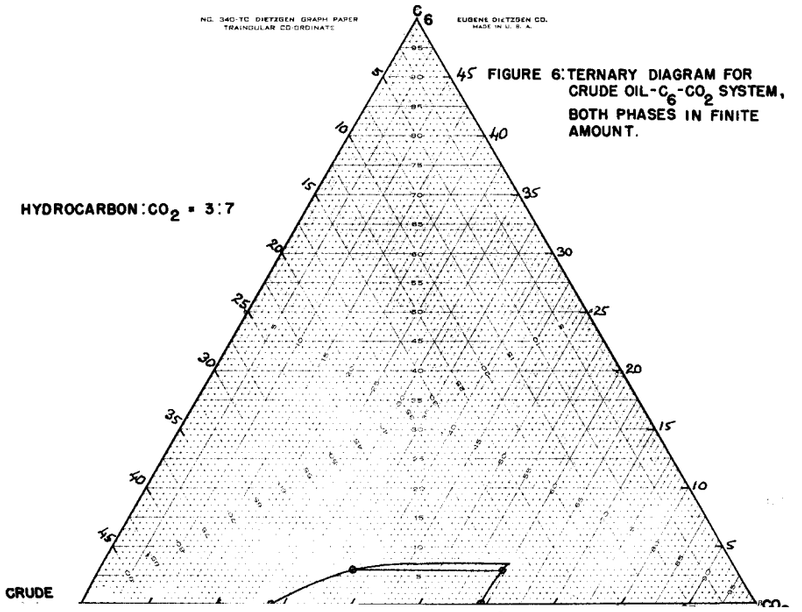

FIGURE 6: TERNARY DIAGRAM FOR CRUDE OIL - C_6 - CO_2 SYSTEM, BOTH PHASES IN FINITE AMOUNT.

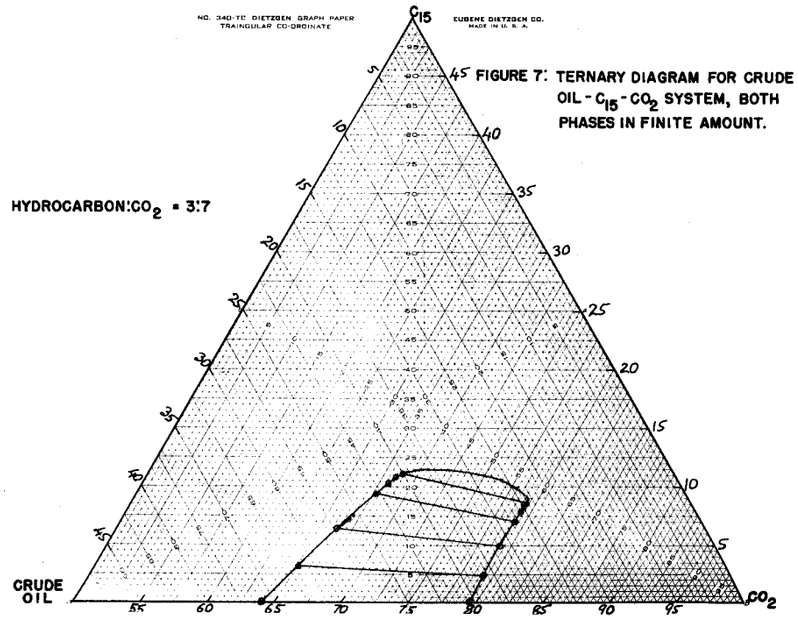

FIGURE 7: TERNARY DIAGRAM FOR CRUDE OIL - C_{15} - CO_2 SYSTEM, BOTH PHASES IN FINITE AMOUNT.

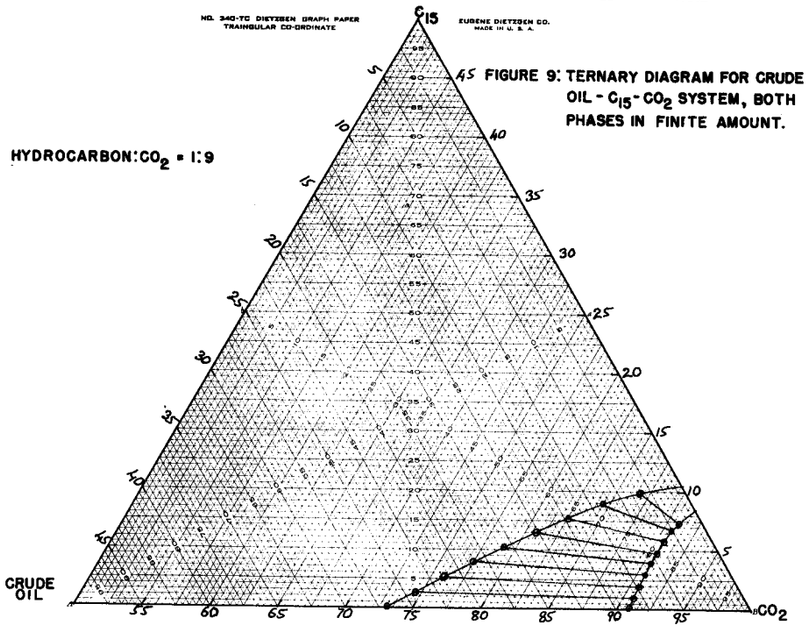

FIGURE 9: TERNARY DIAGRAM FOR CRUDE OIL - C_{15} - CO_2 SYSTEM, BOTH PHASES IN FINITE AMOUNT.

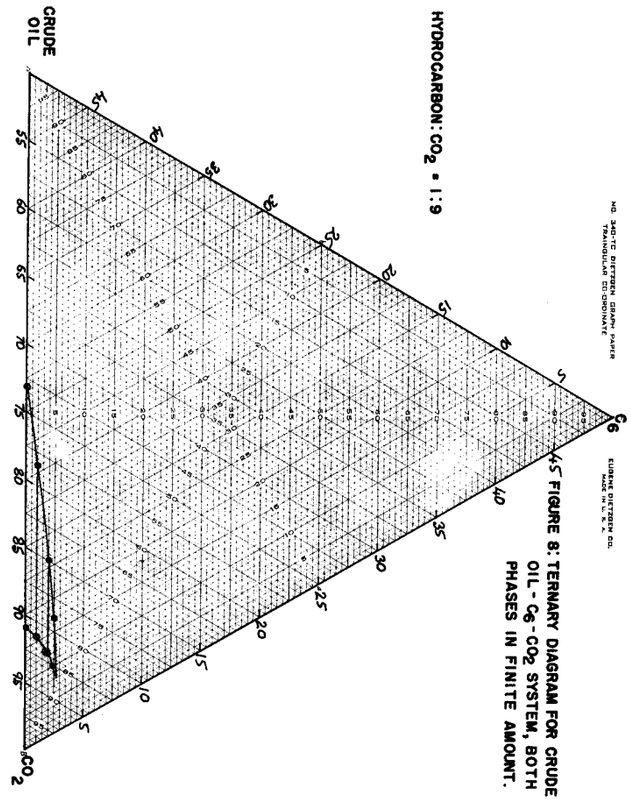

FIGURE 8: TERNARY DIAGRAM FOR CRUDE OIL - C_6 - CO_2 SYSTEM, BOTH PHASES IN FINITE AMOUNT.

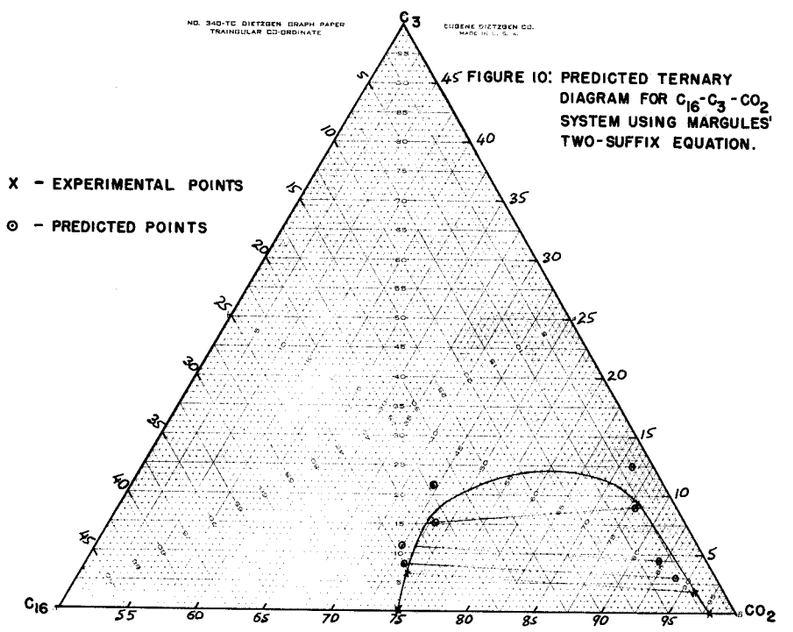

FIGURE 10: PREDICTED TERNARY DIAGRAM FOR C_{16} - C_3 - CO_2 SYSTEM USING MARGULES' TWO-SUFFIX EQUATION.